Mechanisms of Photosynthetic High-Light Tolerance

Synechocystis sp. PCC6803 as an Experimental Platform

Dissertation der Fakultät für Biologie
der Ludwig-Maximilians-Universität München

Marcel Dann

Planegg, 2019

Diese Dissertation wurde
unter der Leitung von Prof. Dr. Dario Leister

an der Fakultät für Biologie

der Ludwig-Maximilians-Universität München

angefertigt.

Erstgutachter: Prof. Dario LEISTER

Zweitgutachter: Prof. Dr. Thomas NÄGELE

Tag der Abgabe: 07.11.2019

Tag der mündlichen Prüfung: 06.02.2020

ERKLÄRUNG: Ich versichere hiermit an Eides statt, dass meine Dissertation selbstständig und ohne unerlaubte Hilfsmittel angefertigt worden ist. Die vorliegende Dissertation wurde weder ganz, noch teilweise bei einer anderen Prüfungskommission vorgelegt. Ich habe noch zu keinem früheren Zeitpunkt versucht, eine Dissertation einzureichen oder an einer Doktorprüfung teilzunehmen.

München, den 05.11.2019

Der Mist von heute ist ja häufig der Dünger von morgen.

- Christoph Bals

Acknowledgement

I would like to sincerely thank everyone who was involved in making this thesis happen. Many thanks to Professor Dr. Dario Leister for taking me in and supplying this rich and stimulating working environment, to the people of GRK2062 for taking care of me, and to Chiara and Francesca for helping me so very much to get started and for fostering my coffee addiction right from the start. Moreover I would like to thank everyone in the lab, especially Sabine, Natalia, Belén, Giada and Thilo for their help and support, as well as Bennet and Theo for tons of fun, beverages, and their endurance regarding my bottle issue. A big thank you also to my collaboration partners Edgardo, Hanno and Aurélien for their shared interest and for demanding analysis of piles of data.

Most special thanks to my friends in and around Munich, as well as those who already moved away – without you this weird village would have routed me out long ago. This one is especially to Jani, Alex, Rebecca, Axel, Anna and Bennet (again), who kept me well-fed and cosy, as well as to Martin and Matthias, who dedicatedly kept me from getting too fat on the other hand. Also, I'd like to thank Greta, Laura, Fabian, David and Carsten back around Cologne, who'd always make sure I'm coming back home from time to time.

Of course I am most grateful for my family's support; especially my Dad's help in getting me started adulting, and my Grandma's unswerving backup and inexhaustible inquisitiveness regarding my work. Equally, I'd like to thank Christoph for getting me into biology so many years ago. If it wasn't for you, I'd probably be baking cakes right now.

Last but not least I'd like to thank my girlfriend Steffi for bearing with me during the past one and a half years and in general. You helped me more with pulling through this than you can imagine.

Contents

Figures

Tables

Abbreviations

AA	antimycin A
Abs	absorbance
AL	actinic light (wavelength λ = 635 nm; driving PSI and PSII photochemistry)
APS	ammonium peroxodisulfate
ATP	adenosine 5'-triphosphate
at	*Arabidopsis thaliana*
BG11(G)	blue-green medium 11 (with glucose)
BSA	bovine serum albumin (fraction V)
°C	degrees Celsius
CDS	coding sequence
CEF	cyclic electron flow (around PSI)
Cytb_6f	cytochrome b_6/f (complex)
d(A/C/G/T)TP	deoxy-(adenosine/cytidine/guanosine/thymidine)5'-triphosphate
Da	daltons (atomic mass units)
DCMU	3-(3,4-dichlorophenyl)-1,1-dimethylurea
DMSO	dimethyl sulfoxide
DNA	deoxyribonucleic acid
DR	downstream region (3' of reference)
DTT	DL-dithiothreitol
E	Einstein [mol photons m^{-2} s^{-1}]
E (-value)	expectation value
EDTA	ethylenediaminetetraacetic acid
EtOH	ethanol
FC	*-fold* change
$Fd_{ox/red}$	ferredoxin oxidized/reduced
Fig.	figure
FNR	ferredoxin-$NADP^+$ oxidoreductase
FQR	ferredoxin-plastoquinone oxidoreductase
FR	far-red (light; wavelength λ = 720 nm; driving only PSI photochemistry)
F_v/F_m	photosystem II maximum quantum efficiency
Φ_{II}	photosystem II effective quantum efficiency
g	gram(s)
GTP	guanosine 5'-triphosphate
h	hour(s)
i.e.	that means/is
J	Joule [$kg \cdot m^2$ s^{-2}]
k	kilo-
l	liter(s)
λ	wavelength [nm]
LB	Lysogeny broth
LEF	linear electron flow
M	molar [mol l^{-1}]
m	milli-
µ	micro-
MeOH	methanol

min	minute(s)
MMS	methyl methanesulfonate
MOPS	3-morpholinopropane-1-sulfonic acid
n	nano-
n	sample size
NAD(P)H	nicotinamide adenine dinucleotide (phosphate)
NDH	NADH dehydrogenase-like (complex)
NPQ	non-photochemical quenching
OD(XXX)	optical density (at wavelength λ = XXX nm)
ORF	open reading frame
P (-value)	probability value
PAM	pulse amplitude modulation
PAGE	polyacrylamide gel electrophoresis
PAR	photosynthetically active radiation
PBS	phosphate buffered saline
PCC	Pasteur culture collection
PCR	polymerase chain reaction
PGR5	proton gradient regulation 5
PGRL1	PGR5-like photosynthetic phenotype
PMSF	phenylmethylsulfonyl fluoride
PSI	photosystem I
PSII	photosystem II
PVDF	polyvinylidene fluoride
rcf	-*times* gravity (relative centrifugal force)
RNA	ribonucleic acid
ROS	reactive oxygen species
rpm	rotations per minute
s	second(s)
SDS	sodium dodecyl sulfate
sp.	species
SSC	saline-sodium citrate
syn	*Synechocystis*
$t_{0.5}P700_{ox}$	PSI reaction centre oxidation half time
$t_{0.5}P700^{+}_{red}$	PSI reaction centre re-reduction half time
Tab	table
TBS(T)	Tris-buffered saline (+ Tween® 20)
TEMED	N,N,N′,N′-Tetramethylethylenediamine
TES	2-[(2-Hydroxy-1,1-bis(hydroxymethyl)ethyl)amino]ethanesulfonic acid
Tricine	N-[Tris(hydroxymethyl)methyl]glycine
Tris (base)	Tris(hydroxymethyl)aminomethane
Tween® 20	Polyethylene glycol sorbitan monolaurate
UR	upstream region (5’ of reference)
UV	ultra violet (light)
v/v	volume/volume
w/v	weight/volume

Abstract

Plants and cyanobacteria use a process called oxygenic photosynthesis to convert light into chemical energy, which in turn sustains most life on Earth. Oxygenic photosynthesis is an elaborate interplay of multi-subunit transmembrane protein complexes, two of which, the photosystems I and II (PSI and PSII), harvest light energy and use it to catalyze photochemical redox reactions. The PSII-catalyzed reaction results in water oxidation and the eponymous release of molecular oxygen, while the PSI-driven reaction results in reduction of ferredoxin. These light-driven enzymes have evolved once and are being used by all oxygenic photosynthesizers with little to no structural variation.

Photosynthesis is commonly assumed to have evolved under extremely low light intensities originally. In order to conquer elevated-light-intensity environments it had to be supported by evolution of numerous protective mechanisms, however. One of these mechanisms is called cyclic electron flow (CEF) around PSI, which is assumed to serves as energy valve and balancing agent. CEF recycles surplus electrons until acceptor molecules become available, resulting in formation of a proton gradient and consequent induction of excitation energy dissipation mechanisms. The proton gradient also is harvested for ATP synthesis, and CEF can be employed to adjust proton gradient formation to cellular ATP demands without generation of reductive equivalents. CEF is channeled through several, partially redundant routes, one of which is characterized by its sensitivity to the antibiotic antimycin-A (AA). AA-sensitive CEF is common to most cyanobacteria and plants, but remains poorly understood to date. Two plant components of AA-sensitive CEF termed PGR5 and PGRL1 have been identified in the model plant *Arabidopsis thaliana* (*Arabidopsis*), but their mode of action and actual involvement in CEF and/or its regulation is still elusive. We have established a prokaryotic expression system for plant PGR proteins based on the cyanobacterial model organism *Synechocystis* sp. PCC6803 (*Synechocystis*) to, upon deletion of endogenous PGR5, assess the function of *Arabidopsis* PGRL1 and PGR5 on a presumably orthogonal platform. We could demonstrate functional complementation of the *Synechocystis* PGR5 knockout mutant by the plant PGRL1*PGR5 couple, confirmed the system to be suitable for functional assays with different PGR protein isoform, and identified a new *Synechocystis* component that apparently fulfils parts of the functional role of plant PGRL1 (synPGRL1-LIKE Sll1217). Besides offering a new approach to study this known light stress adaptive mechanism, we could establish an experimental pipeline to evolve new strategies of high-light-intensity tolerance in *Synechocystis* and confirmed the adaptive value of two candidate mutations, one of which seemingly confers increased CEF activity. CEF upregulation by means of evolution and genetic engineering was found to result in similar degrees of high-light tolerance, demonstrating feasibility and power of adaptive evolution, and suggesting its great potential as optimization tool for photosynthetic research and production strains.

Zusammenfassung

Pflanzen und Cyanobakterien nutzen oxygene Photosynthese, um Licht in chemische Energie zu konvertieren, welche den Großteil des Lebens auf der Erde versorgt. Zwei an der oxygenen Photosynthese beteiligte, membranständige Multi-Protein-Komplexe, die Photosysteme I und II (PSI und PSII), absorbieren Lichtenergie und nutzen diese um Redox-Reaktionen zu katalysieren. Dabei oxidiert PSII Wasser, was zur namensgebenden Freisetzung von Sauerstoff führt, während PSI Ferredoxin reduziert. Diese lichtgetriebenen Enzyme wurden einmalig evolviert und werden fast unverändert von allen oxygen-photosynthetischen Organismen genutzt.

Es wird angenommen, dass Photosynthese ursprünglich unter extrem niedrigen Lichtintensitäten evolvierte. Wachstum unter erhöhten Lichtintensitäten setzte die Entwicklung neuer Schutzmechanismen voraus. Einer dieser Mechanismen ist *zyklischer Elektronentransport* (ZET) um PSI, welcher überschüssige Anregungsenergie abführt und an der Balancierung zellulärer Energie- und Redox-Träger beteiligt ist. ZET führt „überschüssige“ Elektronen zurück zur PSI-Donorseite, bis Akzeptormoleküle verfügbar werden. Dabei werden ein Protonengradient aufgebaut und Energiedissipationsmechanismen induziert. Es existieren mehrere, partiell überlappende ZET-Routen, von denen eine empfindlich gegenüber Antimycin A (AA) ist. AA-sensitiver ZET existiert in den meisten Cyanobakterien und Pflanzen, ist aber bis heute kaum verstanden. Zwei pflanzliche Komponenten dieser ZET-Route, PGRL1 und PGR5, wurden in *Arabidopsis thaliana* (*Arabidopsis*) identifiziert, aber ihre Funktion im ZET und/oder seiner Regulation sind umstritten. Zu deren funktionaler Analyse wurde ein prokaryotisches Expressionssystem für pflanzliche PGR-Proteine im Cyanobakterium *Synechocystis* sp. PCC6803 (*Synechocystis*) etabliert. Deletion des *Synechocystis*-eigenen PGR5 schaffte dabei einen physiologisch orthogonalen Hintergrund, in dem eine funktionelle Komplementation der *Synechocystis pgr5* Mutante durch das pflanzliche PGRL1*PGR5-Pärchen gezeigt, und die Eignung unseres Systems für die funktionale Analyse verschiedener PGR-Protein-Isoformen bestätigt werden konnte. Zudem wurde eine neue ZET-Komponente in *Synechocystis* identifiziert, die teilweise die Funktion pflanzlichen PGRL1 übernehmen kann (synPGRL1-LIKE Sll1217). Neben diesem neuen Ansatz zur Erforschung von ZET konnten wir einen experimentellen Aufbau zur Evolution neuer Strategien zur Erhöhung der Lichtstresstoleranz etablieren. Zudem konnte der adaptive Mehrwert zweier Kandidatenmutationen experimentell bestätigt werden, von denen eine erhöhte ZET-Aktivität hervorruft. Die künstliche Anregung von ZET-Aktivität durch gentechnische und evolutive Ansätze resultierte in einer vergleichbaren Erhöhung der Starklicht-Toleranz, was die Möglichkeiten und Umsetzbarkeit adaptiver Evolutionsexperimente demonstriert, und deren Potential als Optimierungswerkzeug für die Photosyntheseforschung und bakterielle Produktionsstämme verdeutlicht.

1 Introduction

1.1 Oxygenic photosynthesis: Fuelling life

All terrestrial life forms known are built from the same set of carbon-based (macro-) molecules including lipids, carbohydrates, nucleic acids, and proteins. These building blocks are near-exclusively provided by photoautotrophic organisms, which harness solar energy and convert it into chemical energy carriers. With these energy carriers they assimilate – among others – inorganic carbon, nitrogen, sulfur and phosphorous compounds into biomass. Most photoautotrophs today are oxygenic (i.e. oxygen-releasing) photosynthesizers, a heterogeneous group comprised of prokaryotes (cyanobacteria) and eukaryotes (algae, plants, protists). A set of pigment-binding multi-protein complexes absorb and convert solar energy by carrying out a sequence of light-driven redox reactions. These reactions catalyze oxidation of water to molecular oxygen and reduction of universal cellular redox carriers, which are used to reduce carbon dioxide to carbohydrates ($C_nH_{2n}O_n$).

The evolutionary origin of oxygenic photosynthesis dates back approximately 3–3.5 billion years, meaning it has fueled heterotrophic life on earth (dating back approximately 3.8–4 billion years) for most of its existence (Blankenship 2010 and references therein). It is still debated whether the key functional modules were evolved in different organisms and were later combined by horizontal gene transfer, or whether they originated in the same organism (Blankenship et al. 2007, Cardona 2017). However, the earliest oxygenic photosynthesizers are presumed to have closely resembled modern cyanobacteria (Allen 2014). Modern plants are hypothesized to have acquired oxygenic photosynthesis by endosymbiotic uptake of a primordial cyanobacterium, resulting in the evolution of semi-autonomous cell organelles termed *plastids* (Keeling 2010). Chloroplasts are a subtype of plastid endosymbionts which harbor special pigment-binding multiprotein complexes. Chlorophylls (Greek χλωρός, khloros "*pale green*" and φύλλον, phyllon "*leaf*") are the most prominent pigment class prevalent in chloroplasts, characteristically tinting these organelles and giving them their name. Chlorophylls are arguably the most crucial components in photosynthesis. They are not only responsible for most of the solar-energy absorption, but also for its enzyme-assisted conversion into chemical energy by photon-absorbance induced charge separation (for a profound compilation, see Grimm et al. 2007).

1.2 Light is a key substrate of photosynthesis

As mentioned before, light is one of the key substrates for photosynthesis (hence the Greek origin of the term, φῶς, phōs, "*light*", and σύνθεσις, synthesis, "*putting together*"). The basic principle of photosynthesis lies in coupling highly endergonic chemical reactions, such as splitting of water (H_2O) into two protons ($2*H^+$), two electrons ($2*e^-$), and molecular oxygen (½ O_2), with absorbance of a red photon. In this process, absorbed photons provide enough energy (175.9 kJ/mol for λ = 680 nm) to oxidize water (requiring ΔG° = 317 kJ/mol) in a two-step process, encompassing absorption of two photons and consequent charge separation events per water molecule (Johnson 2016).

In all organisms performing full-fledged oxygenic photosynthesis, four multiprotein complexes work in concert (Nelson and Ben-Shem 2004). All of them are embedded into intracellular membrane systems forming closed compartments called *thylakoids*, which resemble flattened vesicle structures. Photosystem (PS) II is a chlorophyll-binding, light-driven, water-splitting enzyme. Upon excitation of its reaction center P680, P680* reduces small organic intra-thylakoid-membrane electron carrier termed plastoquinone (PQ), subsequently oxidizes H_2O, and then releases O_2; hence, PSII is a light-driven H_2O-PQ oxidoreductase. PQ is oxidized by the cytochrome b_6/f complex (Cytb_6f), which reduces the soluble protein redox-carriers plastocyanin (PC) or cytochrome c_6 (cyt c_6), and in the process translocates six protons (H^+) per oxidized H_2O across the thylakoid membrane, which acidify the thylakoid lumen. Photosystem I (PSI), another chlorophyll-binding, light-driven multi-protein enzyme, reduces oxidized ferredoxin (Fd_{ox}) to Fd_{red} upon excitation of its reaction center P700 (P700*), and in turn oxidizes PC (or cyt c_6); hence, PSI is a light-driven PC-Fd oxidoreductase. Fd_{red} then acts as potent cellular reductive equivalent and is required for NADPH/H^+ formation and CO_2 reduction/assimilation. Finally, an F_0/F_1 type ATP synthase harvests the proton gradient built up across the thylakoid membrane in order to drive ADP phosphorylation to ATP, a universal cellular equivalent of chemical energy (Rochaix 2011). A fifth thylakoid membrane protein complex, a homologue of respiratory complex I called NDH (NADH DeHydrogenase) can additionally generate a proton gradient coupled to reduction of PQ with stromal electrons. NDH is not common to all oxygenic photosynthesizers, however, and has been shown to be evolutionarily lost in *Pinus thunbergii* (Wakasugi et al. 1994) and *Chlamydomonas reinhardtii* (Peltier and Cournac 2002), for example.

1.3 Light utilization underwent evolutionary changes and shifts of optima

Although light energy is crucial to photosynthetic catalysis, excess light energy can be highly detrimental to integrity and activity of the pigment-binding complexes (e.g. Barber and Andersson 1992). So-called photoinhibition primarily occurs upon lack

of adequate electron donors or acceptors, leading to unspecific oxidation or reduction of nearby molecules or the photosystems themselves (Nishiyama et al. 2006, Sonoike 2010, Li et al. 2018). However, when they started to colonize the land masses, photosynthetic organisms had to adapt to severely increased incidence of light and therefore in part drastically shifted their physiological optima of ambient light intensity.

1.3.1 Original state: Low-light photosynthesis

The first oxygenic photosynthesizers are hypothesized to have originated in the ocean, where they could easily avoid detrimentally high light intensities since light incidence is depth-dependent. Variants of this hypothesis locate their origin at depths where photosynthetically active radiation was highly limited, or even next to hydrothermal vents, where original phototrophs would have harnessed the vents' black body radiation rather than sunlight (reviewed by Martin et al. 2018). Considering the evolutionarily conserved proneness of PSII core protein D1 to photodamage (Andersson and Aro 2001) and the low-light ecological niches still occupied by most modern cyanobacteria (Stal 1995), it seems plausible that low light intensities were preferred by or even vital to ancient photosynthesizers.

Later, more light-tolerant progenitors of cyanobacteria optimized light harvesting efficiency evolutionarily, employing alternative antenna pigments absorbing light of wavelengths 400–650 nm (Bryant et al. 1967), which are bound to elaborate multiprotein complexes called phycobilisomes (reviewed by Glazer 1977). These complexes allow modern cyanobacteria, as well as red algae sharing their general photosynthetic setup (Allen et al. 2011 and references therein), to strive in the shade of other photoautotrophs that rely solely on carotenoids and chlorophylls for light harvesting (Fig 1.1).

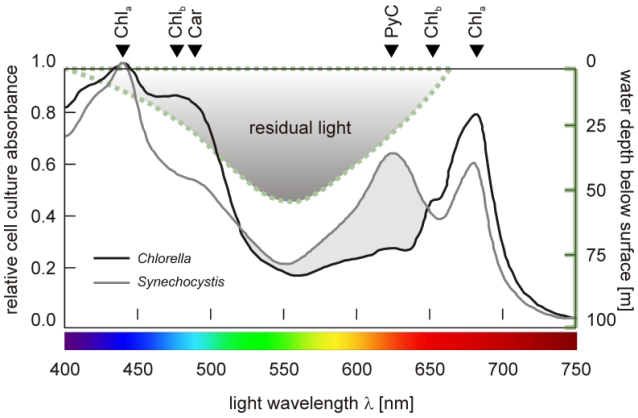

Fig 1.1. **Cyanobacterial antenna pigments allow utilization of light inaccessible to green plants.** Schematic absorbance spectra of green algae (*Chlorella sorokiniana*) and cyanobacteria (*Synechocystis* sp. PCC6803) cell cultures (adapted from Luimstra et al. 2018) illustrate additional light harvesting capacities regarding green, yellow, and orange light (solid grey area) due to alternative antenna pigments. The penetration depth of visible light in water (grey gradient; secondary y-axis; Chandler et al. 2016) underpins the selective advantage of cyanobacterial light harvesting. Absorbance maxima of common chlorophyll a (Chl$_a$) and carotenoids (Car), as well as plant-specific chlorophyll b (Chl$_b$) and cyanobacterial phycocyanin (PyC), are indicated with triangles.

Combined with typically low physiological maintenance costs (Van Liere and Mur 1979, Zevenboom and Mur 1984) cyanobacteria at large are well-adapted to low-light competitiveness. In this context, it appears unsurprising that the photoautotrophs with the lowest growth-light-energy requirements

known are the cyanobacterial species *Acaryochloris marina* and *Chroococcidiopsis thermalis*. Both species rely on far-red-light absorbing chlorophyll variants to drive photosynthetic water splitting with wavelengths around 725 and 727 nm instead of 680 nm (Renger and Schlodder 2008, Nürnberg et al. 2018).

1.3.2 Derived state: High-light photosynthesis

Green algae and land plants (summarized in *Viridiplantae*, literally "green plants") have adapted their light harvesting machinery to excessive light abundance in upper water layers and terrestrial habitats. In the course of this process they lost phycobilisomes and evolved several plant-specific mechanisms to quench or re-allocate excitation energy. Many land plants and algae in fact depend on growth-light intensities at least an order of magnitude above those sufficient of cyanobacterial growth. While most cyanobacterial liquid cultures require a minimum of 3–5 µmol photons m^{-2} s^{-1} (µ*Einstein,* µE) to grow photoautotrophically (e.g. Litchman 2003, Foy and Gibson 1982, Fallowfield and Osborne 1985) and red algae (Leukart and Lüning 1994) have been reported to undergo cell division under as little as 0.1 µE, green algae require approximately 15–25 µE for minimum growth (rewieved by Richardson et al. 1983). Most higher plants were described to require a minimum of 3–4 moles photons per m^2 per day (corresponding to approximately 52 µE at 16 h light/8 h dark cycles) to successfully reproduce (reviewed by Poorter et al. 2019). This trend suggests a pronounced physiological trade-off between high-light tolerance and low-light performance.

As compared to cyanobacteria, land plants display an array of molecular mechanisms granting enhanced high-light resilience. Among the most prominent are the xanthophyll cycle (an enzymatic carotenoid-pigment-derivation cycle, which initiates non-photochemical quenching of excitation energy by heat dissipation (Demming-Adams and Adams 1996, Jahns and Holzwarth 2012), and re-allocation of PSII-associated light-harvesting complexes (LHCBs) to PSI, a process termed “state transition” (Minagawa 2011). And while also cyanobacteria have evolved a carotenoid-dependent mode of non-photochemical heat dissipation *via* the so-called orange carotenoid protein (OCP; Wilson et al. 2006), this mode can prevent only about 50 % of excitation energy from the phycobilisomes from reaching the PSII reaction centers (Gorbunov et al. 2011). Plants in turn have been reported to display NPQ capable of dissipating *all* excess light energy that solar incidence can possibly provide (Ruban and Belgio 2014 and references therein), at least mathematically.

Finally, plants can employ morphological adaptations such as altered leaf architecture, reflective trichoma and cuticulae to reduce incident light intensity (Boardman 1977, Klich 2000), all of which require tissue or cellular differentiation unattainable to bacteria.

1.3.3 The key components of photosynthesis remain conserved

Despite their divergent growth-light optima, the core components of photosynthetic electron transport are highly conserved from cyanobacteria to plants (reviewed by Allen et al. 2011, Leister 2019). In fact, for PSII and PSI, only a total of 7 and 5 polypeptides are known to be specific for either phylogenetic branch, respectively, with 19 and 10 subunits being common to cyanobacteria and plants, respectively (Tab 1.1). Moreover, no plant/cyanobacteria-specific subunits of Cytb_6f, ATP synthase, or the NDH complex have been described, with the sole exception of PetO, a non-conserved Cytb_6f subunit present in certain green algae (Takahashi et al. 2016). Hence, the light-reaction protein-complex setup retained virtually complete structural conservation over the course of hundreds of millions of years of divergent evolution, estimates of which range from 580 million (Cavalier-Smith 2011) to 1.2 billion years ago (Parfrey et al. 2011).

This in turn implies that shifts in growth-light preferences/requirements are likely a result of small mutational changes of the key components, or of the employment of vastly different sets of accessory, plant/cyanobacteria-specific factors.

Tab 1.1. Recognized structural subunits of photosynthetic multiprotein complexes. Subunits as described by Allen et al. (2011) and Leister (2019). Centre: common subunits; margins: cyanobacteria (left) and plant (right) specific subunits.

	cyanobacteria		**plants**
PSII		D1, D2, CP43, CP47, E, F, H, I, J, K, L, M, N, O, T, W, X, Y, Z	
	U, V		P, Q, R, S, Tn
Cytb_6f		Cyt b_6, Cyt f, IV, G, L, M, N, Rieske	
			(O)
PSI		A, B, C, D, E, F, I, J, K, L	
	M		G, H, N, O
ATP synthase		α, β, γ, δ, ε, a, b, b', c	
NDH		A, B, C, D, E, F, G, H, I, J, K, L, M, N, O, P, Q, R, S	

1.3.4 Do cyanobacteria lack potential? Genetic innovation as possible consequence of endosymbiosis

The endosymbiotic uptake initiated massive evolutionary changes in the plant plastid precursor. The majority of protein-coding genes were exported into the host cell nucleus (Weeden 1981, Timmis et al. 2004), and numerous originally eukaryotic proteins were implemented into plastid structures, such as nucleoids (Kobayashi et al. 2015), and metabolic pathways, such as starch biosynthesis (Ball et al. 2011). Coinciding with the altered environmental challenges faced by *Viridiplantae*, the vast majority of specific PSII and PSI subunits (71 % and 80 %, respectively) are found in plants nowadays (see Tab 1.1). Red algae in turn display, with exception of presence of LHCI,

cyanobacteria-type photosystem architecture, as well as cyanobacteria-type light-harvesting machinery (Gantt et al. 2003). Consequently, red algae strive in deeper (up to 15 m), low light aquatic environments (Lüning 1970), very much like cyanobacteria themselves, which dominate deeper water layers in nature (Källqvist 1981).

1.3.5 Study branch 1:

Experimental exploration of high-light adaptive potential in *Synechocystis*

To investigate the effective limitations of cyanobacterial high-light adaptation, we issued an experimental exploration of the high-light adaptive potential of the model cyanobacterium *Synechocystis* spec. PCC6803 (hereafter *Synechocystis*). By directed evolution of high light tolerance we aimed to assess whether, if at all, such tolerance could rather be achieved by genetic convergence towards the set of presumably high light adaptive alleles found in modern plant photosynthetic genes, or by developing truly novel genetic variants. Assuming the accessory components of *Synechocystis* wildtype to be unsuitable to convey elevated high light tolerance, adaptive changes should occur in the photosynthetic core machinery and primary metabolism. This in turn might grant us valuable insight into the effective degrees of freedom regarding genetic variability and possible targets for improvement in algal and land plant photosynthesis.

1.4 In spite of opposite preferences:

High-light acclimation to short-term exposure

Although mostly favoring low-light habitats, cyanobacteria display some high light acclimation capacity. While continuous high-light exposure compromises growth in many cyanobacterial species (Van Liere and Mur 1980), intermittent exposure to elevated light intensities – about half of the maximum prevalent in the respective habitat – has been observed to actually stimulate maximum growth (Loogman 1982). Several mechanisms of short- to mid-term high-light acclimation have been described for *Synechocystis*, among which there is accumulation of so-called high-light inducible polypeptides (HLIPs), the loss of which severely compromises high-light cell survival (He et al. 2001). HLIPs are homologues to plant light-harvesting complexes (Funk and Vermaas 1999) involved in biosynthesis of chlorophyll (Xu et al. 2004), its allocation to PSII (Hernandez-Prieto et al. 2011), as well as PSII photoprotection (Komenda and Sobotka 2016 and references therein, Tibiletti et al. 2018). Also, chlorophyll biosynthesis and turnover are fostered by high-light exposure (Kopečná et al. 2012).

Another mechanism fostering high-light tolerance in *Synechocystis* is cyclic electron flow (CEF) around PSI, with according loss-of-function mutations resulting in decreased high-light tolerance (Yeremenko et al. 2005, Gao et al. 2016). The phenomenon of CEF around PSI has initially been described as *photosynthetic phosphorylation* (Arnon et al. 1954, Allen et al. 1958) and was found to result in light driven ATP-biosynthesis without $NADP^+$ reduction or CO_2 fixation. Later, it has been re-labeled *cyclic photophosphorylation* to distinguish it from the then newly discovered *non-cyclic photophosphorylation* (Arnon et al. 1958, Whatley and Arnon 1963) which encompasses linear photosynthetic electron flow from H_2O through PSII and PSI to ferredoxin/$NADP^+$.

1.4.1 Cyclic electron flow around PSI: Valve and working horse

Today CEF is widely accepted to return electrons from the PSI acceptor site back to PQ, thus preventing unspecific reduction and reactive oxygen species (ROS) formation in case of terminal-electron-acceptor limitation (Munekage et al. 2002, Scheller and Haldrup 2005, Suorsa et al. 2013). CEF is encompassed by enhanced thylakoid lumen acidification through fostered Cytb_6f activity, and concordantly increased ATP synthesis. While thylakoid lumen acidification induces non-photochemical quenching and thus protects PSII from photodamage (Shikanai 2016), additional ATP is required for cellular repair mechanisms, such as the D1 repair cycle to sustain PSII activity (Takahashi et al. 2009, Murata and Nishiyama 2018). Effectively returning electrons to the PSI donor side meanwhile alleviates dangerous PSI acceptor side limitation, a prominent consequence of reduced Calvin cycle activity (Golding and Johnson 2003, Miyake et al. 2005).

There are several partially overlapping routes of CEF described in cyanobacteria (summarized by Mullineaux 2014), two of which they share with plants. The first route of CEF around PSI that was discovered is ferredoxin-dependent and sensitive to antimycin A (AA)-inhibition (Tagawa et al. 1963), and was early hypothesized to entail the activity of a ferredoxin-plastoquinone oxidoreductase (FQR; Moss and Bendall 1984). Molecular components of this route have long remained elusive, until rather recently two involved proteins were identified in the model plant *Arabidopsis thaliana* (hereafter *Arabidopsis*). PGR5 (proton gradient regulation 5; Munekage et al. 2002) and PGRL1 (*pgr5*-like photosynthetic phenotype 1; DalCorso et al. 2008) cause severe impairment of AA-sensitive CEF upon their inactivation, and PGRL1 is required for PGR5-protein accumulation *in vivo*. Both proteins apparently are necessary for AA-sensitive CEF activity in *Arabidopsis*, and a PGRL1*PGR5 complex could be shown to catalyze reduction of a plastoquinone analogue in an Fd_{red}-dependent manner (Hertle et al. 2013). Besides PGR5 and PGRL1, ferredoxin-$NADP^+$ oxidoreductase (FNR) has been a long-standing candidate enzyme for FQR-related electron injection into PQ/Cytb_6f (Bendall and Manasse 1995). FNR catalyzes the final step in photosynthetic linear electron flow (LEF),

but has repeatedly been hypothesized to play a role in CEF as well (Mulo 2011). This connection was initially made due to its Fd-binding capacity and close association with Cytb_6f (Clark et al. 1984, Zhang et al. 2001) and, more recently, due to its interaction with PGRL1 (DalCorso et al. 2008). *Arabidopsis*-knock-down mutants of FNR do not display reduced but rather increased CEF activity as indicated by enhanced NPQ, however (Lintala et al. 2012). At the same time, it cannot be excluded that residual FNR is preferentially channeled into thylakoid membrane association and CEF activity (Bölter et al. 2010) as a result PSI acceptor side limitation; this is suggested by enhanced PGRL1 accumulation, accelerated $P700^+$ dark re-reduction, and fostered xanthophyll-de-epoxidation (Lintala et al. 2012).

The second CEF route common to plants and cyanobacteria is AA-insensitive (Joët et al. 2001) and employs the NDH (NAD[P]H dehydrogenase) complex (Ogawa 1991, Shikanai et al. 1998). NDH contributes to PQ-reduction-coupled proton translocation across the thylakoid membrane (Burrows et al 1998) while being a plastid/cyanobacterial homologue to respiratory complex I (Berger et al. 1993) that lacks a canonical NAD(P)H-docking site (Laughlin et al. 2019). Recently, *Thermosynechococcus elongatus* photosynthetic complex I has been demonstrated *in vitro* to directly receive electrons from PSI *via* Fd_{red} (Schuller et al. 2019), implying it to be an actual FQR rather than an NADPH-PQ-oxidoreductase, albeit not *the* FQR hypothesized to be involved in AA-sensitive CEF. A schematic overview of the CEF routes described above is provided in Fig 1.2.

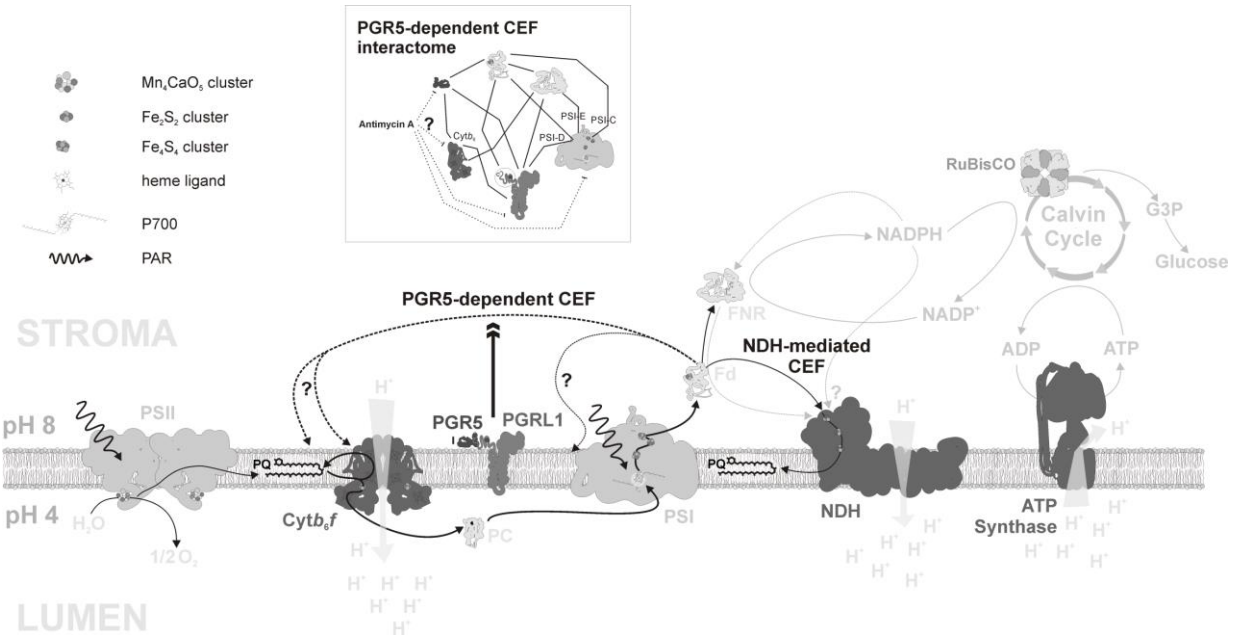

Fig 1.2. **Schematic overview of photosynthetic electron transport routes.** Discussed CEF routes are highlighted bold. Known protein-protein interactions (solid lines; Clark et al. 1984, Andersen et al. 1992, van Thor et al. 1999, Zhang et al. 2001, DalCorso et al. 2008, Hertle et al. 2013, Buchert et al. 2018) of potential participants in PGR5-mediated CEF are summarized in the box; possible AA-binding/inhibition sites as outlined below (section 1.4.2) are indicated with dotted lines. PAR, photosynthetically active radiation.

The physiological relevance of CEF under field conditions has long been doubted; however, nowadays it is widely accepted that CEF is pivotal to efficient photosynthesis (reviewed by Yamori and Shikanai 2016, Finazzi and Johnson 2016). CEF plays a key role in poising chloroplast/cellular ATP:NADPH ratios (Slovacek et al. 1978, Allen 2002), especially in C_4 plant bundle sheath cells (Takabayashi et al. 2005), in inducing non-photochemical quenching of excess light energy (Munekage et al. 2002), and in buffering PSI from fatal photodamage under fluctuating light conditions (Suorsa et al. 2012). *Arabidopsis pgr5 ndh* (i.e. chlororespiratory reduction *crr2*) double mutants deficient in both AA-sensitive and AA-insensitive CEF displayed no *in vitro* CEF activity, and severe photoautotrophic growth defects even under continuous light (Munekage et al. 2004). This supports the notion that CEF actually plays a key role not only under stress, but also in steady state photosynthesis by supplying extra ATP required for efficient carbon fixation and cellular maintenance that LEF cannot provide (Allen 2003).

In the cyanobacterial model *Synechocystis*, both CEF routes described above have been shown to be active (Mi et al. 2000, Yeremenko et al. 2005). However, the relative contribution of both routes is inverted as compared to plants. Initial estimates placed PGR5-dependent CEF-activity around 13 % of LEF activity (Avenson et al. 2005). Recent estimates in *Arabidopsis* attribute approximately 35 % of total thylakoid proton gradient formation to CEF, approximately 86 % of which (i.e. 30 %) correspond to AA-sensitive CEF (Kawashima et al. 2017). In *Synechocystis*, approximately 52 % of total photosynthetic electron transport activity has been attributed to CEF under not light-limited/inorganic carbon-limited conditions (Nogales et al. 2012), and approximately 80 % of total light energy storage by CEF around PSI has been found to correspond to AA-insensitive CEF (Yeremenko et al. 2005).

Synechocystis, as most cyanobacteria, possesses an obvious PGR5 homologue encoded by open reading frame (ORF) ssr2016, but, as all cyanobacteria, lacks a clear PGRL1 homologue. Intriguingly, in *Synechocystis* the loss of PGR5 results in increased susceptibility to high light (Yeremenko et al. 2005), but not to fluctuating light (Allahverdiyeva et al. 2013).

1.4.2 CEF conundrums

In addition to questions raised by the absence of cyanobacterial PGRL1, the characterization of PGR5-dependent CEF as AA-sensitive CEF might need to be re-evaluated. Shikanai and co-workers identified a PGR5 variant from *Pinus taeda* that alleviates AA-sensitivity by a V3K substitution in the mature PGR5 protein. This effect could be reproduced upon introduction of an according mutation in *Arabidopsis* PGR5 (Sugimoto et al. 2013). A corresponding substitution has been found in *Chlamydomonas reinhardtii* (hereafter *Chlamydomonas*) strain 137c PGR5, coinciding with

AA-insensitivity of CEF around PSI (Iwai et al. 2010, Antal et al. 2013). The N-terminal sequence containing the according V3 (K1-G8 in *Arabidopsis* mature PGR5), however, is absent from cyanobacterial PGR5; yet, AA sensitivity has been reported in *Synechococcus* spec. PCC7002 (Charlebois and Mauzerall 1999) and *Synechocystis* (Yeremenko et al. 2005). AA is a respiration inhibitor, that binds to the Q_i site of the mitochondrial cytochrome *bc*1 complex and there suppresses respiratory electron transport (Kim et al. 1999). Counterintuitively, AA does not bind to the corresponding site of the plastid Cytb_6f complex as initially suggested (Mills et al. 1978), but to PSI-containing thylakoid protein fractions (Davies and Bendall 1987). *In vitro*, AA inhibits reduction of the PQ analogue 2,6-dimethoxy benzoquinone (DMBQ) by heterologously expressed PGRL1, suggesting PGRL1 or the PGRL1*PGR5 complex as site of action (Hertle et al. 2013). Indeed PGRL1 physically interacts with the stromally exposed PSI subunit PSI-D (DalCorso et al. 2008), potentially giving rise to a PSI-PGRL1/PGR5 hybrid AA binding site. With both PGRL1 and the suggested AA-binding site of PGR5 being absent from AA-sensitive cyanobacteria, however, the actual binding site of AA is still unclear. Finally, in *Chlamydomonas*, induction of maximum CEF rates has been observed in absence of PGRL1 and PGR5 (Nawrocki et al. 2019), questioning both proteins' integral role to AA-sensitive CEF, at least in *Chlamydomonas*. Then, again, in *Chlamydomonas* strain 137c (the genetic background of the *pgrl1* mutant used in the corresponding study; Tolleter et al. 2011), CEF is precisely *not* AA-sensitive (see above), rendering this observation potentially exclusive to the 137c strain.

Further potentially confounding evidence stems from cyanobacterial studies with *Phormidium laminosum* (Manasse and Bendall 1993) and *Anacystis nidulans*/*Synechococcus elongatus* sp. PCC7942, for both of which CEF has been reported to be insensitive to AA (Bothe 1969, Lee-Kaden and Simonis 1979). In fact, however, the *Synechococcus elongatus* sp. PCC7942 genome (Holtman et al. 2005) apparently encodes no PGR5 homologue at all. For *Phormidium laminosum* meanwhile no genome or proteome data is available.

Just as the actual AA binding site remains unclear, so does the actual mode of electron transfer during AA-sensitive/PGR5-dependent CEF. The most popular models suggest either (i) formation of a PSI-Cytb_6f super-complex and concordantly "hard-wired" electron flow from PSI to PQ or directly to Cytb_6f, or (ii) diffusion-based electron transfer employing relatively small and mobile electron shuttle proteins (recently reviewed in Yamori and Shikanai 2016).

Solid evidence for PQ reduction by the NDH-dependent CEF route can be observed in form of a post-illumination fluorescence rise (PIF), putatively owed to delayed PQ-pool reduction by CEF and resultant PSII acceptor-side limitation (Gotoh et al. 2010). This effect appears to be exclusive to NDH complex mutants in *Arabidopsis* with *pgr5-1* mutants showing no or very weak PIF defect (Munekage et al. 2004), and could be reproduced in *Synechocystis* (Deng et al. 2003, Gao et al. 2016). These observations oppose the interpretation of large-scale PGR5-dependent PQ-pool reduction, and

favors hypotheses of direct electron injection into Cytb_6f/the Q-cycle semi-quinone, possibly through an atypical heme discovered on the stromal face at the Q_i site of *Chlamydomonas* Cytb_6f (Stroebel et al. 2003). PSI-Cytb_6f super-complexes have been proposed for spinach chloroplasts as early as 1967 (Boardman and Anderson 1967) and are still being debated regarding their potential to facilitate direct electron transfer during CEF (Alric 2015). The actual existence of *Arabidopsis* PSI*Cytb_6f*LHCB*NDH (Yadav et al. 2017) and *Chlamydomonas* PSI*Cytb_6f*LHCA (Iwai et al. 2010, Steinbeck et al. 2018) super-complexes could be demonstrated very recently, however. The implications of these findings for the precise mechanisms of AA-sensitive CEF and possible direct electron injection into Cytb_6f remain matter of debate as well, with a key counter argument being that pH-dependent impairment of Cytb_6f Q-cycle activity in the *pgr1* mutant due to a P194L amino-acid exchange in the Rieske-protein subunit (Munekage et al. 2001, Jahns et al. 2002) does not give rise to a *pgr5* phenocopy regarding Fd-dependent PQ reduction (Okegawa et al. 2005, Shikanai 2007).

1.4.3 Study branch 2: Establishing an orthogonal test system for *Arabidopsis* PGR5-dependent CEF in *Synechocystis* sp. PCC6803

While NDH-dependent CEF is considerably well-understood phenomenologically, as by now, there is no scientific consensus regarding AA-sensitive/PGR5-dependent CEF. Many puzzles remain to be solved, among which there are (i) components involved in AA-sensitive CEF, (ii) the degree of phylogenetic and functional conservation across the green lineage, (iii) the site and generality of AA activity/sensitivity, and (iv) the mode of electron transfer conferred by this route of CEF. Moreover, the minimal molecular setup of this CEF route remains unknown. For the model organisms *Arabidopsis* and *Chlamydomonas* not even the effects of known players can be assessed individually in *pgrl1* and *pgr5* loss of function mutants, since *pgrl1* mutants fail to accumulate PGR5 protein (DalCorso et al. 2008, Johnson et al. 2014).

In order to access the conundrum posed by AA-sensitive/PGR5-dependent CEF around PSI, we decided to establish an (as far as possible) orthogonal test system for *Arabidopsis* AA-sensitive/PGR5-dependent CEF in a prokaryotic chassis. Upon investigation/confirmation of general compatibility of eukaryotic PGRL1/PGR5-dependent CEF with a photosynthetic prokaryote, such a system would allow us to investigate the functionality of individual plant CEF components, and efficiently generate and assess variants thereof. For this endeavor *Synechocystis* constitutes an appealing chassis organism. It harbors an oxygenic-photosynthetic apparatus and a PGR5 homologue,

implying general compatibility with the plant system. *Synechocystis* can easily be genetically modified due to its natural competence, efficient homologous recombination, and a big variety of bacterial molecular biology tools available. Lacking clear PGRL1 homologues and bearing only one PGR5 homologue it presumably can be transformed into a “clean” test system displaying little to no interference with the *Arabidopsis* PGRL1/PGR5 couple with comparably little effort.

1.5 Aims of the doctoral study

This study aims to elucidate the evolutionary constraints of high-light tolerance in the model cyanobacterium *Synechocystis* and initial assessment of its backwards compatibility with plant-derived photo-protective mechanisms, exemplified by PGR5-dependent CEF around PSI. Eventually, these two branches are intended to converge into a prokaryotic proxy system in which plant photosynthetic components can be investigated and evolutionarily modified to an extent and within timeframes that are impracticable in plants.

2 Methods

2.1 Databases, data analysis and software tools

Synechocystis gene sequences were obtained from CyanoBase (http://genome.microbedb.jp/cyanobase/Synechocystis; Fujisawa et al. 2016); *Arabidopsis* gene sequences were obtained from TAIR (https://www.arabidopsis.org/index.jsp; Berardini et al. 2015); protein sequences were obtained from NCBI (https://www.ncbi.nlm.nih.gov/) and UniProt (https://www.uniprot.org/). Protein structures were predicted using I-TASSER (https://zhanglab.ccmb.med.umich.edu/I-TASSER/; Yang et al. 2015); protein sequence alignments and phylogenetic analyses were conducted with MEGA X (https://www.megasoftware.net/; Kumar et al. 2018). Protein sequence similarity/identity scores were calculated using MatGAT 2.01 (Campanella et al. 2003), and alignment visualization was done using the BoxShade Server v 3.2.1 (https://embnet.vital-it.ch/software/BOX_form.html; Hofmann and Baron 1996). Local protein alignment searches were performed using the NCBI or CyanoBase pBLAST tools. Plant protein transit peptide prediction was done using the ChloroP 1.1 Server (http://www.cbs.dtu.dk/services/ChloroP/; Emanuelsson et al. 1999), and plant protein domain prediction was done using the Batch Web CDD-search Tool (https://www.ncbi.nlm.nih.gov/Structure/bwrpsb/bwrpsb.cgi; Marchler-Bauer et al. 2017). Transmembrane helices were predicted with the TMHMM Server v. 2.0 (http://www.cbs.dtu.dk/services/TMHMM/; Krogh et al. 2001). Statistical analyses were performed with Microsoft Office Excel or via Astatsa (https://astatsa.com/).

2.2 Chemical materials

Chemicals were purchased from Sigma-Aldrich (Steinheim, Germany), Roth (Karlsruhe, Germany), Applichem (Darmstadt, Germany), Serva (Heidelberg, Germany) and Invitrogen (Darmstadt, Germany). Radioactive dCTP was purchased from Hartmann Analytic (Braunschweig, Germany).

2.3 Enzymes, kits, primers, size markers, and antibodies

All restriction enzymes, T4 DNA ligase, kits for Gibson Assembly and Q5® Site-Directed Mutagenesis, and Q5® High-Fidelity DNA Polymerase were obtained from New England Biolabs (NEB; Ipswich, MA, USA). The Phire Plant Direct PCR Kit and DNA molecular weight markers GeneRuler™ 1 kb / 1 kb Plus DNA ladder were purchased from Thermo Fisher Scientific

(Waltham, MA, USA). DNA purification and Plasmid miniprep kits were purchased from QIAGEN (Venlo, Netherlands). All primers were purchased from Metabion GmbH (Martinsried, Germany). The protein molecular weight marker used was BlueStar Prestained Protein Marker (10–170 kDa; NIPPON Genetics EUROPE GmbH, Düren, Germany). Antibodies, unless stated otherwise, were purchased from Agrisera (Vännäs, Sweden). αPGR5 antibody (Munekage et al. 2002) and αPGRL1 antibody (DalCorso et al. 2008) were supplied by the respective working groups.

2.4 Molecular cloning

2.4.1 Genomic DNA extraction from *Synechocystis*

To obtain *Synechocystis* genomic DNA, cells of 5 ml late exponential phase culture were harvested by centrifugation (7000 rcf, 3 min, 25 °C) and re-suspended in 50 µl TE buffer. 750 µl of DNA extraction buffer were added, and cell suspensions were transferred into 2 ml reaction tubes. Samples were incubated for 3 hours at 70 °C and inverted twice every 30 min to facilitate membrane lysis. After completed thermolysis, samples were vortexed for 10 s and subsequently incubated on ice for 30 min. Precipitated detergents and cell debris were removed by centrifugation (13000 rcf, 20 min, 4 °C), and 650 µl of the supernatant were transferred into a new 1.5 ml reaction tube. 650 µl isopropanol and 150 µl 3 M Na-acetate (pH 5.4) were added and nucleic acids were precipitated on ice for 30 min. Subsequently, nucleic acids were pelleted by centrifugation (13000 rcf, 30 min, 4 °C). The supernatant was discarded; the pellet was washed twice with 70 % EtOH, and dried overnight at room temperature under a fume outlet. DNA pellets were suspended in 50 µl H_2O supplied with 25 µg/ml RNase A and incubated at 37 °C for 2 hours at 650 rpm shaking. Samples were mixed carefully by flicking, and centrifuged (13000 rcf, 10 min, 25 °C) to remove insoluble precipitates. The DNA-containing supernatant was transferred into new 1.5 ml reaction tubes and subjected to agarose-gel electrophoresis to assess yield and structural integrity of extracted DNA.

DNA extraction buffer

Potassium ethyl xanthogenate	1 % (w/v)
Tris/HCl (pH 7.4)	100 mM
EDTA/HCl (pH 8.0)	20 mM
NH_4O acetate	800 mM
SDS	1 % (w/v)

TE buffer

Tris/HCl (pH 7.4)	10 mM
EDTA/HCl (pH 8.0)	1 mM

2.4.2 DNA agarose gel electrophoresis

DNA was size separated electrophoretically at 120 V on agarose gels 0.5-2 % (w/v in TAE buffer) using TAE as running buffer. DNA fragments were visualized by ethidium bromide staining (1:10000 v/v in gel) and subsequent UV fluorescent detection.

TAE buffer

Tris	40 mM
Acetic acid	20 mM
EDTA-Na_2	1 mM

2.4.3 Growing and transforming *Escherichia coli* (*E. coli*) strains

Plasmid DNA for *Synechocystis* transformation and bacteria-two-hybrid assays was cloned and amplified in *E. coli* Dh5α cells. Plasmids assembled by restriction/ligation-based traditional cloning, Gibson assembly, Golden Gate cloning, or Q5® site-directed mutagenesis were added to 25 µl aliquots of chemically competent *E. coli* cells (strain Dh5α), incubated on ice for 30 min, heat shocked for 30 s (42 °C), incubated on ice for another 10 min, and regenerated in 500 µl of LB medium for 60 min at 37 °C without agitation. Cell suspensions were split in 90 % and 10 % volume aliquots and plated on LB solid media supplied with appropriate antibiotics. Clones were grown for 16–24 hours at 37 °C and pre-selected by colony PCR. Positive clones were transferred into liquid culture, plasmid DNA was extracted and correct assembly was confirmed by restriction pattern analysis and Sanger sequencing. DH5α liquid cultures were grown in glass tubes overnight at 37 °C and at 220 rpm shaking.

LB

Yeast extract	5 g l^{-1}
NaCl	5 g l^{-1}
Peptone (Casein)	10 g l^{-1}
pH 7.5 (NaOH)	

For solid media 1 % bacteriological agar (w/v) was added.

Supplements

Sucrose	5 % (w/v)
Kanamycin	50–100 µg/ml
Spectinomycin	25–50 µg/ml
Chloramphenicol	8.5–17 µg/ml
Gentamycin	12.5–25 µg/ml

2.4.4 Restriction-based molecular cloning

Fusion protein constructs for B2H assays were obtained by PCR-amplification of ORFs of interest entailed by primer-extension based restriction-site addition. After agarose-gel electrophoresis, PCR amplicons of correct size were excised and purified from agarose gels using the

QIAquick Gel Extraction Kit (QIAGEN, Hilden, Germany). Subsequently, amplicons and empty plasmids pKT25 and pUT18C were digested with appropriate restriction endonucleases, subjected to gel electrophoresis, and re-extracted. DNA concentrations were determined using a NanoDrop 1000 spectrophotometer (Peqlab, Erlangen, Germany), and 200 ng of plasmid DNA and insert DNA corresponding to a 3x molar excess relative to the plasmid DNA were ligated with T4 DNA ligase for 2 h at room temperature in final reaction volume of 20 µl. Subsequently, ligation products were transformed into chemically competent *E. coli* Dh5α cells (see 2.4.3). Clones were selected on LB agar supplied with 50 µg ml^{-1} kanamycin for pKT25 derivates, and 100 µg ml^{-1} ampicillin for pUT18C derivatives, respectively. Good clones were pre-selected by colony PCR, and correct plasmid assembly was confirmed by restriction pattern analysis and Sanger sequencing.

Primers used to clone candidate genes into B2H vectors with according restriction sites and target vectors are listed below (table 2.1).

Tab 2.1. **Cloning primers for B2H constructs.** Restriction enzyme cutting sites (**bold**) and bases added to keep correct reading frame (grey) are indicated. 3' melting temperature (Tm) is given for specifically annealing part of the respective primer.

Gene	primer	sequence	enzyme	target	3' Tm [°C]
atPGR5	B2H atPGR5 Fw 1	GGTGGT**CTGCAG**TATGCAACAAGCCAGAGTCTCAAG	PstI	pUT18C	67
	B2H atPGR5 Fw 2	GGTGGT**CTGCAG**TTATGCAACAAGCCAGAGTCTCAAG	PstI	pKT25	67
	B2H atPGR5 Rv	GGTGGT**TCTAGA**TTAGCAAGGAAACCAAGCCTC	XbaI	pUT18C, pKT25	65
synPGR5	B2H ssr2016 Fw 1	TCAGAT**CTGCAG**GATGTTCGCCCCCATC	PstI	pUT18C	62
	B2H ssr2016 Fw 2	GGTGGT**CTGCAG**TTATGTTCGCCCCCATC	PstI	pKT25	62
	B2H ssr2016 Rv	TCAGAT**TCTAGA**TTAGGCCAATAAACCGAG	XbaI	pUT18C, pKT25	59
bfr1	B2H sll1341 Fw	GTAGTC**GGATCC**CATGAAAGGTAAACCCGC	BamHI	pUT18C	59
	B2H sll1341 Rv	GTAGTC**GAGCTC**CTAGCTCATTTGAGATTGC	SacI	pUT18C	58
bfr2	B2H slr1890 Fw	GTAGTC**GGATCC**CATGGGTAAAAATGGAAACAACAAC	BamHI	pUT18C, pKT25	62
	B2H slr1890 Rv	GTAGTC**GAGCTC**TTACTCTTCCCCCATCATGG	SacI	pUT18C, pKT25	64
bfd	B2H ssl2250 Fw	GTAGTC**GGATCC**CATGTATATCTGCGTTTGCCG	BamHI	pUT18C, pKT25	63
	B2H ssl2250 Rv	GTAGTC**GAATTC**CTAGGTTAATTTCCTTCTGGCG	EcoRI	pUT18C, pKT25	63
nadA	B2H sll0622 Fw	GCATTC**GGATCC**CGTGTTCACCGCCGTTG	BamHI	pUT18C, pKT25	64
	B2H sll0622 Rv	ACCACC**GAATTC**CTAGGACATGGCCAGC	EcoRI	pUT18C, pKT25	62
Unknown protein	B2H sll1217 Fw 1	GTAGTC**CTGCAG**GATGTCAGAGCTTCAAACCCTG	PstI	pUT18C	65
	B2H sll1217 Fw 2	GTAGTC**GGATCC**CATGTCAGAGCTTCAAACCCTG	BamHI	pKT25	65
	B2H sll1217 Rv	GTAGTC**GGTACC**CTAGAAAGCAATTTCCGTTAAGCG	KpnI	pUT18C, pKT25	64
unknown protein	B2H slr1353 Fw	GTAGTC**CTGCAG**GATGCCAATGTCCAGTCTG	PstI	pUT18C	62
	B2H slr1353 Rv	GTAGTC**GAATTC**TTAATTTGGGTCTGGCTGTTG	EcoRI	pUT18C	63
putative transcription factor	B2H sll0149 Fw	GTAGTC**CTGCAG**GATGGGTATGCCATGGACC	PstI	pUT18C	65
	B2H sll0149 Rv	GTAGTC**GAGCTC**CTAAAAGTCTAGGTCAACTCCC	SacI	pUT18C	62

2.4.5 Gibson assembly cloning of *Synechocystis* knock-out constructs

Constructs to knock out *Synechocystis* genes were designed to replace the ORF of interest with a suitable antibiotic-resistance cassette by homologous recombination. A non-replicative vector backbone derived from pICH69822 (E. Weber, Icon Genetics GmbH, Halle, Germany) as was used to build all plasmids for *Synechocystis* genomic integration mutagenesis (Viola et al. 2014). ORF/resistance couples were ssr2016/*synPGR5*-kanamycin, sll0622/*nadA*-kanamycin, sll1217-spectinomycin, and slr1353-erythromycin. Constructs were assembled by Gibson assembly (Gibson et al. 2009) or, in case of pΔssr2016, derived from a knock-in construct for ssr2016 (*synPGR5*) variants (pKssr2016) by Q5® SDM. Primers used for deletion of the ssr2016 CDS from pKssr2016 were identical to the respective Gibson cloning primers. The vector backbone was amplified from pDSlux (Viola et al. 2014) by Q5® PCR. Vector maps of knock-out plasmids and primers used to assemble the according plasmids are shown below (Fig 2.1, Tab 2.2).

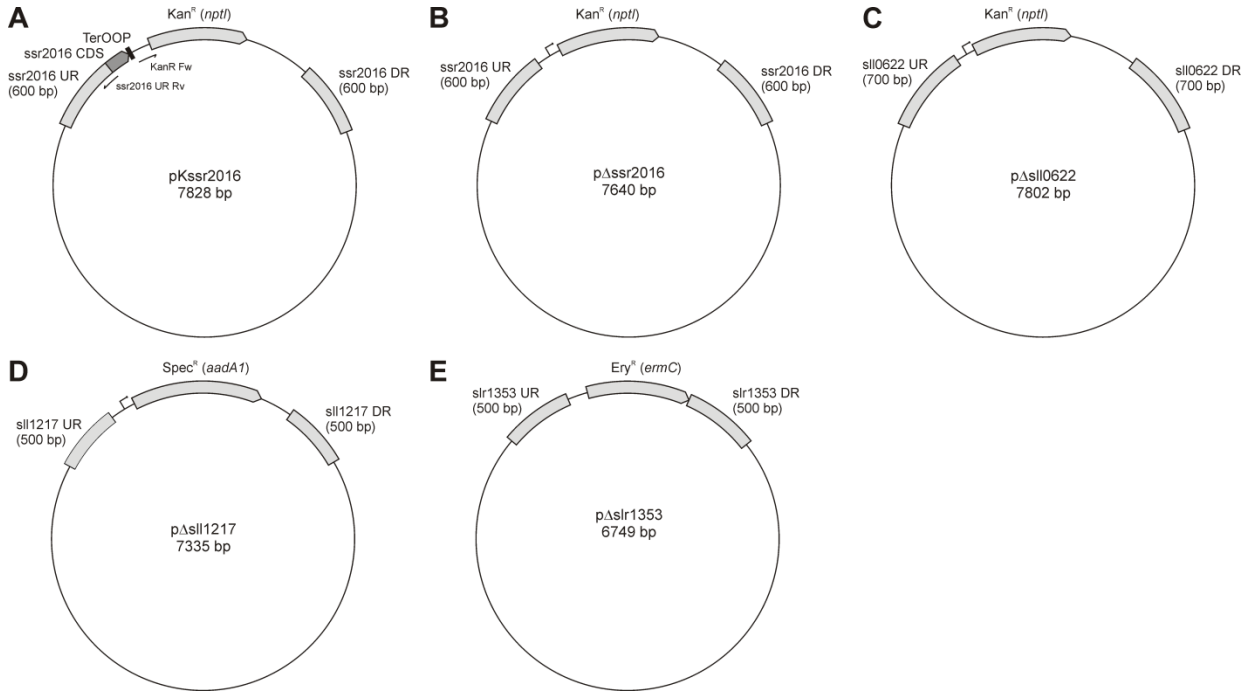

Fig 2.1. **Vector maps of *Synechocystis* genomic knockout constructs.** (**A**) Knock-in construct of *Synechocystis* PGR5-encoding gene followed by bacteriophage lambda transcription terminator oop (TerOOP) and kanamycin-resistance cassette (Kan^R), targeting the ssr2016 locus. (**B**) Knock-out construct of *Synechocystis* PGR5-encoding gene for replacement of the ssr2016 ORF with Kan^R. (**C**) Knock-out construct of *Synechocystis* NadA-encoding gene for replacement of sll0622 ORF with Kan^R. (**D**) Knock-out construct of unknown protein Sll1217-encoding gene for replacement of sll1217 ORF with spectinomycin-resistance cassette Spec^R. (**E**) Knock-out construct of unknown protein Slr1353-encoding gene for replacement of slr1353 ORF with erythromycin-resistance cassette Ery^R. Primer binding sites for pKssr2016 vector editing are indicated as curved arrows, promoters are indicated as kinked arrows. Antibiotic resistance genes are given in parentheses. CDS, coding sequence. UR, upstream region. DR, downstream region.

Tab 2.2. **Cloning primers for genomic knockout vectors.** For Gibson assembly primers, sequences annealing specifically are given in capital letters, while adapter overhangs are given in lowercase letters. 3' melting temperatures (Tm) correspond to the specifically annealing subsequence, respectively. CDS, coding sequence. UR, upstream region. DR, downstream region.

primer	sequence	3' Tm [°C]
Backbone-fwd	ACCTGGGCCCACTGCATCC	73.8
Backbone-rev	GCTTACCTGTTTAAACTATCAGTG	60.7
sll0622-UR-fwd	acactgatagtttaaacaggtaagcGTTTACTGTCCCTGCTCC	62.4
sll0622-UR-rev	acgtgagaccaaaTATGTTTCGGCTCCTGGAATATTTATAG	63.6
KanR-sll0622-fwd	gagccgaaacataTTTGGTCTCACGTTGGAATTC	62.7
KanR-sll0622-rev	gattatgccacccGTAAAACAGCCAGCGCTG	64.5
sll0622-DR-fwd	ctggctgttttacGGGTGGCATAATCAGGCTC	65.8
sll0622-DR-rev	tggggtggatgcagtgggcccaggtTATTGCCACTAGAATTAGCCG	61.6
ssr2016-UR-fwd	gatagtttaaacaggtaagcCCGGGTAATCCGGGTGGC	71.9
ssr2016-UR-rev	gggcgaacatggcagtgactCCTAAATTCCTACG	67.0
ssr2016-CDS-fwd	agtcactgccATGTTCGCCCCCATCGTTATC	67.4
ssr2016-CDS-rev	aaaaacgcccggcggcaaccgagcgttgTTAGGCCAATAAACCGAGGG	64.4
KanR-ssr2016-fwd	caacgctcggttgccgccgggcgtttttTTTGGTCTCACGTTGGAATTC	62.7
KanR-ssr2016-rev	aaacgaagagGTAAAACAGCCAGCGCTG	64.5
ssr2016-DR-fwd	gctgttttacCTCTTCGTTTTCAATAATTCTTGCCAAAC	64.6
ssr2016-DR-rev	tggatgcagtgggcccaggtTTTCCACCGAAGGGCTGG	68.1
sll1217-UR-fwd	gatagtttaaacaggtaagcAGGACGGGGGGGAAATTTC	64.7
sll1217-UR-rev	tgttcttctagagGGAAGAAACTGAGATAACTGATTG	60.5
SpecR-sll1217-fwd	agtttcttccCTCTAGAAGAACAGCAAGGCCG	67.6
SpecR-sll1217-rev	aagtctggaaGCCGCTCAATTCGCTGCG	70.9
sll1217-DR-fwd	attgagcggcTTCCAGACTTAAAATATTTATCACCTTTACTTC	62.4
sll1217-DR-rev	tggatgcagtgggcccaggtCCGCACAATGGTGTAGGG	66.3
slr1353-UR-fwd	gatagtttaaacaggtaagcCTGCATCGGCCACTTCCTGG	71.6
slr1353-UR-rev	gtatgaatgaCTGGTTGCGGAGGGCCGT	74.4
EmR-slr1353-fwd	ccgcaaccagTCATTCATACAGACAAATCC	56.2
EmR-slr1353-rev	atcaatccgaTTACTTATTAAATAATTTATAGCTATTGAAAAG	55.9
slr1353-DR-fwd	ttaataagtaaTCGGATTGATCCTGCTTTTG	62.5
slr1353-DR-rev	tggatgcagtgggcccaggtCTTGGAAGACATTGCCAAC	61.3

2.4.6 Golden Gate assembly cloning and site directed mutagenesis of *PGR*-gene knock-in constructs

Expression systems for *atPGRL1A* (At4g22890) and/or *atPGR5* (At2g05620) were derived from plasmid pDSpgrl1_Cm^R (PhD thesis Stefania Viola; Viola 2014) encoding both genes under translational control of the D1 protein promoter *PpsbA2*. The original pDSpgrl1_Cm^R encodes atPGRL1A without chloroplast transit peptide (cTP) and atPGR5 with cTP. To generate an *atPGRL1A*-only expression system, a fragment containing *PpsbA2*:*atPGR5* was deleted by PCR amplifying the rest of the vector and auto-ligation of the PCR product. To generate an *atPGR5*-only expression system, Golden Gate assembly (Engler et al. 2008) was used to delete two interspaced DNA fragments containing *PpsbA2*:*atPGRL1A*-5'CDS upstream, and the entire *atPGRL1A* CDS downstream of a Cm^R/$Sucr^S$ double selection cassette (DSC). Then, Q5 SDM was used to delete a subsequence encoding the atPGR5 cTP (codons 2-44) from the *atPGRL1A*+*atPGR5*, as well as the *atPGR5*-only expression vector. This yielded a set of three transformation vectors suitable to introduce genes encoding mature atPGRL1A (pP1), atPGR5 (pP5), or both (pP15) into a *Synechocystis* genomic neutral site (ORF slr0168) under control of *PpsbA2*. The synPGR5 over-expression constructs pOE-synP5 HisN/HisC were generated by replacing the *atPGR5* CDS in pP5 with C- or N-terminally 6xHis-tagged *synPGR5* CDS by Golden Gate assembly. Vector topologies were confirmed by restriction analysis, integrity of the promoter:transgene cassette was confirmed by Sanger sequencing, and selective marker functionality was assayed on LB agar plates supplemented with kanamycin and chloramphenicol or with 5 % (w/v) sucrose.

Point mutant alleles of *atPGRL1A* and *atPGR5* were introduced into *Synechocystis* employing the same expression systems, respectively. Point mutations were introduced into pP1, pP5 and pP15 by Q5® SDM and resulted in non-synonymous amino-acid exchanges. These exchanges were S115F for atPGRL1A (identified as possible suppressor mutation of the *Arabidopsis pgr5-1* phenotype; see Results Fig 3.20), and G130S for atPGR5 (mutation causing the *pgr5-1* mutant phenotype; Munekage et al. 2002). Vector maps of resultant plasmids bearing PGR gene expression constructs are shown below (Fig 2.2). Primers used for pDSpgrl1_Cm^R modification and subsequent point mutagenesis or gene exchange are listed below (Tab 2.3).

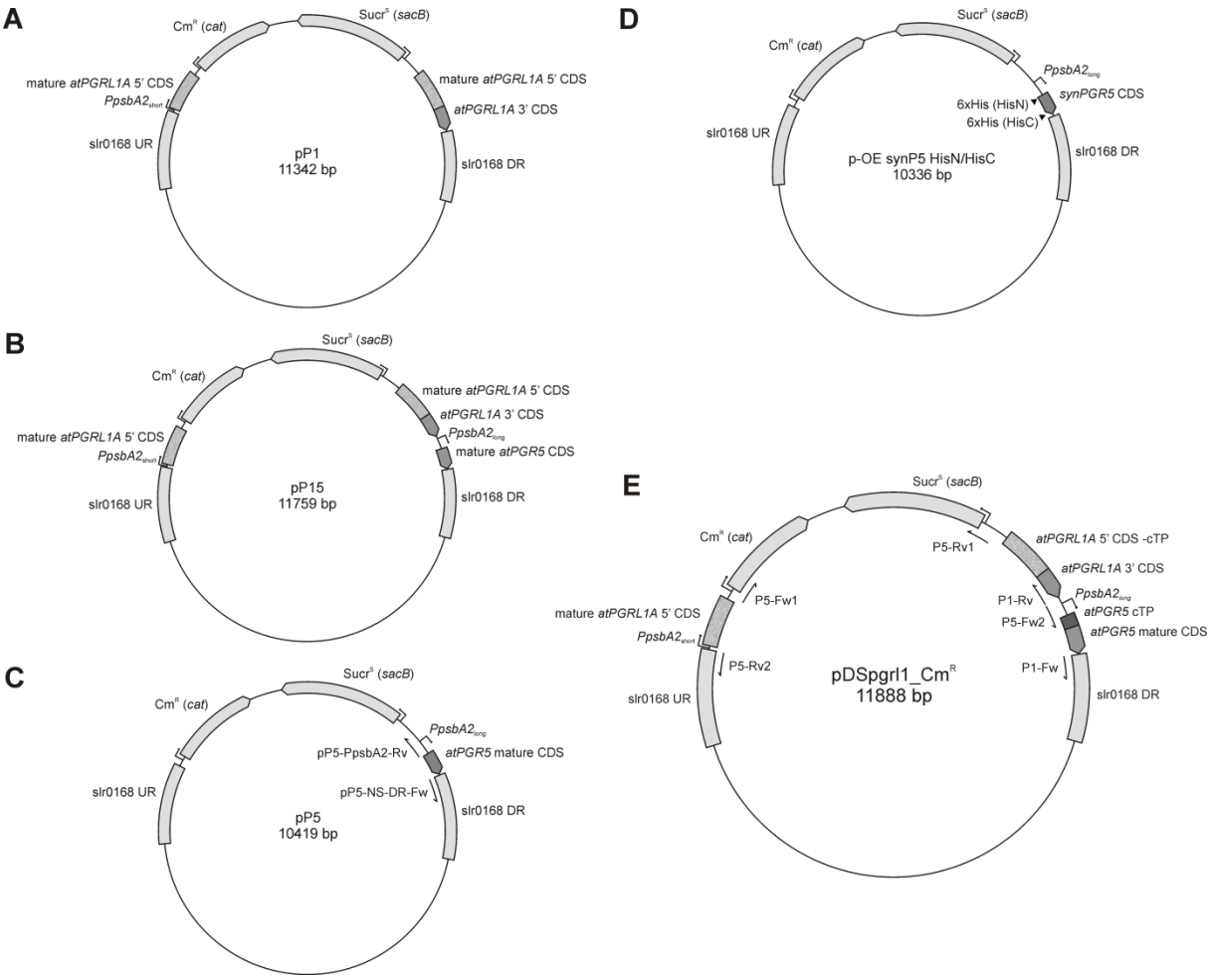

Fig 2.2. **Vector maps of *atPGR*-gene expression-system plasmids.** (**A**) *PpsbA2*:*atPGRL1A*-only expression vector. (**B**) *PpsbA2*:*atPGRL1A* and *PpsbA2*:*atPGR5*-only co-expression vector. (**C**) *PpsbA2*:*atPGR5*-only expression vector. (**D**) *PpsbA2*:*sybPGR5* over-expression vector(s) with N- or C-terminal 6xHis-tag (indicated by black arrow heads). (**E**) Original template plasmid generated by Dr. Stefania Viola (Viola 2014). Primer binding sites for vector editing are indicated as curved arrows, promoters are indicated as kinked arrows. Antibiotic resistance and sucrose sensitivity genes are given in parentheses. CDS, coding sequence. UR, upstream region. DR, downstream region. Cm^R, chloramphenicol-resistance cassette. $Sucr^S$, sucrose-sensitivity cassette.

Tab 2.3. **Primers used for pDSpgrl1_Cm editing and site-directed mutagenesis.** For Golden-Gate primers, BsaI recognition sites (**bold**) and generated overhangs are indicated (grey). For site-directed mutagenesis primers, introduced SNPs are highlighted in black. Sequences annealing specifically are given in capital letters, while adapter overhangs are given in lower case letters. 3' melting temperatures (Tm) refer to specifically annealing part of the respective primer.

Primer	Sequence	3' Tm [°C]
P5-Rv2	ttt**ggtctct**tcgcGCCACTGTTATTTTGATTGGTGGC	67.0
P5-Fw2	ttt**ggtctct**ccatGCCAGAAGGAAGCCAAGCTTAACCCA	74.0
P5-Fw1	ttt**ggtctct**gcgaCGTTGGAATTCGATTGATCCGTCGAC	70.0
P5-Fw1	ttt**ggtctct**atggCATACTTTAGGCCCGTAGTCTGCA	68.0
P1-Fw	ttt**ggtctct**tgggTTAAGCTTGGCTTCCTTCTGGC	74.0
P1-Rv	ttt**ggtctct**ttcgTTTGCGAATTTACACCAG	63.0
pP5-NS-DR-Fw	ttt**ggtctct**tcgcTTCGTTTGCGAATTTACACC	61.0
pP5-PpsbA2-Rv	ttt**ggtctct**gatgTTGGTTATAATTCCTTATGTATTTGTCG	60.0
synPGR5-HisN-Fw	ttt**ggtctct**catcatgcatcaccatcaccatcacTTCGCCCCCATCG	61.0
synPGR5-unmodified-Rv	ttt**ggtctct**gcgaTTAGGCCAATAAACCGAGG	60.0
synPGR5-unmodified-Fw	ttt**ggtctct**catcATGTTCGCCCCCATC	62.0
synPGR5-HisC-Rv	ttt**ggtctct**gcgattagtgatggtgatggtgatgGGCCAATAAACCGAGG	60.0
atPGR5-cTPdeletion-Fw	CAACAAGCCAGAGTCTCAAGG	66.0
atPGR5-cTPdeletion-Rv	CATTTGGTTATAATTCCTTATGTATTTGTCGATGTTCAG	66.0
atPGR5- G130S-SDM-Fw	GAGAGGCTTAGTTTCCTTGCTTAG	65.0
atPGR5-G130S-SDM-Rv	CATTCTTCTTAGCAAGCCTGATAAGC	66.0
atGRL1A-S115F-SDM-Fw	GATCATGTTTAATGAAGAGTTTGATAACCTTAAAG	64.0
atGRL1A-S115F-SDM-Rv	GCTTTGCCATCATAATAGAAAGATTGCAAC	66.0

2.4.7 Gibson assembly and site directed mutagenesis of *allele-swapping* constructs for introduction of high-light adaptive point mutations in *Synechocystis*

Candidate point mutations were introduced into WT cells by homologous recombination using a marker-less gene-replacement system developed in our lab (Viola et al. 2014). Transformation vectors were cloned using Gibson Assembly (NEB), and point mutations were introduced by Q5® site-directed mutagenesis (SDM; NEB). Candidate ORFs and fragments thereof were amplified from WT genomic DNA, while the double selection cassette (DSC) and vector backbone were amplified from pDSlux (Viola et al. 2014) using Q5® high fidelity polymerase (NEB). Correct assembly of vectors was tested by restriction analysis, while functionality of negative selection markers was assayed on LB supplemented with 5 % (w/v) sucrose. Correctly assembled plasmid DNA was used as template for Q5® SDM PCR, followed by plasmid re-circularization according to manufacturer's instructions, and transformed into Dh5α *E. coli* cells. Successful point mutagenesis and lesion-free auto-ligation were confirmed by Sanger sequencing, yielding the plasmids pDS_ndhF1-F124L (pHL1), pDS_fusB-R461C (pHL2). Vector maps of the plasmids used to generate the artificially reconstituted high light mutant strains HL1 and HL2, as well as primers used for plasmid assembly are given below (Fig 2.3, Tab 2.4).

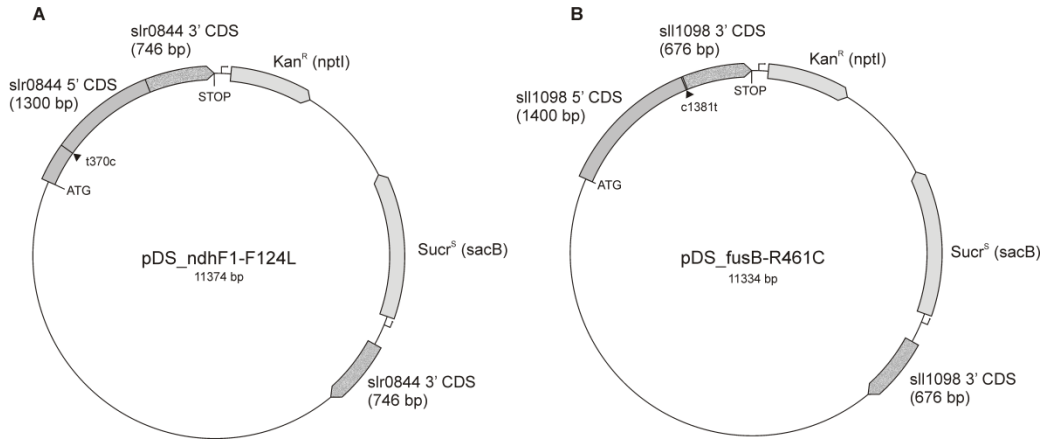

Fig 2.3. **Plasmid maps of high-light-mutant-reconstitution vectors**. (**A**) *Allele-swapping* vector for introduction of HL1 (F124L) mutation in ndhF1 (ORF slr08844). (**B**) *Allele-swapping* vector for introduction of HL2 (R461C) mutation in fusB (ORF sll1098). CDS, coding sequence. Kan^R, kanamycin resistance. $Sucr^S$, sucrose sensitivity. Introduced point mutations are indicated by black arrow heads. Redundant sub-sequences for double selection-cassette deletion are marked in textured grey.

Tab 2.4. **Cloning primers for marker-less genome-editing/*allele-swapping* vectors.** For Gibson assembly primers, sequences annealing specifically are given in capital letters, while adapter overhangs are given in lowercase letters. 3' melting temperatures T_m correspond to the specifically annealing subsequence, respectively. Start and stop codons marking the ends of respective coding sequences (CDS) cloned are indicated in **bold font**. For site-directed mutagenesis (SDM) primers, introduced SNPs are highlighted in black.

Primer	5'-3' Sequence	3' Tm [°C]
Backbone Fw	ACCTGGGCCCACTGCATCC	73.8
Backbone Rv	GCTTACCTGTTTAAACTATCAGTG	60.7
slr0844 CDS Fw	acactgatagtttaaacaggtaagc**ATG**GAATTACTCTATCAATTAGC	60.7
slr0844 CDS Rv	tcccgcggccgcc**CTA**GGTGAGGCTAAAAAC	56.7
DSC slr0844 Fw	tagcctcacctagGGCGGCCGCGGGAATTCG	56.4
DSC slr0844 Rv	gtggcccaacccaAGTTCTTTAGGCCCGTAGTCTGCAAATCC	76.4
slr0844 3' Fw	ggcctaaagaactTGGGTTGGGCCACCGCCG	71.9
slr0844 3' Rv	tggggtggatgcagtgggcccaggt**CTA**GGTGAGGCTAAAAACAATTACAAAGCCTAACACCGC	78.1
sll1098 CDS Fw	acactgatagtttaaacaggtaagc**ATG**GCTCGCACAGTGCCC	71.9
sll1098 CDS Rv	tcccgcggccgcc**TTA**GGCATAGCCTCTGCTTTTGG	67.1
DSC sll1098 Fw	aggctatgcctaaGGCGGCCGCGGGAATTCG	76.4
DSC sll1098 Rv	attggcctccaccAGTTCTTTAGGCCCGTAGTCTGCAAATCC	71.9
sll1098 3' Fw	ggcctaaagaactGGTGGAGGCCAATGTGGG	69.4
sll1098 3' Rv	tggggtggatgcagtgggcccaggt**TTA**GGCATAGCCTCTGCTTTTG	64.8
slr0844 F124L Fw	CGTCTCTATGCCTATCTCAGTC	64.0
slr0844 F124L Rv	CACATAACCCGGATCGTG	63.0
sll1098 R461C Fw	GACTGCATGCTACGGGAATTTAAGGTG	70.0
sll1098 R461C Rv	CACCAGAATTTCTAAATGCAATTCTCCCATGC	70.0

2.5 Growing *Synechocystis* sp. PCC6803 strains

Experiments were conducted with glucose-tolerant (GT) *Synechocystis* sp. PCC 6803. Wildtype cells were provided by Prof. Dr. Himadri Pakrasi (Washington University, St. Louis, USA) and mutant strains were generated in our lab. Cultures were grown under continuous illumination with 30 µE white fluorescent light at 30 °C. Liquid cultures were grown in BG11 photoautotrophic medium by default (Rippka et al. 1979), which was supplemented with 5 mM glucose (BG11G) for pre-transformation cultures. Liquid cultures were agitated at 120 rpm on a rotary shaker. Cultures on solid media were supplied with 5 mM glucose by default, with exception of cultures/clones used in the high-light tolerance evolution study. Antibiotics were added to the media in appropriate concentrations (see below).

BG11 liquid

$FeNH_4$ citrate	0.023 mM
Na_2CO_3	0.198 mM
K_2HPO_4	0.175 mM
$NaNO_3$	17.60 mM
$MgSO_4$*7 H_2O	0.304 mM
$CaCl_2$*2 H_2O	0.245 mM
Citric acid *1 H_2O	0.031 mM
Na-EDTA*1 H_2O	2.790 µM
H_3BO_3	46.30 µM
$MnCl_2$*2 H_2O	9.15 µM
$ZnSO_4$*7 H_2O	0.77 µM
Na_2MoO_4*2 H_2O	1.61 µM
$CuSO_4$	0.32 µM
$Co(NO_3)_2$*6 H_2O	0.17 µM

pH 7.4 (HCl)

BG11 solid

BG11 liquid +	
TES	10 mM
pH 8.2 (KOH)	
$Na_2S_2O_3$*5 H_2O	29 mM
bacteriological agar	0.75 % (w/v)

Supplements

Glucose	5 mM
Sucrose	5 % (w/v)
Kanamycin	10–100 µg ml^{-1}
Spectinomycin	5–50 µg ml^{-1}
Chloramphenicol	6.5–17 µg ml^{-1}
Gentamycin	5–20 µg ml^{-1}
Erythromycin	1–20 µg ml^{-1}

2.6 Generation of *Synechocystis* mutant strains

2.6.1 Transformation and homologous recombination

2.6.1.1 Transformation of *Synechocystis* cells

Mutant generation and genome editing of *Synechocystis* was achieved by homologous recombination, using non-replicative vectors derived from pICH69822 (E. Weber, Icon Genetics GmbH, Halle, Germany) as vector backbone. *Synechocystis* cells were grown to early exponential phase (OD_{730} = 0.2–0.4) in BG11G media supplemented with appropriate antibiotics. A total of OD_{730} = 5 cells were harvested by centrifugation (3000 rcf, 5 min, 25 °C) in 50 ml reaction tubes, washed with BG11

twice, and re-suspended in 500 µl BG11 prior to addition of ~500 ng plasmid DNA. Cells were incubated at 5 µE and 25 °C for two hours without mixing, followed by incubation at 20 µE and 140 rpm rotational shaking for 3 hours. 4.5 ml of fresh BG11 were added to the cells, tubes were wrapped in aluminum foil and dark-incubated overnight (140 rpm, 25 °C). The next morning, cells were harvested by centrifugation (3000 rcf, 25 °C) and plated on selective BG11 solid medium containing appropriate antibiotic and/or glucose concentration. Clones were then propagated under increasing antibiotic concentrations (1x > 2x > 5x > 10x antibiotic concentration used for transformation) and mutant segregation was confirmed by PCR.

Selective media supplements

Glucose	0–5 mM
Sucrose	0–5 % (w/v)
Kanamycin	10 µg/ml
Spectinomycin	5 µg/ml
Chloramphenicol	6.5 µg/ml
Gentamycin	5 µg/ml
Erythromycin	1 µg/ml

2.6.1.2 Mutant genotyping

Genotyping PCRs were conducted using the Phire Plant Direct PCR Kit (Thermo Fisher Scientific, Waltham, MA, USA). Whenever relevant, point mutations were confirmed by Sanger sequencing (in-house service, Genomics Service Unit, Genetics, LMU Munich).

2.6.1.3 Double recombination and genomic deletion of selection cassettes

Segregated mutant strains transformed with constructs fit for marker-less gene replacement (Viola et al. 2014) were selected for intra-chromosomal homologous recombination events by negative selection on BG11G supplemented with 5 % (w/v) sucrose. Strains were grown in liquid BG11G supplemented with antibiotics up to OD ~2.0. 10 µl of these cultures were used to inoculate 25 ml of antibiotic-free liquid media, 250 µl of which were plated on sucrose media upon reaching early stationary phase (OD ~ 1.0-1.5). Double-recombinant clones were selected 7-10 days after plating. Successful deletion of the DSC was confirmed by cultivation on BG11 agar containing the formerly used antibiotic. Clones that regained antibiotic sensitivity were tested for desired transgenic DNA and selection-cassette loss by PCR.

2.6.2 Random mutagenesis and high-light adaptive evolution of *Synechocystis*

The evolution experiment was conducted as outlined in Fig 3.2. Mutagenesis was performed as described (Tillich et al. 2012) either by treatment with 1 % (v/v) MMS for 60 s, or by exposure to 50 J m^{-2} UV-C radiation (λ = 254 nm) in a Stratalinker® UV Crosslinker 1800 (Stratagene, La Jolla, CA, USA). Cells were selected/grown in a Multi-Cultivator MC 1000-OD equipped with an AC-700 cooling unit and a warm-white LED panel (Photon Systems Instruments, Drásov, Czech Republic). Cultures were constantly illuminated and aerated with atmospheric air. After each cultivation cycle, cells of 10 ml of mature culture were collected and cryo-preserved at -80 °C in BG11G supplemented with 8 % DMSO (v/v). After the final selection round, single clones were isolated by streaking on solid BG11 media. Clones for whole genome re-sequencing were selected based on their chlorophyll-fluorescence phenotypes (see 2.11.3, Fig 3.6, Fig 3.7) and transferred into liquid culture. Genomic DNA was extracted as outlined above (2.4.1).

2.7 RNA isolation and Northern blot analysis

2.7.1 Total RNA isolation from *Synechocystis* cells

RNA isolation was conducted according to Dienst (2017; dx.doi.org/10.17504/protocols.io.j3scqne). Reaction tubes and equipment was pre-cooled on ice, centrifuges were pre-cooled to 4 °C.

Sterile 50 mL tubes were filled with ice and stored in an ice bath. 20–25 ml of late exponential phase cell culture (OD_{730} < 1.0) were transferred into the ice-filled tubes (up to ~45 ml mark) and harvested by centrifugation (3000 rcf, 5 min). The supernatant including ice was discarded; the cell pellet was re-suspended in residual water (~1 ml) and transferred into 2 ml safe lock reaction tubes. Cells were collected by centrifugation (13000 rcf, 15 s) and the supernatant was completely removed by pipetting. The cell pellet was re-suspended in 1 mL TRIzol reagent (Invitrogen, Carlsbad, CA, USA) and frozen at -80 °C for 60 min. Frozen samples were incubated at 65° C for 15 min under constant agitation (600 rpm). 200 µl ice cold chloroform/isoamyl alcohol (24:1) were added to each tube, and samples were vortexed for 30 sec. Cell debris was collected by centrifugation (11000 rcf, 10 min) and the upper, aqueous phase was transferred into to fresh 1.5 ml tubes. One volume of ice cold phenol/chloroform/isoamyl alcohol (25:24:1) was added, samples were mixed gently, and phases were separated by centrifugation (11000 rcf, 10 min). The upper, aqueous phase was transferred into fresh 1.5 ml tubes, and one volume of isopropanol and 10 µl of 3 M Na-acetate (pH 5.2) were added. RNA was precipitated at -20 °C overnight. RNA was collected by centrifugation (13000 rcf, 30 min), the supernatant was completely removed, and the pellet was washed twice with 70 % (v/v) ice cold

ethanol and re-collected by centrifugation (13000 rcf, 10 min). The supernatant was discarded, and the RNA pellet was air-dried for 1 hour. RNA was suspend in 30 µl ultra-pure water and stored at -80 °C until needed.

2.7.2 RNA size separation, capillary blotting, and radio-detection

*Note: The protocol outlined below has been applied as described in Dr. Evgenia Vamvaka's doctoral thesis (*Vamvaka 2016*).*

Northern blot analysis was performed according to Sambrook and Russel (2001). RNA samples were mixed with 2x RNA loading dye and denatured at 95 °C for 5 min. Subsequently, the samples were loaded on a denaturing agarose gel (1.2% [w/v] agarose in 1x MOPS buffer and 1% [v/v] formaldehyde) and separated for ~3 hours at 40 V in 1x MOPS buffer. RNA was capillary transferred onto a nylon membrane (Hybond N+; GE Healthcare, Freiburg, Germany) pre-equilibrated with 2x SSC, using 10x SSC as transfer buffer. Transfer was performed overnight (16–20 h).

After successful transfer the membrane was washed with 2x SSC and air-dried for 30 min at room temperature. RNA was cross-linked to the membrane with UV-C radiation (λ =254 nm; Stratalinker® UV Crosslinker 1800, Stratagene, USA) at 1200 µJ cm^{-2}.

The membrane was equilibrated in 2x SSC buffer and placed into a glass cylinder containing 20 ml pre-hybridization buffer and 160 µl denatured herring sperm DNA (10 µg ml^{-1}). The membrane was incubated at 65 °C for at least 4 h prior to probe hybridization. The radioactively-labeled probe was added and hybridization was performed for 16 h at 65 °C. The hybridization buffer was discarded. The blot was washed twice for 30 min with 10 ml of pre-warmed washing buffer at 65 °C. A final washing step was carried out with RT buffer for at least one hour on a shaker at room temperature. A radioactivity-sensitive screen (Storage Phosphor Screen, Fujifilm, Minato, Tokyo, Japan) was exposed to the membrane for 1–7 days. Signals were then detected with a Typhoon™ scanner (GE Healthcare, Chicago, USA).

2x RNA loading dye

Formamide	95 % (v/v)
SDS	0.02% (w/v)
bromophenol blue	0.02% (w/v)
Xylene cyanol	0.01 % (w/v)
EDTA	0.5 mM

1x MOPS buffer

MOPS	200 mM
sodium acetate	50 mM
EDTA	10 mM
pH 7.0 (HCl)	

SSC buffer

NaCl	1.5M
trisodium citrate ($Na_3C_6H_5O_7$)	150 mM
pH 7.0 (HCl)	

Pre-hybridization buffer

SDS	7 % (w/v)
Na_2HPO_4	0.25 M
pH 7.0 (HCl)	

Washing buffer

SDS	0.1 % (w/v)
NaCl	0.2 M
NaH_2PO_4	20 mM
EDTA	5 mM
pH 7.4 (HCl)	

RT buffer

NaH_2PO_4	6 mM
EDTA	1 mM
SDS (w/v)	0.2 %
pH 7.0 (HCl)	

OLB buffer

Tris/HCl (pH6.8)	50 mM
MgOAc	10 mM
DTT	50 mM
BSA	0.5 mg ml^{-1}
dATP, dTTP and dGTP	each 33 µM

2.7.3 Radioactive probe preparation

Approximately 100 ng of DNA template (purified PCR product) was diluted in 12 µl ddH_2O and used for radioactive labeling. The template was denatured for 5 min at 100 °C and put on ice for 2 min to avoid re-annealing. 4 µl of OLB buffer, 1 µl Klenow DNA polymerase (NEB), and 3 µl of radioactive ^{32}P-dCTP were added to the probe. The reaction was incubated at 37 °C for 60 min and the probe was purified with Microspin™ G-25 Columns (Illustra, Freiburg, Germany) according to the manufacturer's instructions. The probe was added to 40 µl herring sperm DNA (10 µg ml^{-1}), denatured at 100 °C for 5 min, and added to the hybridization solution (pre-hybridization buffer and membrane after 4 h of incubation; see above). Primers used for the amplification of the ssr2016 probe were identical to ssr2016-CDS-fwd and ssr2016-CDS-rev used for Gibson assembly cloning (see 2.4.5).

2.8 Protein sample preparation and immunodetection

2.8.1 *Synechocystis* whole-cell protein extracts

OD_{730} = 4 cells were pelleted by centrifugation (8000 rcf, 2 min, 25 °C) and re-suspended in 100 µl of 2x Tris/Tricine loading dye. Samples were incubated at 95 °C for 15 min under occasional agitation. Insoluble cell debris was collected by centrifugation (16000 rcf, 10 min, 25 °C). The supernatant was collected in fresh 1.5 ml reaction tubes and stored at -20 °C until separation by SDS-PAGE.

2x Tris/Tricine loading dye

Tris pH 6.8 (HCl)	100 mM
glycerol	24 % (v/v)
SDS	5 % (w/v)
bromophenol blue	0.02 % (w/v)
DTT	100 mM (freshly added)

2.8.2 *Synechocystis* soluble and thylakoid protein preparation

Notes: All the steps are carried at dim light, on ice and in cooled centrifuges. Protocol modified from Gandini et al. 2017.

OD_{730} = 10–20 cells were collected by centrifugation (5000 rcf, 3 min, 4 °C) and supernatant media was discarded. Cell pellets were re-suspended in 1 ml homogenization buffer, supplied with ~1 ml of glass beads (0.065–0.25 mm, Sigma Aldrich, St. Louis, MO, United States) and physically ruptured in a TissueLyser II (QIAGEN, Hilden, Germany) by five cycles of shaking and re-cooling (5 min, 30 Hz > 15 min on ice) in 2 ml safe-lock reaction tubes. TissueLyser racks were pre-cooled for 60 min at -20 °C, and re-cooled at -20 °C between rupture cycles. Glass beads and unbroken cells were collected by centrifugation (16000 rcf, 1 min, 4 °C) and the supernatant was transferred into in a new 1.5 ml reaction tube. The membrane fraction was collected by centrifugation (16000 rcf, 60 min, 4 °C), the supernatant was collected as soluble protein fraction and stored at -80 °C until needed. The pellet was washed twice in 500 µl of Tricine buffer by gentle re-suspension by pipetting and subsequent re-collection of membranes by centrifugation (13000 rcf, 15 min, 4 °C). Pellets were re-suspended in homogenization buffer supplied with 20 % (v/v) glycerol and lacking Na ascorbate. Membrane fractions were stored at -80 °C until needed.

Homogenization buffer

Sucrose	0.4 M
NaCl	10 mM
$MgCl_2$	5 mM
Tricine	20 mM

pH 7.9 (HCl)

freshly added:

Na ascorbate	10 mM
NaF	10 mM

Tricine buffer

Tricine	5mM

pH 7.9 (HCl)

freshly added:

NaF	5mM

2.8.3 Immuno-detection of proteins in *Synechocystis* extracts (Western blot)

For whole cell proteins 7.5 µl of protein extract (corresponding to ~$1.5*10^7$ cells) were loaded per sample. For soluble and thylakoid protein extracts aliquots corresponding to 30-50 µg of protein were loaded. Protein concentration was approximated by Bradford protein assay (Bio-Rad, Hercules, CA, USA) using 2 µl of protein sample (typically corresponding to ~1–3 µg of protein) and 998 µl of Bradford reagent. Proteins were separated electrophoretically on 10 % or 12.5 % Tris-Tricine SDS polyacrylamide gels at 0.01 mA cm^{-3} according to Schägger and Jagow (1987). Stacking gels were prepared with 4 % polyacrylamide and 1.5-fold amount of APS and TEMED.

Tris-Tricine SDS Polyacrylamide Stacking/Separation Gels

Acrylamide 40 (29:1)	4 % / 10 – 12.5 %
Tris/HCl (pH 8.45)	1 M
SDS	0.1 % (w/v)
APS	1.3 ‰ / 0.65 ‰ (w/v)
TEMED	1.3 ‰ / 0.065 ‰ (v/v)

Anode buffer

Tris	0.2 M

(pH 8.9, HCl)

Cathode buffer

Tris	0.1 M
Tricine	0.1 M
SDS	0.1 % (v/v)
EDTA	1 mM

pH 8.9 (NaOH)

After PAGE was completed, proteins were blotted onto 0.45 µm pore size Immobilon-P PVDF membrane (Merck Milipore, Billerica, MA, USA) by capillary transfer using 1x phosphate-buffered saline (PBS) as transfer buffer. PVDF membranes were activated with 100 % MeOH for 10 min prior to blot assembly (see Fig 2.4). Cotton paper covering the PVDF membrane was pre-wetted with PBS to avoid membrane desiccation and to trigger capillary flow into the overlaid tissue/towel paper. Transfer times varied depending on the size of the protein of interest, ranging from 12 h (≤ 20 kDa) to 24 h (≤ 40 kDa); proteins bigger that 40 kDa were transferred incompletely within the given time frame.

Upon completion of transfer, membranes were air-dried, re-activated with 100 % MeOH, and air-dried again to fix proteins on the PVDF matrix. Dried membranes were stored at room temperature until needed. Prior to immuno-detection membranes were re-activated with 100 % MeOH and equilibrated with 1x TBST. Further antibody-related steps were performed at 4 °C, with exception of final detection. Unbound membrane areas were blocked with 3 % (w/v) BSA in TBST for 2 h under gentle horizontal shaking (45 rpm). Primary antibodies were added to BSA-TBST to generate appropriate dilutions ranging from 1:1000–1:20000. Primary antibody decoration was performed overnight under gentle shaking (45 rpm). After removal of primary antibodies, membranes were washed four times for 10 min each with TBST, and horse-radish-peroxidase coupled secondary antibody was added to TBST at a final dilution of 1:20000. Secondary antibody decoration was performed for 2-3 h. Membranes were washed five times for 10 min in TBST to remove excess secondary antibody prior to chemiluminescent signal detection. Proteins were detected using PierceTM ECL western blotting substrate (Thermo Fisher Scientific, Waltham, MA, USA).

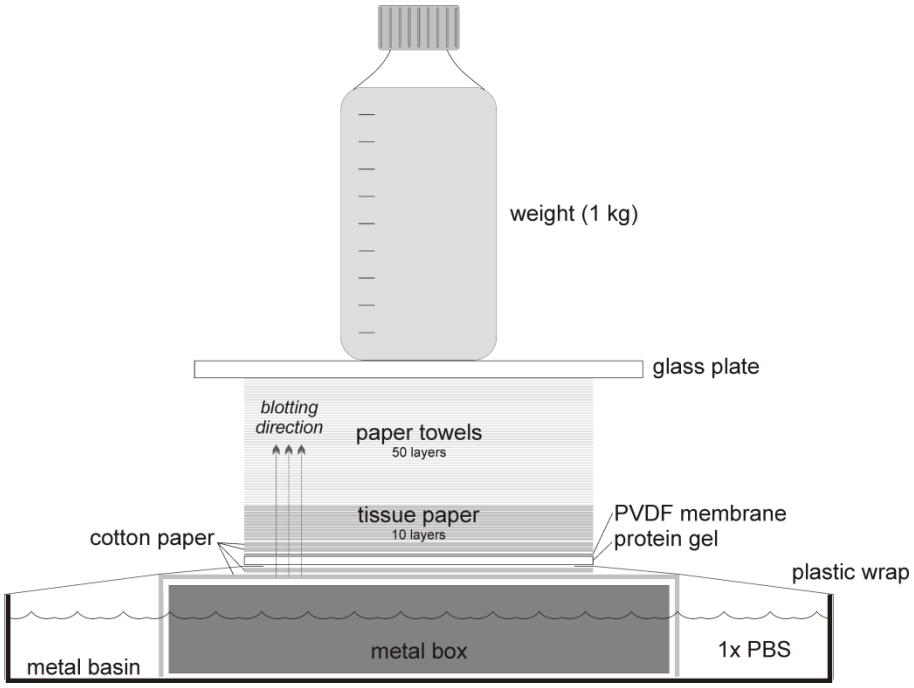

Fig 2.4. Capillary-transfer setup for blotting of proteins onto PVDF membranes.

PBS

NaCl	140.3 mM
KCl	26.8 mM
Na_2HPO_4	8.03 mM
KH_2PO_4	1.84 mM
pH 7.4 (HCl)	

TBST

NaCl	150 mM
Tris	20 mM
pH 7.5 (HCl)	
Tween® 20	0.25 % (v/v)

2.9 Co-Immunoprecipitation (Co-IP) of atPGR5 interaction partners

To identify possible interaction partners of atPGR5 in *Synechocystis*, atPGR5 and physically interacting proteins were immuno-precipitated using αPGR5-decorated magnetic beads as outlined below.

2.9.1 Whole cell protein extraction for Co-IP

Synechocystis cells were grown in 500 ml culture volume, using 2000 ml Erlenmeyer flasks at 30 °C and under rotary shaking (120 rpm) in BG11G. Cells were harvested seven days past inoculation by centrifugation (2000 rcf, 10 min, 4 °C) and re-suspended in 3 ml of protein extraction buffer. Cell suspensions were split into 1 ml aliquots and placed in 2 ml reaction tubes. Glass beads (0.25–0.65 mm) were added to a final volume of 1.75 ml, and samples were homogenized in a TissueLyser II for 2x5 minutes at 30 Hz in sample racks pre-chilled to -20 °C. Unbroken cells and glass beads were collected by centrifugation (16000 rcf, 1 min, 4 °C). The supernatant was transferred into new 1.5 ml reaction tubes and cell debris was removed by centrifugation (16000 rcf, 120 min, 4 °C). The supernatant was collected in a new reaction tube, protein concentration was estimated by Bradford assay, and samples were stored on ice until needed.

Protein extraction buffer

Tris/HCl (pH 7.4)	50 mM
NaCl	150 mM
$MgCl_2$*$6H_2O$	1 mM
glycerol	5 % (v/v)
Nonidet P40	1 %
EDTA/HCl (pH 8.0)	1 mM
freshly added:	
PMSF (in EtOH)	100 µM
Benzamidine (in HEPES/NaOH pH 7.5)	665 µM
ε-aminocapronic acid	500 µM

Binding buffer

Tris/HCl (pH 7.4)	50 mM
NaCl	150 mM
glycerol	5 % (v/v)
Nonidet P40	0.05 %

Washing buffer

Tris/HCl (pH 7.4)	50 mM
NaCl	150 mM
glycerol	5 % (v/v)

2.9.2 Decoration of magnetic protein A beads with αPGR5 antibody

All steps were performed at 4 °C and, if not stated otherwise, on ice. Ambient light intensity was kept below 5 µE to protect photoactive compounds used. Magnetic beads were collected for at least 5 min in order to cover small beads, unless stated otherwise.

For one reaction, 25 µl of protein A magnetic beads (NEB catalogue number S1425S) were washed two times with 0.1 M Na_2PO_4 (pH 8.0) and were re-collected magnetically using a magnetic separation rack

(NEB catalogue number S1509S; pre-cooled to 4°C). Beads were equilibrated by washing them two times with binding buffer. 80 µl of binding buffer were mixed with 20 µl of antibody serum and applied to the magnetic beads. Beads were gently re-suspended by flicking, decorated with antibodies for 1.5 h under orbital mixing, recollected, and washed once with binding buffer. Beads were re-suspended in 100 µl binding buffer and set aside on ice until needed.

2.9.3 Magnetic labelling

100 µl of equilibrated beads were mixed with 900 µl of protein extract (corresponding to 5-10 mg total protein) in 2 ml reaction tubes, wrapped in aluminum foil, and incubated overnight under rotational shaking (60 rpm). The next day, beads were recollected for 15 min, washed three times with 800 µl binding buffer, and two times with 500 µl washing buffer. After the final washing step, the supernatant was discarded as thoroughly as possible, and beads were stored on ice until needed.

2.9.4 Processing of precipitated protein samples

Further processing steps were performed at room temperature and under regular illumination, unless stated otherwise.

Proteins were eluted from magnetic beads twice by application of 2x50 µl of 0.1 M glycine solution (pH 2.5), incubation for 10 min at room temperature on a rotary shaker, and subsequent magnetic collection of the beads. The beads were then discarded; the eluate fractions were combined and transferred into new 1.5 ml test tubes. Sample pH was neutralized by adding 100 µl of 100 mM ammonium bicarbonate (NH_4HCO_3). To reduce protein disulfide bonds, 10 µl of 45 mM DTT were added and samples were incubated for 30 min at 37 °C. Samples were re-cooled to room temperature for 10 min prior to thiol group alkylation by addition of 10 µl of 100 mM iodoacetamide (ICH_2CONH_2). Alkylation was performed for 30 min at room temperature and in the dark. Sample pH was verified to range between 7.5 and 8.0, and 15 µl of 0.1 µg μl^{-1} trypsin in 50 mM acetic acid were added. Samples were mixed gently by flicking, and tryptic digestion was performed overnight (~16 h) at 37 °C under constant mixing (350 rpm).

2.9.5 Peptide purification for mass-spectrometric analysis

Digested protein samples were acidified to pH 2–3 by addition of formic acid to a final concentration of 10 % (v/v). Residual protein aggregates were pelleted by centrifugation (16000 rcf, 10 min, RT) and clear supernatant was set aside in new reaction tubes until needed.

To desalt peptides and exclude undigested protein residues, home-made C18 STAGE tips (Rappsilber et al. 2003) were used, consisting of a C18 Empore™ Disk (3M™, Saint Paul, MN, USA) matrix column (diameter 0.4 mm, length 0.5) inserted into a 200 µl pipet tip. Washing, binding and elution steps were conducted at room temperature, assisted by gentle centrifugation at 500 rcf with STAGE tips placed in 2 ml reaction tubes to minimize back-pressure of passing liquid. The column matrix was activated with 100 % MeOH and equilibrated with 100 µl 0.5 % formic acid. Tips were transferred into new, non-autoclaved 2 ml reaction tubes, and digested protein samples were loaded onto the column. Flow-through was collected in new, non-autoclaved 1.5 ml reaction tubes and re-loaded onto the column upon completion of the first passage. After second matrix passage was completed, flow-through was collected, and columns were washed with 100 µl of 5 % formic acid. STAGE tips were placed into new, non-autoclaved 1.5 ml reaction tubes, and peptides were eluted with 2x50 µl of elution buffer (80 % acetonitrile (CH_3CN), 0.5 % formic acid). Samples were near-dried to a residual volume ≤ 3 µl using a vacuum rotary evaporator and re-suspended in 0.1 % formic acid to a final volume of 15 µl. Samples were frozen in liquid nitrogen and stored at -80 °C. Mass-spectrometric analysis and data processing was conducted by Dr. Giada Marino.

2.10 Bacteria-two-hybrid (B2H) assay for protein-protein interaction

In order to test for protein-protein interaction *in vivo*, a split adenylate cyclase reconstitution assay was employed. The assay is based on a split adenylate cyclase whose N- or C-terminal domain is fused to a bait or a prey protein, respectively, and are expressed under control of the IPTG (Isopropyl β-D-1-thiogalactopyranoside) inducible *lacZ* promoter (Karimova et al. 1998). Upon physical interaction of bait and prey, adenylate cyclase activity is restored, leading to the formation of cAMP, which in turn induces a promoter controlling β-galactosidase expression. The two-plasmid system is co-transformed into adenylate-cyclase deficient (Δ*cya*) *E. coli* cells. After induction of fusion protein expression, β-galactosidase enzyme activity results in *o*-nitrophenyl-β-D-galactopyranoside cleavage, which is measured *in vitro* by photometric detection of yellow dye formation. Δ*cya E. coli* cells bearing a cAMP-inducible lacZ gene (strain BTH101), as well as plasmids pKT25 (C-terminal fusion of the target protein to the T25 fragment of adenylate cyclase) and pUT18C (C-terminal fusion of the target protein to the T18 fragment of adenylate cyclase) were obtained from Euromedex (Souffelweyersheim, France).

Candidate genes for synPGR5 interactors, as well as a set of control proteins including atPGR5 and positive controls for transient *Synechocystis* protein-protein interactions were cloned into pKT25 and pUT18C by classical restriction-ligation molecular cloning (see Methods 2.4.4).

Interaction strength upon IPTG-induction of fusion proteins was quantified using an ONPG-based β-galactosidase activity assay according to manufacturer's instructions, with two exceptions. First, cells were grown for 72 h at 30 °C and 140 rpm, resulting in weak interactions being detectable reliably. Second, we employed pKT25_ssl2250 and pUT18C_sll0149 rather than empty vectors as negative control. Empty vectors have been found to generate unspecific signals earlier than fusion constructs. Since observed interactions between *Synechocystis* and/or plant proteins were weak and presumably transient in nature, we resorted to controls generating as little background signal as possible.

2.11 Phenotyping and physiological measurements in *Synechocystis*

2.11.1 Dry mass determination

Cells of 2 ml mature culture volume were harvested by centrifugation (3 min, 12000 rcf, 25 °C). Supernatant media was removed thoroughly with a pipette, pellets were centrifuged once more as previously and residual media was completely removed. Cells were desiccated for 3 h at 30 °C using a vacuum rotary evaporator. Pellets were flicked out of the tube and weighed on an analytical scale.

2.11.2 Pigment extraction

Synechocystis cellular hydrophobic pigments were extracted and quantified based on a method proposed by Zavřel et al. (2015). *Synechocystis* cells corresponding to OD_{730} = 0.75 were harvested into 1.5 ml reaction tubes by centrifugation (15000 rcf, 7 min, 25 °C), and supernatant media was removed thoroughly by pipetting. 1 ml MeOH (100 %) was added to the cell pellets and tubes were wrapped in aluminum foil to avoid light exposure. Pigments were extracted for a minimum of 2 h or overnight at 4 °C under gentle shaking. Cells and precipitates were removed by centrifugation (15000 rcf, 10 min, 4 °C), and pigment extracts were transferred into plastic cuvettes for spectrophotometric analysis. Chlorophyll a (Chl_a) and carotenoid contents were calculated as follows:

Chl_a [µg ml^{-1}]	=	$12.9447*(Abs_{665}-Abs_{720})$	(Ritchie 2006)
Carotenoids [µg ml^{-1}]	=	$[1000*(A_{470}-A_{720})-2.86*(Chl_a[\mu g\ ml^{-1}])]/221$	(Wellburn 1994)

OD_{730} = 0.75 cells were empirically determined to yield extracts with maximum absorbance ≤ 0.5 and thus were suitable for approximate pigment quantification. Hence, biomass input for pigment extraction was set to OD 0.75 cells routinely.

2.11.3 Determination of PSII quantum yield

For liquid cultures, maximum and efficient PSII quantum yield (F_v/F_m and Φ_{II}) were determined with a DUAL-PAM-100 P700 & chlorophyll fluorescence measuring system (WALZ, Effeltrich, Germany) using the Fluo measuring mode, following the instructions by Ogawa et al. (2017). Cultures were dark incubated for 15 min prior to measurements. Non-default settings were: Gain 5 (high), damping 1 ms (high), measuring light intensity 5 (12 µE), block frequency MF low 20 / MF high 2000 (auto-high), actinic light (AL) intensity 5 (50 µE), acquisition rate 10 s^{-1}, saturation pulse (SP) intensity 3 (3000 µE), SP width 800 ms, acquisition rate 10 ms^{-1}. Measurement routine was 10 s dark > SP >60 s dark > 290 s AL > SP > 10 s AL >300 s dark > 150 s actinic light. During the second actinic light phase maximum chlorophyll fluorescence was determined upon addition of 5 µM DCMU.

For culture drops on BG11 agar plates, F_v/F_m was determined using a FluorCam 800MF (Photon Systems Instruments, Drásov, Czech Republic), employing the quenching analysis routine. Measuring durations were set to 5 s for F_o, 800 ms F_m pulse duration, 10 s dark pause after F_m measurement, 60 s actinic light exposure, 20 s relaxation interval, and 9 s first pulse after actinic light trigger, giving a total of 6 pulses (5 pulses during Kautsky induction; 1 pulse during relaxation).

2.11.4 P700 Dual-PAM measurements

The antenna system of PSI contains a set of “far-red” chlorophylls in the core antenna that absorb light of λ>700 nm. These far red (FR) wavelengths are – to the largest extend – energetically insufficient to excite the reaction center of PSII, but lead to oxidation of the PSI reaction center (P700). Oxidized P700 displays strong absorbance in the infra-red spectrum, peaking between 800 and 840 nm, allowing tracing its redox kinetics by means of a simple absorbance measurement. To measure P700 redox kinetics as $\Delta(Abs_{830}\text{-}Abs_{875})$, *Synechocystis* cells were prepared as follows:

Liquid cultures of 50 ml volume were grown photoautotrophically in 100 ml Erlenmeyer flasks covered with aluminum (foil) caps at 30 °C and 30 µE of continuous white fluorescent light, and under constant rotary shaking at 140 rpm. Cultures were supplied with transformation-level concentrations of appropriate antibiotics and grown to exponential phase (OD_{730} = 0.4–0.8). Cells were harvested in sterile 50 ml reaction tubes by centrifugation (3000 rcf, 5 min, 25 °C) and washed two times with BG11 media. Cells were then re-suspended, adjusted to OD_{730} = 5.0 with fresh BG11 media, transferred into 2 ml reaction tubes, and dark incubated overnight (≥ 16 h) at 25 ° and under constant shaking at 140 rpm. P700 PAM measurements were conducted in a darkened room with a DUAL-PAM-100 P700 and chlorophyll fluorescence measuring system. Sample application into the measuring cuvette was

performed minimizing exposure to air and thus oxygen input. P700-oxidation kinetics were measured in single-channel P700 mode over 60 s of constant far-red (FR) light exposure (3 s dark > 60 s FR > 30 s dark). We used measuring light intensity 4, FR light intensity 3 (38 µE), acquisition rate 200 s^{-1}, and high gain (5) and damping (1 ms).

In order to obtain representative correlation between physiological and protein detection data samples were re-collected after P700 measurements, subjected to thylakoid protein preparation as described before (Methods 2.8.2; Gandini et al. 2017), and used for Western blot analysis (see 2.8).

2.11.5 Electrochromic shift (P515) Dual-PAM measurements

Cells for P515 measurements were prepared just like for P700 measurements (see 2.11.4). The Dual-PAM-100 P515 module was used in P515 dual channel mode and, unless stated otherwise, settings were chosen in accordance to default parameters described by Schreiber and Klughammer (2008). We used measuring light intensity 5, actinic light (AL) intensity 10 (216 µE), acquisition rate 50 s^{-1}, measuring frequency (MF) low 200, MF high 2000, and high gain and damping. P515 signal measuring routine consisted of 15 s dark > 600 s AL > 135 s dark.

2.12 Protein-sequence analysis

Protein sequences used for multi-species alignments and subsequent phylogenetic analyses were obtained from NCBI genbank and UniProt. Full species descriptions and NCBI/UniProt protein IDs are listed below (Tab 2.5). Chloroplast transit peptides for plant PGRL1 sequences were predicted using ChloroP 1.1 (Emanuelsson et al. 1999) and removed prior to phylogenetic reconstruction. N-terminal transit peptides spanned 60, 49, 40, 67, and 61 amino acids for *Arabidopsis* (a, b), *Chlamydomonas*, *Physcomitrella*, and *Zea* PGRL1, respectively. For *Arabidopsis* PGR5 the actual N-terminal sequence was determined experimentally (Sugimoto et al. 2013), and other plant PGR5 transit peptide subsequences were removed accordingly. The removed sequences spanned 60, 69, 56, and 54 amino acids for *Arabidopsis*, *Chlamydomonas*, *Physcomitrella*, and *Zea* PGR5, respectively.

Tab 2.5. **Protein sequences used for phylogenetic reconstruction.** NCBI/Uniprot IDs as of Sept. 10th 2019. Lowercase letters in parentheses refer to respective PGRL1 isoforms.

	NCBI ID						UniProt ID
Organism	**NadA**	**Sll1217/UDG4**	**Slr1353**	**PGRL1**	**NdhF(1)**	**EF-G(2)**	**PGR5**
Acaryochloris marina	WP_041659169.1	WP_012164391.1	WP_012164533.1				
Anabaena sp. PCC7108	WP_016951391.1	WP_016951772.1	WP_016950996.1				
Aphanothece minutissima	WP_106220220.1	WP_106220097.1	WP_106220105.1				
Cyanobium usitatum	WP_106501607.1	WP_106501549.1	WP_106501712.1				
Geminocystis sp. NIES3708	WP_066348861.1	WP_066345990.1	WP_066343513.1				
Gloeocapsa sp. PCC 73106	ELR96448.1	WP_006527475.1	WP_015189282.1				
Gloeomargarita lithophora	WP_071454470.1	WP_071453505.1	WP_099092488.1				
Microcystis aeruginosa NIES-843	B0JLU4.1	BAG01530.1	WP_104397852.1				
Pleurocapsa sp. PCC 7327	AFY76937.1	AFY77210.1	WP_144054260.1				
Prochlorococcus marinus str. MIT 9303	A2C9Z7.1	ABM78179.1	KZR71644.1				
Roseofilum reptotaenium AO1-A	OJJ26673.1	OJJ26952.1	OJJ21918.1				
Synechococcus sp. PCC 7502	WP_015167217.1	WP_015169319.1	WP_015169185.1				
Synechocystis sp. PCC6803	WP_010874167.1	WP_010872728.1	WP_010872797.1		WP_010873758.1	WP_010872942.1	P73358
Thermosynechococcus sp. NK55a	WP_024123981.1	WP_024124991.1	WP_024124928.1				
Vulcanococcus limneticus	WP_094590265.1	WP_094589427.1	WP_094591835.1				
Bacillus subtilis					WP_120027728.1	WP_071584208.1	
Escherichia coli	WP_000115290.1						
Thermotoga maritima		WP_004081422.1					
Chlamydomonas reinhardtii				XP_001692513.1		XP_001701845.1	A8I547
Chaetosphaeridium globosum					NP_683848.1		
Physcomitrella patens (b)				XP_024386479.1	NP_904235.1	XP_024390742.1	A9SSW4
Arabidopsis thaliana (a)				NP_567672.1	NP_051106.1	NP_564801.1	Q9SL05
Arabidopsis thaliana (b)				NP_192933.2			
Zea mays (b)				XP_008652279.1	NP_043084.1	PWZ41790.1	A0A3L6F657

2.12.1 Protein-sequence alignments used for pairwise similarity/identity calculations and phylogenetic reconstruction

Protein sequence pairwise similarities and identities were calculated using MatGAT 2.01 (Campanella et al. 2003). Input multiple protein alignments of NadA:Sll1217/UDG4.PGRL1 (Fig 2.5) NadA:PGRL1 (Fig 2.6), Sll1217/UDG4:PGRL1 (Fig 2.7), and Slr1353 (Fig 2.8) were generated using MUSCLE (Edgar 2004) with default parameters as implemented in MEGA X (Kumar et al. 2018) using the proteins sequences described above (Tab 2.5). NdhF and EF-G2 multiple-protein-sequence alignments (Fig 3.10, 3.11) were generated with MUSCLE default settings likewise.

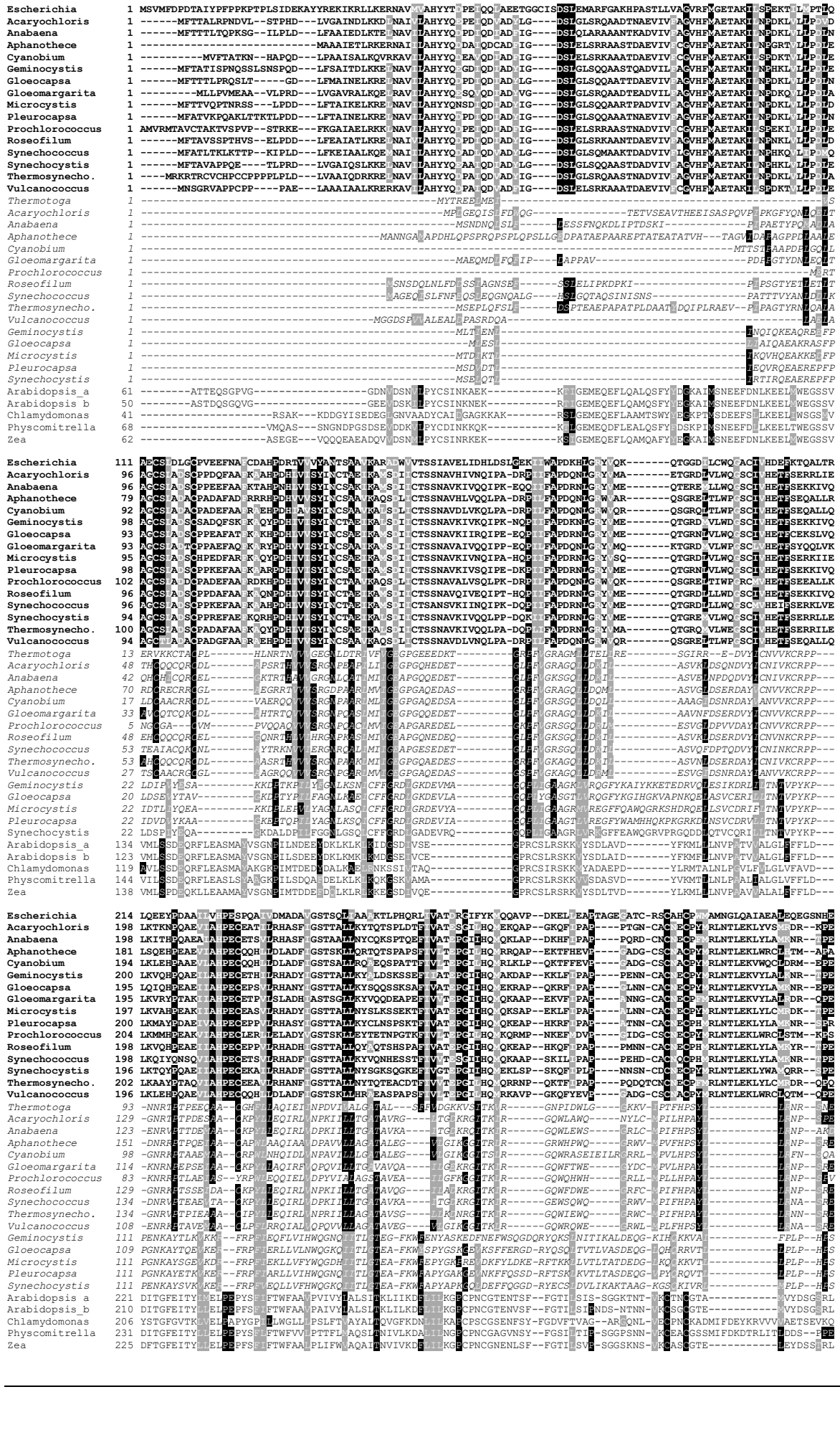

Fig 2.5. **Multi-protein-sequence alignment of cyanobacterial NadA, UDG4/Sll1217-homologues, and plant PGRL1.** Residues conserved/similar in ≥50 % of sequences are highlighted in black/grey. PGRL1 sequences are displayed without transit peptides as predicted by ChloroP v 1.1. ***Escherichia*** (***coli***) serves as outgroup for the **NadA-like protein family** (labelled with **bold font**); *Thermotoga* (*maritima*; Thermatogales) serves as *UDG4-like protein family* outgroup (labelled *in italics*).

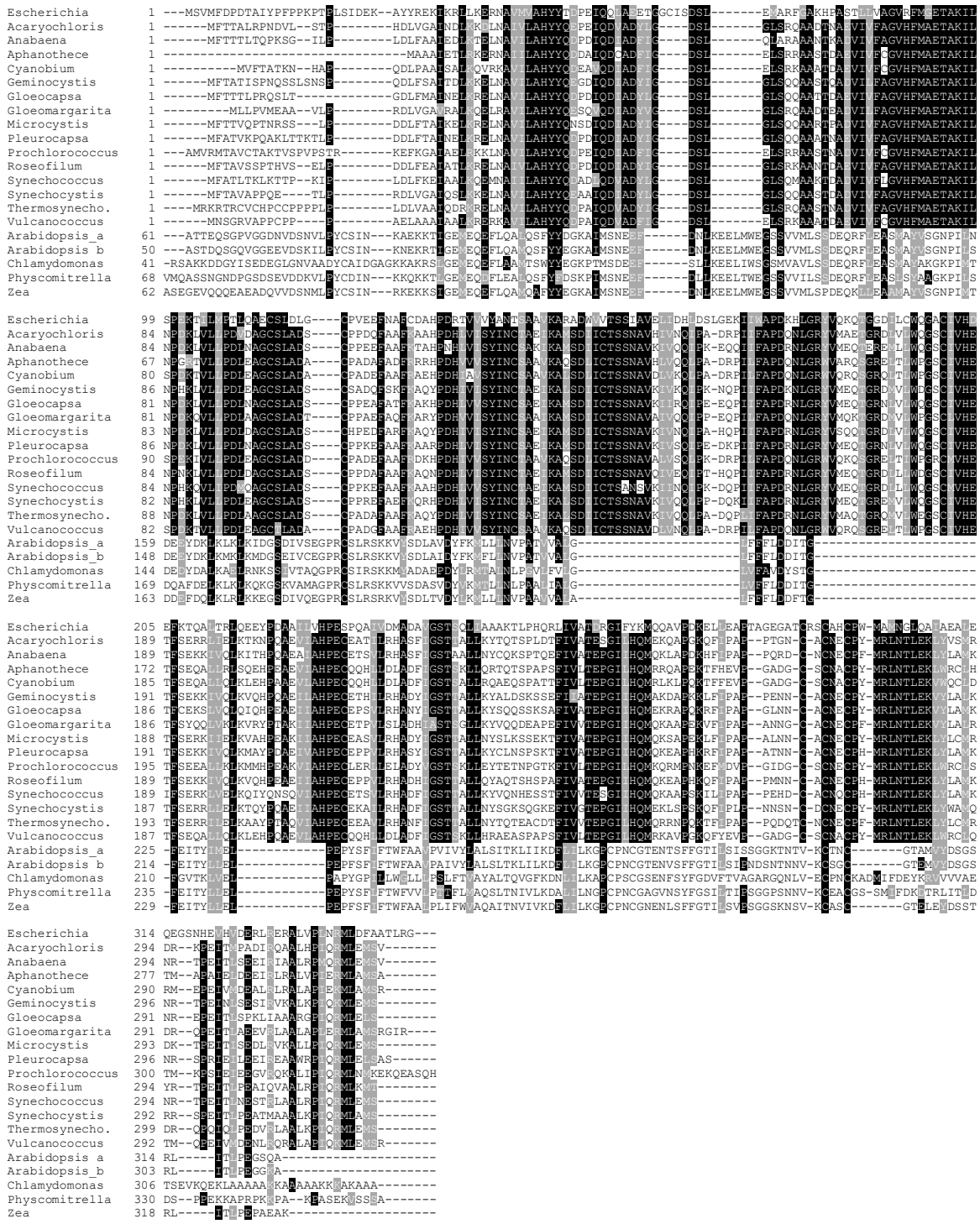

Fig 2.6. **Multi-protein-sequence alignment of cyanobacterial NadA and plant PGRL1.** Residues conserved/similar in ≥ 70 % of sequences are highlighted in black/grey. PGRL1 sequences are displayed without transit peptides as predicted by ChloroP v 1.1. *Escherichia* (*coli*) serves as NadA-like protein family outgroup.

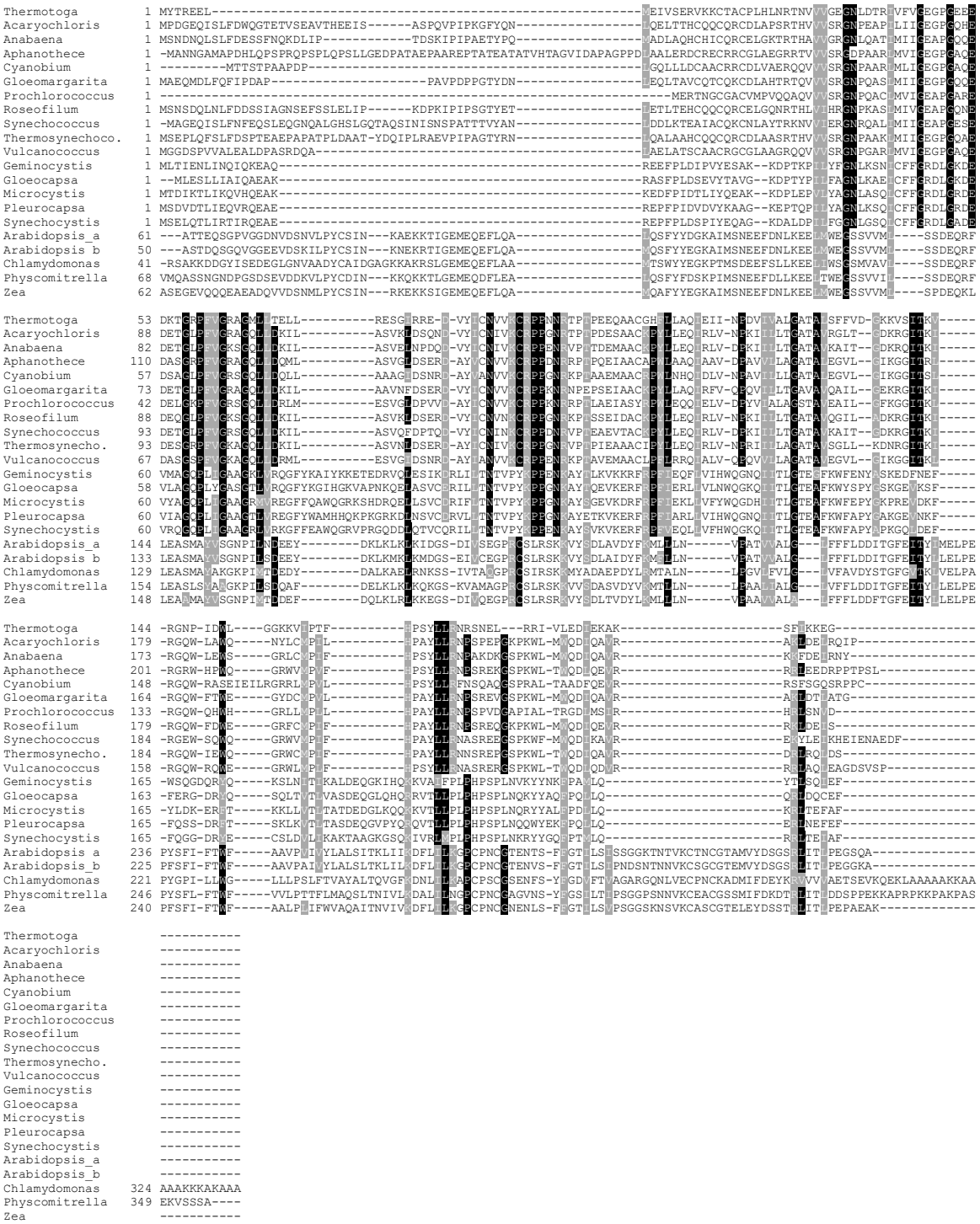

Fig 2.7. **Multi-protein-sequence alignment of cyanobacterial UDG4/Sll1217-homologues and plant PGRL1.** Residues conserved/similar in ≥ 70 % of sequences are highlighted in black/grey. PGRL1 sequences are displayed without transit peptides as predicted by ChloroP v 1.1. *Thermotoga* (*maritima*; Thermatogales) serves as UDG4-like protein family outgroup.

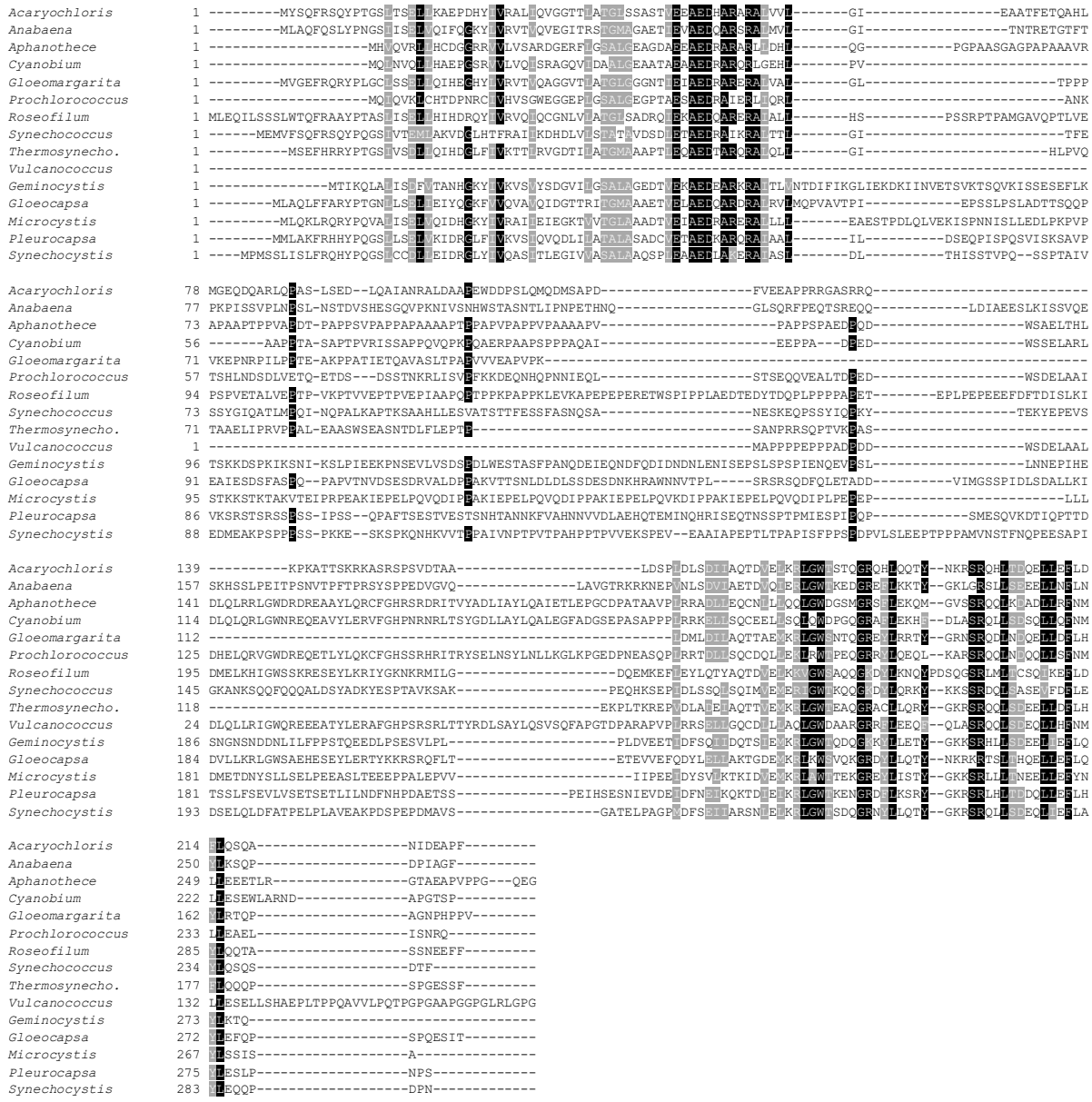

Fig 2.8. **Multi-protein-sequence alignment of cyanobacterial Slr1353-homologues.** Residues conserved/similar in ≥ 70 % of sequences are highlighted in black/grey.

2.12.2 Phylogenetic Reconstruction

Phylogenetic reconstruction was performed using maximum likelihood (ML) and maximum parsimony (MP) methods as implemented in MEGA X with the protein alignments shown above as input. Optimum evolutionary models for ML reconstruction were determined by ModelTest (Posada and Crandall 1998) as implemented in MEGA X. Confidence of tree inference was tested by 500–5000-fold bootstrapping (i.e. repetition of the statistical analysis and derivation of a most likely consensus tree topology (Felsenstein 1985). Details of the respective reconstructions are given below.

2.12.2.1 PGRL1-NadA-Sll1217/UDG4 Maximum Parsimony analysis

Initially, the evolutionary history of plant PGRL1, cyanobacterial Sll1217/UDG4-like proteins with UDG4-family founding member *Thermotoga maritima* as outgroup, and cyanobacterial NadA proteins with NadA-family founding member *Escherichia coli* was inferred using the Maximum Parsimony method. A bootstrap-consensus tree inferred from 5000 replicates was calculated to represent the evolutionary history of the taxa analyzed. The MP tree was obtained using the Subtree-Pruning-Regrafting (SPR) algorithm (Nei and Kumar 2000) with search level 1 in which the initial trees were obtained by the random addition of sequences (10 replicates). The analysis involved 37 amino-acid sequences. There were a total of 362 positions in the final dataset.

2.12.2.2 PGRL1-NadA-Sll1217/UDG4 Maximum Likelihood analysis

The evolutionary history of plant PGRL1, cyanobacterial Sll1217/UDG4-like proteins with UDG4-family founding member *Thermotoga maritima* as outgroup, and cyanobacterial NadA proteins with NadA-family founding member *Escherichia coli* was inferred by using the Maximum Likelihood method based on the Whelan-And-Goldman model (WAG; Whelan and Goldman 2001). 500 bootstrap replicates were calculated. Initial tree(s) for the heuristic search were obtained automatically by applying Neighbor-Join and BioNJ algorithms to a matrix of pairwise distances estimated using a JTT model, and then selecting the topology with superior log likelihood value. A discrete Gamma distribution was used to model evolutionary rate differences among sites (5 categories (+*G*, parameter = 2.1453)). The analysis involved 37 amino acid sequences with a total of 362 positions in the final dataset.

2.12.2.3 PGRL1-Sll1217/UDG4 Maximum Parsimony analysis

The evolutionary history of plant PGRL1 and cyanobacterial Sll1217/UDG4-like proteins with UDG4-family founding member *Thermotoga maritima* as outgroup was inferred using the Maximum Parsimony method. 5000 bootstrap replicates were calculated. The MP tree was obtained using the Subtree-Pruning-Regrafting (SPR) algorithm with search level 1 in which the initial trees were obtained by the random addition of sequences (10 replicates). The analysis involved 21 amino acid sequences. There were a total of 341 positions in the final dataset.

2.12.2.4 PGRL1-Sll1217/UDG4 Maximum Likelihood analysis

The evolutionary history of plant PGRL1 and cyanobacterial Sll1217/UDG4-like proteins with UDG4-family founding member *Thermotoga maritima* as outgroup was inferred by using the Maximum Likelihood method based on the WAG model. 500 bootstrap replicates were calculated. Initial tree(s) for the heuristic search were obtained automatically by applying Neighbor-Join and

BioNJ algorithms to a matrix of pairwise distances estimated using a JTT model, and then selecting the topology with superior log likelihood value. A discrete Gamma distribution was used to model evolutionary rate differences among sites (5 categories (+*G*, parameter = 1.7582)). The analysis involved 21 amino acid sequences. There were a total of 341 positions in the final dataset.

2.12.2.5 Slr1353 Maximum Likelihood analysis

The evolutionary history of cyanobacterial Slr1353 homologues was inferred by using the Maximum Likelihood method based on the WAG+*Frequency* model (WAG+F). 500 bootstrap replicates were calculated. Initial tree(s) for the heuristic search were obtained automatically by applying Neighbor-Join and BioNJ algorithms to a matrix of pairwise distances estimated using a JTT model, and then selecting the topology with superior log likelihood value. A discrete Gamma distribution was used to model evolutionary rate differences among sites (5 categories (+*G*, parameter = 2.6592)). The rate variation model allowed for some sites to be evolutionarily invariable ([+*I*], 2.53 % of sites). The analysis involved 15 amino acid sequences. There were a total of 356 positions in the final dataset.

3 Results

3.1 High-light adaptive evolution

The evolutionary potential of *Synechocystis* sp. PCC6803 for high light intensities was explored experimentally. Adaptive evolution experiments have been conducted before to generate heat-tolerant *Synechocystis* strains (Tillich et al. 2012, Tillich et al. 2014), but so far photosynthesis, and specifically the light reaction, has not been subject of such research yet.

To yield the maximum number of adaptive mutations the adaptive-evolution experiment was conceptualized to contain as many favorable aspects and to exclude as many detrimental aspects of natural evolution as possible. This encompassed:

- Induction of high mutation rates at the cost of relatively low mortality (Tillich et al. 2012) to speed up the experiment
- Re-inoculation of batch cultures with supposedly representative cell sample sizes to minimize genetic drift leading to loss of favorable alleles (Lande 1976)
- Splitting of an original high-light mutant batch several times and subjecting the resultant progeny branches to different mutagenesis and selection protocols. The rationale behind this was
    - to allow for a more thorough exploration of the mutation space
    - To avoid large-scale loss of adaptive diversity in any single culture upon evolution of a highly adaptive allele, leading to a *selective sweep* (i.e. excessive competitive exclusion of other less adapted genotypes; Majewski and Cohan 1999).
- Cryo-conservation of representative portions of each cultivation cycle's mature cultures to preserve "past" genetic diversity and haplotypes in form of a resurrectable fossil record. This would not only allow to reconstruct evolutionary trajectories and to detect epistatic (i.e. sequentially fixed) evolution of adaptations, but also to resume adaptive evolution of any batch starting from any given point backwards in time as demonstrated by Lenski and co-workers (Blount et al. 2008).

The evolution experiment was aimed to be conducted with as small as possible operational effort and culture volumes in order to enhance method accessibility, throughput, and transferability.

3.1.1 Evolution of high light tolerant *Synechocystis* mutants

High light adaptive evolution experiments were performed with culture volumes of approximately 80 ml volumes which were re-inoculated at OD_{730} = 0.1, corresponding to approximately $4*10^8$ cells (Viola et al. 2014). This number was considered a representative sample containing most prevalent genotypes, and thus to grant quasi-continuous evolution of batch cultures. Mutagenesis was performed with UV-C radiation (λ = 254 nm) and the alkylating agent methyl-methanesulfonate (MMS) according to the optimal mutagen dosages described by Frohme and co-workers (Tillich et al. 2012).

Lethal light intensity for non-adapted WT in photoautotrophic media (BG11) was empirically determined to be approximately 1100 µE at 23 °C under atmospheric aeration. We chose approximately 2/3 of the lethal light intensity as starting point for adaptive evolution, which was observed to exert high light stress, yet to allow for productive growth rates (Fig 3.1).

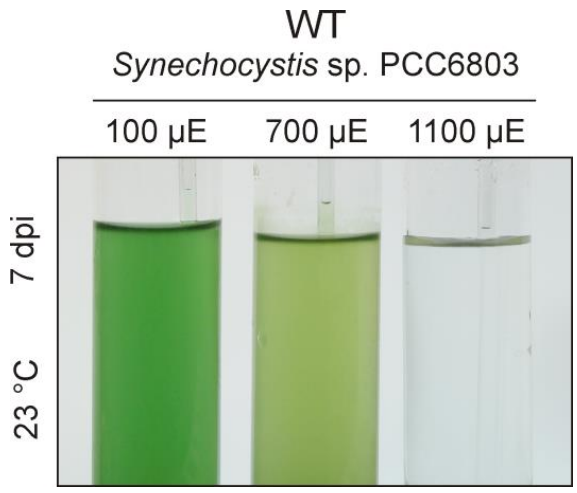

Fig 3.1. ***Synechocystis* WT high-light tolerance.** WT cells in photoautotrophic liquid culture tolerate 700 µE growing light at 23 °C, but do not survive under 1100 µE. Subsequent high-light adaptive evolution aimed at shifting the WT physiological pessimum beyond 1100 µE. Cultures were inoculated at OD_{730} = 0.05 from liquid culture.

Subsequently, WT cells were sequentially mutagenized with 50 J m^{-2} UV-C or 1 % (v/v) MMS and subjected to increasing light intensities according to the protocol outlined in Fig 3.2, resulting in mutants tolerating 1900–2300 µE at 23 °C and thus about twice the light intensity found lethal for WT.

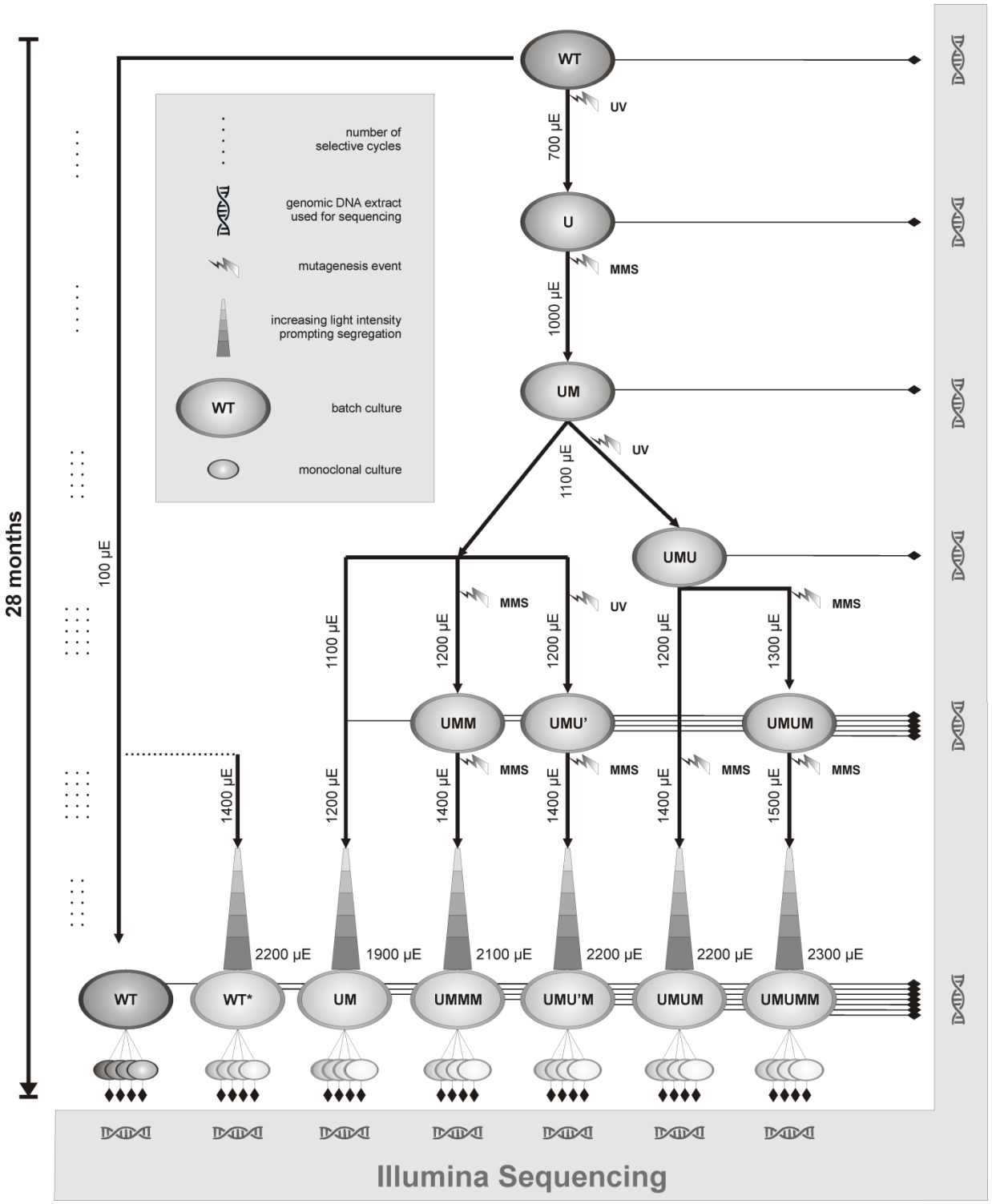

Fig 3.2. **High-light adaptive evolution experimental design.** High-light adaptive evolution was performed according to the outlined protocol of repeated mutagenesis, and by application of increasing selective pressure. Batch cultures (large ovals) were mutagenized (indicated by lightning bolts) with 1 % (v/v) MMS for 1 min, or with 50 J m^{-2} UV-C radiation, respectively. After mutagenesis, selective light intensities were increased to the µmol photons m^{-2} s^{-1} (µE) indicated in the flow chart and applied for the given number of cultivation cycles (represented by dots on the left). Following the last mutagenesis event and subsequent 15 selection cycles, light intensities were increased stepwise over the course of ten more selective cycles to drive mutant allele segregation prior to single clone isolation. Whole genome sequencing was performed on four monoclonal strains per batch (small ovals), as well as intermediate and final batch cultures were selected for whole genome sequencing (diamond-tipped arrows represent genomic DNA sampling events for whole genome sequencing indicated by double helices). A WT culture unexpectedly surviving under control high light conditions in midst of the experiment was henceforth propagated in parallel with the mutagenized culture, giving rise to the high light adapted yet never mutagenized WT*.

All evolutionary trajectories we explored yielded heterogeneous batches of high light adapted mutants, and we observed pronounced between-cultivation cycle heterogeneity regarding batch culture phenotype (Fig 3.3). The number of post-mutagenesis selective cycles was increased in the course of the experiment (5–5–10–15; Fig 3.2). This was meant to allow for enrichment of the best-performing mutant alleles prior to the next mutagenesis event while accounting for the expectedly rising number of adaptive genotypes.

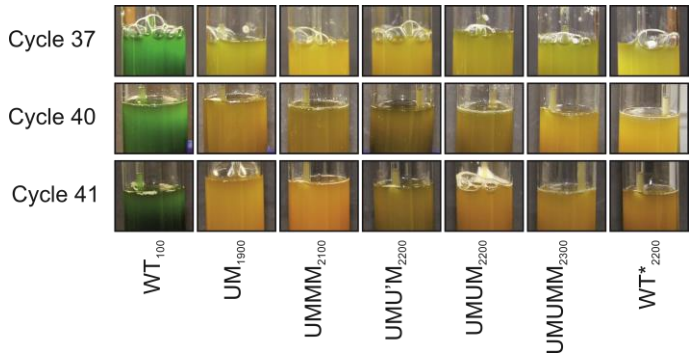

Fig 3.3. **Phenotypical heterogeneity between selective cycles.** Cycle number corresponding to selection protocol outlined in Fig. 3.2. Subscript numbers correspond to respective selective light intensity [µE].

After the final mutagenesis-regeneration-cycle, selective pressure was gradually increased to drive segregation of adaptive alleles. This was deemed necessary due to multiple genome copies present in each *Synechocystis* cell (2–10; max. approximately 50/cell; Zerulla et al. 2016). We hypothesized oligo-/polyploidy to favor dominant mutations to prevail in adapted strains without full segregation. Since partial segregation would obscure single clone genome sequence analysis and SNP call reliability, enforcing within-clone allele fixation was favored over quick mutation analysis.

Final high-light adapted mutant batches displayed pronounced phenotypic variability

Final batch cultures were grown comparatively under high (2000 µE) and low light intensity (50 µE) for twelve days, revealing pronounced among-batch phenotypic heterogeneity (Fig 3.4 A). Photosynthetic marker protein detection (Fig 3.4 B), pigment content and culture dry mass determination (Fig 3.4 C, D), as well as maximum and effective PSII quantum yield measurements (F_v/F_m and Φ_{II}; Fig 3.4 E, F) indicated pronounced heterogeneity. This in turn suggested successful exploration of different evolutionary trajectories by different batches.

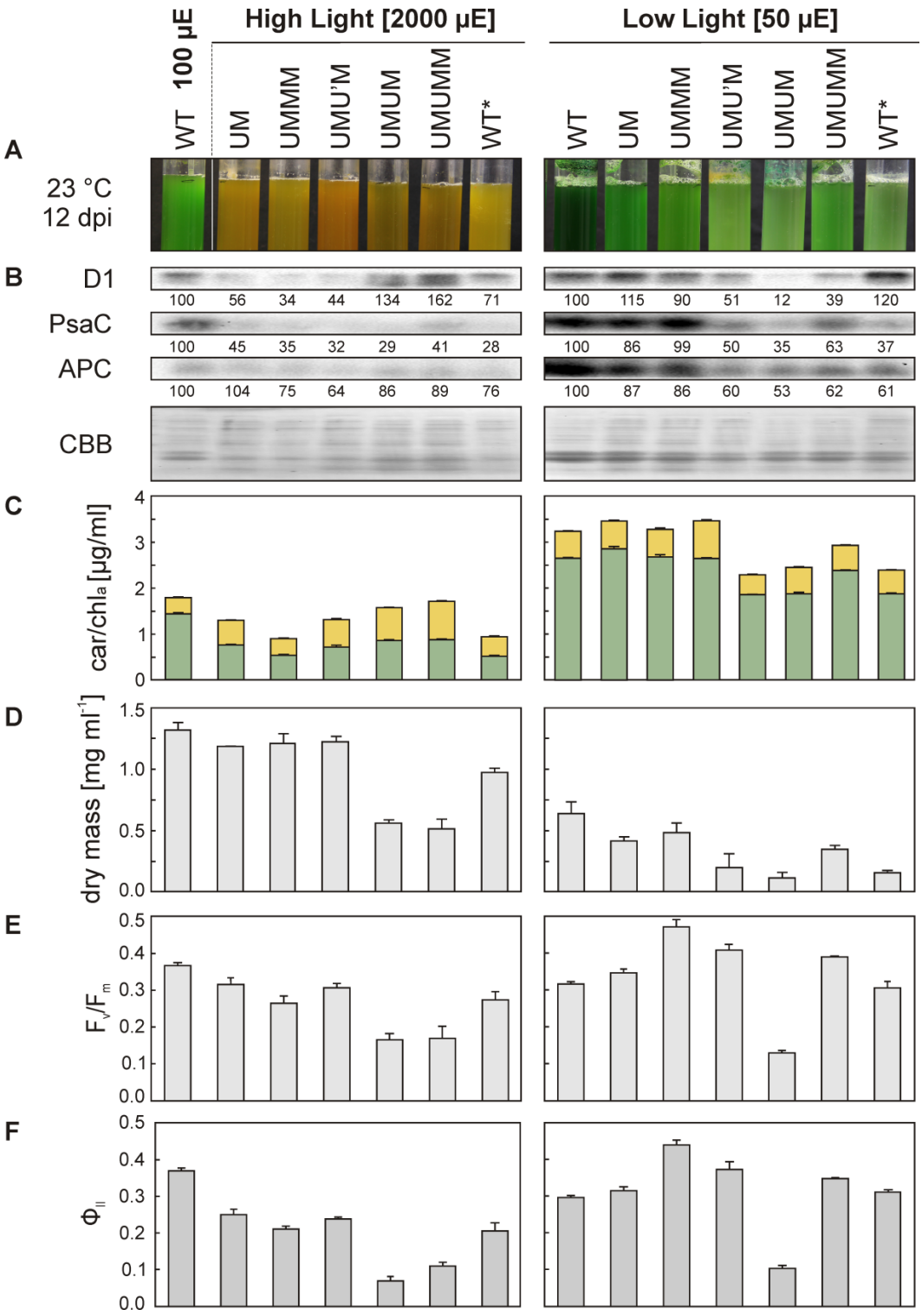

Fig 3.4. **Characterization of high-light tolerant batch cultures.** (**A**) Final batch cultures were cultivated at 23 °C for twelve days under atmospheric aeration at 2000 µE (i.e. µmol photons m^{-2} s^{-1}) and 50 µE each to allow for direct phenotypical comparison. As controls for the respective experiments, WT cells were cultivated at 100 µE and 50 µE. (**B**) Marker proteins of PSII (D1), PSI (PsaC), and phycobilisomes (apophycocyanin APC) were immunodetected on blots of whole cell protein extracts of OD_{730} = 0.3 cells. Numbers indicate protein content relative to WT control (average over three replicates). Staining with Coomassie Brillant Blue (CBB) served as loading control. (**C**) Methanolic pigment extracts of chlorophyll a (chl_a; green) and carotenoids (car; yellow) contents for OD_{730} = 0.75 cells. (**D**) Dry mass accumulation per ml of culture volume. (**E**) maximum (F_v/F_m) and (**F**) effective (Φ_{II}) quantum yield of PSII. Data have been derived from three replicates taken from the same cultivation batch (n = 3). Western blots shown are representative for three replicates, and marker proteins have been detected on the same membrane. PAM measurements were conducted in a Dual-PAM-100 with samples being taken straight from the cultivation device after 15 min of dark incubation. Cultures were grown at 23 °C in BG11 medium under continuous light and aeration with atmospheric air.

High light tolerant mutants were viable under light intensities exceeding the applied selective pressure, and, with exception of UMMM, could be shown to grow to high optical densities under as much as 3000 µE (Fig 3.5), which corresponds to about 150 % of full sunlight incidence at sea level (2000 µE; Torzillo et al. 2008) and delineates the maximum capacity of our experimental setup.

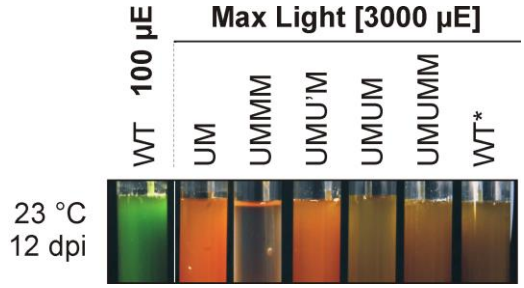

Fig 3.5. **High-light tolerance of batch cultures under maximum light exposure.** Batch cultures shown in Fig. 3.4 were grown for 12 days at 3000 µE. As a control a WT strain simultaneously grown at 100 µE is shown.

3.1.2 Sampling high-light adapted batch cultures genetic diversity

Obvious differences among mature batch cultures implied distinct adaptive mechanisms to have arisen. This rendered the multiple-parallel-evolution approach a success in terms of non-redundant exploration of *Synechocystis* high light adaptive evolutionary potential. In order to capture a broad array of adaptive mutations with as little redundancy as possible, batch culture samples were streaked on BG11 agar to isolate single clones; this practice revealed obvious phenotypic diversity among same-batch clones (Fig 3.6 A). In order to select mutant clones as diverse as possible for sequencing, 24 single clones were picked from each batch culture and subjected to chlorophyll fluorescence analysis to determine basic fluorescence F_o and maximum PSII quantum yield F_v/F_m values (Fig 3.6 B, Fig 3.7 C).

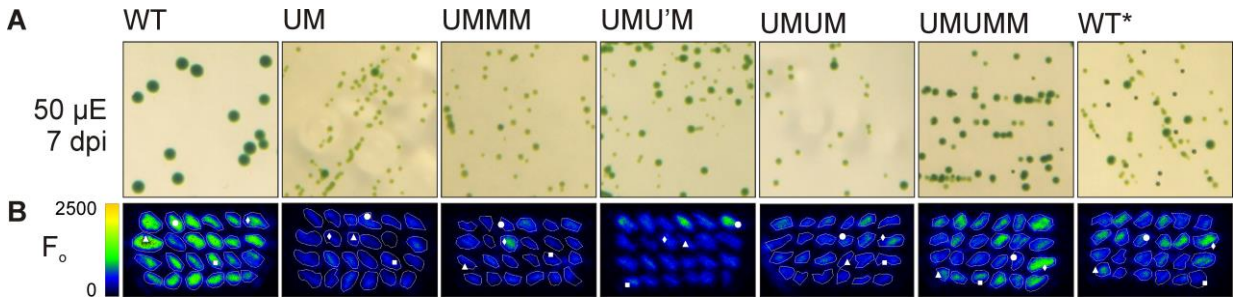

Fig 3.6. **Single-clone isolation from batch cultures for genome re-sequencing.** (**A**) Individual clones of evolved batch cultures isolated by plate streaking technique display pronounced phenotypic heterogeneity regarding colony size and coloration. A total of 24 clones per batch culture were isolated. (**B**) Isolated clones and differed strongly in basic Chl_a fluorescence F_o and PSII maximum quantum yield F_v/F_m (see Fig 3.7 **C**). Clones representing the quantile edges of the F_v/F_m distribution were selected for whole genome sequencing. The according clones are tagged with circles (clone 1), diamonds (clone 2), triangles (clone 3), and squares (clone 4) in (**B**), respectively.

Out of each batch, 4 clones representing the quantile edges of the F_v/F_m distribution (Fig 3.7 C) were selected for whole genome re-sequencing. To confirm successful sampling of variable phenotypes, aliquots of the liquid cultures of selected clones used for genomic DNA extraction were diluted to OD_{730} = 0.05, dropped onto BG11 agar plates, and cultivated for five days at 30 °C and 100 µE. The selected clones displayed pronounced phenotypical variability in growth and pigmentation (Fig 3.7 A) and basic chlorophyll fluorescence (Fig 3.7 B). Moreover, F_v/F_m distributions of post-selection clones (Fig 3.7 D) broadly recapitulated those of the original samples of 24 clones per batch (Fig 3.7 C).

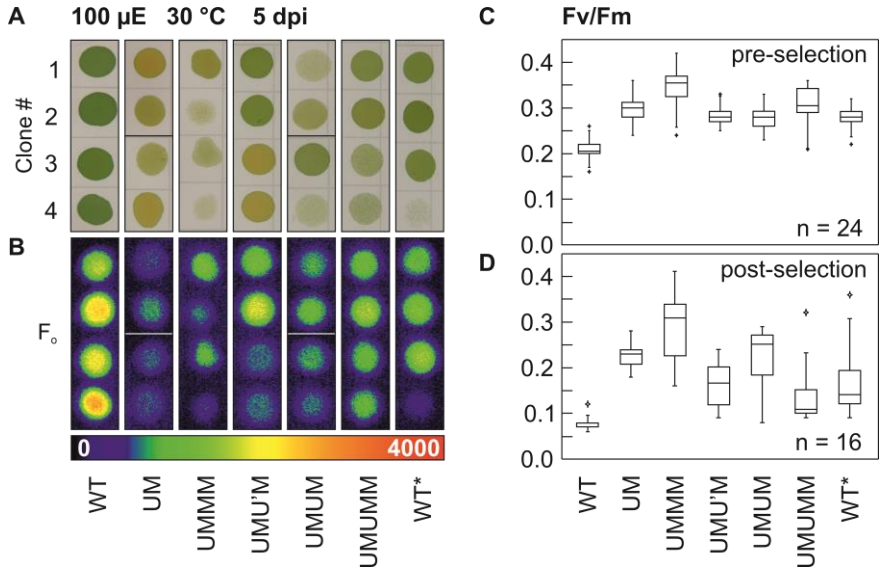

Fig 3.7. **Confirmation of to-be-sequenced clone phenotypic diversity.** (**A**) Single clones selected for whole genome sequencing cultivated on BG11 agar (100 µE, 30 °C, 5 days) displayed pronounced differences in growth, pigmentation, and (**B**) basic chl_a fluorescence F_o. (**C**, **D**) F_v/F_m distributions obtained from four plate replicates differed strongly from one another in both original clone isolation plates (**C**; see Fig 3.6) and after selection of four representative clones each (**D**). Diamonds correspond to outliers ranging beyond ±1.5 standard deviations.

Beyond single clones, whole batch genomic DNA was sequenced for batch cultures representing branching points of the experimental pedigree (see Fig. 3.2). Like this, single alleles could later be traced backwards in time in order to reconstruct approximate time points of their emergence, as well as the sequence of allelic haplotype evolution.

3.1.3 Evolved *Synechocystis* genome re-sequencing and candidate mutations

Genome sequencing data analysis was conducted by our collaboration partners Dr. Edgardo Oritz Valencia and Prof. Dr. Hanno Schäfer at the WZW (TU Munich, Freising, Germany). Genome and phylogenetic data presented below was provided by Dr. Edgardo Oritz Valencia. Single nucleotide polymorphisms (SNPs) were identified as deviations from the published Synechocystis WT genome sequence (Kaneko and Tabata 1997). *Figures were prepared by Marcel Dann.*

Overall average genome coverage for isolated-clone whole-genome re-sequencing (Fig 3.8 A) was 997±115-fold. For batch cultures, overall coverage was 1001±218-fold. Averages of median insert sizes of sequencing libraries were 309±9 bp for either group, respectively. The total amount of detected single nucleotide polymorphisms (SNPs) did not differ in a consistent manner between WT control clones and high-light adapted clones with respect to intergenic regions, nonsense mutations (i.e. giving rise to a stop codon), non-synonymous mutations (i.e. giving rise to amino-acid exchanges), or synonymous mutations (i.e. not affecting the encoded amino acid; Fig 3.8 B). Overall SNP count patterns (i.e. lower or higher numbers of any kind of SNPs in general) were consistent within same-clone sequencing data, however. The number of newly acquired high-allele frequency (> 75 %) non-synonymous (non-syn) and synonymous (syn) SNPs was increased two- to five-fold in high light adapted clones as compared to WT controls (Fig 3.8 C, D). For synonymous and nonsense SNPs, no changes in the distribution of SNPs among codon positions 1–3 were observed, while for non-synonymous mutations a shift from predominantly first position SNPs in WT to predominantly second position SNPs in high-light adapted clones was observed (Fig 3.8 E). Maximum likelihood phylogenetic reconstruction based on single-clone genome data (Fig 3.8 F) partially recovered the experimental mutant pedigree (see Fig 3.2). Lineages UMUM and UMUMM that were separated early from other lineages clustered as expected, while later derivates of the UM lineage were not resolved into separate lineages reliably, but clustered with the non-mutagenized evolved WT* lineage.

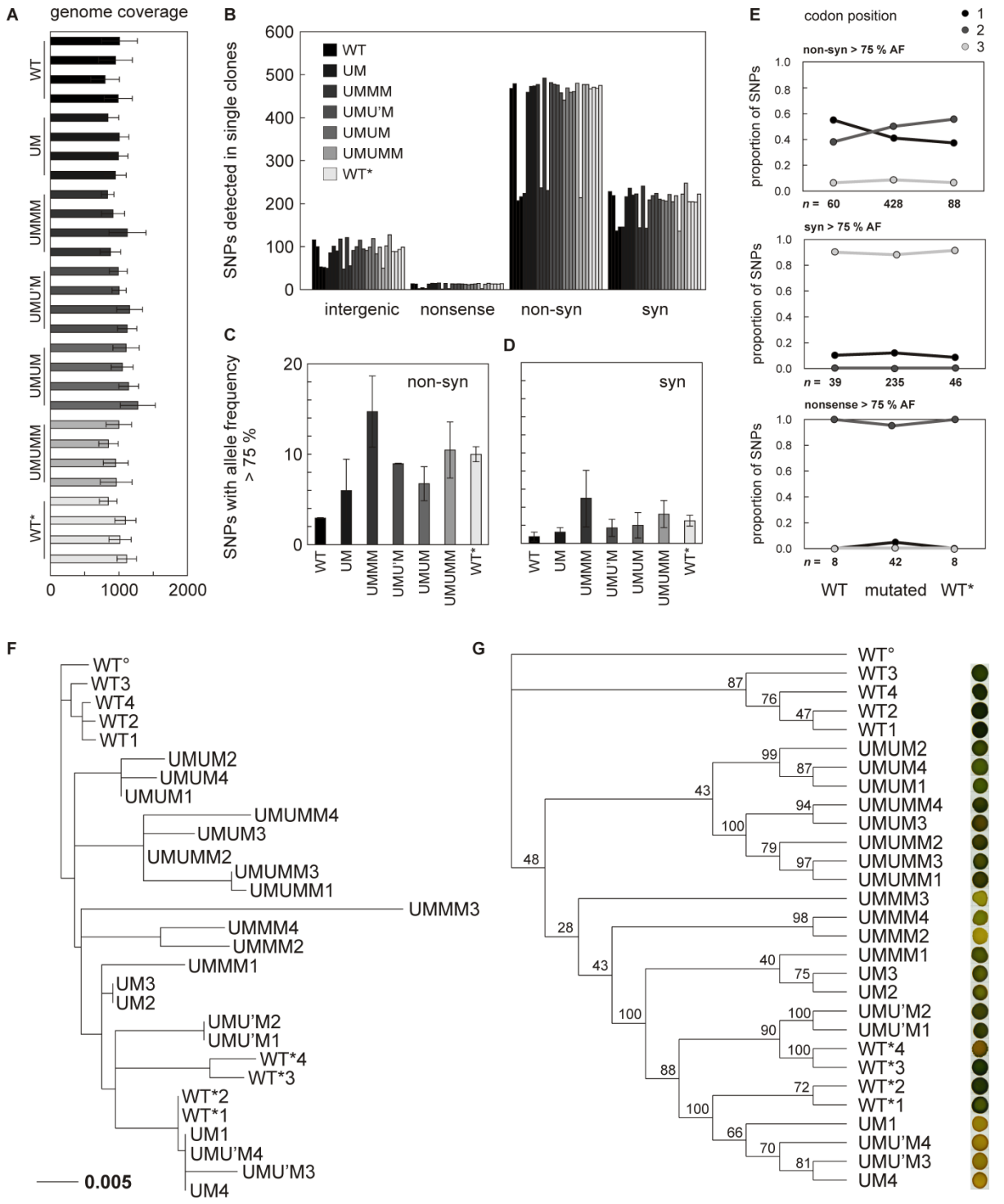

Fig 3.8. **Graphical summary of single clone whole genome sequencing data.** (**A**) Average *fold*- genome coverages of four single clones per experimental lineage plus/minus standard deviation. (**B**) Total number of identified SNPs (i.e. deviation from the reference genome; Kaneko and Tabata 1997) resulting in intergenic, nonsense, non-syn(onymous) and syn(onymous) mutations. Data corresponds to four clones per experimental lineage (from left to right: 1-4, respectively). (**C**) Average number of high frequency (>0.75) non-synonymous mutations over four clones of respective experimental lineage plus/minus standard deviation. (**D**) Average numbers of high frequency (>0.75) synonymous mutations over four clones of respective experimental lineage plus/minus standard deviation. (**E**) Codon positions of high allele frequency (>0.75) SNPs resulting in non-synonymous, synonymous, and nonsense mutations, separated into WT control (WT), artificially mutagenized and evolved clones (mutated), and non-mutagenized evolved WT clones (WT*). (**F**) Maximum likelihood tree for single clone whole genome sequences; the tree is drawn to scale, with branch lengths measured in the number of substitutions per site (see scale bar). (**G**) The consensus tree topology over 100 bootstrapping replicates is shown. The percentage of replicate trees in which the associated taxa clustered together in the bootstrap test is shown next to the branches. *Synechocystis* culture drops corresponding to the sequenced clones are shown next to their respective tips on the consensus topology tree.

We identified a total of 228 non-synonymous SNPs with allele frequency > 0.75 in our 24 sequenced high-light adapted clones, and 12 such SNPs in the control WT. While most alleles occurred only once in individual clones and most genes were only represented once, a small set of 12 protein coding genes acquired multiple mutations along several independent evolutionary pathways (Tab 3.1), indicating pronounced significance of these genes to evolved high-light tolerance. The comparably small overlap regarding mutational content was unsurprising, since maximum phenotypic diversity of clones was selected for prior to genome re-sequencing.

3.1.4 Experimental assessment of high-light adaptive candidate alleles

In order to evaluate the effect of individual candidate alleles, a variant of a marker-less gene replacement strategy developed in our lab (Viola et al. 2014) was designed. *Allele swapping* of high-light adapted and wildtype alleles was designed to (i) at no time disrupt the full coding sequence length of the gene of interest, and (ii) leave behind the exact genomic conformation of WT with the exception of a single nucleotide exchange after deleting the double selection cassette (Fig 3.9). Like this, expression rates and gene dosage would remain unaltered, so that artificially high-light adapted strains recapitulate the situation of evolved clones as exactly as possible.

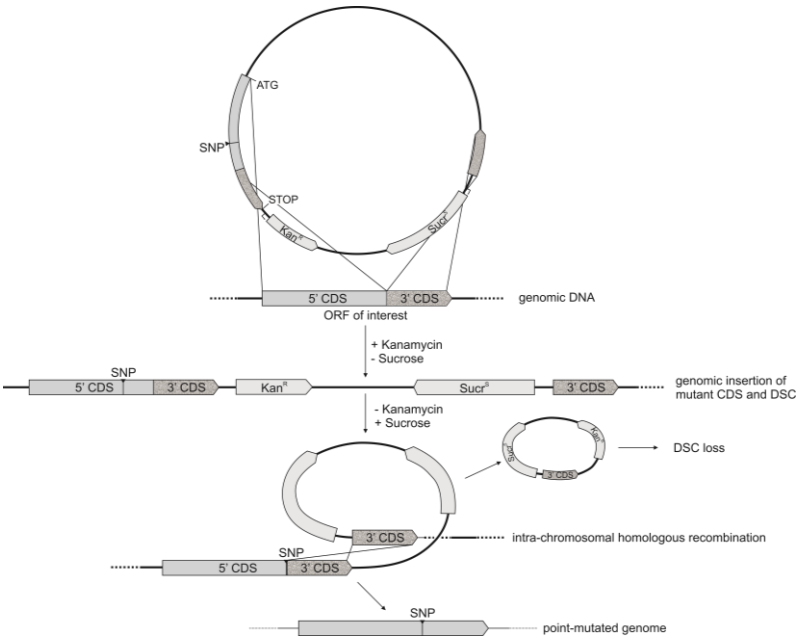

Fig 3.9. ***Allele-swapping*** **strategy based on marker-less gene replacement**. The whole coding sequence (CDS) of the gene of interest was cloned into a *Synechocystis* non-replicative vector 5' of a kanamycin resistance (Kan^R) / sucrose sensitivity ($Sucr^S$) double-selection cassette (DSC), followed by 500 bp of the 3' end of the CDS. Point mutations were introduced by Q5® site-directed mutagenesis. Clones having incorporated the construct into their genome by homologous recombination were selected on kanamycin, replacing the original allele by the allele of interest in the process. Upon full segregation, removal of kanamycin from the media allowed for intrachromosomal homologous recombination of the redundant 3' CDS stretches, removing the DSC from the genome and leaving behind only the to-be-introduced point mutation. Clones devoid of the DSC were selected on 5 % w/v sucrose agar, and point mutations were confirmed by Sanger sequencing.

Tab 3.1. **Overview on all genes with two or more independent non-synonymous mutations.** Genes including corresponding genomic ORFs are categorized by biological processes they are involved in. Annotated functions and detected amino-acid exchanges are listed for each gene. # non-syn = number of independent non-synonymous mutations. a, UM; b, UMMM; c, UMU'M; d, UMUM; e, UMUMM; f, WT; g, WT*. Candidate mutations HL1 and HL2 used for consecutive adaptive allele experimental verification are highlighted in **bold** font.

Gene	Function/annotation	# non-syn	Origin						
			a	b	c	d	e	f	g
Transcription									
rpoC1 (slr1265)	RNA polymerase γ-subunit	3		x	x	x	x		
	K226E, K504I, D551V								
sigA/*rpoD1* (slr0653)	principal RNA polymerase sigma factor	4				x	x	x	
	R96L, K206R, Q316R, M383K								
sigC (sll0184)	group2 RNA polymerase sigma factor	2		x			x		
	A274V, E298V								
kaiC-like protein 1 (sll1595)	circadian clock protein homolog	2				x	x		
	F337S, K395E								
Translation									
fusB (sll1098)	elongation factor G2	7	x	x	x				x
	R29Q, D138N, D189G, V284A,								
	K304N, Y328N, **R461C** (***HL2***)								
Photosynthesis/Respiration									
ndhF1 (slr0844) *ndhF3* (sll0026)	NDH complex subunit 5	3		x					x
	NdhF1: **F124L** (***HL1***)								
	NdhF3: A283D, A347G								
Metabolism									
slr2124	3-oxoacyl-[acyl-carrier protein] reductase	4		x		x			
	L57P, L116H, I126T, F230L								
ppc (sll0920)	phosphoenolpyruvate carboxylase	2	x				x		
	T252M, R1031C								
pykF (sll1275)	pyruvate kinase 2	2				x		x	
	A260V, P406T								
spoT (slr1325)	Probable guanosine-3',5'-bis(diphosphate)	2		x					
	3'-pyrophosphohydrolase								
	N202D, Q416R								
Unknown function									
slr6022	transmembrane protein, unknown function	2		x					
	G136A, S138G								
ssr5117	HicB family protein, unknown function	2	x						x
	A38T, R47H								

Consecutive to allele swapping, the high-light adaptive value of candidate alleles was assessed by applying the original selective regime used in the first step of the experiment (i.e. 700 µE, 23 °C, atmospheric aeration). Evolved alleles were hypothesized to confer better adaptation as compared to WT alleles at least under this degree of high light stress.

3.1.5 Tested candidate alleles

Out of the genes hit multiple times, *ndhF1* (slr0844 encoding an isoform of the NAD(P)H-plastoquinone oxidoreductase subunit 5) and *fusB* (sll1098 encoding elongation factor EF-G2) were chosen for a proof of concept regarding adaptiveness of our evolved SNPs. The NDH complex confers the largest proportion of *Synechocystis* CEF around PSI; thus, it is a major contributor to PSI photoprotection (Gao et al. 2016) and a mutation of a core-subunit protein might well be of immediate relevance for cyanobacterial photosynthetic high-light tolerance. EF-Gs have already been described to be involved in D1 protein expression and turnover in a redox-regulated manner (Kojima et al. 2007), and cysteine constitutive reduction mimetic mutants have been found to express approximately 40 % more D1 within a 60 min time course (Kojima et al. 2009). Thus, the additional alleles we evolved represent good candidates to enhance D1 steady state accumulation under high-light stress.

3.1.5.1 HL1: NdhF1$_{F124L}$ (Slr0844)

NdhF1 is an isoform of the structurally essential subunit 5 of the NDH complex and an eleven-transmembrane helix thylakoid protein involved in proton translocation across the thylakoid membrane (Battchikova and Aro 2007, Saura and Kaila 2019). NdhF isoforms are specific to certain NDH complex isoforms, with NdhF1 being prevalent in NDH-1L/L' which confers respiration and CEF (Battchikova et al. 2011 and references therein).

A potentially high-light adaptive F124L mutation was found in NdhF1 (encoded by ORF slr0844). A multi-species protein sequence alignment of NdhF homologues (Fig. 3.10) revealed the mutated site F124 to be highly conserved in the NdhF primary structure. F124 resides at the N-terminal luminal end of NdhF transmembrane helix 4 and is conserved across the green lineage, and even the homologous position in *Bacillus subtilis* is occupied by a physio chemically similar aromatic residue (tyrosine Y).

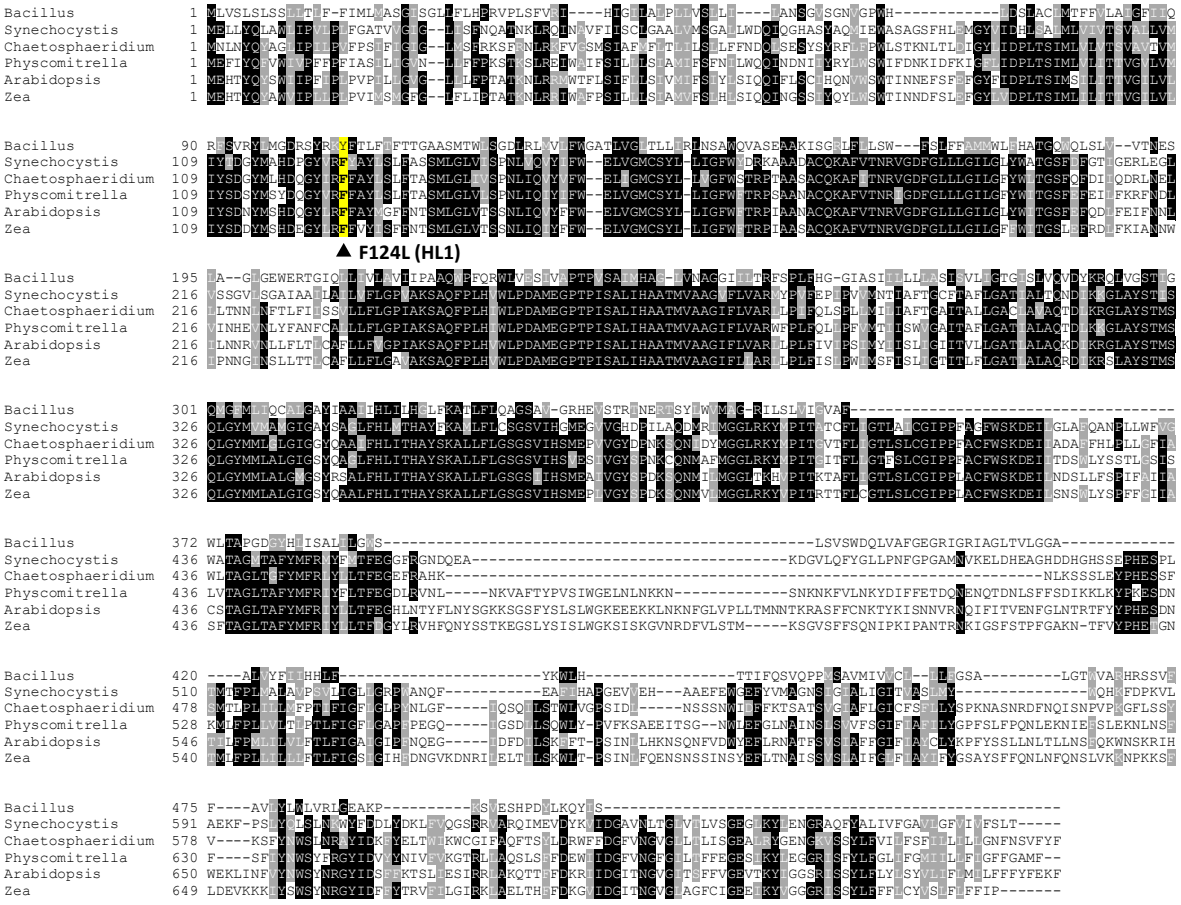

Fig 3.10. **The mutated position in NdhF is conserved across photosynthetic taxa.** The HL1 amino acid exchange (F124L; highlighted in yellow) is strictly conserved in photosynthesizers, and similar in the heterotrophic bacterium *Bacillus* (*subtilis*; Firmicutes), implying structural and/or functional relevance of the mutated residue. *Synechocystis* (spec. PCC6803; Cyanophyceae/cyanobacteria), *Chaetosphaeridium* (*globosum*; Charophyta/green algae), *Physcomitrella* (*patens*; Bryophyta/mosses), *Arabidopsis* (*thaliana*; dicotyledons), *Zea* (*mays*; monocotyledons). Note that *Chlamydomonas* does not possess an ndhF gene and was thus substituted for with another green alga, *Chaetosphaeridium globosum*. NCBI IDs of protein sequences used are provided in Methods (Tab 2.5).

3.1.5.2 HL2: EF-G2$_{R461C}$ (Sll1098)

A subset of HL mutations we detected were found to induce amino-acid exchanges R29Q, D138N, D189G, V284A, K304N, Y328N, and R461C in elongation factor G2 (EF-G2; Sll1098). A multi-species protein sequence alignment of Sll1098 homologues (Fig. 3.11) revealed mutated positions arginine R29, aspartate D138, tyrosine Y328, and arginine R461 to be strictly conserved across the green lineage and down to *Bacillus subtilis*. Aspartate D189 has been found to be conserved in bacteria and to be replaced by the similar glutamate (E) in most assayed plants, with exception of *Physcomitrella patens*. The position homologous to *Synechocystis* EF-G2 valine V284 is partially occupied with the similar amino acids leucine (L) or isoleucine (I) and hence conserved regarding physiochemical properties. The position homologous to *Synechocystis* EF-G2 lysine K304 is atypical and otherwise mostly occupied by acidic residues.

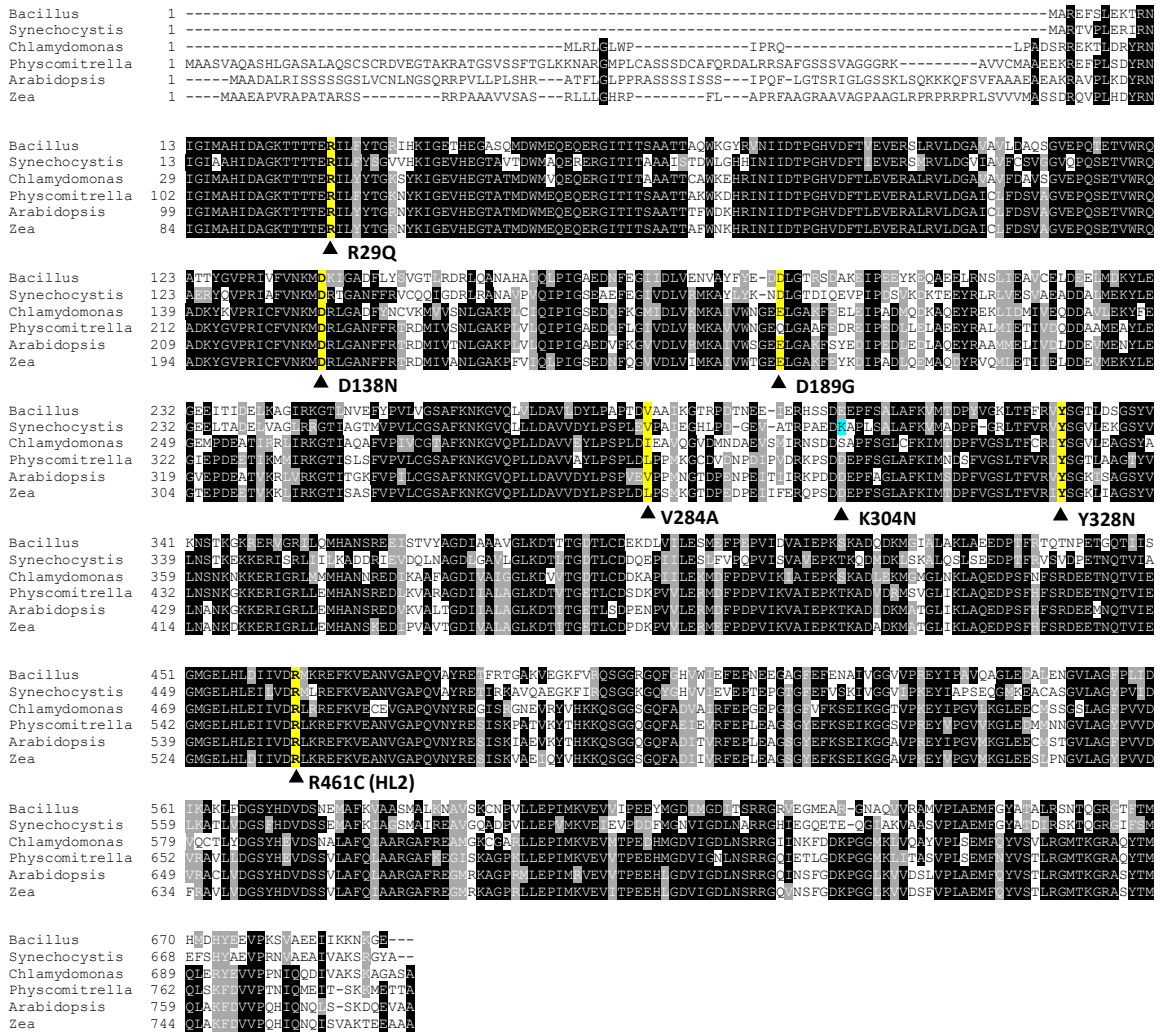

Fig 3.11. **The positions mutated in *Synechocystis* EF-G2 are mostly conserved across plant and bacterial taxa.** Four out of seven mutated positions are strictly conserved across *Synechocystis* EF-G2 homologues (R29, D138, Y328, R461; highlighted yellow + **bold** font). Two positions are occupied by mostly (D189; Q in *Chlamydomonas*) or exclusively (V284; I in *Chlamydomonas*; L in *Physcomitrella* and *Zea*) similar amino acids (highlighted yellow + normal font). One mutated position (K304) is private to *Synechocystis* (highlighted cyan). *Bacillus* (*subtilis*; Firmicutes), *Synechocystis* (spec. PCC6803; Cyanobacteria), Chlamydomonas (reinhardtii; Chlorophyceae), *Physcomitrella* (*patens*; Bryophyta), *Arabidopsis* (*thaliana*; Dicotyledons), and *Zea* (*mays*; Monocotyledons). NCBI IDs of protein sequences used are provided in Methods (Tab 2.5).

3.1.6 Reconstitution of mutant alleles confers elevated high-light tolerance in *Synechocystis* WT background

The candidate mutations NdhF1 F124L and FusB/EF-G2 R461C (hereafter termed HL1 and HL2, respectively) were confirmed to confer enhanced high-light tolerance at 700 µE and 23°C as compared to WT cells in terms of pigment and biomass accumulation (Fig 3.12 A). Under control low light of 50 µE, cellular chlorophyll a content was found reduced in both HL1 (-16 %) and HL2 (-9 %) as compared to WT. Cellular carotenoid contents, however, were significantly increased in both HL1 (+53 %; $P = 4.6*10^{-4}$) and HL2 (+25 %; $P = 2.2*10^{-2}$). Under high light of 700 µE, cellular chlorophyll a content was found increased in both HL1 (+31 %; $P = 5.6*10^{-2}$) and HL2 (+28 %; $P = 4.0*10^{-2}$)

as compared to WT. Cellular carotenoid contents were significantly increased in both HL1 (+56 %; $P = 4.5*10^{-3}$) and HL2 (+32 %; $P = 3.7*10^{-2}$) at 700 µE (Fig 3.12 B).

Under control low light of 50 µE, average biomass accumulation per culture volume was found reduced in both HL1 (-21 %; $P = 2.5*10^{-1}$) and HL2 (-35 %; $P = 1.5*10^{-1}$) as compared to WT. Under high light, however, average biomass accumulation was found increased in both HL1 (+32 %; $P = 5.6*10^{-2}$) and HL2 (+24 %; $P = 7.8*10^{-2}$) as compared to WT (Fig 3.12 C).

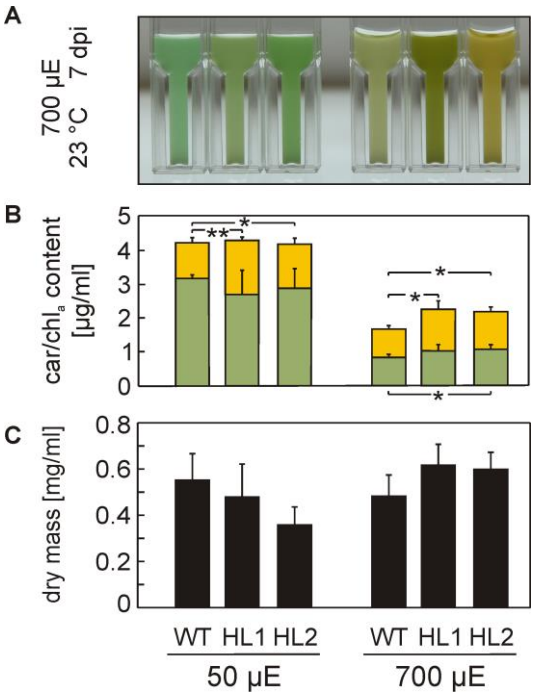

Fig 3.12. **High-light adaptiveness of candidate alleles HL1 and HL2.** (**A**) Culture phenotype of WT, HL1 ($NdhF1_{F124L}$) and HL2 ($EF\text{-}G2R_{461C}$) cells 7 days past inoculation (dpi) under high light treatment (700 µE, 23 °C). Cultures were inoculated at initial OD_{730} = 0.05. (**B**) Methanolic pigment extracts of cellular chlorophylls (green) and carotenoids (yellow) corresponding to OD_{730} = 0.75 cells. (**C**) Biomass accumulation per ml of final culture. Statistically significant differences with $P \leq 0.05$ (*) or $P \leq 0.01$ (**) according two-sided Student's *t*-tests Holm-corrected for multiple simultaneous comparisons of HL mutants to the respective WT control (* $P \leq 0.05$, ** $P \leq 0.01$). Results of 4 independent experiments for each HL mutant with double amount of WT controls are shown. Bar charts represent averages with standard deviations.

3.1.7 Physiological and biochemical assessment of adaptive mechanisms

Photosynthesis was strongly affected by both the HL1 and HL2 mutations. Observed effects were, however, qualitatively distinct and contrary despite resulting in similar degrees of high light tolerance. While HL1 displayed delayed PSI-reaction-center oxidation under far-red (FR) light and faster re-reduction upon its offset, in HL2 oxidation and re-reduction were accelerated and delayed, respectively (Fig 3.13 A). Time passed until oxidation/re-reduction of half of the P700 population ($t_{0.5}P700_{ox}/t_{0.5}P700^{+}_{red}$) was used as a comprehensive measure to quantify the according kinetics. Direct comparisons of revealed significant differences for $t_{0.5}P700_{ox}$ between WT and HL1 (+50 %; $P = 5.4*10^{-8}$) and WT and HL2 (-51 %; $P = 4.3*10^{-8}$), as well as for $t_{0.5}P700^{+}_{red}$ between WT and HL1 (-87 %; $P = 2.4*10^{-5}$) and WT and HL2 (+59 %; $P = 1.7*10^{-3}$) upon on- and off-set of FR light, respectively (Fig 3.13 B).

Chlorophyll-a-fluorescence measurements revealed significantly decreased F_v/F_m in HL1 (-11 %; $P = 8.9*10^{-7}$), and significantly increased F_v/F_m in HL2 (+12 %; $P = 9.6*10^{-9}$; Fig 3.13 C/D). Moreover, in HL2, a pronounced P700 over-reduction upon offset of actinic light exciting both PSII and PSI was observed (Fig 3.13 A), implying increased PSII capacity to donate electrons to PSI. Basic fluorescence F_o was observed to be altered in mutants as well. In both, HL1 and HL2, F_o was reduced as compared to WT, however, and hence could not explain the contrasts in PSII maximum quantum yield F_v/F_m we observed.

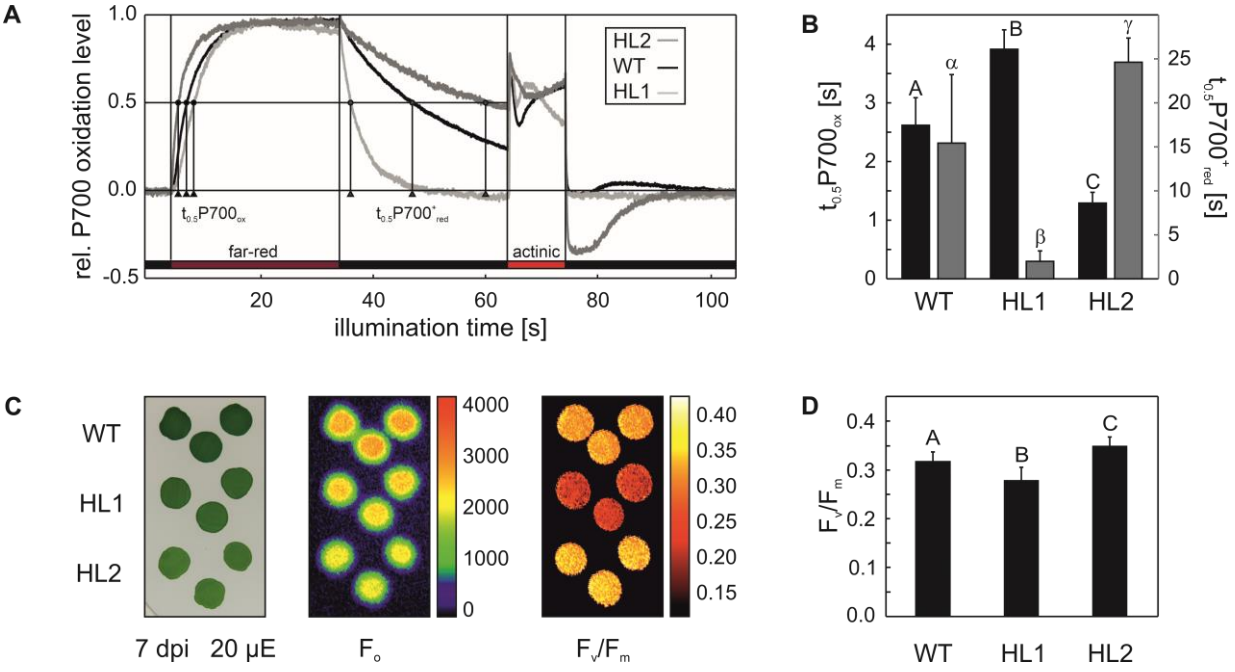

Fig 3.13. **Photosynthetic performance of PSI and PSII is differentially affected in candidate mutants HL1 and HL2.** (**A**) PSI reaction center P700 oxidation kinetics of WT, HL1 and HL2 under far-red (FR) and actinic light (AL) treatment measured as differential absorbance change ΔI/I at 830/875 nm wavelength. Half times of P700 oxidation ($t_{0.5}P700_{ox}$) and $P700^+$ re-reduction ($t_{0.5}P700^+_{red}$) are indicated with black and grey triangles, respectively. Dark red bar indicates FR illumination, and light red bar indicates AL illumination. (**B**) Mean $t_{0.5}P700_{ox}$ (black bars) and $t_{0.5}P700^+_{red}$ (grey bars) with standard deviations for *n* = 8/7/15 measurements in HL1/HL2/WT from a total of 4 independent experiments. Cells were cultivated for seven days at 30 °C and 30 µE of constant light, concentrated to OD_{730} = 5, and dark-incubated for 16 hours prior to measurement. (**C**) Chlorophyll fluorescence measurements on culture drops seven days past inoculation (dpi) grown at 20 µE low light and 30 °C. F_o, basic fluorescence; F_v/F_m PSII maximum quantum yield. (**D**) Mean F_v/F_m with standard deviations for *n* = 18/24/42 measurements in HL1/HL2/WT from a total of four independent experiments. Letters in (**B**) and (**D**) correspond to statistically significant differences with $P \leq 0.05$ according to one-way ANOVA and post-hoc Tuckey HSD test. Experiments were performed with the same cultures (four biological replicates of HL1 and HL2; eight biological replicates for WT) described in in Fig 3.12.

The HL1 and HL2 mutants were assayed for photosynthetic marker protein accumulation (Fig 3.14). For HL1, immunoblot detection indicated lower accumulation of PSII (-49 % D1) and higher accumulation of PSI (+135 % PsaC) under low light as compared to WT. Also, under high light, HL1 accumulated less PSII (-54 % D1) but more PSI than WT cells (+59 % PsaC).

For HL2, immunoblot detection indicated increased accumulation of both PSII (+170 % D1) and PSI (+263 % PsaC) under 50 µE low light intensity as compared to WT. Under 700 µE high light intensity, HL2 still accumulated more PSII (+147 % D1, but slightly less PSI than WT cells (-7 % PsaC).

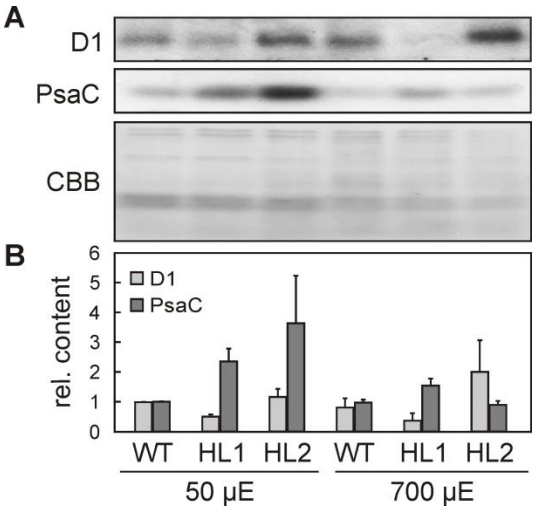

Fig 3.14. **PSI and PSII marker protein accumulation is differentially affected in HL1 and HL2 in both high and low light.** (**A**) Immunoblot detection of photosystem marker protein accumulation. D1 (PSII) and PsaC (PSI) were detected in whole cell protein extracts corresponding to OD_{730} = 0.3 cells. Cells were grown for seven days at 23 °C under continuous illumination and atmospheric aeration. Signals representative for *n* = 3 replicates are shown. A Coomassie Brillant Blue (CBB) staining of the blot is provided as loading control. (**B**) Marker protein content in OD-normalized samples relative to the WT 50 µE control (mean and standard deviation for *n* = 3 replicates). Protein extracts were derived from the same cultures described in Fig 3.12.

In summary, both candidate alleles could be shown to confer enhanced high-light tolerance in *Synechocystis* sp. PCC6803 WT cells. The underlying physiological reactions appear to differ drastically from each other, however, encompassing opposite effects on PSI and PSII photosynthetic parameters and protein accumulation trends, as well as obvious differences in liquid-culture phenotypes. Therefore, from observations of just two tested candidate alleles we infer that similar levels of high-light tolerance can be achieved by altering seemingly unrelated and opposite cellular processes.

3.2 Results cyclic electron flow (CEF)

3.2.1 Preface

CEF around photosystem I (PSI) is an essential and apparently rather ancient mechanism of photosynthetic resilience, protecting cyanobacterial and plant photosynthesis from environmental detriment in very similar fashions. CEF is not restricted to a single pathway, but rather a network of several partially redundant electron transport routes. One of these routes designated "antimycin A-sensitive CEF" depends on the highly conserved protein PGR5 in both cyanobacteria and plants. PGR5 in turn requires an additional component in plants, PGRL1, to fully function.

In the model plant *Arabidopsis,* the nuclear encoded *PGR5* gene (At2g05620) encodes a small protein with a predicted molecular weight of approximately 14 kDa, approximately 6 kDa of which correspond to a chloroplast transit peptide (cTP) which is cleaved off upon plastid import. Apart from a short plant-specific N-terminus of approximately 6 aa (Sugimoto et al. 2013), the protein sequence is remarkably conserved from cyanobacteria to higher plants (Fig 3.15).

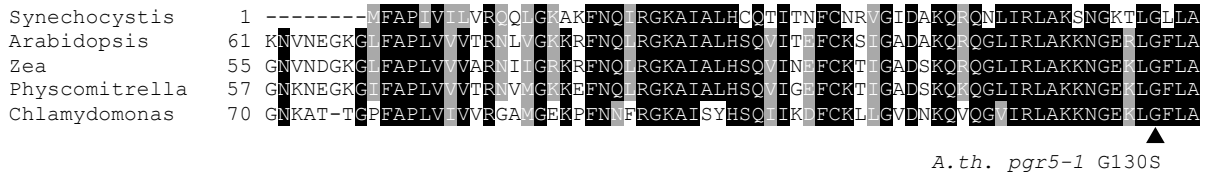

Fig 3.15. **Sequence alignment of mature PGR5 proteins.** Residues conserved/similar in ≥ 70 % of sequences are highlighted in black/grey. The position of a non-synonymous mutation giving rise to the original *Arabidopsis pgr5-1* mutant phenotype (glycine 130 to serine G130S; Munekage et al. 2002) is indicated (black triangle). Genus names displayed short for *Synechocystis* (sp. PCC6803), *Chlamydomonas* (*reinhardtii*), *Physcomitrella* (*patens*), *Arabidopsis* (*thaliana*), *Zea* (*mays*).

Experimental evidence for similar molecular functions of PGR5 exists for *Synechocystis* (Ssr2016; Yeremenko et al 2005), *Chlamydomonas* (Johnson et al. 2014), *Pinus* (Sugimoto et al. 2013) and rice (Nishikawa et al. 2012). A function of PGR5 as electron shuttle has been suggested due to the presence of potentially redox-active cysteine residues, one of which is strictly conserved throughout the green lineage. PGR5 is localized on the stromal face of the thylakoid membrane, but seems not to be a transmembrane protein itself (Munekage et al. 2002). Rather, it displays an estimated net charge of +11 at pH 7 which might facilitate adsorption to the negatively charged phospholipid bilayer surface of the thylakoid membrane, or mediate electrostatic interactions with negatively charged thylakoid proteins. Several direct interaction partners of PGR5 have been identified, among which there are Cyt b_6 and Fd, as well as the plant-specific transmembrane protein PGRL1 (DalCorso et al. 2008).

The *Arabidopsis* genome encodes two functionally redundant PGRL1 homologues, atPGRL1A (At4g22890) and atPGRL1B (At4g11960). A double knockout of *PGRL1A* and *PGRL1B* causes a proton gradient (mis)regulation phenotype very similar to that of *pgr5* (hence *pgrl1* = *pgr5-like photosynthetic phenotype* 1; DalCorso et al. 2008). PGRL1 is a two-transmembrane-helix thylakoid protein with stromally exposed N- and C-termini. It is essential for efficient PGR5-protein accumulation in plants (DalCorso et al. 2008), contains three pairs of putatively redox-sensitive cysteine residues, and has been suggested as a possible candidate for the elusive FQR (Hertle et al. 2013). The molecular interaction between PGRL1 and PGR5 has been investigated by yeast-two-hybrid assay (DalCorso et al. 2008) and *in vitro* pulldown assays, the latter of which indicated protein–protein interaction with the stromally exposed C-terminus of PGRL1 (Hertle et al. 2013). In addition, *pgr5* plants accumulate less PGRL1 protein, indicating that reciprocal regulation of protein accumulation is exerted by either component (DalCorso et al. 2008). PGRL1 was found to have a similar yet broader interactome as compared to PGR5, containing Fd and Cytb_6, FNR1/2, and PSI-D (DalCorso et al. 2008). While the observed *pgr* phenotype, as well as the involvement with a set of (putatively) CEF-associated proteins (Bendall and Manasse 1995), serve as viable indication of PGRL1 being a key component of AA-sensitive CEF, its precise role is matter of an ongoing debate. Recent experiments in *Chlamydomonas* (Nawrocki et al. 2019) and *Arabidopsis* (our group; unpublished) imply PGRL1 to play a modulatory role in PGR5-mediated CEF rather than being the very enzyme catalyzing its core reaction. This raises questions about the reliability of *in vitro* enzyme activity assays conducted with a PGRL1*PGR5 complex (in which case the latter was notably still in possession of its otherwise to-be-removed cTP, and thus an additional and potentially redox-active cysteine residue), which demonstrated oxidation of FD_{red} and subsequent reduction of a PQ analogue in the presence of PGRL1*PGR5.

In order to elucidate the actual function of the PGRL1/PGR5 couple, we decided to employ an orthogonal yet photosynthetically active working system in the form of *Synechocystis*. True orthogonality (i.e. functional independence of PGRL1*PGR5 on *Synechocystis* endogenous CEF components and an according gain-of-function regarding CEF activity upon heterologous expression) could turn out a crucial piece of evidence to discriminate between the suggested accessory and mechanistic roles of PGRL1/PGR5 in CEF around PSI. Moreover, identifying novel components in *Synechocystis* PGR5-mediated CEF may allow us to trace back the evolutionary pathway leading from NDH-centered CEF in cyanobacteria towards PGR5-centered CEF in higher plants.

3.2.2 Establishment of *Arabidopsis* PGR5-dependent CEF in *Synechocystis*

The results presented in sections 3.2.2 and 3.2.3 have in part been published in *Nature Communications* (Dann and Leister 2019).

3.2.2.1 Introduction of *Arabidopsis*-gene expression systems in *Synechocystis*

In order to establish atPGRL1/atPGR5-dependent CEF around PSI in *Synechocystis*, a deletion mutant of the endogenous synPGR5-encoding open reading frame (ORF) ssr2016 (*Δsynpgr5*; Fig 3.16 A) was used as genetic background for heterologous CEF installation to avoid interference of the highly conserved synPGR5 with the introduced *Arabidopsis* components.

Upon genomic segregation (Fig 3.16 B), our *Δsynpgr5* mutant was confirmed to be more sensitive to high light than WT (Fig 3.16 D) and to display higher PSI-oxidation rates under far-red (FR) light, as well as lower re-reduction rates upon offset of FR illumination, implying lower CEF activity (Fig 3.16 D). Both phenotypes were in line with observations of a former study investigating an independent *ssr2016* knockout mutant (Yeremenko et al. 2005). Hence, *Δsynpgr5* was considered a suitable platform for further experiments.

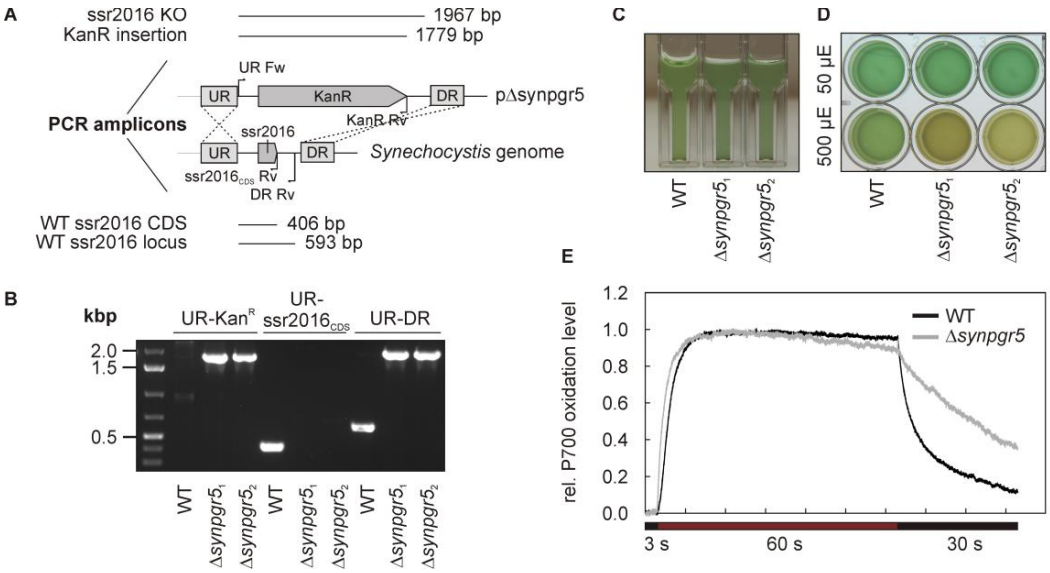

Fig 3.16. **Generation of an ssr2016 deletion mutant (Δ*synpgr5*).** (**A**) Design of the genomic knockout construct. A kanamycin-resistance kassette (Kan^R) was introduced into the genomic ssr2016 ORF encoding synPGR5 by homologous recombination *via* ~700 bp of genomic DNA sequence 5' (upstream region UR) and 3' (downstream region DR) of ssr2016, using a non-replicative vector as shuttle. Genotyping primer binding sites with 5'-3' orientation are indicated by labeled arrows. Expected amplicon origins and sizes are indicated. (**B**) Genomic replacement of ssr2016 by Kan^R and full segregation of the ssr2016 deletion (Δ*synpgr5*) were confirmed by PCR. (**C**) Δ*synpgr5* does not display an obvious phenotype under standard growing-light intensity of 30 µE. (**D**) Δ*synpgr5* does not differ from WT cell phenotype at 50 µE, but bleaches under elevated light intensities of 500 µE. (**E**) P700 oxidation of Δ*synpgr5* upon far red light (red bar) onset is accelerated, and P700 re-reduction upon offset is delayed.

In order to assess heterologous atPGRL1 and atPGR5 functionality reliably, robust expression of the *Arabidopsis* components had to be achieved. Hence, *Arabidopsis* coding sequences for PGR5 (*atPGR5*) and PGRL1A (*atPGRL1A; hereafter atPGRL1*) were expressed under the control of the *Synechocystis* D1 promoter (*PpsbA2*), a widely used promoter yielding high and robust expression rates (Englund et al. 2016). Originally contained sub-sequences encoding N-terminal chloroplast transit peptides according to ChloroP prediction (see methods 2.12) were deleted to obtain the respective mature *Arabidopsis* proteins in *Synechocystis.* Deleted subsequences spanned residues 2–60 for atPGRL1, and residues 2–44 for atPGR5, respectively.

Expression strains were generated by incorporation of gene cassettes with *PpsbA2*:*atPGRL1*, *PpsbA2*:*atPGR5*, *PpsbA2*:*atPGRL1* + PpsbA2:*atPGR5,* or into a genomic *neutral site* (slr0168) by homologous recombination. Likewise, over-expression (OE) strains of N- or C-terminally 6xHis-tagged synPGR5 protein were generated as intended positive controls for enhanced CEF activity, harboring either *PpsbA2*:6xHis-*synPGR5 or PpsbA2*:*synPGR5*-6xHis expression cassettes in the *neutral site*. See Fig 3.17 A–D for construct and recombination maps. Transgene presence and mutational segregation were verified by PCR (Fig 3.17 E).

Heterologous expression of atPGRL1 and/or atPGR5 was confirmed on the protein level by immuno-detection. In *Arabidopsis,* PGRL1 and PGR5 have been shown to be integral or peripheral thylakoid membrane proteins, respectively. Consistently, in *Synechocystis*, both proteins could only be detected in the membranous, but not in the soluble fraction of cellular protein preparations. Intriguingly, strains co-expressing atPGRL1 and atPGR5 were found to accumulate higher amounts of atPGR5 (Fig 3.18).

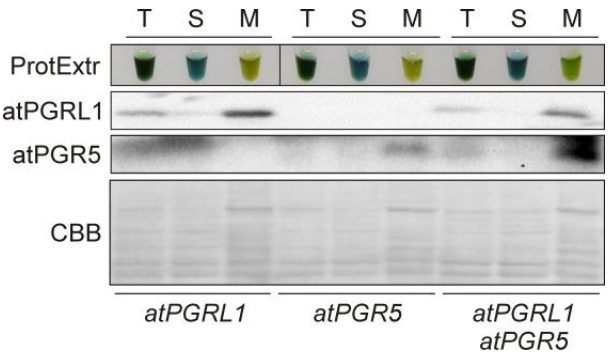

Fig 3.18. **Subcellular localization of atPGR proteins in *Synechocystis* expression strains.** Immunodetection of atPGRL1 and atPGR5 in the membranous fraction of according expression strain protein extracts (ProtExtr). Soluble (S) fractions are blue due to phycobiliproteins; membrane (M) fractions are green-yellow due to chlorophylls and carotenoids; Total (T) protein extracts are blue-green, accordingly. 50 µg of protein were separated by SDS-PAGE and blotted onto PVDF by capillary transfer with PBS prior to chemiluminescent immunodetection of PGRL1 and PGR5. Coomassie Brilliant Blue (CBB) staining of the PVDF membrane served as a loading control. All strains have been generated in the Δ*synpgr5* background.

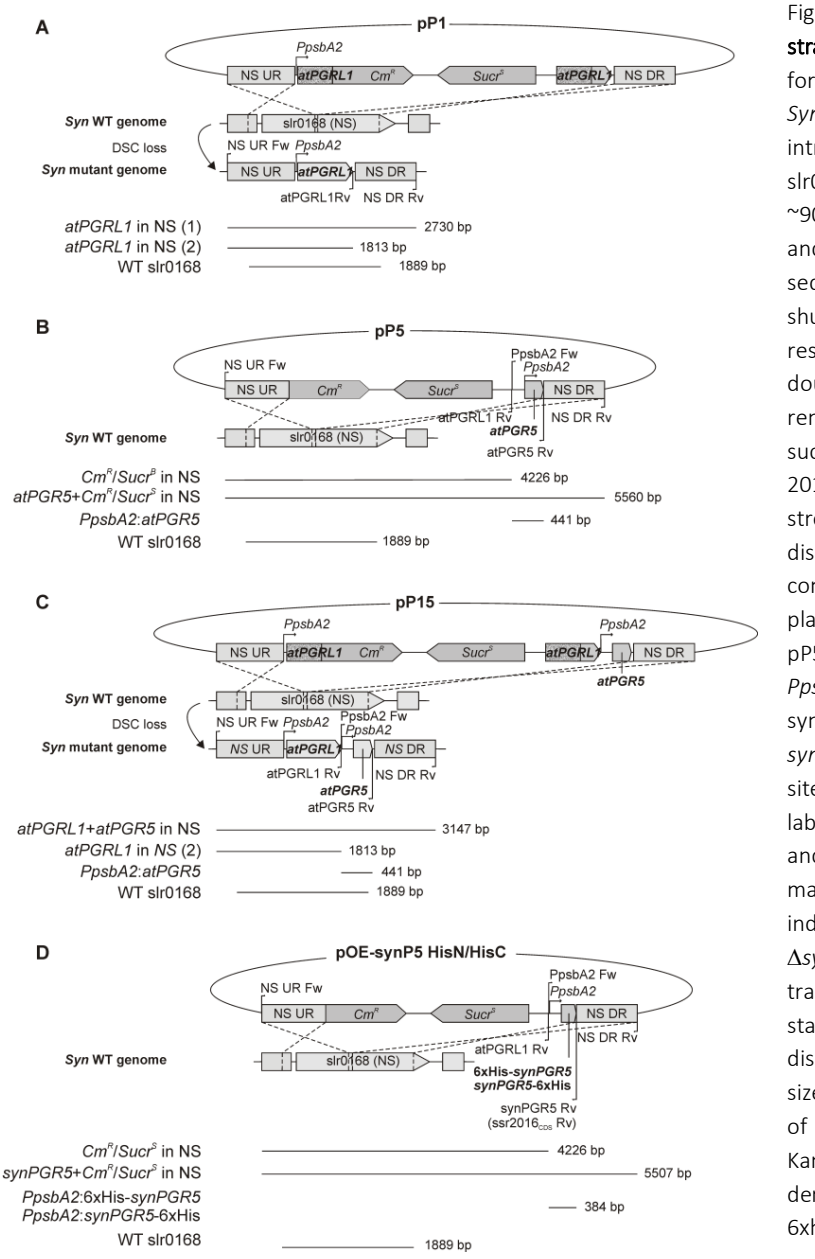

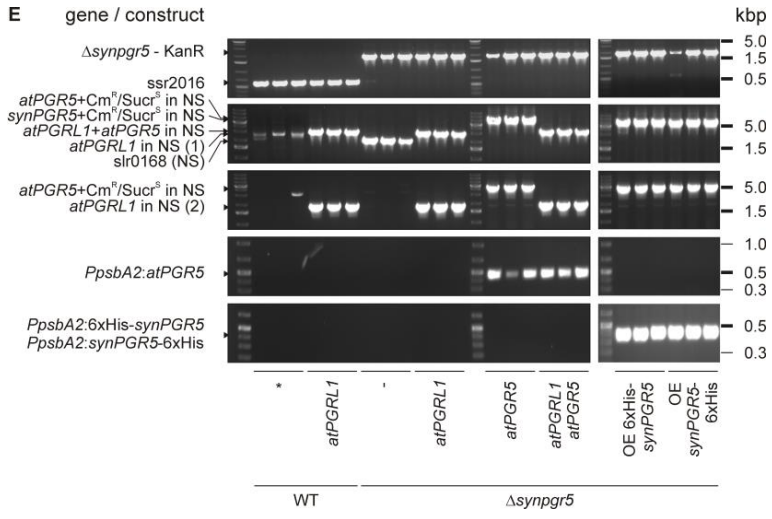

Fig 3.17. **Generation of *atPGR* gene expression strains in *Synechocystis*.** Expression constructs for *atPGR* genes under control of the *Synechocystis* D1 promoter (*PpsbA2*) were introduced into the genomic *neutral site* (NS) slr0168 by homologous recombination via ~900 bp of slr0168 5' (upstream region UR) and 3' (downstream region DR) genomic DNA sequences, using a non-replicative vector as shuttle. When appropriate, chloramphenicol resistance /sucrose sensitivity (Cm^R/$Sucr^S$) double selection cassettes (DSC) were removed by negative selection on 5 % (w/v) sucrose agar as described earlier (Viola et al. 2014; see Fig 3.9). Redundant sequence stretches for double-recombination are displayed in textured grey. Expression construct and recombination maps of plasmids (**A**) pP1 with *PpsbA2*:*atPGRL1*, (**B**) pP5 with *PpsbA2*:*atPGR5*, (**C**) pP15 with *PpsbA2*:*atPGRL1* + *PpsbA2*:*atPGR5, (**D**)* pOE-synP5 HisN/HisC *with PpsbA2*:6xHis-*synPGR5 / synPGR5*-6xHis. Genotyping primer binding sites with 5'-3' orientation are indicated by labeled arrows; expected amplicon origins and sizes are indicated below respective maps. (**E**) Genotyping PCR of three independent transformants each confirmed Δ*synpgr5* genetic background, as well as transgene cassette presence and segregation status. Note that the WT control does not display an slr0168 amplicon of the expected size (2183 bp) because of complete deletion of the slr0168 ORF by replacement with a Kan^R-selection cassette. 6xHis-/-6xHis denotes addition of an N-or C-terminal 6xhistidine tag, respectively.

Over-expression of synPGR5 protein could not be confirmed on the protein level despite labelling with a 6xHis tag and expression under the same promoter as *Arabidopsis* PGRL1 and PGR5. Neither αHis nor αPGR5 antibodies were found sensitive or specific enough to detect a reliable signal. Hence, alternatively, Northern blot analysis was performed to confirm over-accumulation of *synPGR5* transcripts (see next section). With atPGRL1 and atPGR5 being expressed and localized to the correct subcellular compartment, physiological assessment of their functionality could be performed. As CEF is thought to return electrons to oxidized PSI reaction centers ($P700^+$) after donation to Fd, its activity is hypothesized to be the main contributor to dark-starved cell P700 redox kinetics under far-red light (FR; λ = 720 nm) treatment, which does not drive PSII photochemistry (Mi et al. 1994, Mi et al. 2000). FR-P700-oxidation kinetics offers a comparably easy, non-invasive, and thus less error-prone assessment of *in vivo* CEF activity and effects of *Arabidopsis*-transgene expression. P700-redox kinetics was measured with a Dual-PAM-100 device using photoautotrophic, late exponential phase cultures. Cells were washed twice with BG11, adjusted to OD_{730} = 5.0, and dark incubated overnight for approximately 16 h under shaking (120 rpm) and at ambient temperatures (23 °C).

3.2.2.2 Phenotypic assessments of atPGR protein functionality in *Synechocystis*

The time which passed from FR-light onset until achieving half-maximum P700-oxidation level ($t_{0.5}P700_{ox}$) was employed as a comprehensive measure for CEF activity around PSI (see section 3.1.7; Fig 3.13 A/B). Isolated expression of atPGRL1 did not have an effect on $t_{0.5}P700_{ox}$ in either WT or *Δsynpgr5* cells. Expression of atPGR5 alone led to a moderate yet significant delay of $t_{0.5}P700_{ox}$ in *Δsynpgr5* but did not fully complement the mutant phenotype. A combination of atPGRL1 and atPGR5 however caused delay in $t_{0.5}P700_{ox}$ beyond WT level. Co-expression also recovered the sigmoid shape of WT early P700-oxidation-kinetics curve. Thus, atPGRL1 and atPGR5 in concert were able to (over-)complement the *Δsynpgr5* mutant (Fig 3.19 E). Correct transgene expression in the measured strains could be confirmed by western blot (Fig 3.19 B). Over-expression of synPGR5 could not be confirmed on protein level despite being 6xHis-tagged N- or C-terminally, respectively, neither using αPGR5 nor α6xHis antibodies, nor by mass spectrometry of crude protein extracts or extracts treated with Ni-NTA for 6xHis-synPGR5 enrichment (data not shown). However, *synPGR5* transcript levels were confirmed to be increased more than 100-fold as compared to WT cells (Fig 3.19 C). Over-expression strains of synPGR5 displayed an even more severe decrease in P700-oxidation rates than strains co-expressing atPGRL1 and atPGR5 under the same promoter, implying enhanced functionality of endogenous *Synechocystis* PGR5 protein (Fig 3.19 E). N- and C-terminally tagged synPGR5 gave rise to nearly identical phenotypes, implying neither tag crucially impaired synPGR5 functionality.

Finally, both atPGRL1+atPGR5 co-expression and synPGR5 over-expression strains displayed a paler culture phenotype than other mutants assayed (Fig 3.19 A).

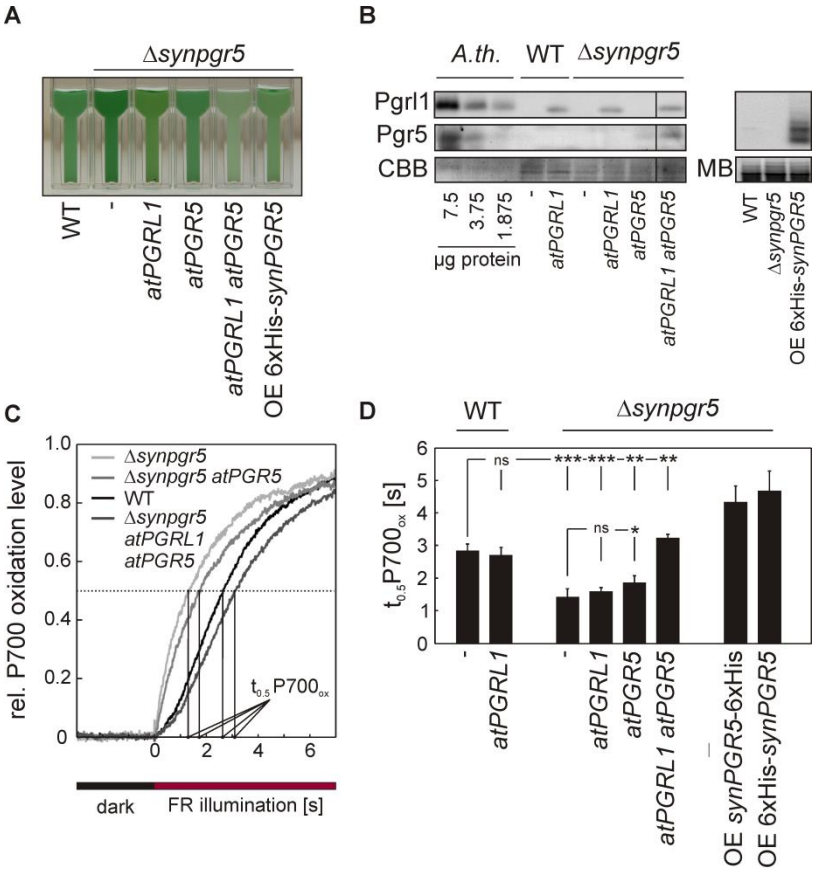

Fig 3.19. **Expression of *Arabidopsis* PGR proteins differentially affects P700 oxidation kinetics in *Synechocystis*.** (**A**) Expression strain mutant phenotypes prior to P700 PAM measurement. Cultures were grown for seven days at 30 °C under 30 µE of constant illumination. (**B**) Heterologous protein accumulation in protein extract membrane fractions corresponding to 30 µg of protein was confirmed by western blot. Proteins were separated by SDS-PAGE and blotted onto PVDF by capillary transfer with 1x PBS prior to chemiluminescent immunodetection of atPGRL1 and atPGR5. Coomassie Brilliant Blue (CBB) staining of the PVDF membrane served as a loading control. (**C**) Over-accumulation of the *synPGR5* (ssr2016) transcript could be confirmed by northern blot. 20 µg of total RNA were separated by agarose gel electrophoresis, capillary transferred onto nylon membrane, and probed with the entire ssr2016 coding sequence (198 bp) labelled with P^{32}. (**D**) P700 oxidation half time upon FR illumination ($t_{0.5}P700_{ox}$) was used as comprehensive parameter of mutant CEF phenotypes, with higher $t_{0.5}P700_{ox}$ values presumably corresponding to higher CEF activity. (**D**) The bar chart shows average $t_{0.5}P700_{ox}$ values as a proxy for CEF activity in plant PGR5 and/or PGRL1 expression or synPGR5 over-expression strains, together with the appropriate controls. Error bars correspond to the standard deviations for n = 6/6/6/4/6/3/7/16 (order as displayed) independent experiments. Statistically significant differences with respect to WT or Δ*synpgr5* according to Holm- corrected two-sided Student's *t*-tests are indicated by asterisks (* $P \leq 0.05$, ** $P \leq 0.01$, *** $P \leq 0.001$, ns, not statistically significant).

Functionality of the atPGRL1+atPGR5 couple could be demonstrated in terms of an expected effect on P700-oxidation kinetics. This suggested general compatibility of the *Synechocystis* and *Arabidopsis* PGR5-dependent CEF system, albeit atPGR5 depends on atPGRL1 for full functionality. Also, atPGR5 was found to accumulate more efficiently in strains co-expressing atPGRL1 (Fig 3.18, Fig 3.19). Contrarily, atPGRL1 accumulation was not affected by presence or absence of atPGR5, contrasting the decrease in PGRL1 accumulation in *Arabidopsis pgr5-1* mutants (DalCorso et al. 2008).

After demonstrating above the general system compatibility, we could begin to elucidate the atPGRL1/atPGR5 joint functionality in a working system much more accessible to genetic engineering than the original plant.

To test the suitability of the established heterologous expression system as test platform experimentally we decided to introduce (i) an *atPGR5* point mutation of known and (ii) an *atPGRL1* point mutation of to-be-confirmed effect on plant-type PGRL1/PGR5-mediated CEF into *Synechocystis*.

3.2.2.3 Exploring the heterologous CEF system as a genetic test platform

In *Arabidopsis* the *pgr5-1* mutation results in severely reduced CEF activity (Munekage et al. 2002) and drastically reduced PGR5 protein accumulation (Yamamoto and Shikanai 2019). Moreover, loss of PGR5 functionality results in a lethal phenotype under fluctuating light conditions (5 min low light 50 µE – 1 min high light 500 µE) in *Arabidopsis* (Suorsa et al. 2012), but not in *Synechocystis* (Allahverdiyeva *et al. 2013*). Surprisingly, not a nonsense mutation, but a point mutation in the atPGR5 gene giving rise to a G130S amino-acid exchange is responsible for the *pgr5-1* phenotype (Munekage et al. 2002). Recently, an *Arabidopsis pgr5-1* suppressor screen applying fluctuating light as selective condition was conducted by a member of our lab (Dr. Belén Naranjo) and yielded a *PGRL1B* point mutant termed *pgr5-1* S30 (suppressor 30) as a possible suppressor of *pgr5-1* lethality (Fig 3.20 A). The according point mutation results in an S104F amino acid exchange in a highly conserved region of the PGRL1B N-terminus (Fig 3.19 B).

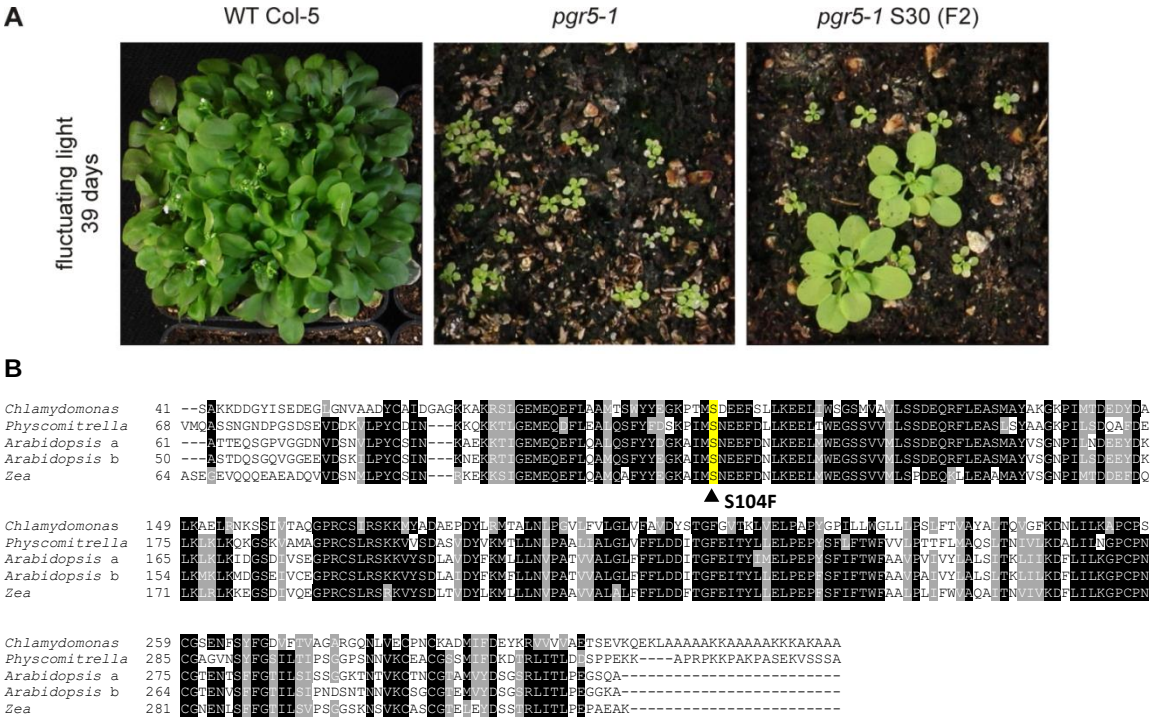

Fig 3.20. **Suppressor mutant *pgr5-1* S30 bearing a non-synonymous mutation in *PGRL1B* rescues *pgr5-1* lethality under fluctuating light.** (**A**) *Arabidopsis* WT (Col-5), *pgr5-1*, and *pgr5-1* S30 mutant plants after 39 days of fluctuating light treatment (5 min 50 µE / 1 min 500 µE; 12 h daylight). In the F2 generation, S30 suppressor mutants homozygous for a second site mutation in *atPGRL1B* are viable under fluctuating light. (**B**) Alignment of mature PGRL1 proteins reveals the S30 mutation (PGRL1B S104F) affects a highly conserved serine residue (highlighted in yellow), allowing for direct transfer into the *atPGRL1A* expression system established in *Synechocystis*. Residues conserved/similar in ≥ 70 % of sequences are highlighted in black/grey. NCBI IDs of protein sequences used and predicted cTP lengths are provided in Methods (section 2.12). Images and mutants shown have been generated, identified, and supplied by Dr. Belén Naranjo (unpublished).

The intriguing combination of the two *pgr5-1* and S30 point mutations was investigated within the newly-established *Synechocystis* atPGRL1/atPGR5 expression system. First, the *pgr5-1* mutant allele was reconstituted. An according point mutation resulting in a G130S amino acid exchange was introduced into the pP5 and pP15 plasmids by Q5® site directed mutagenesis, giving rise to the atPGR5 expression systems $pP5_{G130S}$ and $pP15_{G130S}$ mimicking the plant loss of function allele. Second, to reconstitute the S30 mutation in *Synechocystis*, a point mutation altering the homologous serine S115 of atPGRL1A to phenylalanine (S115F) was introduced into pP1 and $pP15_{G130S}$ in the same way, giving rise to $pP1_{S115F}$ and $pP1_{S115F}$ 5_{G130S}.

Transgene introduction and segregation status were confirmed by PCR (Fig 3.21 A). The culture phenotype was strongly affected by $atPGRL1_{S115F}$+$atPGR5_{G130S}$, resulting in pronounced culture paleness. Co-expression of atPGRL1 and $atPGR5_{G130S}$, contrarily, cancelled out the bleaching effect observed upon expression of the *Arabidopsis* wildtype atPGRL1+atPGR5 couple (Fig 3.21 B). Subsequently, the single and combinatory effects of both mutations on P700-FR-oxidation kinetics, as well as atPGRL1 and atPGR5 protein accumulation were examined. The *pgr5-1* mutation was shown to neutralize the $t_{0.5}P700_{ox}$ effects of both atPGR5 and atPGRL1+atPGR5 co-expression. While $atPGRL1_{S115F}$ alone did not affect P700, it caused a strong delay in $t_{0.5}P700_{ox}$ in combination $atPGR5_{G130S}$ very similar to that caused by wildtype atPGRL1+atPGR5 proteins (Fig 3.21 C). On the protein level the reconstituted *pgr5-1* mutation abolished atPGR5 protein accumulation and neutralized the synergistic effect of co-expression with atPGRL1 on $atPGR5_{G130S}$ accumulation likewise, confirming *pgr5-1* as a loss of function allele in a heterologous system. Protein accumulation of $atPGR5_{G130S}$, however, could be partially restored by the $atPGRL1_{S115F}$ second site mutation. Protein accumulation or immuno-detectability was strongly affected by the S115F mutation in $atPGRL1_{S115F}$ and $atPGRL1_{S115F}$+$atPGR5_{G130S}$ (co-)expression strains (Fig 3.21 D).

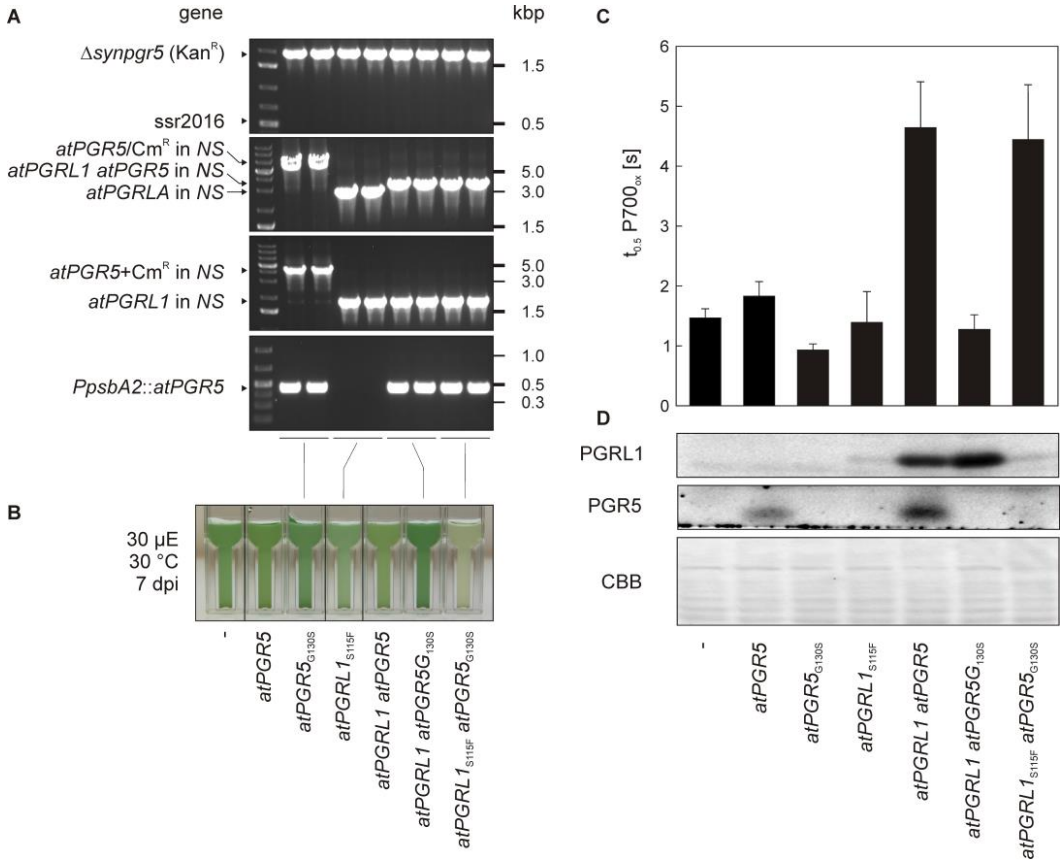

Fig 3.21. **Effects of the *pgr5-1* and *pgr5-1* S30 mutations in *Synechocystis* recapitulate *Arabidopsis* phenotypes.** (**A**) Genotyping PCRs of two independent transformants each confirm Δ*synpgr5* genetic background, transgene cassette presence, and segregation status of *atPGR* mutant allele expression constructs. (**B**) Phenotypes of *atPGRL1*$_{S115F}$ *atPGR5*$_{G130S}$ mutant cultures and corresponding control strains prior to P700 PAM measurements. Cultures were grown for 7 days at 30 °C under 30 µE of constant illumination. (**C**) Average $t_{0.5}P700_{ox}$ values in mutated atPGR5 and/or atPGRL1 expression strains, together with the appropriate controls. Error bars correspond to the standard deviations for *n* = 4/8/6/9/10/3/6 (order as displayed) independent experiments. (**D**) Immunoblot detection of heterologous protein accumulation in membrane protein fractions corresponding to 40 µg of protein. Proteins were separated by SDS page and blotted onto PVDF by capillary transfer with 1x PBS prior to chemiluminescent immunodetection of PGRL1 and PGR5. Coomassie Brilliant Blue (CBB) staining of the PVDF membrane served as a loading control.

In summary, heterologous expression of atPGRL1 and atPGR5 in *Synechocystis* yielded several pieces of information regarding the supposed two-component system.

- *Arabidopsis* PGRL1 and PGR5 in concert complement the *Δsynpgr5* P700 phenotype and thus probably confer CEF in the heterologous system.
- atPGR5 accumulates in *Synechocystis* in absence of atPGRL1, but displays limited functionality.
- Full functionality of atPGR5 in *Synechocystis* apparently requires atPGRL1.
- atPGRL1 enhances atPGR5 protein accumulation also in *Synechocystis*.
- Mutant atPGR5$_{G130S}$ does not accumulate to detectable degrees in *Synechocystis*, regardless of atPGRL1 being present or not.
- atPGR5$_{G130S}$ accumulation and functionality are (partially) recovered by mutant atPGRL1$_{S115F}$.
- No tested *Arabidopsis* protein expression system reaches the effect of over-expressing endogenous synPGR5.

3.2.3 *Synechocystis* PGRL1 functional analogue

Our findings outlined above suggest that, within the newly-established *Synechocystis* test system, atPGR5 is only fully functional in presence of atPGRL1. Still, atPGR5 expression caused a small but reproducible delay of P700-FR oxidation. Moreover, it accumulates in absence of atPGRL1 and gets degraded or fails to accumulate in the presence of the *pgr5-1* G130S mutation. These facts imply that at least one unknown *Synechocystis* component is involved in atPGR5 stabilization and functionalization.

Since no clear PGRL1 homologues exist in *Synechocystis,* the hypothetical protein could represent the result of convergent evolution, rendering it a functional PGRL1 analogue. Alternatively, it could have evolutionarily diverged from PGRL1 since the split of chloroplast and *Synechocystis* lineages beyond the threshold of clearly detectable sequence homology. To find candidates for the putative *Synechocystis* PGRL1-like component (hereafter synPGRL1-LIKE), protein local alignment search was performed using the pBLAST (protein basic local alignment search tool) implemented in CyanoBase with heavily reduced stringency (http://genome.microbedb.jp/blast/blast_search/cyanobase/genomes; for parameters, see legend of Fig 3.22). The soluble N-terminus of atPGRL1A (amino acid (aa) 61–198, i.e. first aa of mature protein to first transmembrane helix) was chosen as query sequence as (i) it was presumed to be crucial for proper atPGRL1*atPGR5 functionality (see section 3.2.2.3; Fig 3.21), and (ii) the C-terminus of PGRL1 is shorter and harbors two CXXC sequence motifs which might provoke false-positive alignment hits due to their relative rarity. The pBLAST search yielded two potential distant homologues of atPGRL1A: the quinolate synthase NadA encoded by ORF sll0622, and an unknown protein encoded by ORF sll1217, which is homologous to uracil DNA glycosyl transferases (Fig 3.22).

A **>atPGRL1A**

```
        10         20         30         40         50         60
mgskmlfslt sprlfsavsr kpsssfspsp pspssrtqwt qlspgksisl rrrvfllpak
        70         80         90        100        110        120
ATTEQSGPVG GDNVDSNVLP YCSINKAEKK TIGEMEQEFL QALQSFYYDG KAIMSNEEFD
       130        140        150        160        170        180
NLKEELMWEG SSVVMLSSDE QRFLEASMAY VSGNPILNDE EYDKLKLKLK IDGSDIVSEG
       190        200        210        220        230        240
PRCSLRSKKV YSDLAVDYFK MLLLNVPATV VALGLFFFLD DITGFEITYI MELPEPYSFI
       250        260        270        280        290        300
FTWFAAVPVI VYLALSITKL IIKDFLILKG PCPNCGTENT SFFGTILSIS SGGKTNTVKC
       310        320
TNCGTAMVYD SGSRLITLPE GSQA
```

Fig 3.22. **CyanoBase pBLAST search against the atPGRL1A N-terminus.** (**A**) Only the mature atPGRL1A N-terminus (**UPPERCASE BOLD**) without the predicted transit peptide (lowercase; aa 1–60) was used as query sequence. Transmembrane helix sequences are highlighted in grey; redox sensitive cysteines are highlighted in black with white font. (**B**) Best pBLAST hits for potential *Synechocystis* PGRL1 homologues with key statistics of local alignments. (**C**) Local alignments of the atPGRL1A N-terminus and NadA/Sll1217. Expectation (*E*) value threshold for CyanoBase pBLAST was increased to 10^4 to reduce alignment search stringency. "+" signifies physio chemically similar residues.

B

protein	candidate range	*E*-value	identity	positives	gaps
NadA	aa 173-217	0.65	12/38 (31%)	20/38 (52%)	0/38 (0%)
Sll1217	aa 103-143	1.1	13/41 (32%)	23/41 (56 %)	1/41 (2 %)

C **quinolate synthase NadA**

```
atPGRL1A  63  KEELMWEGSSVVMLSSDEQRFLEASMAYVSGNPILNDE  100
              +E ++W+GS +V  +  E+R LE    Y     I + E
NadA     173  REMVLWQGSCIVHETFSERRLLELKTQYPQAEIIAHPE  210
```

unknown protein Sll1217

```
atPGRL1A  16  SNVLPYCSI-NKAEKKTIGEMEQEFLQALQSFYYDGKAIMS  55
              +N +PY    NKA    + E  + F++ L  F++ GK I++
Sll1217  103  TNTVPYKPPENKAYSVKVKERFRPFVEQLLVFHWQGKQIIT  143
```

3.2.3.1 Similarity and phylogenesis of synPGRL1-LIKE candidates

The synPGRL1-LIKE candidate protein sequences were examined for additional evidence of homology or functional analogy to PGRL1. Protein sequences of 15 cyanobacterial species (Tab 3.2) were selected to cover most of the cyanobacterial phylogeny (6/8 orders), while focusing on the order containing *Synechocystis* (Synechococcales; 7/15 species investigated). Protein sequences were obtained from NCBI genbank, and alignments were generated using MUSCLE (Edgar 2004; see Methods section 2.21 for details).

Tab 3.2. **Cyanobacterial species and corresponding orders used for multiple-protein-sequence alignments.**

Species	Order	Species	Order
Acaryochloris marina	Synechococcales	*Pleurocapsa* sp. PCC 7327	Pleurocapsales
Anabaena sp. PCC7108	Nostocales	*Prochlorococcus marinus* str. MIT 9303	Synechococcales
Aphanothece minutissima	Chroococcales	*Roseofilum reptotaenium* AO1-A	Oscillatoriales
Cyanobium usitatum	Synechococcales	*Synechococcus* sp. PCC 7502	Synechococcales
Geminocystis sp. NIES3708	Chroococcales	*Synechocystis* sp. PCC6803	Synechococcales
Gloeocapsa sp. PCC 73106	Chroococcales	*Thermosynechococcus* sp. NK55a	Synechococcales
Gloeomargarita lithophora	Gloeobacterales	*Vulcanococcus limneticus*	Synechococcales
Microcystis aeruginosa NIES-843	Chroococcales		

Quinolate synthase NadA

In *E. coli* the quinolate synthase NadA has been investigated intensively (Ceciliani et al. 2000, Ollagnier-de Choudens et al. 2005, Cicchillo et al. 2005, Saunders et al. 2008), and its molecular function in condensation of iminoaspartate with dihydroxyacetone phosphate to form quinolate is well established. While not being a transmembrane protein such as PGRL1, NadA displays several features potentially linking it to the putative ferredoxin-plastoquinone oxidoreductase PGRL1, such as

- presence of redox-active cysteine motifs (Saunders et al. 2008)
- coordination of an iron cofactor (Fe_4S_4 cluster; Ollagnier-de Choudens et al. 2005)
- functional involvement with quinole-like compounds

rendering synNadA a viable synPGRL1-LIKE candidate.

A multiple protein sequence alignment revealed that the NadA primary structure is highly conserved across cyanobacteria and down to the NadA-like protein-family founding member from *E. coli* (Fig. 3.23). Importantly, all cysteine residues shown or suggested to be involved in Fe_4S_4-cluster coordination were found strictly conserved.

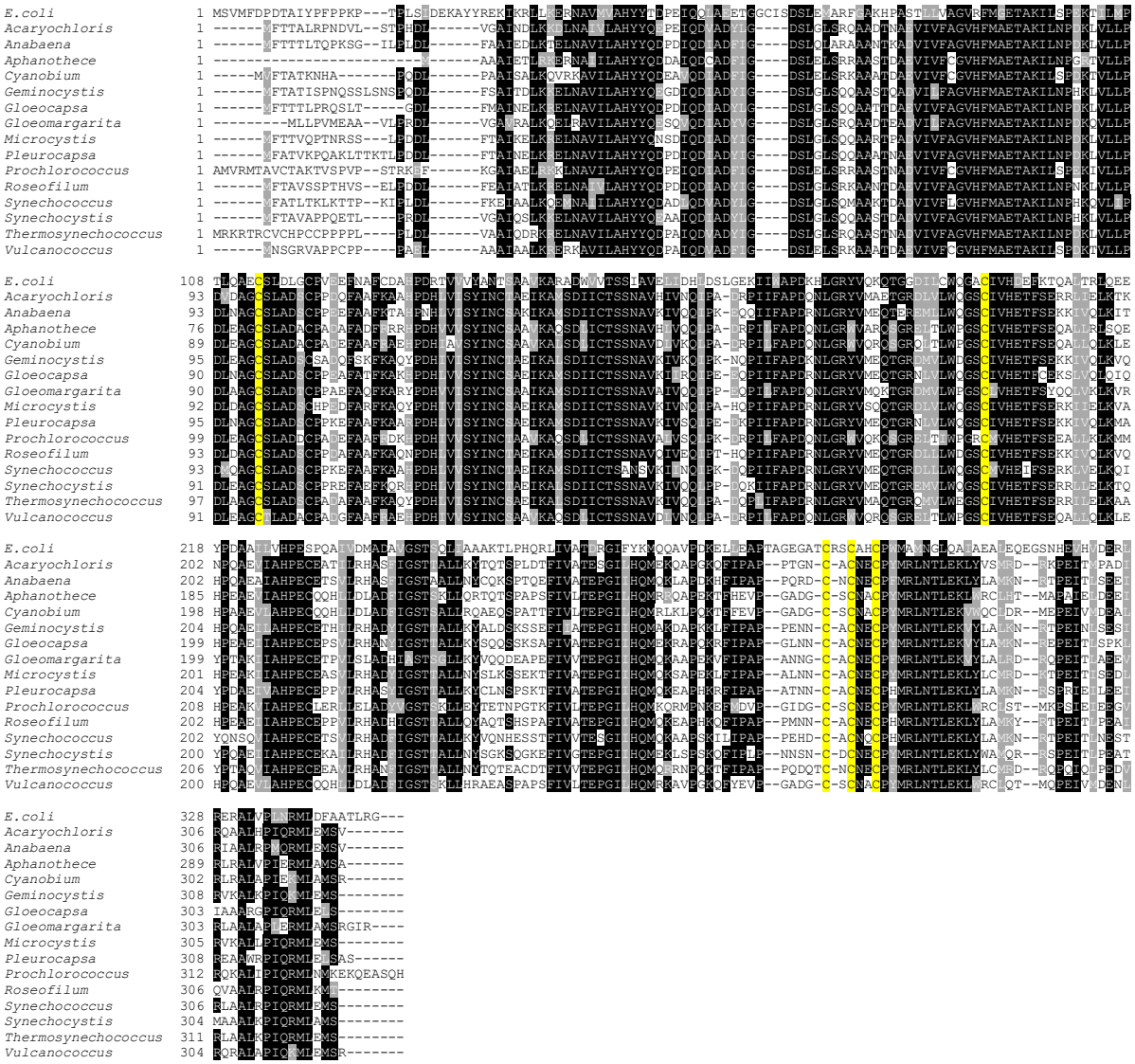

Fig 3.23. **Multi-protein-sequence alignment of cyanobacterial NadA homologues**. Residues conserved/similar in ≥ 70 % of sequences are highlighted in black/grey. Conserved cysteine residues (potentially) involved in coordinating the NadA Fe_4S_4 cluster are highlighted in yellow. For full species and strain names, see Tab 3.2.

Unknown protein Sll1217

The second synPGRL1 candidate Sll1217 lacks defining features of PGRL1 such as

- three pairs of presumably redox-active or iron cofactor-coordinating cysteine residues
- two transmembrane helices embedding PGRL1 in the thylakoid membrane.

Functional prediction for Sll1217 suggests a function as uracil-DNA glycosyltransferase 4 (UDG4)-like protein containing a PFAM UDG domain (PF03167). These proteins remove uracil bases from DNA (Sandigursky et al. 1999, Sandigursky et al. 2001). Canonical UDG4 proteins coordinate an Fe_4S_4 cluster (Hoseki et al. 2003).

Surprisingly, an alignment of Sll1217-protein sequences from the same 15 cyanobacterial species outlined above revealed a phase separation between a sub-group of five cyanobacteria (*Geminocystis*, *Gloeocapsa*, *Microcystis*, *Pleurocapsa*, and *Synechocystis*) and the residual species, which clustered with the UDG4-like protein family founding member sequence from *Thermotoga maritima* (Thermatogales; Fig 3.24). Members of the *Synechocystis*-type subgroup lack the residues coordinating the Fe_4S_4-cluster, distinguishing them from otherwise close UDG4 homologues in other cyanobacteria.

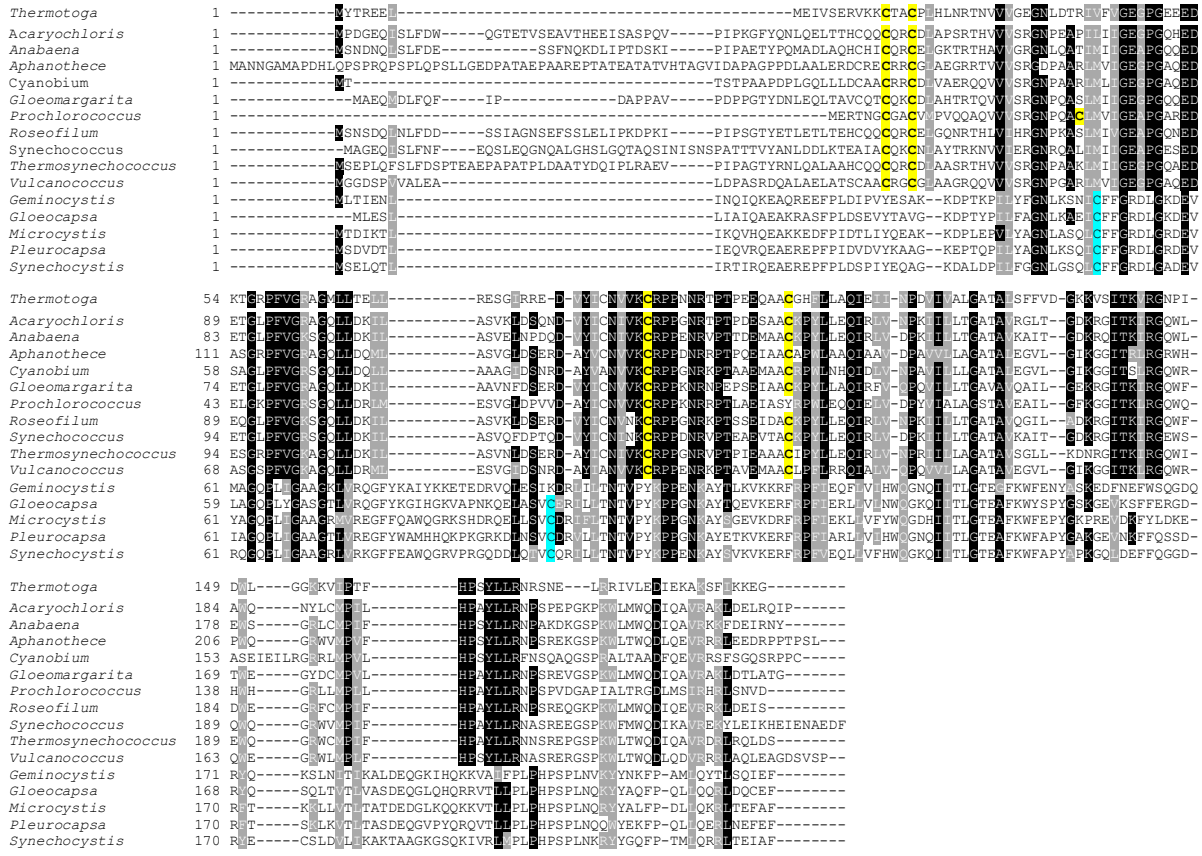

Fig 3.24. **Multi-protein-sequence alignment of cyanobacterial Sll1217 homologues**. Residues conserved/similar in ≥ 70 % of sequences are highlighted in black/grey. Conserved cysteine residues involved in coordinating the UDG4 Fe_4S_4 cluster are highlighted in yellow. A *Synechocystis*-type subgroup of UDG4 homologues harbors a pair of distinct, broadly conserved cysteine residues (highlighted in cyan), but none of the Fe_4S_4 cluster coordinating cysteines. For full species and strain names, see Tab 3.2.

As *Synechocystis* Sll1217 lacks the Fe_4S_4 cluster and is rather dissimilar to the UDG4 archetype, its supposed UDG function is questionable, and its actual molecular function can be considered unclear. Due to its actual protein sequence features Sll1217 constitutes a by far weaker synPGRL1-LIKE candidate than NadA, however.

To explore NadA and Sll1217 as potential strongly diverged PGRL1 homologues, the PGRL1-NadA-Sll1217/UDG4-complex was analyzed for pairwise sequence similarity/identity, and its phylogeny was reconstructed.

Sequence similarity

Pairwise protein-sequence similarities and identities were calculated with MatGAT2 (Campanella et al. 2003) based on global protein alignments of NadA:PGRL1, as well as Sll1217/UDG4:PGRL1, of the same bacterial species covered above. Sequence alignments (see Methods Fig 2.6 and 2.7) contained plant PGRL1 sequences from four species (*Chlamydomonas reinhardtii* [green alga], *Physcomitrella patens* [moss], *Arabidopsis thaliana* [dicotyledon], and *Zea mays* [monocotyledon];). Alignment analysis yielded average pairwise similarities/identities of 33.75±1.74 / 17.01±1.46 % and 31.76±2.12 / 16.08±1.50 % for NadA:PGRL1 and Sll1217/UDG4:PGRL1, respectively. Average similarity/identity of PGRL1 to only *Synechocystis*-type Sll1217 was 32.88±2.04 / 16.92±1.61 %, while similarity/identity of canonical UDG4-like proteins to *Synechocystis*-type Sll1217 was 40.18±2.32 / 20.01±2.02 %. This rendered the *Synechocystis*-type Sll1217 subgroup slightly more similar to PGRL1 than canonical UDG4 sequences, but overall more similar to UDG4 than to PGRL1, and also slightly more dissimilar to PGRL1 than NadA. This result again favored NadA over Sll1217 as synPGRL1-LIKE candidate. Since both proteins were found in an identity range that has been described to be populated by divergent homologues and convergent analogues alike (Rost 1997), phylogenetic reconstruction was issued to investigate potential common ancestry more thoroughly.

Phylogenetic reconstruction of synPGRL1-LIKE candidates

A global alignment of NadA:UDG4/Sll1217:PGRL1 sequences of all organisms used previously was generated (Methods Fig 2.5). The alignment matrix was used for *phylogenetic reconstruction* by Maximum Parsimony (MP) and Maximum Likelihood (ML) methods. MP is a phylogenetic reconstruction method favoring the shortest tree possible, i.e. the phylogenetic tree requiring the lowest total number of mutations needed to derive the input sequence alignment from a common ancestor sequence. ML phylogenetic reconstruction is a method searching the most likely estimate of molecular phylogenesis (i.e. a phylogenetic tree with certain topology and branch lengths) based on the input protein alignment and a statistical model of protein evolution.

Phylogenetic reconstruction in this case was used to examine which candidate protein could more parsimoniously or (assuming an evolutionary model) more likely be transitioned into PGRL1 *via* a hypothetical common ancestor. Hence, in this case, hypothetical trajectory and clustering are sought after rather than actual evolutionary relationships, since at least one (if not both) candidates might not actually share common ancestry with PGRL1.

Both MP and ML analyses placed PGRL1 as sister clade to UDG4/Sll1217 in the majority of bootstrap repetitions (99 % for MP, 57 % for ML; Fig 3.25), suggesting that common evolutionary ancestry of PGRL1 and Sll1217 is more likely than predicted protein properties imply.

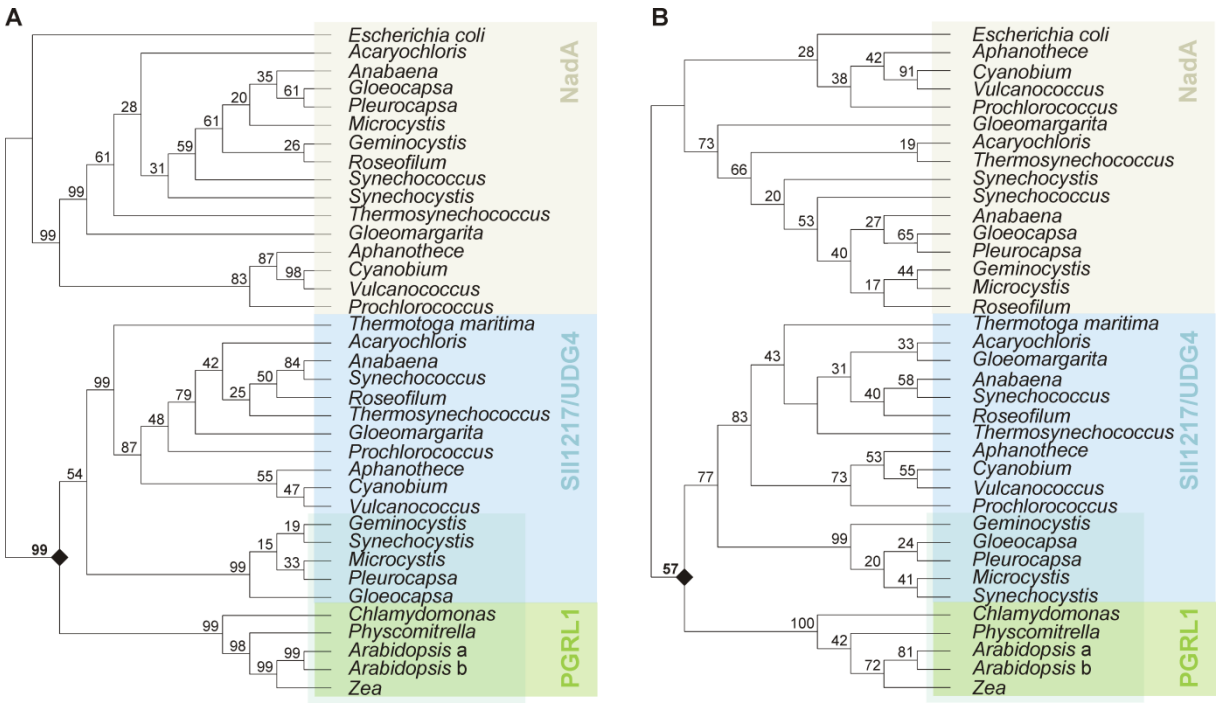

Figure 3.25. **Phylogenetic reconstruction of PGRL1, NadA, and UDG4/Sll1217 protein sequence evolution.** The evolutionary history of synPGRL1-LIKE candidate proteins and PGRL1 was inferred using Maximum Parsimony (MP) and Maximum Likelihood (ML) (see Material and Methods 2.12.2). Confidence of the maximum likelihood tree inference was tested by 5000-fold (MP) and 500-fold (ML) bootstrapping (i.e. 500-fold repetition of the statistical analysis and derivation of a most likely consensus tree topology. The bootstrap consensus trees are taken to represent the evolutionary history of the taxa analyzed. The percentages of replicate trees in which the associated taxa clustered together in the bootstrap test are shown next to the branches. Diamonds highlight the PGRL1-UDG4/Sll1217 dichotomy which was preferred over other pairings by both algorithms; the according clade is highlighted in cyan. (**A**) MP consensus tree. (**B**) ML consensus tree.

If PGRL1 and UDG4/Sll1217 actually share common ancestry, chloroplast PGRL1 would be expected to cluster with cyanobacterial UDG4/Sll1217 rather than *Thermotoga maritima* UDG4, unlike the situation shown above. To exclude confounding effects on sub-topologies of a putative cyanobacterial UDG4/Sll1217-PGRL1 clade induced by enforced non-homologous alignment with NadA, the multi-sequence alignment used to estimate PGRL1:UDG4/Sll1217 pairwise distances (see above and Fig 2.7) was subjected to ML phylogenetic reconstruction.

The resulting maximum likelihood tree (Fig 3.26 A), as well as the consensus tree over 500 bootstrapping replicates (Fig 3.26 B), placed PGRL1 within cyanobacterial UDG4/Sll1217 as sister clade to the aberrant *Synechocystis*-type Sll1217 clade. This implied that artificial simultaneous alignment with non-homologous NadA sequences might indeed have masked the weak residual phylogenetic signal grouping PGRL1 with *Synechocystis*-type Sll1217 proteins.

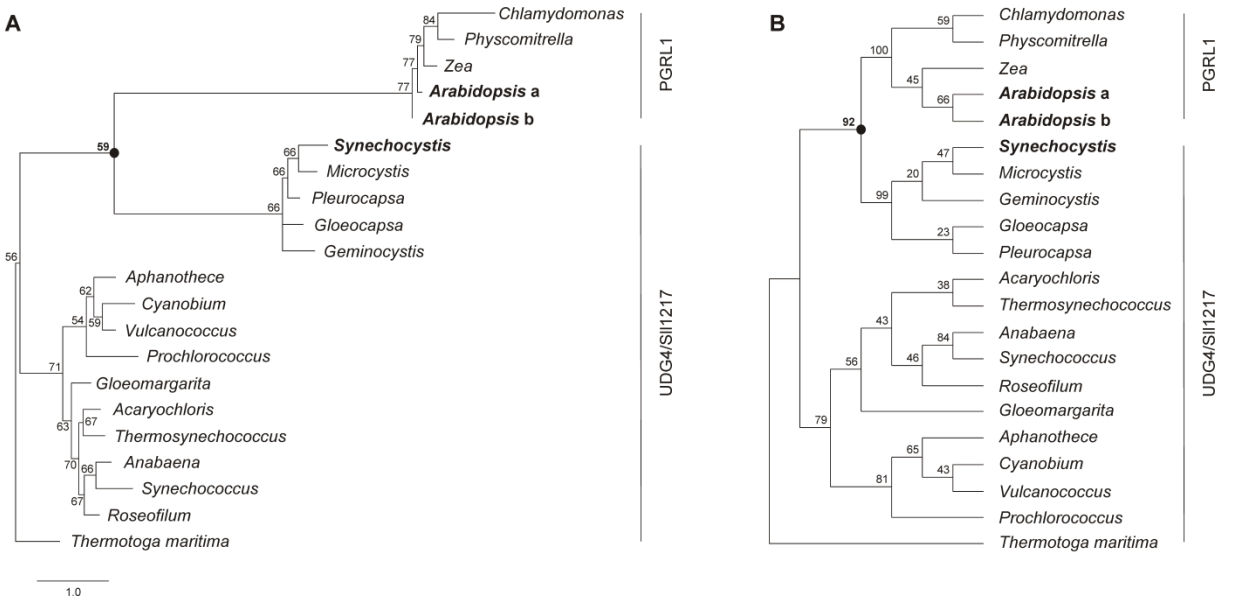

Figure 3.26. **Molecular phylogenetic analysis of PGRL1 and UDG4/Sll1217 by Maximum Likelihood method.** The evolutionary history of PGRL1 and UDG4/Sll1217 was inferred using the Maximum Likelihood method based on the Whelan-And-Goldman model. (**A**) The tree with the highest log likelihood (-8526.53) is shown. A discrete Gamma distribution was used to model evolutionary rate differences among sites (for details, see Methods 2.12.2). The tree is drawn to scale, with branch lengths measured in the number of substitutions per site. (**B**) The bootstrap consensus tree inferred from 500 replicates of ML tree estimation. The percentages of replicate trees in the bootstrap test in which the associated taxa clustered together are shown next to the branches. Black dots (●) highlight the *Synechocystis*-type Sll1217-PGRL1 dichotomy. Trees were rooted on *Thermotoga maritima* UDG4, meaning *Thermotoga* was defined as most-distant relative (outgroup) to all other species/sequences.

In phylogenetic reconstruction, *Synechocystis* Sll1217 preferentially clusters with PGRL1, despite yielding a less specific pBLAST hit and sharing a lower degree of overall sequence similarity with PGRL1 than NadA. This flagged Sll1217 as a more likely synPGRL1-LIKE candidate, assuming actual evolutionary relatedness to plant PGRL1. Given the higher amount of shared molecular features between PGRL1 and NadA, however, the latter could not be discarded as a potential functional PGRL1 analogue. Therefore, biochemical and mutant phenotype analyses were conducted in order to assess actual functional links between the two synPGRL1-LIKE candidates and PGR5.

3.2.3.2 synPGRL1-LIKE candidates protein-protein-interaction assays

Co-immunoprecipitation

To assess potential *in-vivo* interaction of atPGR5 with NadA or Sll1217 a co-immunoprecipitation (Co-IP) with αPGR5 antibody was performed on whole cell extract of WT cells expressing atPGR5 (i.e. WT cells transformed with pP5; see Fig 3.17). WT genetic background was chosen in order to avoid that the loss of synPGR5 would reduce expression levels of its interaction partners, as described in *Arabidopsis* (*pgr5-1* lacking approximately 60% of PGRL1; DalCorso et al. 2008). This happened at the risk of synPGR5 titrating out this very interaction partner. With synPGR5 abundance falling below protein detection thresholds of mass spectrometry to date, however, this risk was considered negligible. Co-IP was performed in two independent experiments, with three and two biological replicates, respectively. In short, magnetic beads covered with protein A were decorated with αPGR5 antibody and incubated with whole-cell-protein extract. Antibody-bound proteins were washed, eluted and digested with trypsin, yielding peptides that were subjected to mass-spectrometric analysis. Most-enriched and synPGRL1-LIKE candidate proteins detected by mass spectrometry are summarized below (Tab 3.3).

Tab 3.3. **synPGRL1-LIKE candidate proteins co-immunoprecipitated with atPGR5.** Whole cell protein extracts of *Synechocystis* WT expressing atPGR5 were immunoprecipitated with antibodies recognizing atPGR5, digested with trypsin, and purified on C18-STAGE-tip columns (Rappsilberet et al. 2003). Peptides were analyzed by liquid-chromatography-tandem mass spectrometry with an electrospray-ionization-ion-trap instrument to identify atPGR5-associated proteins. -*fold* changes (FC) in peptide abundance and corresponding *P*-values of two-sided *t*-tests were determined relative to co-immunoprecipates from WT control not expressing atPGR5 (* $P \leq 0.05$; ** $P \leq 0.01$; *** $P \leq 0.001$). Two independent biological replicates (Exp 1 and Exp 2) with three technical replicates each were analyzed. Candidates for synPGRL1-LIKE, as well as the best unexpected interaction partner candidate (bacterioferritin Bfr1), its close and likewise precipitated homologue Bfr2, and the proposed Sll1217 interaction partner Slr1353 are shown.

		Exp1		Exp2	
Protein	UniProt ID	FC	*P*-value	FC	*P*-value
atPGR5	Q9SL05	22.13	2.51E-03**	638.64	3.00E-03**
Bfr1	P24602	13.48	2.89E-05***	40.55	2.32E-02*
Bfr2	P73287	2.83	1.40E-01	9.39	6.72E-02
Sll1217	P74030	ND	ND	1.45	5.57E-01
Sll0622	P74578	ND	ND	ND	ND
Sll1353	P42350	1.31	7.77E-01	2.61	1.87E-02*

A total of 241 and 648 proteins were detected in experiments 1 and 2. The most enriched protein was atPGR5, confirming successful heterologous expression and antibody specificity. It should be noted that synPGR5 was not detected in any sample. The protein second-most enriched in WT+atPGR5 samples was bacterioferritin 1 (Bfr1). Also Bfr2, a homologue and physical interaction partner of Bfr1 in several bacterial species (Andrews 1998, Uebe et al. 2019), has been found

markedly enriched in both experiments, rendering bacterioferritins strong candidates for physical interaction with PGR5. Bacterioferritins are soluble proteins that form homo- and hetero-dimers catalyzing ferrous iron mineralization and conferring its storage in many bacteria. *Synechocystis* Bfr1 and Bfr2 have been demonstrated to share other known bacterioferritins' characteristics such as oligomer formation and being crucial components in cellular iron storage (Laulhere et al. 1992, Keren et al. 2004). It is therefore unlikely that they are directly involved in PGR5-mediated CEF.

NadA was not detected in any experiment. Sll1217 was found slightly enriched in the course of experiment 2, but enrichment was statistically insignificant. Hence, no direct evidence supporting either NadA or Sll1217 as PGR5-interaction partner could be found. However, an uncharacterized protein called Slr1353 was found moderately, and, in case of experiment 2, significantly enriched. Slr1353 is the only Sll1217-interaction partner reported in *Synechocystis* to date (Sato et al. 2007), raising the possibility of a three-component interaction including atPGR5, Slr1353, and Sll1217.

Bacteria-two-hybrid assay

In order to validate the Co-IP results in an independent test system, candidate proteins were subjected to bacteria-two-hybrid (B2H) assays for protein-protein interaction with PGR5 (see Methods 2.10). The system was preferred over yeast-two-hybrid assays in this study due to the prokaryotic origin of proteins of interest and the higher sensitivity to transient interactions since a persistent second messenger (cAMP) conveys reporter-gene expression rather than the fusion-protein complex itself. Moreover, the assay is insensitive to membrane association of candidate proteins.

Both Sll1217 and NadA were assayed for physical interaction with PGR5. In addition, the best Co-IP interaction partner candidates for atPGR5, Bfr1 and Bfr2, as well as a Bfr-associated ferredoxin (Bfd, encoded by ORF ssl2250) reportedly interacting with Bfr in *Pseudomonas aeruginosa* (Wang et al. 2015), were incorporated into the analysis as positive controls.
Furthermore, Slr1353 was assayed as a putative positive control for interaction with Sll1217, and as a PGR5 interaction partner candidate as suggested by Co-IP. The same analysis was performed for synPGR5, the presumed natural interaction partner of any synPGRL1-LIKE protein. The results of the B2H assay are summarized in Fig 3.27.

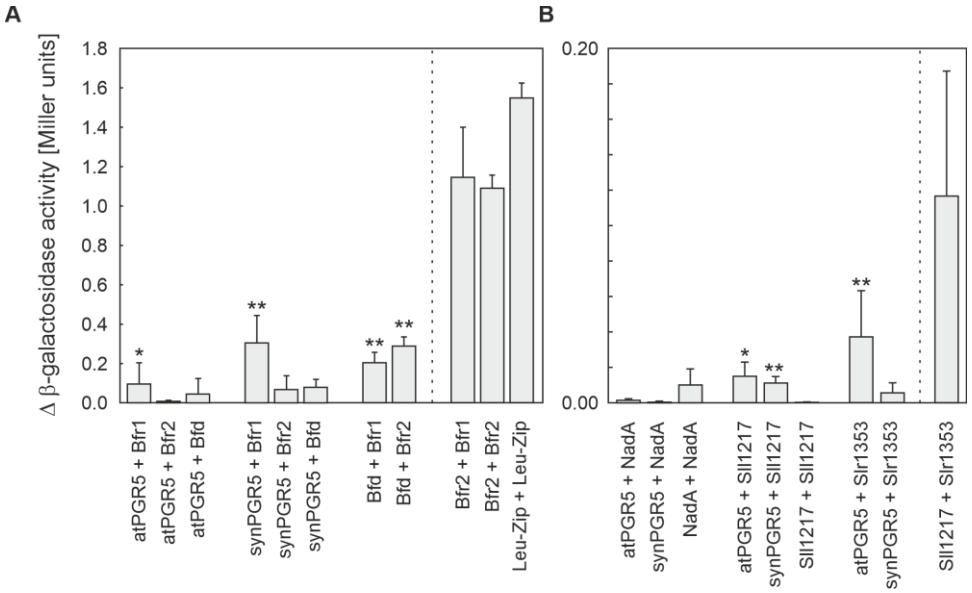

Fig 3.27. **B2H assays for interaction of synPGRL1-LIKE candidates with PGR5.** The degree of protein - protein interaction is indicated as mean differential β-galactosidase activity (i.e. activity above the baseline activity of a negative control of two non-interacting proteins; see Methods 2.10). Error bars correspond to the standard deviation for n = 4 independent experiments for test combinations; n = 16 for negative control. Asterisks indicate significant interaction according to two-sided Student's t-test Holm-corrected for multiple simultaneous comparisons of test combinations to the negative control (* $P \leq 0.05$,** $P \leq 0.01$). Positive controls were excluded from statistical analysis (indicated by dotted lines). (**A**) Interaction of Bfr1, Bfr2, and Bfd (bacterioferritin associated ferredoxin Ssl2250; transient interaction positive control) with atPGR5 and synPGR5, as well as with each other. Bfr dimers yield signals similar to a commercial leucine-zipper positive control (Leu-Zip*Leu-Zip). (**B**) Assay for synPGRL1-LIKE candidate homo-dimerization and interaction with atPGR5 and synPGR5.

Beyond confirmation of Bfr1 as PGR5 interaction partner, significant reporter enzyme activity was detected for atPGR5/synPGR5 and Sll1217, as well as atPGR5 and Slr1353, but not for any PGR5 and NadA. The interaction strength of the atPGR5/synPGR5*Sll1217 couples corresponded to about ten percent of the transient Bfr1/Bfr2*Bfd interactions, indicating a transient or weak interaction. Moreover, the Sll1217*Slr1353-interaction couple discovered by Sato et al. (2007) could be confirmed. In summary, as they corresponded well with the Co-IP results, the B2H results substantiated the candidate status of Sll1217.

3.2.3.3 Knockout phenotypes of synPGRL1-LIKE candidates

To complement the findings of the Co-IP and B2H assays, potential involvement of Sll1217 and NadA in CEF around PSI was assessed in Δ*nadA* and Δ*sll1217* knockout mutants. Knockout of a tentative synPGRL1-LIKE encoding gene was expected to yield a Δ*synpgr5* phenocopy, and to suppress heterologous atPGR5 activity. Knockouts of both candidate genes were generated by homologous recombination, replacing the sll0622 and sll1217 ORFs with kanamycin- and spectinomycin-resistance cassettes, respectively (Kan^R and $Spec^R$; Fig 3.28/3.29 A). Gene deletion was confirmed by PCR (Fig 3.28/3.29 B), and mutant strains (Fig 3.28/3.29 C) were subjected to P700-oxidation kinetics analysis as described earlier (Fig 3.28/3.29 D,E).

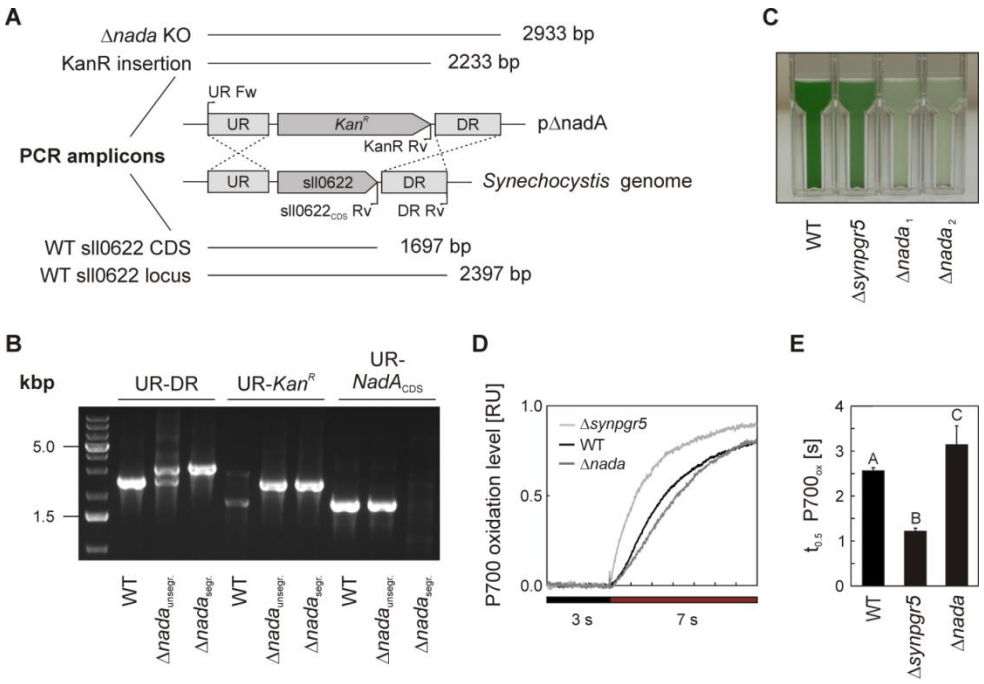

Fig 3.28. **Generation and initial phenotypical assessment of a Δ*nada* knockout mutant.** (**A**) The genomic ORF encoding NadA (sll0622) was replaced with a kanamycin-resistance cassette (*Kan*^{R}) by homologous recom-bination *via* 700 bp of genomic DNA sequence 5' (upstream region UR) and 3' (downstream region DR) of sll1217, using a non-replicative vector as shuttle. Genotyping-primer-binding sites and expected amplicon sizes are indicated. (**B**) Segregation of the Δ*nada* mutation was confirmed by PCR. (**C**) Δ*nada* cultures grown under continuous low light (30 µE) at 30 °C for 7 days displayed pronounced bleaching. (**D**) P700 oxidation in 16 h dark-adapted cells (OD_{730} = 5) upon far-red light onset (indicated by dark red bar). Curves in represent average values of *n* = 5/3/5 independent measurements for WT/Δ*synpgr5*/Δ*nada*, respectively. (**E**) Mean P700-oxidation half-time under far-red illumination ($t_{0.5}P700_{ox}$) with standard deviations for same samples as in (**D**). Letters correspond to statistically significant differences with $P \leq 0.05$ according to one-way ANOVA and post-hoc Tuckey HSD test.

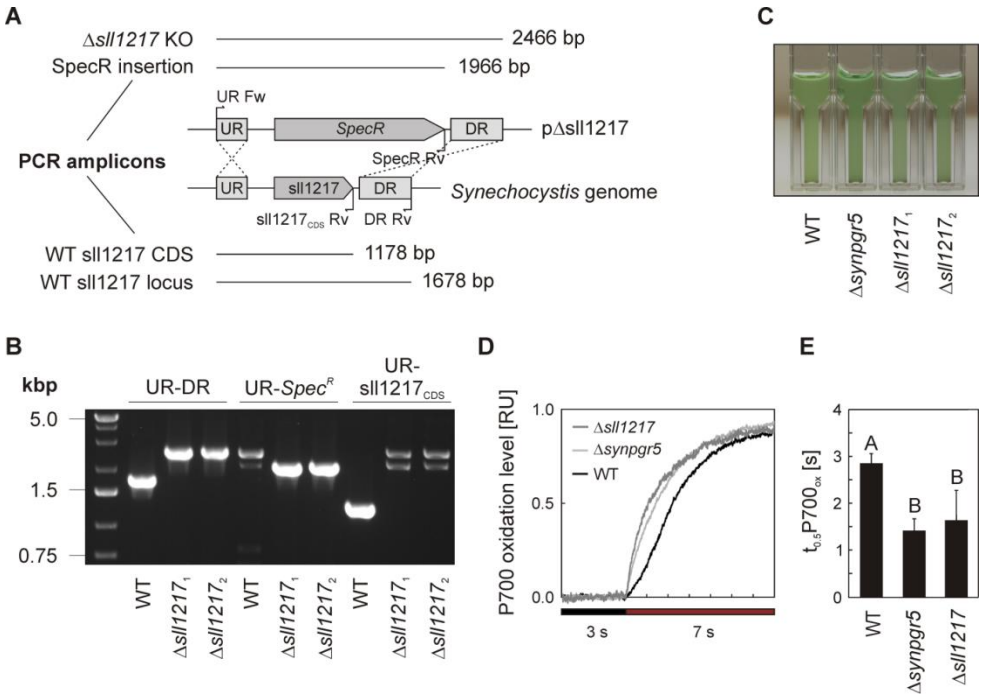

Fig 3.29. **Generation and initial phenotypical assessment of a *Δsll1217* knockout mutant.** (**A**) The genomic sll1217 ORF was replaced with a spectinomycin-resistance cassette (*Spec*^{R}) by homologous recom-bination *via* 500 bp of genomic DNA sequence 5' (upstream region UR) and 3' (downstream region DR) of sll1217, using a non-replicative vector as shuttle. Genotyping-primer-binding sites and expected amplicon sizes are indicated. (**B**) Segregation of the Δ*sll1217* mutation was confirmed by PCR. (**C**) Δ*sll1217* cultures grown under continuous low light (30 µE) at 30 °C for 5 days displayed no obvious phenotype. (**D**) P700 oxidation in 16-h-dark adapted cells (OD_{730} = 5) upon far-red light onset (indicated by dark red bar). Curves in represent average values of *n* = 3/4/2 independent measurements for WT/Δ*synpgr5*/Δ*sll1217*, respectively. (**E**) Mean P700-oxidation half-time under far-red illumination ($t_{0.5}P700_{ox}$) with standard deviations for same samples as in (**D**). Letters correspond to statistically significant differences with $P \leq 0.05$ according to one-way ANOVA and post-hoc Tuckey HSD test.

Δ*nada* mutants displayed a pronounced pale cell culture phenotype (Fig 3.28 C) and decreased P700-oxidation rates in FR light as compared to WT and Δ*synpgr5 (*Fig 3.28 D), while Δ*sll1217* mutants displayed P700-oxidation rates significantly increased as compared to WT, and very similar to Δ*synpgr5 (*Fig 3.29 D). Moreover, no pronounced effect on culture phenotype was observed in Δ*sll1217*, again similar to Δ*synpgr5* (Fig 3.29 C), and no qualitative change was observed after two more days, prior to PAM measurements (data not shown). Combined with the phylogenetic and protein interaction data presented above, these observations finally disqualified NadA as synPGRL1-LIKE candidate. At the same time, Sll1217 was underpinned as a promising candidate.

3.2.3.4 Genetic interaction of synPGRL1-LIKE candidates with PGR5

As mentioned earlier, loss of a synPGRL1-like component was expected to corrupt atPGR5 functionality in *Synechocystis*. To test for such effects, the sll1217 ORF was deleted from the genomes of the Δ*synpgr5* strains expressing atPGR5, atPGRL1+atPGR5, and from synPGR5 over-expressors. Successful gene deletion and presence of transgene constructs was confirmed by PCR (Fig 3.30) using primer combinations established earlier (Fig 3.17, Fig 3.29).

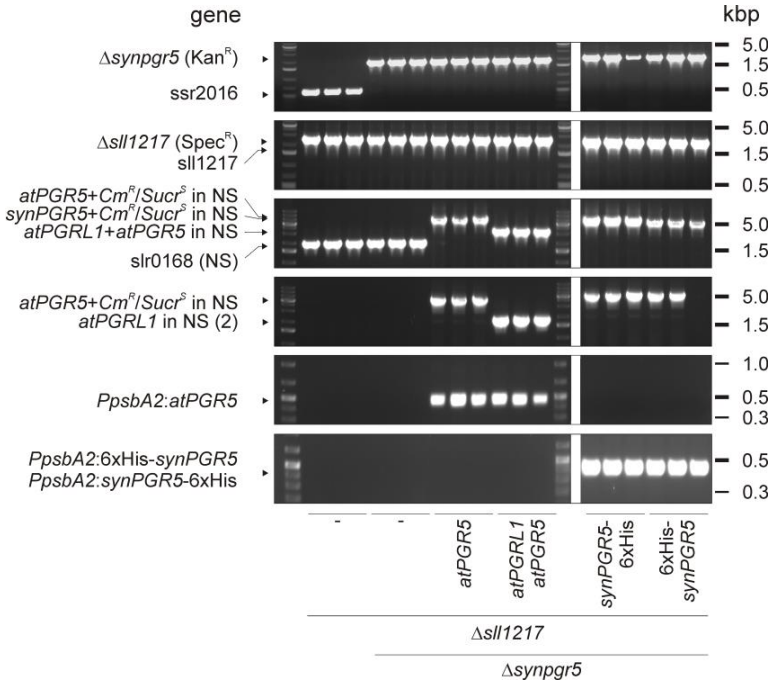

Fig 3.30. **Generation of Δ*sll1217* mutants in CEF mutant backgrounds.** Genotyping PCR of three independent transformants each confirmed the Δ*sll1217* mutation, Δ*synpgr5* genetic background, as well as transgene-cassette presence, and full segregation status. Genotyping-primer combinations and expected amplicon sizes correspond to those described in Fig 3.17 and Fig 3.29.

To assess the effect of Δ*sll1217* on the functionality of atPGR5 and atPGRL1 proteins in *Synechocystis*, mutant strains were subjected to Dual-PAM P700-oxidation-kinetics analysis (Fig 3.31 A) as described above (Sections 3.1.7 and 3.2.2.2). The Δ*sll1217* single and Δ*synpgr5* Δ*sll1217* double mutants displayed accelerated P700-FR oxidation similar to Δ*synpgr5.* Δ*synpgr5* Δ*sll1217* double mutants expressing atPGR5 did display P700-oxidation rates that were equal to those in Δ*synpgr5*, and significantly increased as compared

to the Δ*synpgr5* atPGR5 parental mutant (corresponding to a decrease in P700-oxidation half-time $t_{0.5}P700_{ox}$). Δ*synpgr5* Δ*sll1217* double mutants expressing both atPGRL1 and atPGR5 did not differ from Δ*synpgr5*, however. Both atPGRL1 and atPGR5 protein could be detected in expression strains with Δ*sll1217* mutation (Fig 3.31 B).

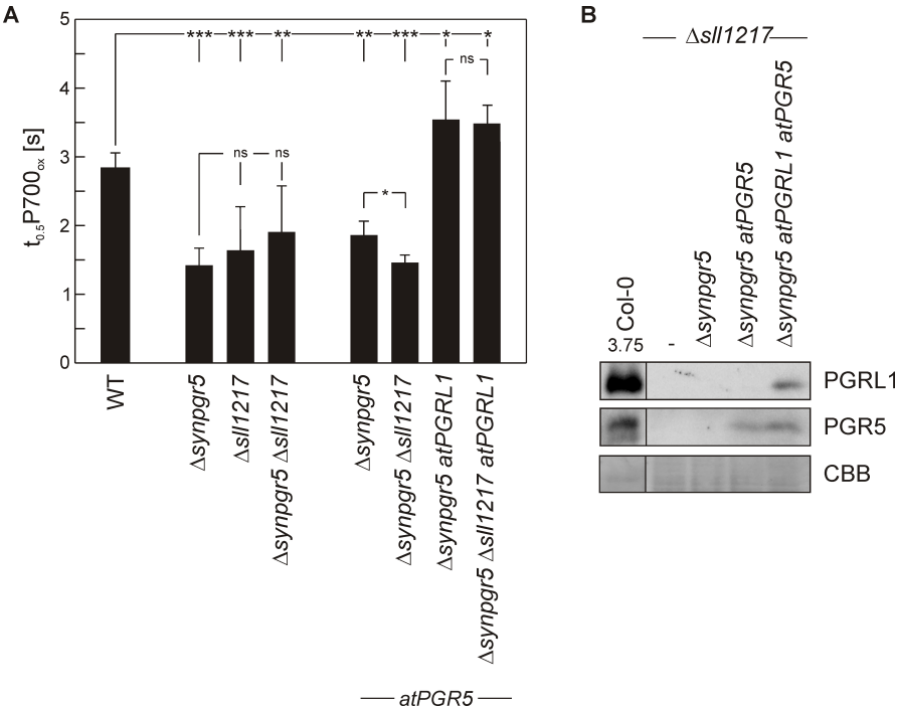

Fig 3.31. **atPGR5 functionality depends on Sll1217 in absence of atPGRL1.** (**A**) Effects of Δ*sll1217* on mean P700-FR-oxidation half-time ($t_{0.5}P700_{ox}$) of atPGR5 and atPGRL1 atPGR5 (co-)expression strains; cultures were grown under continuous low light (30 µE) at 30 °C for seven days. P700 oxidation was measured in 16-h-dark-adapted cells (OD_{730} = 5). Error bars correspond to standard deviations of *n* = 6/6/5/5/4/3/6/4 independent measurements (order as displayed). Statistically significant differences according to Holm-corrected two-sided Student's *t*-tests are indicated with asterisks (* $P \leq 0.05$, ** $P \leq 0.01$, *** $P \leq 0.001$; ns, not statistically significant). (**B**) Immunoblot detection of atPGRL1 and atPGR5 proteins in 30 µg of SDS-PAGE separated thylakoid-protein extracts of various *Synechocystis* Δ*sll1217* strains. Extracts of Δ*sll1217*, Δ*synpgr5* Δ*sll1217*, and WT *Arabidopsis thaliana* (Col-0; 3.75 µg) were used as controls. A segment of the Coomassie Brilliant Blue (CBB) stained blot is provided as a loading control. Please note that the measurements shown above were conducted within the same cultivation batch as measurements shown in Fig 3.19, resulting in shared data for WT, Δ*synpgr5*, Δ*synpgr5 atPGR5* and Δ*synpgr5 atPGR5 atPGRL1* controls.

Effects of Δ*sll1217* on atPGRL1/atPGR5 activity were in line with expected effects of loss of a *Synechocystis* PGRL1 functional counterpart. To test whether Sll1217 actually plays an equivalent role in synPGR5 functionalization, the Δ*sll1217* mutation was introduced into the *Δsynpgr5 synPGR5* over-expression strains described earlier (see section 3.2.2.2). Segregation was confirmed by PCR (Fig 3.30).

P700-oxidation kinetics of synPGR5 over-expressors did not indicate corruption of synPGR5 functionality by loss of Sll1217 (Fig 3.32 A). This effect was unaffected by positioning of the added 6xHis-tag. Also, Northern-blot analyses of the synPGR5 over-expressor *PpbsA2*:*ssr2016*-transcript levels indicated no impairment of transcript accumulation upon introduction of Δ*sll1217* (Fig 3.32 B).

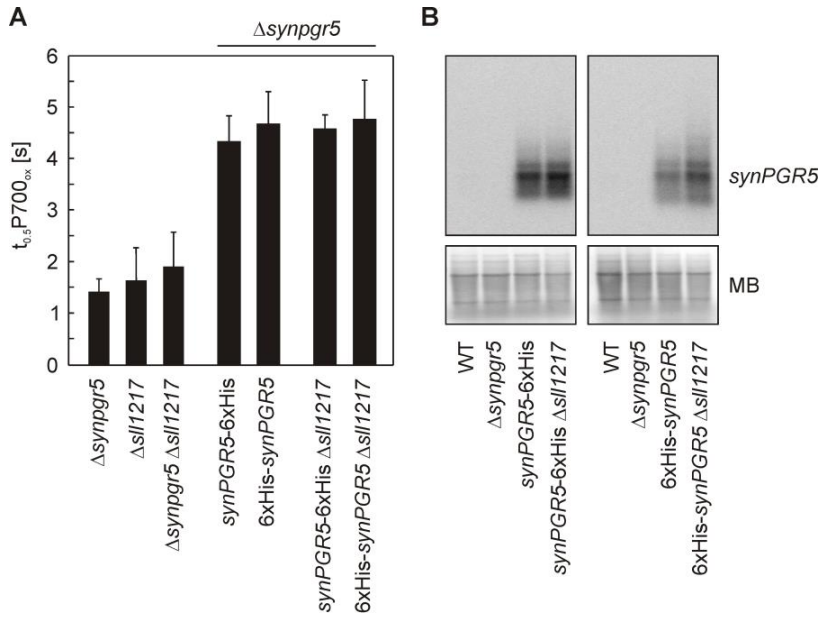

Fig 3.32. **Δ*sll1217* does not accelerate P700-FR oxidation in synPGR5-over-expression strains and does not impair *synPGR5*-transcript accumulation.** (**A**) Effects of Δ*sll1217* on mean P700-FR oxidation half-time ($t_{0.5}P700_{ox}$) of synPGR5-over-expression strains and according controls. Error bars correspond to standard deviations of *n* = 6/5/5/5/9/13/8 independent measurements (order as displayed). Differences were found not statistically significant according to Holm-corrected two-sided Student's *t*-tests. (**B**) Northern-blot detection of *PpsbA2*:*ssr2016* (*synPGR5*). 20 µg of total RNA were loaded per lane. Methylene blue (MB) staining served as loading control. Please note that the measurements shown were conducted within the same cultivation batch as measurements in Fig 3.19 and Fig 3.31, resulting in common data for Δ*synpgr5* and Δ*sll1217* controls.

The findings shown above suggested Sll1217 to be dispensable for *Syn*PGR5-dependent CEF around PSI and basically disqualified Sll1217 as a singular *Synechocystis* FQR. Also, an unexpected effect of Δ*sll1217* was observed regarding the dark-re-reduction of oxidized P700 ($P700^+$) upon FR-illumination offset (i.e. an increase of $P700^+$-re-reduction half-time $t_{0.5}P700^+_{red}$; Fig 3.33).

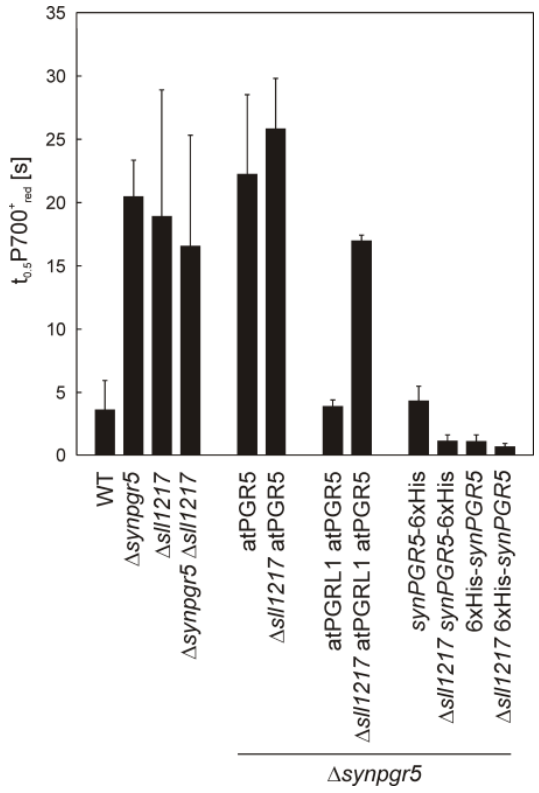

Fig 3.33. **Δ*sll1217* differentially affects $P700^+$ dark re-reduction in strains (over)expressing atPGRL1/atPGR5 or synPGR5.** Cultures were grown photoautotrophically under continuous light (30 µE) at 30 °C for seven days. Columns represent average half time of $P700^+$ re-reduction upon offset of far-red illumination ($t_{0.5}P700^+_{red}$) in 16 h dark-adapted cells (OD_{730} = 5); error bars indicate corresponding standard deviations for *n* = 6/6/5/5/4/3/6/4/5/9/13/8 independent measurements (order as displayed). Please note that the measurements shown above were conducted with the same cultures shown in Fig 3.19, Fig 3.31, and Fig 3.32.

Expectedly, Δ*sll1217* and Δ*synpgr5* Δ*sll1217* constituted Δ*synpgr5* phenocopies with strongly delayed $P700^+$-re-reduction rates as compared to WT. Expression of atPGRL1 and atPGR5 restored Δ*synpgr5* $t_{0.5}P700^+_{red}$ back to WT levels, while expression of atPGR5 alone did not. Intriguingly, Δ*sll1217* caused a major decrease in $P700^+$-re-reduction rates of Δ*synpgr5* atPGRL1 atPGR5 expression strains, but not in synPGR5 over-expression strains. Also, $P700^+$-re-reduction rates in Δ*synpgr5* atPGR5-only expression strains were not affected by Δsll1217.

3.2.3.5 Electrochromism-based CEF assay

The effects of Δ*sll1217* on P700$^+$-dark-re-reduction in different PGR-protein expression strains were puzzling. To substantiate the suggested link between observed P700 oxidation effects and atPGRL1/atPGR5-induced CEF activity, an independent *in vivo* assay for CEF was aimed to be established. To this end, the so-called electrochromic shift (ECS) of thylakoid membrane pigments upon build-up of an electric potential across the thylakoid membrane was measured. In short, ECS is a shift mainly in carotenoid absorbance at 515 nm wavelength (P515) induced by an electric field that alters the energy difference ΔE between the ground state and the excited state of a pigment, resulting in a shift of a respective pigment's absorption band (reviewed in Bailleul et al. 2010). CEF activity somewhat conveniently results in formation of a strong proton gradient across the thylakoid membrane, rendering ECS a potentially viable alternative to P700-redox kinetics to estimate CEF activity *in vivo*. Since CEF has been described to dominate over LEF under conditions limiting electron-sink capacity of the Calvin cycle, we decided to measure ECS upon actinic-light exposure after prolonged dark incubation (≥ 16 h overnight), which should inactivate Calvin cycle enzymes.

ECS was measured in cell suspensions prepared exactly as described for P700 Dual-PAM measurements (see Methods 2.11.5) as P515 $\Delta I/I*10^{-3}$ (see Methods 2.11.5). We observed obvious qualitative differences in P515 spectra of Δ*synpgr5*, WT, and synPGR5 over-expression strains, with Δ*synpgr5* displaying the weakest and synPGR5 over-expressors displaying the strongest positive absorbance shifts. Δ*synpgr5* strains expressing atPGRL1 and atPGR5 displayed an ECS signal intermediate to WT and synPGR5 over-expressors, while atPGR5 expression strains, after an initial positive shift, converged towards the Δ*synpgr5* P515 trace (Fig 3.34 A).

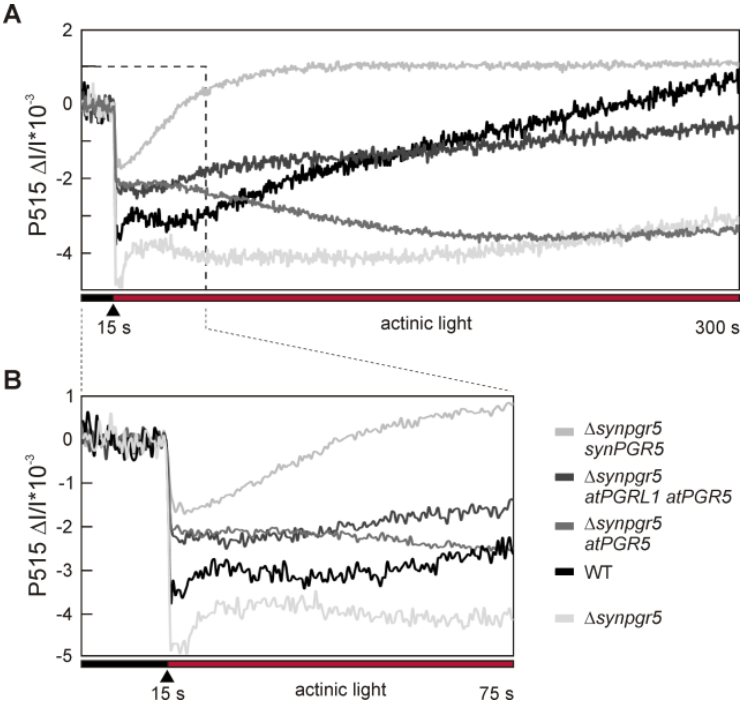

Fig 3.34. **Electrochromic shift is differentially affected in *Synechocystis* CEF mutants and heterologous expression strains.** (**A**) P515 absorbance traces over 4:45 min of actinic-light illumination (symbolized by red bar). Cells were cultivated for seven days at 30 °C and 30 µE of constant light, concentrated to OD_{730} = 5, and dark-incubated for 16 hours prior to measurement. (**B**) Focus on the first minute of actinic light illumination. P515 curves represent averages over *n* = 10 independent measurements (exception: Δ*synpgr5 synPGR5 n* = 9). The absorbance baseline in the dark was set to 0.

Detected ECS signals, especially within the first two minutes after onset of actinic light, mostly correlated well with the findings of P700 FR oxidation measurements (i.e. delayed P700 oxidation coincided with strong initial ECS signal), with exception of atPGR5-only expressors, which displayed a hybrid phenotype of initially strong ECS and subsequent decay to Δ*synpgr5* levels. This pattern might correspond to the intermediate atPGR5-expressor P700 phenotype ranging between the atPGRL1+atPGR5 co-expressor and Δ*synpgr5* phenotypes, however. Still, the clear dichotomy of Δ*synpgr5* and synPGR5 over-expressor phenotypes implied that early ECS and P700 FR oxidation might qualitatively capture the same underlying effect.

To further investigate the effect of loss of Δ*sll1217* on heterologously expressed atPGR5 and atPGRL1+atPGR5 joint activity, ECS measurements were performed with the according strains (Fig 3.35). Strikingly, Δ*sll1217* mutants strongly resemble the Δ*synpgr5* ECS phenotype. Moreover, loss of Sll1217 was found to reduce early ECS in both atPGR5 expressors and atPGRL1+atPGR5 co-expressors, albeit Δ*sll1217* Δ*synpgr5 atPGR5* was found to be affected much more severely, converging towards the Δ*synpgr5* trace within seconds rather than minutes as observed in Δ*synpgr5* atPGR5, and ultimately undershooting it. ECS in Δ*sll1217* Δ*synpgr5 atPGRL1 atPGR5* was affected only mildly, and at a much later time point than Δ*sll1217* Δ*synpgr5 atPGR5*, however.

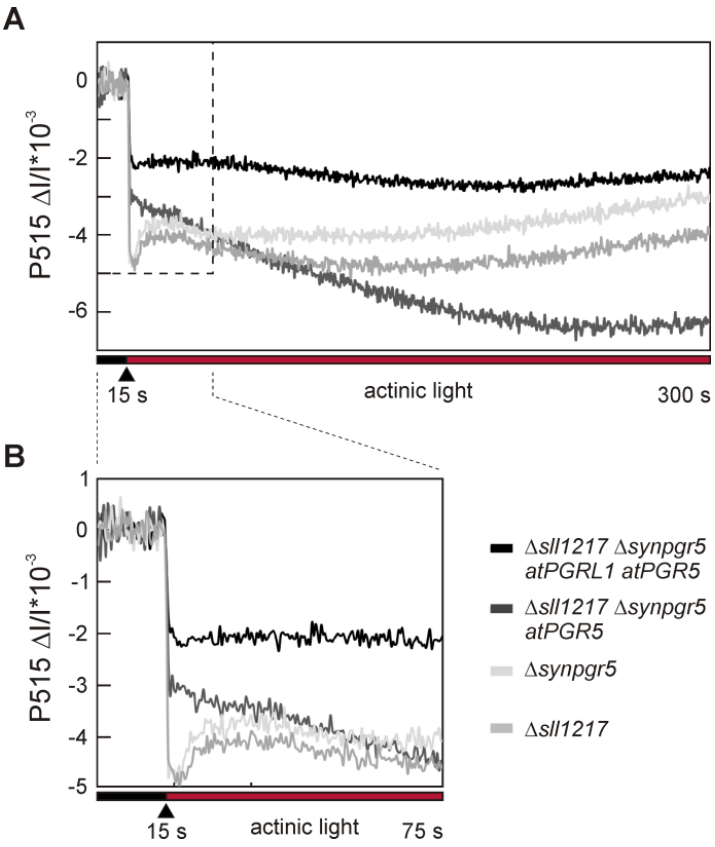

Fig 3.35. **The Δ*sll1217* mutant recapitulates the Δ*synpgr5* electrochromic shift phenotype and negates the effect of atPGR5 expression.** (**A**) P515-absorbance traces over 4:45 min of actinic-light illumination (symbolized by red bar). Cells were cultivated for seven days at 30 °C and 30 µE of constant light, concentrated to OD_{730} = 5, and dark-incubated for 16 hours prior to measurement. (**B**) Focus on the first minute of actinic-light illumination. P515 curves represent averages over *n* = 10 independent measurements. Absorbance baseline in the dark was set to 0. Please note Δ*synpgr5* data is the same as presented in Fig 3.34 since measurements were conducted within the same cultivation batch.

In summary, the effects of *Δsll1217* on P700-redox kinetics under FR treatment clearly imply a functional involvement in CEF around PSI. ECS measurements of the *Δsll1217* single mutant confirmed that it displays a phenotype very similar to Δ*synpgr5*, potentially associated to proton-gradient regulation due to altered CEF activity. In addition, the ECS results essentially reflect the findings of P700-FR-oxidation analyses regarding atPGR5 functionality being seemingly dependent on or influenced by Sll1217 in absence of atPGRL1. However, Sll1217 cannot be assumed to fulfill the exact same role as suggested for PGRL1 in plants, since its loss still affects atPGRL1+atPGR5 co-expressor $P700^+$-re-reduction kinetics and ECS spectra. Upon over-expression, synPGR5 functionality seems to be broadly independent of Sll1217. While atPGR5 functionalization seemingly requires Sll1217 in absence of atPGRL1, atPGR5 protein accumulation does not. Finally, atPGRL1/atPGR5-mediated recycling of electrons to $P700^+$ appears to depend on Sll1217 in the dark, but not under PSI-specific illumination.

To fully explain the observed effects and pinpoint the exact function of Sll1217, additional factors involved in *Synechocystis* PGR5-dependent CEF may need to be identified and characterized. The Sll1217-interacting protein Slr1353 mentioned earlier is a promising candidate for such a factor.

3.2.3.6 Preliminary Slr1353 results

While functionalization of atPGR5 in absence of atPGRL1 apparently depends on Sll1217 in *Synechocystis*, unexpected effects of Δ*sll1217* on synPGR5 over-expressors and atPGRL1+atPGR5 co-expressors implied involvement of at least one, if not several additional factors. Co-IP and B2H assays meanwhile suggested a physical interaction of PGR5 and Sll1217 with the uncharacterized protein Slr1353. In order to assess evolutionary evidence for a potential functional link between *Synechocystis*-type Sll1217 and the Slr1353 protein, protein-sequence analysis of Slr1353 was performed. A global protein alignment did not yield a pattern corresponding to that observed for Sll1217 (i.e. a phase separation between a *Synechocystis*-type and another sub-clade's protein sequences), nor did any distinguished feature on primary structure level become apparent, with exception of a large poorly conserved loop in the middle of the protein sequence (Fig 3.36). Protein BLAST search did not yield any obvious homologue of Slr1353 in non-cyanobacteria or plants.

Maximum likelihood (ML) phylogenetic reconstruction was performed based on the same protein alignment (Fig 3.36; for details, see Methods 2.12.2). ML trees did not yield marked evidence for species of the formerly-described synSll1217-type to cluster separately with respect to Slr1353 (Fig 3.37). Bootstrapping values were < 50 % for most clades, rendering even the most likely tree indicative at most. In summary, no clear evidence for tight co-evolution/co-divergence of a putative Sll1217*Slr1353 couple could be detected.

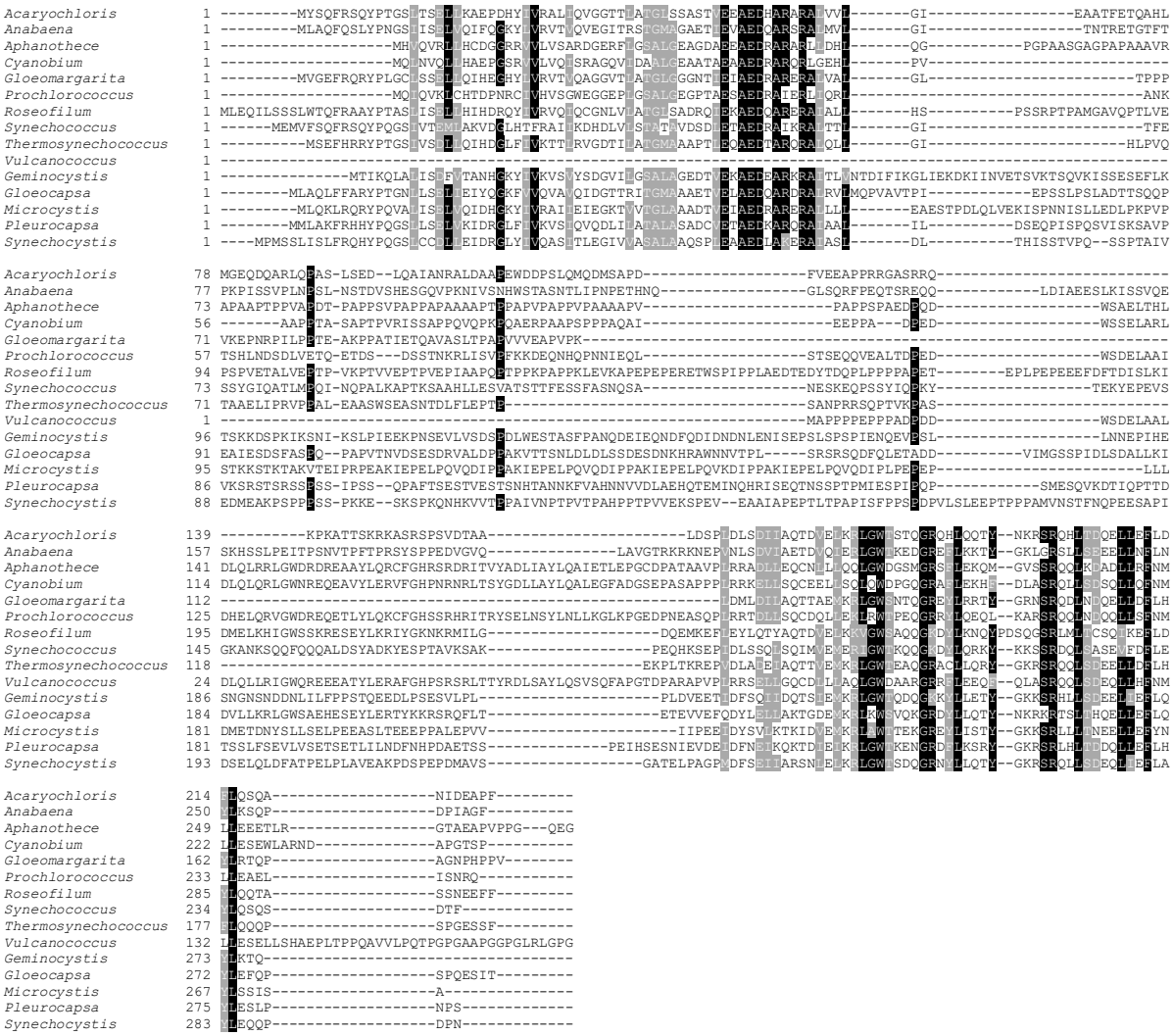

Fig 3.36. **Slr1353 protein alignment.** Protein alignment of Slr1353 sequences from all 15 formerly described cyanobacterial taxa (Tab 3.2). Residues conserved/similar in ≥ 70 % of species are highlighted in black/grey.

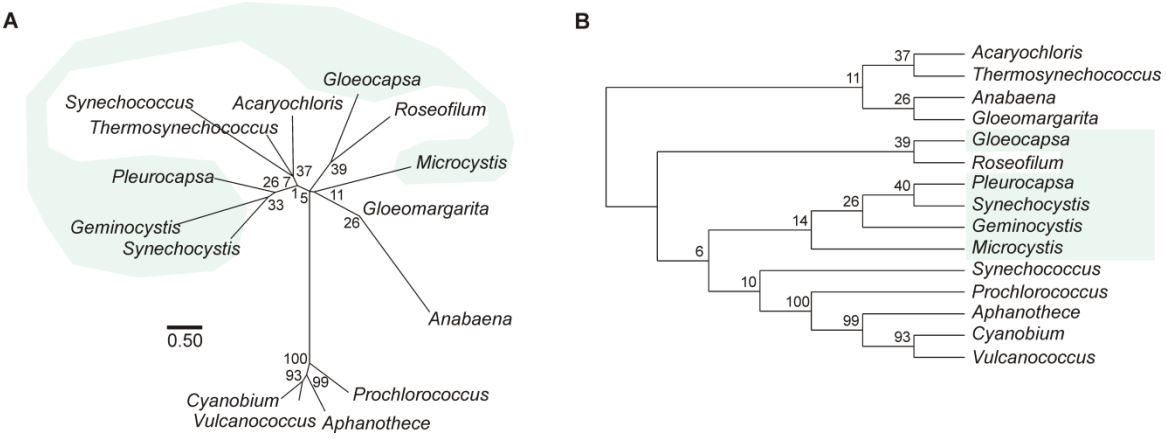

Fig 3.37. **Slr1353 Maximum Likelihood molecular phylogenetic analysis.** Taxa clustering regarding *Synechocystis*-type Sll1217 are highlighted in green. (**A**) Maximum likelihood phylogenetic reconstruction of Slr1353. The tree with the highest log likelihood (-8282.37) is shown. The tree is drawn to scale, with branch lengths measured in the number of substitutions per site (see scale bar). The percentages of replicate trees in which the associated taxa clustered together in the bootstrap test (500 replicates) are shown next to the branches. (**C**) The bootstrap-consensus tree topology inferred from 500 replicates is taken to represent the evolutionary history of the taxa analyzed.

To assess the effect of simultaneous loss of Sll1217 and Slr1353 on synPGR5-over-expressor P700-FR-oxidation kinetics, pΔslr1353 (i.e. a construct to knock out slr1353 by replacement with an erythromycin-resistance gene; see Methods 2.4.5), was transformed into Δ*synpgr5* Δ*sll1217* *synPGR5*-6xHis, as well as the Δ*synpgr5* Δ*sll1217* double mutant. The following data is preliminary and correct insertion/segregation of the Δ*slr1353* construct remains to be verified. Still, several interesting observations were made right after transformation, potentially adding to our understanding of Sll1217 in *Synechocystis* PGR5-mediated CEF; these observations should be mentioned in context of this study.

P700-FR-oxidation rates were measured in liquid cultures supplied with 5 µg ml^{-2} erythromycin derived straight from pΔslr1353 transformation selection plates. Two distinct cultivation batches of tentative Δ*synpgr5* Δ*sll1217* Δ*slr1353** triple mutants were measured independently (Fig 3.38 A) and displayed no difference from Δ*synpgr5* regarding P700 oxidation rates. Transformation of pΔslr1353 into a synPGR5-over-expression strain lacking Sll1217, however, resulted into accelerated P700 FR oxidation as compared to the parental synPGR5 over-expressor (Fig 3.38 B), and caused partial recovery from its pale culture phenotype (Fig3.38 C).

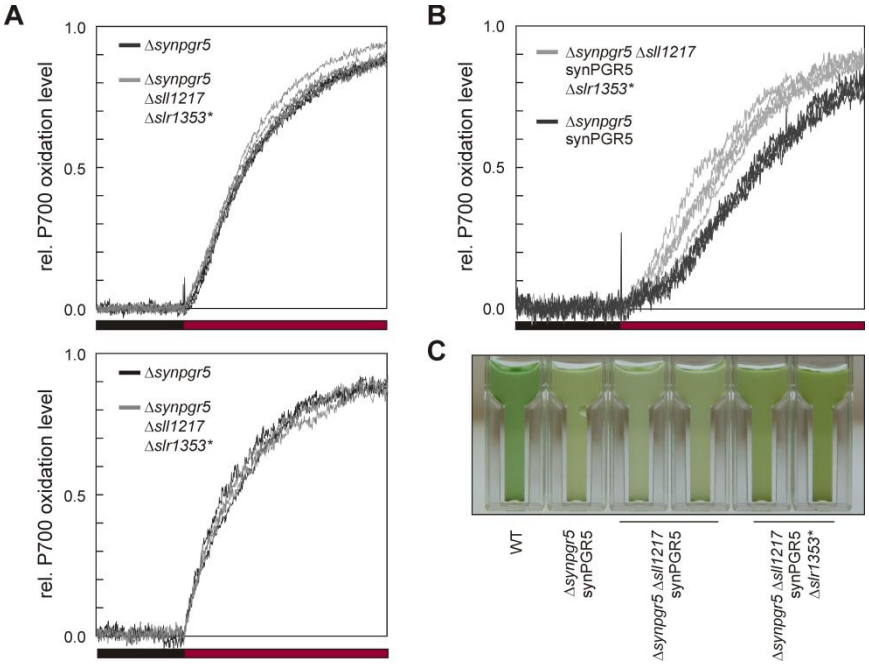

Fig 3.38. **Early-stage pΔslr1353 transformants display a synPGR5-dependent P700-oxidation phenotype**. All cultures were grown photoautotrophically for ten days at 30 °C under continuous light (30 µE). FR oxidation upon far-red-light onset (symbolized by red bar) was measured in 16 h dark-incubated cells (OD_{730} = 5). P700-oxidation curves represent individual biological replicates. (**A**) P700 oxidation in 16 h dark-incubated cells (OD_{730} = 5) of two independent batches of Δ*synpgr5* Δ*sll1217* double mutants transformed with pΔslr1353 (preliminary mutant status signified as Δ*slr1353**). (**B**) P700 FR oxidation rates of Δ*synpgr5* Δ*sll1217* *synPGR5* (synPGR5-6xHis) transformed with pΔslr1353 (Δ*slr1353**). (**C**) Culture phenotype of cultures prior to P700 PAM measurements.

These preliminary results imply that Slr1353 might indeed be involved in PGR5-dependent CEF around PSI in *Synechocystis*. In addition, its physical interaction with Sll1217 (see Fig 3.27) implies functional intertwinements with the former, which requires further experimental investigation.

3.2.3.7 PGRL1-Sll1217 inconsistencies

The Sll1217 protein shares few predicted features with PGRL1. It lacks obvious transmembrane segments and does not possess the set of six redox-sensitive and iron-cofactor coordinating cysteine residues conserved in PGRL1 proteins (DalCorso et al. 2008, Hertle et al. 2013). Moreover, its similarity to UDG4-like proteins does not obviously connect Sll1217 to PGRL1. Some of these discrepancies could potentially be mitigated upon more thorough sequence analysis, however.

Sll1217 uracil-DNA-glycosyltransferase annotation

Functional domain prediction of PGRL1 proteins yielded some intriguing insight regarding the apparent inconsistency of PGRL1 function and Sll1217 predicted uracil-DNA-glycosyltransferase 4 (UDG4)-like structure. Using the Conserved Protein Domain Database (CDD) protein domain classification tool, a distant sequence similarity of PGRL1 proteins to glycosyltransferase superfamily proteins was detected (Tab 3.4). Three out of five assayed plant PGRL1 protein sequences (*Arabidopsis* PGRL1A/B, *Zea* PGRL1B) displayed similarity to glycosyltransferase MraY-like superfamily proteins which use UDP-sugars as a substrate; *Chlamydomonas* PGRL1 meanwhile was similar to the glycosyltransferase sugar-binding region superfamily.

Tab 3.4. **CDD search output indicating distant similarity of PGRL1 to glycosyltransferases.** PSSM-ID, Position-Specific Scoring Matrix ID. Amino acid (aa) positions relative to mature protein sequences. For NCBI sequence IDs of used sequences, see Methods 2.12. Please note that *Zea mays* PGRL1B identification as GT_MraY-like protein is based on an outdated protein domain model (PSSM-ID 324607; labelled with asterisk*). While the NCBI entry for *Zea mays* PGRL1B (XP_008652279) still contains the according annotation, it cannot be obtained from CDD directly.

	PSSM-ID	From aa	To aa	*E*-Value	Accession	Protein superfamily
Chlamydomonas	354516	69	116	0.003	cl19952	glycosyltransferase sugar-binding
Physcomitrella	n.a.	n.a.	n.a.	n.a.	n.a.	n.a.
***Arabidopsis* A**	353087	130	195	1.064	cl10571	MraY-like glycosyltransferase
***Arabidopsis* B**	353087	130	201	0.600	cl10571	MraY-like glycosyltransferase
Zea	324607*	214	273	n.a.	cl10571	MraY-like glycosyltransferase

The according subsequences are conserved among PGRL1 homologues, which indicates prediction of such domains may just have failed for *Physcomitrella*, potentially due to strong divergence of ppPGRL1 – and in general all PGRL1 proteins – from this hypothetical ancient protein function.

Lack of predicted transmembrane helices in Sll1217

Regarding the lack of transmembrane helices (TMHs), an interesting observation was made using the TMHMM tool to predict TMH-forming subsequences. Investigated Sll1217 homologues were found to contain one to three subsequences that yield transmembrane-helix predictions of varying confidence (Fig 3.39 A), and subsequences 2 and 3 happened to align with TMH 1 and 2 of PGRL1 (Fig 3.39 C).

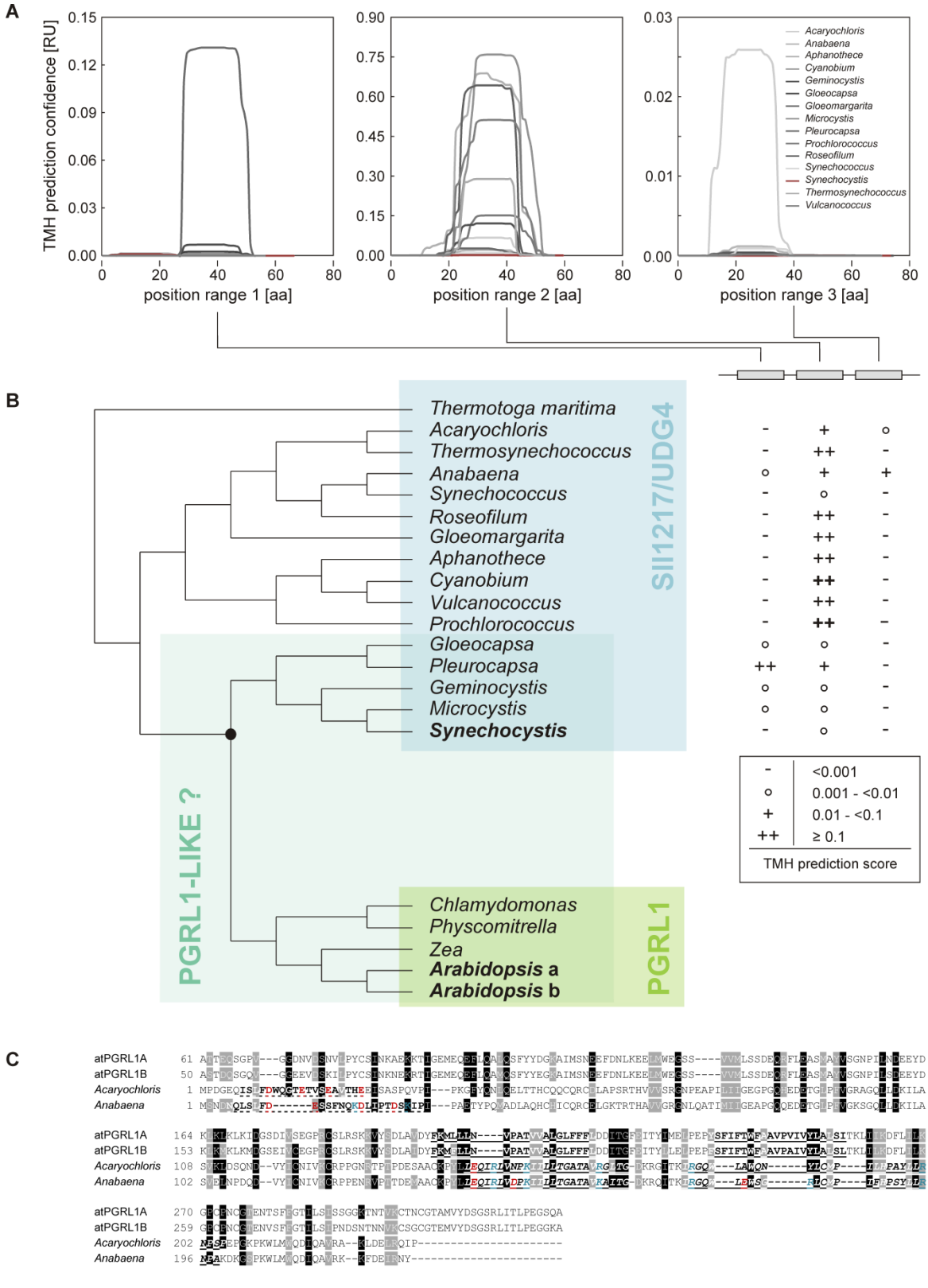

Fig 3.39. **Prediction of possible transmembrane helices in Sll1217/UDG4-like proteins.** (**A**) TMHMM v. 2.0 predictions identified three tentative transmembrane helix (TMH)-forming regions. Since inter-region stretches were not of equal length for all sequences, prediction confidence scores are provided in three subdivided charts spanning 80 amino acids (aa) each. (**B**) Correlating TMH prediction scores with Sll1217/UDG4 phylogenetic reconstruction. The maximum likelihood tree shown is equivalent to Fig 3.26 B. (**C**) Protein-sequence alignment for mature atPGRL1 and cyanobacterial species with cyanobacterial species Sll1217/UDG4 containing TMH 2 and 3 predictions. Predicted TMHs are underlined (interrupted for vague prediction of Sll1217/UDG4 THM 1). Red letters, acidic residues; blue letters, basic residues. Residues conserved/similar in ≥ 70 % of sequences are highlighted in black/grey. Species are abbreviated according to Tab 3.2.

3.2.4 Similarities between PGR5 and Bfr proteins

Our studies in *Synechocystis* expressing plant PGR5-dependent CEF components yielded several interesting implications beyond our original expectations. One of these was the confirmed physical interaction between PGR5 and bacterioferritin Bfr1, as well as possible interactions with Bfr2 and a Bfr-associated ferredoxin (Bfd, Ssl2250; Fig 3.27). Intriguingly, PGR5 shares some features with Bfr beyond physical interaction. An *in silico* prediction of the mature atPGR5-protein 3D structure (I-TASSER, Yang et al. 2015; Fig 3.40 B) displays striking similarities to the known 3D crystal structures of *E. coli* Bfr (Fig 3.40 A; Wong et al. 2009).

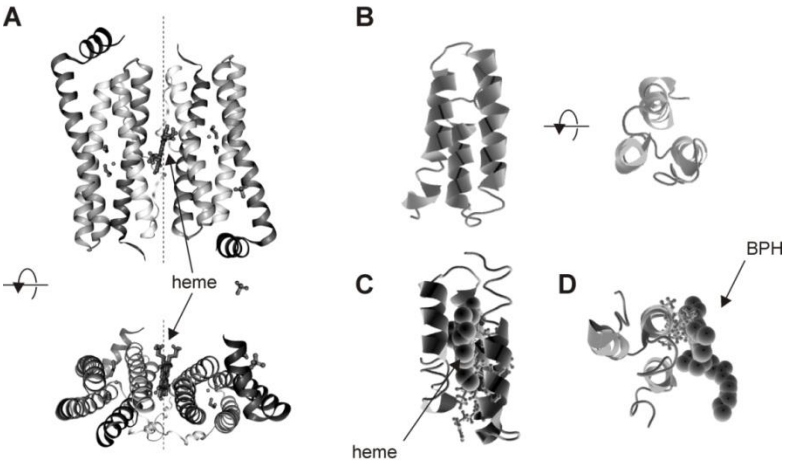

Fig 3.40. **Predicted 3D structure and ligands of atPGR5 resemble bacterioferritin**. (**A**) Crystal structure of *E. coli* Bfr homodimer with heme ligand (PDB-ID 3E2C; Wong et al. 2009). (**B**) I-TASSER prediction of mature atPGR5 protein structure (Yang et al. 2015). (**C**) Predicted heme-binding site (involved residues V16, T17, L20, R30, I34, H37, S38, V40, I41; PDB template Bfr1 [ID: 1BFR; Dautant et al. 1998]; c-score = 0.08). (**D**) Predicted bacteriopheophytin A (BPH) binding site (involved residues K32, A35, L36, V40; PDB template *Rhodobacter sphaeroides* reaction center AijR [ID: 1AIJ; Stowell et al. 1997]; c-score = 0.11); c-scores range from [-2 – 5] with higher values signifying higher prediction confidence.

Both, PGR5 and Bfr proteins consist of roughly parallel α-helix bundles. Moreover, atPGR5 is predicted to laterally bind a tetrapyrrol ligand (Fig 3.40 D), much like Bfr, which dimerizes and *sandwiches* a shared heme ligand between the two monomers. Intriguingly, Bfr1 also is the very template based on which the atPGR5 heme association shown in Fig 3.40 C was modelled.

3.3 Convergent experiment

Regardless of many mechanistic uncertainties, CEF is considered one of the key high-light-acclimation mechanisms in *Synechocystis*. Since CEF is also the apparent subject of one of the high-light tolerant point mutants investigated in this study (HL1; NdhF1$_{F124L}$; see section 3.1.5.1), a direct comparison of the – according to induced delay in P700 oxidation under FR light – most active genetically engineered CEF mutant with the evolved one stirred our interest. Hence, a synPGR5 over-expression strain (Δ*synpgr5* synPGR5-6xHis) and the HL1 mutant were cultivated photoautotrophically under established high-light conditions (700 µE, 23 °C) in a comparative setup. Both mutations gave rise to very similar high-light phenotypes as compared to a WT control regarding general culture phenotype (Fig 3.41 A), pigmentation (Fig 3.41 B), and biomass accumulation (Fig 3.41 C). Comparative P700-oxidation kinetics measurements of cells grown for seven days under standard conditions (30 °C, 30 µE, 140 rpm rotary shaking) revealed similar effects of both mutations (Fig 3.41 D), with synPGR5 over-expression causing an even stronger delay in P700 oxidation relative to WT (+71.4 %) than HL1 (+33.5 %).

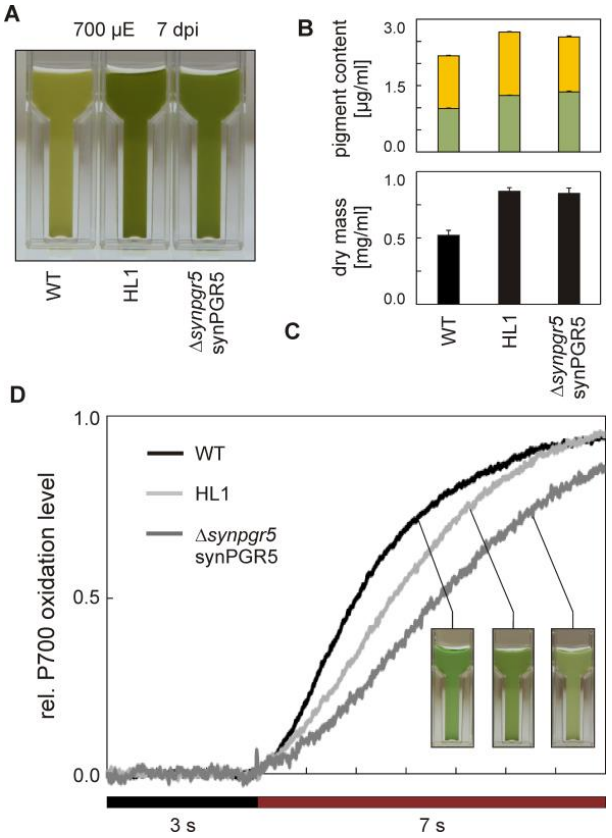

Fig 3.41. **Adaptive values of HL1 and synPGR5 over-expression under high-light treatment.** (**A**) High light culture phenotype of the HL1 point mutant (bearing an NdhF1$_{F124L}$ amino-acid exchange) and a synPGR5 over-expressor (Δ*synpgr5* synPGR5-6xHis) after 7 days at 23 °C and 700 µE continuous light. (**B**) Methanolic pigment extracts of cellular chlorophylls (green) and carotenoids (orange) corresponding to OD_{730} = 0.75 cells. (**C**) Biomass accumulation per ml of final culture. (**D**) P700 oxidation kinetics upon far-red-illumination onset (red bar). Cells were cultivated for seven days at 30 °C and 30 µE of constant light (see inset), concentrated to OD_{730} = 5, and dark-incubated for 16 hours prior to measurement. FR-oxidation kinetics represent averages over *n* = 6, 7, and 6 independent measurements for WT, HL1, and Δ*synpgr5* synPGR5, respectively. Pigment and dry-mass data represents averages and standard deviations over *n* = 3 technical replicates taken from cultures displayed in (**A**).

Interestingly, the presumably higher CEF activity of the synPGR5 over-expression strain did not translate into enhanced pigment content and biomass accumulation. Hence, despite smaller effect size regarding the affected mechanism, on a systemic level the evolved variant performed equally well as the genetically engineered strain.

3.4 Central findings

- In *Synechocystis* oxygenic photosynthesis is a veritable target for high-light adaptive evolution. It is by no means unalterable and can seemingly be made more resilient to photoinhibition by molecular changes in a diverse set of genes including transcription, translation, carbon metabolism, and photosynthesis itself.
- Mutations identified in this study do not make *Synechocystis* proteins converge towards their plant homologues regarding their primary sequence, implying a vastly unexplored space of adaptive molecular mechanisms even in photosynthesis.
- Phenotypic alterations in high-light adapted mutants follow no clear trajectory in detail, with exception of reduction of antenna pigment and increase in protective pigment content.
- Despite the complexity of the trait "high-light tolerance", single non-synonymous amino-acid exchanges can be sufficient to generate measurable and hence selectable improvements in performance.
- Also, under ambient selective pressure, WT cells within a culture diverge from one another, rendering continuous single-clone isolation a good strategy to keep WT homogenous in individual labs. Such practice is likely to compromise among-lab comparability in space as well as within-lab comparability in time considerably, however.
- The plant PGRL1*PGR5 couple suffices to establish CEF in *synpgr5* mutants and restore CEF activity to WT level. Over-expression of synPGR5 results in an even higher CEF activity implying that PGRL1 constitutes either a compensatory component to overcome deficit PGR5 functionality, or a means of achieving more subtle regulation of PGR5.
- An evolutionary pendant to PGRL1 in cyanobacteria might have been discovered in form of Sll1217. Not being a transmembrane protein, a common ancestor of Sll1217 and PGRL1 would have needed to undergo extensive modification and presumably gene fusion events to turn into modern plant PGRL1. However, physical and genetic interaction with synPGR5 and atPGR5 render Sll1217 a viable synPGRL1-LIKE candidate.
- PGR5 might constitute a central hub of high-light-stress integration in *Synechocystis*, interacting with another couple of key players in stress response in form of Bfr1/2 and Bfd.
- Experimentally evolved and artificially induced over-activation of *Synechocystis* endogenous CEF routes yield very similar morphological, physiological and molecular phenotypes. This underlines the potential of adaptive evolution approaches to partially substitute for transgenic approaches.

4 Discussion

4.1 High-light adaptive evolution

4.1.1 Successful evolution of a diverse set of high-light tolerant mutants

In the course an adaptive laboratory-evolution experiment, the tolerance of *Synechocystis* sp. PCC6803 WT cells could be increased from <1100 µE lethal light intensity at 23 °C (Fig 3.1) to > 3000 µE (Fig 3.5). Stemming from one original mutant culture, six batch cultures of high-light tolerant mutants were evolved in parallel (see Fig 3.2). At the end of the experiment batch cultures displayed pronounced phenotypic variability (Fig 3.4, Fig 3.5), and single mutant clones isolated from said batches differed strongly in photosynthetic performance and culture phenotype (Fig 3.6, 3.7). All of this implied that in the course of the experiment different adaptive "strategies" have been realized, rendering the approach itself, as well as the concept of multiple parallel evolutions a success.

Whole genome re-sequencing of isolated clones revealed a high total number of detectable mutations, but no clear increases in mutation incidence in high-light adapted clones as compared to the WT control (Fig 3.8 B). This could either mean that mutagenesis failed to introduce significant amounts of additional genetic variation, or the number of selection cycles after the final mutagenesis step was so high that segregation and new mutations masked the induced increase. The final count of high allele frequency (i.e. > 0.75) synonymous and non-synonymous mutations was increased 2–5-fold in high-light clones, however (Fig 3.8 C, D). Intriguingly, the non-mutagenized evolved WT (WT*; i.e. control WT cells that at one point survived under high-light selection without any mutagenesis) ranged among the mutagenized clones regarding synonymous and non-synonymous high frequency allele count, both of which were increased about 4-fold. These results indicate that neither artificial mutagenesis, nor physiological stress by high-light treatment increased the incidence rate of mutations. Allele-fixation rates, however, were enhanced in high-light treated cultures, as expected of experimental populations under selective pressure in which beneficial mutations arise (Patwa and Wahl 2008 and references therein). Moreover, a predominance shift from first codon position to second codon position mutations was observed for non-synonymous SNPs (Fig 3.8 E). While base exchanges in the first and third codon position mostly preserve hydropathy and polarity of encoded residues, changes in the second codon position mostly result in dissimilar amino-acid substitutions (Haig and Hurst 1991). Dissimilar amino-acid exchanges, however, mostly coincide with protein destabilization or loss/gain of function (Lugo-Martinez et al. 2016). This observation contradicts the common notion that beneficial/adaptive mutations usually derive from similar

amino-acid exchanges that preserve overall protein structure (Castro-Chavez 2010) and might indicate that the harsh selective pressure we applied favored evolution of drastically different protein isoforms after all.

Perplexingly, WT* clones were found to cluster with UM and UMU'M according to maximum likelihood phylogenetic reconstruction (Fig 3.8 F, G). Hence, it cannot be excluded that the sudden occurrence of WT* surviving under control high light was actually caused by contamination with UM and/or UMU'M cell material. In case of no contamination, the only factor left to explain the elevated allele-fixation rates in all high-light strains is selective pressure and, in turn, increased survival rates or reduced generation time of adapted mutants (i.e. greater fitness in bacteria; Wahl and DeHaan 2004). In case of contamination giving rise to WT*, the same combination of mutagenesis and selection affecting the remaining high-light-mutant cultures would be responsible for this effect. Otherwise, the drastically reduced number of selective cycles applied to WT* still would have been sufficient to fix a similar amount of potentially adaptive mutations (Fig 3.8 C, D). This is possible since spontaneously evolved WT* probably would have derived from a single/few cell clone(s) in which many alleles could have been swept into fixation (Majewski and Cohan 1999). Considering the markedly reduced count of high-frequency alleles in less mutagenized but long-term selected UM clones, however, a fixation rate as high as in WT* rather favors contamination of the WT high-light control with UMU'M cell material as origin of WT*. Uncertainties regarding the origin of WT* urgently need to be resolved. In case of independent evolution of WT*, future experiments could refrain from mutagenesis and hence avoid the corresponding risk of contamination, as well as the detrimental effects of narrow genetic bottlenecks without any obvious drawbacks. In case of WT* having descended from a mutagenized culture by accident, mutagenesis might be crucial to achieve the degree of adaptation observed. In order to design follow-up studies ideally, these drastically divergent implications need to be unraveled.

4.1.2 Overlap with candidate genes from other studies

To our knowledge, no other high-light adaptive evolution experiments have been conducted in *Synechocystis* to date. However, studies on evolution of heat tolerance (Tillich et al. 2012, Tillich et al. 2014) and on high-light acclimation over time spans from minutes to a maximum of 15 hours (Hihara et al. 2001, Huang et al. 2002, Tu et al. 2004, Singh et al. 2008; summarized in Muramatsu and Hihara 2012) have been published. If our high-light adaptive candidate-gene set overlapped with genes found mutated during heat-tolerance evolution or differentially regulated during high-light acclimation, this could have provided additional insight regarding common response

elements. However, our candidate genes with mutant allele frequency > 0.5 overlapped only marginally with the published record. This was somewhat surprising, but at the same time implied that our approach might be highly specific in regards to evolving high-light adaptive variants rather than targeting universal stress response factors.

4.1.2.1 Common candidate genes

Our dataset of potentially high-light adaptive mutations contained just two genes overlapping with records of the high-light-acclimation studies. ATP-dependent caseinolytic protease ATP-binding subunit C (*clpC*; sll0020) has been found upregulated in two out of four studies (Huang et al. 2002, Singh et al. 2008) and acquired two independent non-synonymous mutations (I587M and E620D) in our screen. I587M is a low frequency allele (> 0.5; < 0.75), however.

The other shared candidate was slr1855 (repressed in Hihara et al. 2001, Huang et al. 2002; D200G in our screen), encoding an uncharacterized secreted protein (Sergeyenko and Los 2000). Three protein coding genes which were also present in our dataset were found to have acquired non-synonymous mutations in the course of heat-tolerance evolution (Tillich et al. 2014). Said genes/ORFs encode Slr1098, a protein involved in (apo-) phycocyanin oligomerization and hence phycobilisome-rod formation (Hicks 2009; E213V in our screen), pyruvate kinase 2 PykF (Sll1275; A260V and P406T in our screen), and ClpC.

4.1.2.2 clpC

Intriguingly, clpC was found a common target in all three approaches. In plants and cyanobacteria *clpC* is apparently essential (Sjögren et al. 2004, Clarke and Eriksson 1996). In plants its gene product mainly acts as regulatory subunit of the Clp-protease complex (Sjörgen et al. 2014) which is involved in protein homeostasis, embryogenesis and plant development (Olinares et al. 2011). *Synechococcus elongatus* ClpC possesses intrinsic chaperone activity *in vitro* (Andersson et al. 2006), and hence ClpC has been hypothesized to also display standalone activity as independent chaperone *in vivo*. Being high-light induced and subject of heat-and high-light-stress adaptive evolutionary change, ClpC can be considered of central importance to high-light and general stress response in *Synechocystis*.

4.1.2.3 pykF

The second target gene common to both heat and high-light evolution experiments, *pykF*, encodes pyruvate kinase 2, which catalyzes the last step of glycolysis, namely the dephosphorylation of phosphoenolpyruvate and concordant ADP phosphorylation to ATP (Fothergill-Gilmore and Michels 1993, Valentini et al. 2000). Due to its central role in primary metabolism its potential effect on stress tolerance are hardly predictable, but one could speculate on alleviation of stress-induced repression of PykF activity by acquired mutations. Indeed, Pyk activity has recently been shown to constitute a

potential metabolic bottleneck in *Synechococcus elongatus* even under optimal growing conditions (Jazmin et al. 2017), indicating a tentative gain-of-function mutation might foster growth rates under detrimental high-light- or heat-stress conditions.

4.1.2.4 Affected homologues

For three high-light induced genes (**bold**) we found homologues mutated (underlined) in our adaptive evolution screen. These genes encode NDH-subunit 5 (*ndhF3*; **sll1732**, sll0026; involved in inorganic carbon uptake (Zhang et al. 2004)), sigma factor σ^{70} (*rpoD*; **sll2012**, slr0653; primary translation-initiation factor during exponential growth (Jishage et al. 1996 and references therein)), and elongation factor EF-G (*fusD*/*B*; **slr1105**, sll1098; essential GTPase translocating the ribosome along mRNA (Rodnina et al. 1997)). This functional overlap indicates that transcription, translation, and photosynthetic sink capacity play key roles to high-light tolerance, and potentially implies these protein isoforms to contribute differentially to short- and long-term high-light tolerance. If protein homeostasis/repair mechanisms and photosynthetic electron-sink capacity really should be the most limiting factors to cell growth under high light, this might explain why associated genes represent the biggest set of regulatory and mutational targets.

4.1.3 HL1 and HL2 mutants

In order to assess the actual adaptive value of our high-light-mutant-allele library, we introduced two candidate mutations (termed HL1 and HL2) into the WT genetic background and characterized the subsequent changes in high-light performance. This proof of concept yielded promising results for both candidate alleles, but also indicated vastly different adaptive mechanisms to be engaged. These mechanisms are discussed in the following section.

4.1.3.1 HL1

The HL1 mutation (F124L) in NAD(P)H-quinone oxidoreductase subunit 5-1 (NdhF1) has been found to confer increased high-light tolerance in terms of pigment and biomass accumulation under 700 µE of light intensity (Fig3.12). NdhF1 is an integral multi-pass thylakoid-membrane protein involved in proton translocation across the thylakoid membrane (Saura and Kaila 2019). NdhF1 is a constituent of the NDH1 complex isoforms L and L' (Proommenate et al. 2004, Battchikova et al. 2005) which confer NDH-dependent cyclic electron flow (CEF) in *Synechocystis* (Battchikova et al. 2011 and references therein). A *Synechocystis ndhf1* knockout mutant was shown to display an oxidized PQ pool and increased PSII maximum and effective quantum yields (F_v/F_m and Φ_{II}), as well as reduced non-photochemical quenching, probably due to weaker proton-gradient formation in *ndhf1* mutants (Ogawa et al. 2013). This mutant phenotype represents a virtual inversion of the HL1 phenotype.

In HL1, PSI reaction center (P700) FR-oxidation and dark re-reduction were found to be significantly delayed and accelerated, respectively, as compared to a WT control (Fig 3.13 A, B), both of which implies enhanced CEF activity around PSI (Gao et al. 2016). Moreover, HL1 displays reduced F_v/F_m in low-light acclimated cultures (Fig 3.13 C, D) – presumably due to PQ pool over-reduction – and fostered PsaC accumulation under high light (Fig 3.14). Both effects would be expected under enhanced CEF activity, implying PSI protection to underlie the high-light tolerant phenotype of HL1. Under elevated light intensities (240–270 µE) a *Synechococcus* sp. PCC7002 *ndhf1* mutant did not display severe growth defects (Schluchter et al. 1993), but to our knowledge no systematic high-light experiments have been conducted with *Synechocystis ndhf1* so far. Given the opposite phenotypes of *Synechocystis* HL1 and *ndhf1*, the latter can be assumed to be less high-light tolerant than WT, however. Concordantly, the F124L mutation can be assumed to entail an NdhF1 gain of function.

4.1.3.2 HL2

The HL2 mutation (R461C) in elongation factor G2 (EF-G2) has been found to confer increased high-light tolerance in terms of pigment and biomass accumulation under 700 µE of light intensity (Fig 3.12). EF-G is a universally conserved and essential bacterial GTPase that catalyzes unidirectional translocation of mRNA and tRNA through the ribosome (Li et al. 2011, Rodnina and Wintermeyer 2011). EF-G has been suggested as primary target of photosynthetic reactive-oxygen-species (ROS) inhibition of the translational system in *Synechocystis* (Kojima et al. 2007, Kojima et al. 2008). In *Synechocystis,* three isoforms of EF-G have been identified (FusA/B/C or EF-G1/2/3, encoded by slr1463, sll1098, and sll0830, respectively). *In vitro* ROS susceptibility of EF-G1 (Slr1463) was significantly decreased by mutation of two redox-sensitive cysteine residues, C105S and C242S (Kojima et al. 2009); this effect was confirmed *in vivo* for C105S, but not for C242S (Ejima et al. 2012). In addition, heterologous over-expression of Slr1463 and Sll0830, as well as of a putative fourth *Synechocystis* EF-G isoform (Slr1105) in *Synechococcus sp*. PCC 7942, alleviated translational suppression by 1 mM H_2O_2 *in vivo* (Kojima et al. 2007/2008).

In contrast to HL1, P700 FR oxidation in the HL2 mutants was significantly accelerated and dark re-reduction significantly delayed as compared to a WT control, implying reduced CEF activity around PSI (see above). A pronounced $P700^+$ $\Delta I/I$ absorbance dip upon offset of actinic light, which is absent from WT and HL1 (Fig 3.13 A), can be interpreted as P700 dark over-reduction, probably induced by enhanced PSII activity under actinic-light treatment. Equally, significantly enhanced F_v/F_v in low-light acclimated cultures (Fig 3.13 C, D) and increased accumulation of PSII core protein D1 under high-light treatment (Fig 3.14) suggest a PSII-protective mechanism to cause high-light tolerance in HL2 mutants. Taking into account the high ROS susceptibility and the functional involvement of certain

cysteine residues in conferring this susceptibility demonstrated for *Synechocystis* EF-G, it is tempting to speculate the R461C mutation confers ROS protective features, potentially as an additional ROS scavenging group. Indeed, a ROS-protective function of surface-exposed free thiol groups of cellular proteins has been suggested to play a key role on non-glutathione based ROS protection in rat liver mitochondria (Requejo et al. 2010). Hence, *in vivo* experiments to assess alleviation of translational suppression by H_2O_2 due to R461C along the lines of Nishiyama and coworkers (Kojima et al. 2008, Ejima et al. 2012) represent a logical extension of this study.

Regardless of the precise function of the HL2 mutation, EF-G2 can confidently be assumed to play a central role in many high-light adaptive evolutionary pathways, given the sheer number of independent non-synonymous mutations detected in the *fusB* gene. Its apparent importance to high-light adaptation might further hint that, at least for cyanobacteria under high-light stress, the actual bottleneck of coping with PSII photodamage is D1-protein biosynthesis, as already suggested for the moss *Ceratodon* by Aro and coworkers (Rintamäki et al. 1994), rather than D1 degradation (Melis 1999 and references therein). Said degradation crucially depends on FtsH proteases in *Synechocystis* (Silva et al. 2003), much like in plants (Lindahl et al. 2000), and *Synechocystis ftsH* (slr1604) expression has been found upregulated under high-light stress in three out of four high-light-acclimation studies (Muramatsu and Hihara 2012). However, not a single high-light mutation has been detected in *ftsH* genes. In the context of multiple mutations in EF-G2, the complete absence of any *ftsH* homologue (four in *Synechocystis*) mutant from our high light candidate set may be considered an argument for robust protein biosynthesis being a more selectable trait than efficient degradation.

The differences in high-light adaptive mechanisms exploited by HL1 and HL2 suggest that several physiological and metabolic bottlenecks are equally relevant for *Synechocystis* high-light performance. Hence, combinatory effects of HL mutations in different classes of high-light affected genes should be explored experimentally. Such experiments might significantly contribute to our understanding of evolution of vastly different ecotypes by a few point mutations in nature. Taking into account that the two candidate alleles tested are the only ones assessed experimentally so far, and both of them conferred measurably increased high-light tolerance, such studies can be expected to reliably yield interesting insight, and the mutant library produced by this study can be assumed to contain a plethora of rewarding high-light adaptive candidate alleles.

4.2 *Synechocystis* as a test system for plant CEF components

Cyclic electron flow (CEF) around PSI is of crucial importance for efficient photosynthesis under physiologically demanding conditions since it poises cellular ATP/NADPH ratios and prevents stromal/cytoplasmic over-reduction (reviewed by Yamori and Shikanai 2016). While the two major routes of CEF via the NDH complex and via PGR5 are conserved between cyanobacteria and plants, the relative contributions of said routes have shifted in the course of evolution, from mostly NDH-dependent CEF in cyanobacteria like *Synechocystis* (Yeremenko et al. 2005) to predominance of PGR5-dependent CEF in higher plants like *Arabidopsis* (Kawashima et al. 2017). The precise mechanics of PGR5-dependent CEF in plants (and cyanobacteria) are still unclear, and in sum the experimental evidence obtained from different species is puzzling and partially contradictory. Such contradictions include sensitivity *vs.* insensitivity to antimycin A, necessity *vs.* dispensability of PGRL1, and supposed catalytic *vs.* regulatory function of the PGRL1*PGR5 complex (see sections 1.4.2 and 3.2.1).

To resolve some of the pending contradictions we considered a minimal setup of PGR5-dependent CEF on physiologically *neutral ground* (i.e. in a working system mostly orthogonal to all the plant systems out of which said contradictions arose) to be the best possible test system. Therefore, we investigated the transferability of *Arabidopsis* PGR5-dependent CEF into a genetically highly accessible cyanobacterium, *Synechocystis* sp. PCC6803. Upon successful establishment of plant-type CEF such a system would allow us to test the effect of addition or subtraction of candidate proteins, of introduction of mutations, and to assess cross-compatibility of CEF components from different plant and algal species. As such, a prokaryotic test system would pave the road towards a much more systematic and genetic-engineering oriented investigation of PGR5-dependent CEF than it is possible in plants. In *Synechocystis*, the relative contribution of PGR5-dependent CEF has been described to be minuscule (Yeremenko et al. 2005). Therefore, we considered *Synechocystis* (upon removal of endogenous synPGR5; Δ*synpgr5*) as a suitable platform to investigate the effects of gain of function by expression of *Arabidopsis*-type PGR5-dependent CEF, in which open questions can be addressed in a (as compared to plants) quick and easy manner.

4.2.1 Establishing an *Arabidopsis* CEF test system in a Δ*synpgr5* genetic background

We found extensively dark-incubated Δs*ynpgr5* mutants to display a well-measurable phenotype regarding increased P700 oxidation and decreased $P700^+$ re-reduction rates upon far-red (FR) light on- and offset (Fig 3.16), corresponding well with expectations regarding (NDH-dependent) CEF-deficiency phenotypes (Gao et al. 2016). Over-expression strains of synPGR5 meanwhile displayed

the inverse effects on P700-redox kinetics, corresponding exactly to observations in *Arabidopsis pgr5* knockout and PGR5 over-expression lines (Okegawa et al. 2007). This led us to conclude that the phenotypic effect we observed was indeed CEF correlated, and that Δ*synpgr5* was successfully depleted of the respective CEF route.

In order to establish the CEF test system, the *Arabidopsis* proteins atPGR5 and atPGRL1 were expressed in *Synechocystis* independently and in combination. Interestingly, atPGR5 could not fully complement the Δs*ynpgr5* P700 phenotype, while the atPGRL1/atPGR5 couple restored P700 oxidation and re-reduction rates approximately to WT levels (Fig 3.19 E, Fig 3.33); atPGRL1 expression alone meanwhile did not result in any significant effect, neither in absence nor presence of synPGR5 (WT background; Fig 3.19 E, Fig 3.33). These findings implied that atPGR5 crucially depends on atPGRL1 for full functionality in *Synechocystis,* but also that the plant PGRL1/PGR5 system is functionally compatible with the *Synechocystis* photosynthetic machinery without any further plant specific modules. Over-expression of synPGR5 noteworthily caused a stronger effect than atPGRL1/atPGR5 combined. This indicates the capacity for synPGR5-dependent CEF is actually high, unlike previously suggested (Allahverdiyeva et al. 2013). Importantly, our findings contradict interpretations of PGR5 or PGRL1*PGR5 not conferring CEF, but rather regulating LEF (Suorsa et al. 2012). Extensive dark incubation (~16 h without aeration) shutting down the Calvin cycle (reviewed in Buchanan 1980) and PSI-exclusive far-red illumination during P700 measurements should not allow for significant LEF activity. Therefore, delays in P700 oxidation can be excluded with near certainty to be affected by anything but CEF activity.

Our observations also raise questions about interpretations which consider PGRL1 a capacitor of land plant evolution (i.e. a protein that usually acts as physiological buffer and conditionally allows for phenotypic expression of hidden genetic variation; Le Rouzic and Carlborg 2008, Kukuczka et al. 2014). Rather, our results suggest atPGRL1 to reconstitute partially lost functionality of atPGR5. In doing so it potentially adds a layer of regulatory control to PGR5-dependent CEF, perhaps due to the presence and activity of redox-sensitive cysteine residues (Hertle et al. 2013). Conditionally restorable PGR5 functionality instead of constitutive activity may be a necessity in chloroplasts. Detrimental effects of surplus PGR5 activity have been shown in *Arabidopsis* PGR5 over-expression lines which display severe defects in plant development and chloroplast structure (Okegawa et al. 2007). Measurements implying that atPGRL1 is necessary to grant full atPGR5 functionality and CEF activity (Fig 3.19 E) are in line with previous observations made in our lab (DalCorso et al. 2008, Hertle et al. 2013), but puzzling in context of recent findings of Joliot and coworkers. These authors observed maximum CEF activity and duration to be independent of PGRL1 and PGR5 in *Chlamydomonas* (Nawrocki et al. 2019). They concluded that PGRL1 and PGR5 do not play

a mechanistic role in CEF, as already indicated for PGR5 by earlier experiments in *Arabidopsis* (Nandha et al. 2007), but are regulatory elements of the chloroplast redox poise and tune LEF rather than conferring CEF. This of course could be the case in our plant-CEF *Synechocystis* strains as well, but again, measurements were conducted under conditions as specific to CEF as possible, and a plant enzymatic function is presumably easier to transfer into cyanobacteria than a plant photosynthetic regulatory mechanism. Also, these authors did not discuss that crPGR5 does not accumulate in *Chlamydomonas pgrl1* mutant, meaning they in some way described the same mutant (*pgr5*) twice. A facultative alternative CEF route that compensates for the common loss of PGR5 could explain their findings just as well. Such a third CEF route *via* Cytb_6f which recapitulates a "reversed Q-cycle" and is potentially uncoupled from proton translocation has been proposed for *Helianthus annuus* (Laisk et al. 2010) but raised little attention in the field. In addition, the absence of an NDH-1 complex from *Chlamydomonas* chloroplasts (Desplats et al. 2009) and the formation of a composition-wise unique CEF-PSI supercomplex (Iwai et al. 2010, Steinbeck et al. 2018) reflect a fundamentally different setup of CEF around PSI and its possible redundancies in *Chlamydomonas*. The applicability of *Chlamydomonas* CEF experiments on plant questions might need to be re-evaluated at this point. Complementarily, our *Synechocystis* platform can be applied to elucidate the CEF conferring capacities of *Chlamydomonas* PGRL1 and PGR5.

4.2.2 Initial assessment and evaluation of mutant *Arabidopsis* CEF proteins in *Synechocystis*

Our heterologous CEF expression system proved very promising as prokaryotic test platform for plant-CEF-centered questions. To further our understanding of both potential and limitations of the system, we co-introduced a described atPGR5 mutant isoform (loss of function) with a tentative suppressor mutant atPGRL1 isoform into *Synechocystis*.

By reconstitution of the original *Arabidopsis pgr5-1* loss-of-function point mutation (resulting in amino-acid exchange G130S; Munekage et al. 2002) we could demonstrate that the mechanism destabilizing atPGR5$_{G130S}$ *in planta* is apparently conserved in *Synechocystis*. In fact, atPGR5$_{G130S}$ failed to accumulate above detection threshold (Fig 3.21 D) and did not confer CEF activity (Fig 3.21 C), neither alone, nor in combination with wildtype atPGRL1. Co-introduction of a tentative *pgr5-1* suppressor mutation in PGRL1A (S115F; Dr. Belén Naranjo, unpublished; see section 3.2.2.3) reconstituted CEF activity (Fig 3.21 C) and resulted in slight accumulation of atPGR5$_{G130S}$, which coincided with drastically reduced atPGRL1$_{S115F}$ levels (Fig 3.21 D). Interestingly, atPGRL1$_{S115F}$/atPGR5$_{G130S}$ co-expression apparently confers the same CEF activity as the wildtype atPGRL1/atPGR5 couple, indicating that PGR5-dependent CEF

activity does not strictly correlate with PGR5 (or PGRL1) protein abundance. Such a correlation was recently implied by description of a second *atPGR5* allele (*pgr5-2*; S98F) which caused higher residual protein accumulation and less CEF impairment than *pgr5-1* (Yamamoto and Shikanai 2019). The mutant protein couple's enhanced activity might be explained by *Synechocystis* endogenous CEF regulators being unable to recognize the mutant proteins by physical interaction. This might render their activity deregulated and result in *rouge* CEF activity around PSI.

A prominent effect of atPGRL1$_{S115F}$/atPGR5$_{G130S}$ co-expression was pronounced culture bleaching (Fig 3.21 A). A similar effect has been observed in wildtype atPGRL1/atPGR5 co- and synPGR5 over-expressors (Fig 3.19 A), and thus is seemingly linked to enhanced CEF activity. These phenotypes also remarkably resembled that of high-light treated WT cells (Fig 3.12), for which decreased accumulation of PSI and PSII marker proteins could be shown (Fig 3.14). We therefore hypothesize that the bleached phenotypes of high-CEF-activity strains is due to enhanced thylakoid lumen acidification, which initiates physiological responses similar to high-light stress, resulting in a pseudo-high-light-acclimation syndrome. The results obtained for the atPGR5$_{G130S}$/atPGRL1$_{S115F}$ couple were not only in line with expectations regarding a *pgr5-1* suppressor mutant and will contribute to formulation of new working hypotheses on PGR5-dependent CEF regulation, but could also be obtained within a much shorter time frame than according *Arabidopsis* data. This highlights our test platform as a viable option for comparably quick preliminary assessments of artificial and plant-derived alleles alike.

4.3 *Synechocystis* protein Sll1217 may constitute a PGRL1 functional counterpart

PGR5 protein accumulation crucially depends on PGRL1 in *Arabidopsis* (DalCorso et al. 2008) and *Chlamydomonas* (Johnson et al. 2014). However, in *Synechocystis* atPGR5 accumulates in absence of atPGRL1 and confers standalone activity (Fig 3.19). This indicated that a functional counterpart to PGRL1 might exist in *Synechocystis*. Homology-based search for such a synPGRL1-LIKE protein yielded two candidates with distant sequence similarity to the N-terminus of atPGRL1A, the *Synechocystis* quinolate synthase NadA, and an unknown protein, Sll1217, with distant homology to uracil DNA glycosyltransferase subfamily 4 (UDG4; Fig 3.22). NadA could be excluded as synPGRL1-LIKE candidate experimentally for not showing any phenotype associated with CEF deficiency (Fig 3.28) and lacking detectable interaction with PGR5 (Tab 3.3, Fig 3.27). Sll1217, however, was substantiated as a synPGRL1-LIKE candidate by physical protein-protein interaction with both synPGR5 and atPGR5 (Tab 3.3, Fig 3.27). Also, a knockout mutant Δ*sll1217* closely resembles the Δ*synpgr5* P700 phenotype (Fig3.29), and heterologous atPGR5 functionality is lost upon loss of Sll1217 in absence

of atPGRL1 (Fig 3.31). All of these results were in line with expectations regarding behavior of a synPGRL1-LIKE protein and the effects of its loss.

Moreover, phylogenetic reconstruction revealed an Sll1217-subclade including *Synechocystis* Sll1217 to group with plant PGRL1 sequences within the phylogeny of cyanobacterial UDG4-like proteins (Fig 3.26). This indicates potential common ancestry of Sll1217 and PGRL1. This line of evidence has to be considered tentative, however; firstly, because the subclade does not correlate with the cyanobacterial phylogeny and includes scattered species from Chroococcales, Pleurococcales, and Synechococcales, and secondly, because both Sll1217 and PGRL1 clades display extensive evolutionary divergence from their hypothetical common ancestor, as well as from other UDG4-like proteins. Hence, the Sll1217-PGRL1 clade might be an artifact of so-called *long-branch attraction* (Felsenstein 1978, Bergsten 2005), a systematic error of phylogenetic reconstruction due to random accumulation of analogous amino-acid exchanges over evolutionary time, resulting in superficial sequence similarity and thus wrongful placement as homologues. Still, common evolutionary ancestry of PGRL1 and Sll1217 is phylogenetically implied. Sequence identity of Sll1217 to PGRL1 (16.08 ± 1.50 %) could therefore actually be indicative of common descent followed by strong divergent evolution, while observed sequence identity of PGRL1 to NadA (17.01 ± 1.46 %) might be the result of convergent evolution due to several shared functional features (outlined in section 3.2.3.1). In fact, distantly related structural homologues have been found to often have < 15 % pairwise sequence identity and a mere 3–4 % of residues effectively anchor the structure and thus function of a protein (Rost 1997). The same study found evolutionary convergence and divergence to display very similar equilibrium states, making a distinction of the two effects based on protein sequence similarity alone very challenging. Our experimental data implies that NadA and Sll1217 might fall into just that category of uncanny overlap of divergence and convergence.

Assessing PGRL1-Sll1217 inconsistencies

The *Synechocystis* Sll1217 protein lacks several prominent features of *Arabidopsis* PGRL1, among which transmembrane segments and a set of six redox-sensitive and iron-cofactor coordinating cysteine residues conserved in PGRL1 proteins (DalCorso et al. 2008, Hertle et al. 2013) are most intriguing. Also, Sll1217 displays similarity to UDG4-like proteins rather than obvious homology to PGRL1. Both discrepancies might be less severe than initially assumed since (i) Sll1217 homologues have been found to contain sub-sequences that potentially form α-helical transmembrane segments and align with PGRL1 transmembrane helices (Fig 3.39), and (ii) PGRL1 proteins have been found to yield (uracil-) glycosyltransferase predictions (Table 3.4).

Most Sll1217/UDG4 TMH candidates contain a surprising number of interspaced charged residues. This might indicate them to form a couple of amphipathic α-helices. According to *in silico* data such helices may spread on a membrane surface and then pass the membrane in tandem, reciprocally masking their hydrophilic residues (Pohorille et al. 2003). Such amphiphilic helix couples are hypothesized to constitute a major pathway of *de novo* transmembrane segment evolution (Mulkidjanian et al. 2009). Therefore, even if the current *Synechocystis*-type Sll1217 sub-clade does not yield clear TMH predictions and may well not contain any TMHs in fact, a common ancestor of PGRL1 and Sll1217 might have had a much clearer predisposition to evolve a TMH pair at the precise position occupied by modern PGRL1 protein TMHs. Such THM precursors may have evolved into the two TMHs observed in modern plant PGRL1. Also, the weak traces of glycosyltransferase heritage in PGRL1 make an actual common evolutionary origin of PGRL1 and cyanobacterial UDG4-like proteins appear more likely than originally expected.

Eventually, a common descent of PGRL1 and Sll1217 is conceivable despite little similarity on modern protein sequence level. Moreover, Sll1217 can confidently be assumed to play a role in *Synechocystis* PGR5-dependent CEF, and seemingly affects the functionality of atPGRL1 and atPGR5 in a manner mostly in line with expectations of a *Synechocystis* PGRL1-like component. Given the large amount of functional overlap between PGRL1 and Sll1217, we consider re-naming Sll1217 into "synPGRL1-LIKE" henceforth as adequate.

Nonetheless, several questions remain to be addressed, among which the apparent failure of electron return to P700 upon FR light offset in Δ*synpgr5* Δ*sll1217 atPGRL1 atPGR5* (Fig 3.33), the role of the Sll1217 interaction partner Slr1353 (Fig 3.27, Fig 3.38), and a presumed membrane attachment mechanism for Sll1217 (co-migrating at ~600 kDa in native gels; Takabayashi et al. 2013) are the most urgent ones.

4.4 Electrochromism-based CEF assay

Our conclusions regarding successful establishment of a *Synechocystis*-based plant CEF test platform near-exclusively rely on P700 redox kinetics measurements. This is because absorbance measurements tracing oxidation and re-reduction kinetics of PSI reaction center P700/$P700^+$ have become a commonly used method to non-invasively approximate CEF activity *in vivo* and yield robust results in cyanobacteria and plants alike (Mi et al. 1992/1994/2000, Okegawa et al. 2007, Gao et al. 2016). Most other CEF measurements or approximations meanwhile rely on artificial systems, such as isolated thylakoid membranes in ruptured chloroplast assays (Endo et al. 1998), and/or the use of often pleiotropic inhibitors such as NDH-inhibitory Hg^{2+} (Mi et al. 1992,

Mi et al. 1995) and rotenone (Mi et al. 1995, Deng et al. 2003), PSII-inhibitory 3-(3,4-dichlorophenyl)-1,1-dimethylurea (DCMU), and of course antimycin A (Joliot and Joliot 2002, Taira et al 2013). While we consider P700 measurements as applied in this study a reliable CEF proxy, we worked on establishing an independent *in vivo* CEF assay to assess the robustness of our results and substantiate our conclusions.

Electrochromism offers another non-invasive method for probing a CEF-associated phenomenon, namely the generation of an electric field across the thylakoid membrane due to proton gradient formation (ΔpH). Electric fields in turn alter the absorbance spectra of membrane-embedded pigments (Witt et al. 1979). This voltage-induced *electrochromic shift* (ECS) of primarily carotenoid-pigment absorbance at 515 nm wavelength (P515; $\Delta(Abs_{515}-Abs_{550})$) has been repeatedly suggested as CEF probe (Bailleul et al. 2010, Fan et al. 2016). Several plant protocols have been established to monitor proton gradient formation in CEF mutants via ECS (Sacksteder et al. 2000, Joliot and Joliot 2002), but only in one single older study ECS could be measured in a cyanobacterium (Hirano and Katoh 1981). After decades of dismissal of this idea, a new attempt to measure ECS in cyanobacteria has been made very recently (Viola et al. 2019, *published after completion of the practical work covered in this thesis*). However, ECS has not been used to study CEF in *Synechocystis* so far.

CEF is hypothesized to dominate photosynthetic electron transport under certain conditions, such as dark-light-transitions while the Calvin cycle is mostly inactive (Ort and Baker 2002, Johnson 2005, Joliot 2006). This time span has been shown to corresponds to up to two minutes in *Arabidopsis thaliana* and *Hordeum vulgare* (Finazzi et al. 2004), leading us to reason that altered CEF activity and concordant changes in ΔpH formation should be observable in our *Synechocystis* mutants in a semi-quantitative manner by monitoring P515 over minutes upon actinic-light exposure in extensively (~16 h) dark-adapted cells.

We prepared cells exactly like for P700 measurements and indeed we could observe changes in P515 signals in our CEF mutants seemingly specific to different CEF activity levels. The CEF-deficient mutants Δ*synpgr5* and Δ*sll1217* displayed the weakest P515 signals (Fig 3.35), while synPGR5 and atPGRL1 atPGR5 (over-)expression strains displayed the strongest P515 signals (Fig 3.34). This was in line with expectations of CEF resulting in fast and strong ΔpH formation even under LEF-deprived conditions. Other mutant strains' P515 results aligned with the corresponding trends observed in P700 oxidation under far-red light treatment. This means low P700-oxidation rates (presumably due to high CEF activity) coincided with strong ECS (presumably due to strong ΔpH formation) and *vice versa*. Hence, the ECS-based measurement protocol proposed in this study might offer a second non-invasive method complementary to CEF activity approximation by P700-redox kinetics.

An exact interpretation of the P515 kinetics, especially at later time points, certainly requires further experiments. In fact, long-term development of P515 kinetics under actinic light, also in plants, is poorly understood to date (Allorent et al. 2018), and has not been subject of broader interest – presumably due to the complexity of the signal. However, according to Schreiber and Klughammer (2008), absorbance changes in the sub-second to minutes time range are near-exclusively caused by P515, while slow changes ranging from minutes to hours are due to zeaxanthin formation, at least in plants. Indeed, ECS-based CEF approximations usually rely on short-term (i.e. µs-ms) decay kinetics upon dark-pulse application (Sacksteder et al. 2000, Wang et al. 2015, Yamamoto et al. 2016) or offset of previously applied continuous light (Joliot and Joliot 2002). Similar time scales of ECS signal detections have been reported for cyanobacteria (Hirano and Katoh 1981, Viola et al. 2019). In our hands, however, attempts of such measurements failed in *Synechocystis*.

Surprisingly, in our approach *Synechocystis* cells were observed to display a pronounced and quasi-instantaneous P515-signal dip upon onset of actinic light, much in contrast to plants, which display a sharp increase in P515 at this place (e.g. Allorent et al. 2018). We speculate this dip might be an artefact caused by phycobiliprotein fluorescence under actinic light treatment which includes shorter wavelengths than chlorophyll fluorescence (Simis et al. 2012). Such emission might be misinterpreted as *negative absorption* by the DualPAM-100 detector unit. This hypothesis can easily be tested in phycobilisomes-less mutants such as the allophycocyanin A/B double knockout mutant Δ*apc* available in our lab (Viola 2014), which should not display such a dip, accordingly. As already mentioned, the post-dip P515 signals corroborated the trends of P700-oxidation data, indicating the same phenomenon to underlie the observed effects (i.e., presumably, CEF activity delaying P700 FR oxidation and resulting in strong ΔpH formation, increasing ECS). It is important to mention that both approaches we used to assess CEF activity are semi-quantitative in nature, rendering them probably unsuitable for precise description of electron transport rates, but certainly useful tools for mutant phenotype analysis and the identification of new CEF components.

4.5 Convergent experiment: Enhanced high-light tolerance by engineered and evolved CEF

Cyclic electron flow is generally considered a high or fluctuating light adaptive mechanism that buffers the photosynthetic apparatus from photodamage/-inhibition (Takahashi et al. 2009, Suorsa 2015, Alboresi et al. 2019, Yamamoto and Shikanai 2019) and provides additional ATP for carbon fixation and cellular repair (Murata and Nishiyama 2018, Nakano et al. 2019). This conclusion is mostly based on

indirect evidence, such as poor growth of loss-of-function mutants under said challenging lighting conditions (e.g. Yeremenko et al. 2005, Suorsa et al. 2012). In the course of this study, however, we could demonstrate the actual positive high-light adaptive value incurring with strong CEF activity.

In fact, increased high-light tolerance could be observed due to an evolved high-light mutant NdhF1 isoform apparently conferring higher NDH-CEF activity (HL1; $NdhF1_{F124L}$), and in a *Synechocystis* endogenous PGR5 over-expression strain (Fig 3.41). Noteworthily, the effect of the HL1 mutation on CEF activity was milder than that of synPGR5 over-expression, but high light performance of the HL1 strain was equally enhanced. This means that our evolutionary approach was suitable to generate not only new adaptive alleles, but one of these alleles does (and others might do as well) rival the effect size achievable by over-expressing a known component from one of the strongest expression systems available for *Synechocystis* (i.e. D1 promoter *PpsbA2*; Englund et al. 2016). This might be due to a strong demand for physiological poising, and detrimental effects occurring upon unbalancing photosynthetic electron transport, as proposed by Shikanai and coworkers (Okegawa et al. 2007). By employing adaptive evolution, such problems can apparently be avoided. This is somewhat unsurprising, since the HL1 mutation, like all mutations of the high-light screen, was selected for under physiological conditions. Given the majority of fixed mutations actually rose in allele frequency due to natural selection, they must be not only physiologically compatible, but even net beneficial. This criterion does simply not apply to transgenic approaches, and this might explain why only few transgenic attempts of improving plant growth by targeting photosynthesis have succeeded so far apparently (Kromdijk et al. 2017, Głowacka et al. 2018).

4.6 On the evolution of PGR5-dependent CEF

In the course of searching *Synechocystis* PGRL1-like components, we could confirm a physical interaction between PGR5 and bacterioferritin Bfr1, as well as possible interactions with Bfr2 and a Bfr-associated ferredoxin (Bfd, Ssl2250; Tab 3.3, Fig 3.27). *In-silico* atPGR5 protein-structure prediction (Fig 3.40 B) revealed apparent similarities to the known 3D crystal structures of *E. coli* Bfr and a common tetrapyrrol ligand (Fig 3.40 A, C, D). Also, the prediction of atPGR5 heme association was coincidentally modelled based on Bfr1. So the question arises whether PGR5 originally might have been derived from a primordial bacterioferritin-like protein. After all, all photosynthetic complexes presumably involved in CEF heavily rely on iron cofactors (Cytb_6f: 4 hemes and 1 Fe_2S_2 cluster; PSI: 3 Fe_4S_4 clusters; NDH: 3 Fe_2S_2 clusters), and ferredoxin (Fe_2S_2) is the soluble acceptor of PSI electrons. Hence, biogenesis and maintenance of this photosynthetic super-unit demands large amounts of bioavailable iron, which happens to be provided *via* bacterioferritins in cyanobacteria. With such an array of heavily iron dependent redox enzymes and electron carriers, it can be considered rather plausible that CEF may have evolved from a spontaneous short circuit under over-supply of photosynthetic electrons established by iron-delivering proteins that supplied Cytb_6f, PSI and NDH. PGR5 might thus have been derived from such an originally involved bacterioferritin.

In addition to this, two non-synonymous mutations have been found in the ORF encoding Bfr2 (slr1890) in the course of high-light-mutant-batch-culture sequencing (I9L, S76R). While Bfr2 expression is not directly induced by high light (Muramatsu and Hihara 2011), it is induced under 3 mM H_2O_2 treatment (Houot et al. 2007). Since photosynthetic ROS formation is a known result of prolonged high-light exposure in *Synechocystis* (photooxidative stress; Havaux et al. 2005), an association of Bfr2 activity with high-light stress appears plausible. Also, PGRL1 has been suggested to link partitioning of photosynthetic electrons to iron sensing in *Chlamydomonas* (Petroutsos et al. 2009), possibly substantiating a link of PGR5-dependent CEF to iron metabolism. This is highly speculative, and further experiments will be needed to assess the relevance of this hypothesis. It might, however, add to our understanding of the evolutionary origins of the sophisticated and intertwined electron-transport network of modern oxygenic photosynthesis.

5 Conclusion

This study aimed at breeding new high-light tolerant *Synechocystis* strains on the one hand, and at re-building one of the least understood light-stress-tolerance mechanisms of *Arabidopsis thaliana* in *Synechocystis* on the other hand. Both approaches constitute a shortcut to understanding how photosynthetic tolerance to high-light stress may have evolved, and how it is currently realized in plants. Also, both attempts can be considered a success.

De novo evolution of high-light tolerance yielded mutant strains beyond our capacity to select against, and exemplary reconstitution of two high-light mutant alleles in WT cells yielded distinctly high-light adapted phenotypes. Selected mutations appear at highly conserved positions and preferentially cause physio-chemically severe amino-acid exchanges. This implies truly novel adaptive mechanisms to underlie high-light strain evolution, rather than re-iteration of already realized strategies. Moreover, most of our best candidate mutations were found not in photosynthetic, but rather in primary-metabolism genes. This might hint at the true bottleneck of high-light adaptation not being the resilience of the photosynthetic apparatus *per se*, but the cell's capacity to sustain and maintain it under stress. The absence of presumed gain-of-function mutations in designated high-light protective proteins, such as flavodiiron proteins or high-light inducible polypeptides (HLIPs), bears similar implications. Therefore, not only could we demonstrate *Synechocystis* to have great evolutionary potential, but we also may provide photosynthesis research with transferrable building blocks for high-light tolerance. This mutant library may also grant us general insight into the molecular mechanisms and key players of adaptation to photosynthesis-related environmental stresses. Finally, this adaptive-evolutionary approach could in principle be extended to tackle any kind of question, or improve any trait for which an adequate selective pressure can be applied. Evolution-based optimization or trouble shooting of photosynthesis, by standards of this pilot study, is feasible on both spatial and temporal scale in almost every laboratory.

PGR5-dependent cyclic electron flow remains a puzzling process, but the *Synechocystis*-based platform that could be established will doubtlessly prove itself useful to study plant CEF components. Also, it should certainly be extended to other model species such as *Chlamydomonas* to contribute to resolving the current conundrum. Surprisingly, the plant components we introduced turned out to be much less *out of context* and hence orthogonal within the *Synechocystis* chassis than originally assumed. In fact, the *Arabidopsis* PGRL1*PGR5 couple appears to be fully compatible with the *Synechocystis* photosynthetic machinery, and to efficiently confer CEF. In this regard, our setup represents an augmentation of Shikanai and colleagues' work who established a functional heterologous flavodiiron protein electron sink in *Arabidopsis* (Yamamoto et al. 2016). While their

system functioned as dead end for electrons (pseudo-cyclic electron flow) and resulted in water condensation, our setup seemingly extracts *and* re-injects electron from/into the electron transport chain. Moreover, our results imply that PGRL1 (and presumably further yet unknown components) actually possess in part strongly diverged counterparts in *Synechocystis* that yet fulfill a similar functional role. Identification and removal of these components will have to precede the development of purely *Arabidopsis*-protein-driven CEF, but the *Synechocystis* system might allow for much more rapid and efficient identification of the respective candidates. These, in turn, might greatly facilitate final elucidation of PGR5-dependent CEF in plants, and might lead to the conclusion that the original setup of CEF around PSI is much more ancient and conceptually conserved than expected.

6 References

Alboresi, A., Storti, M., & Morosinotto, T. (2019). Balancing protection and efficiency in the regulation of photosynthetic electron transport across plant evolution. *New Phytologist*, 221(1), 105-109.

Allahverdiyeva, Y., Mustila, H., Ermakova, M., Bersanini, L., Richaud, P., Ajlani, G., ... & Aro, E. M. (2013). Flavodiiron proteins Flv1 and Flv3 enable cyanobacterial growth and photosynthesis under fluctuating light. *Proceedings of the National Academy of Sciences*, 110(10), 4111-4116.

Allen, J. F. (2002). Photosynthesis of ATP—electrons, proton pumps, rotors, and poise. *Cell*, 110(3), 273-276.

Allen, J. F. (2003). Cyclic, pseudocyclic and noncyclic photophosphorylation: new links in the chain. *Trends in plant science*, 8(1), 15-19.

Allen, J. F. (2014). Origin of oxygenic photosynthesis from anoxygenic type I and Type II reaction centers. In *The Biophysics of Photosynthesis* (pp. 433-450). Springer, New York, NY.

Allen, J. F., de Paula, W. B., Puthiyaveetil, S., & Nield, J. (2011). A structural phylogenetic map for chloroplast photosynthesis. *Trends in plant science*, 16(12), 645-655.

Allen, Mary B., Frederick R. Whatley, and Daniel I. Arnon. "Photosynthesis by isolated chloroplasts: VI. Rates of conversion of light into chemical energy in photosynthetic phosphorylation." *Biochimica et biophysica acta* 27 (1958): 16-23.

Allorent, G., Byrdin, M., Carraretto, L., Morosinotto, T., Szabo, I., & Finazzi, G. (2018). Global spectroscopic analysis to study the regulation of the photosynthetic proton motive force: A critical reappraisal. *Biochimica et Biophysica Acta (BBA)-Bioenergetics*, 1859(9), 676-683.

Alric, J. (2015). The plastoquinone pool, poised for cyclic electron flow?. *Frontiers in plant science*, 6, 540.

Andersen, B., Scheller, H. V., & Møller, B. L. (1992). The PSI-E subunit of photosystem I binds ferredoxin: NADP+ oxidoreductase. *FEBS letters*, 311(2), 169-173.

Andersson, B., & Aro, E. M. (2001). Photodamage and D1 protein turnover in photosystem II. In *Regulation of photosynthesis* (pp. 377-393). Springer, Dordrecht.

Andersson, F. I., Blakytny, R., Kirstein, J., Turgay, K., Bukau, B., Mogk, A., & Clarke, A. K. (2006). Cyanobacterial ClpC/HSP100 protein displays intrinsic chaperone activity. *Journal of Biological Chemistry*, 281(9), 5468-5475.

Andrews, S. C. (1998). Iron storage in bacteria. In *Advances in microbial physiology* (Vol. 40, pp. 281-351). Academic Press.

Antal, T. K., Kukarskikh, G. P., Bulychev, A. A., Tyystjärvi, E., & Krendeleva, T. (2013). Antimycin A effect on the electron transport in chloroplasts of two Chlamydomonas reinhardtii strains. *Planta*, 237(5), 1241-1250.

Arnon, D. L., Whatley, F. R., & Allen, M. B. (1958). Assimilatory power in photosynthesis. *Science*, 127(3305), 1026-1034.

Arnon, D. I., Allen, M. B., & Whatley, F. R. (1954). Photosynthesis by isolated chloroplasts. *Nature*, *174*(4426), 394-396.

Avenson, T. J., Cruz, J. A., Kanazawa, A., & Kramer, D. M. (2005). Regulating the proton budget of higher plant photosynthesis. *Proceedings of the National Academy of Sciences*, 102(27), 9709-9713.

Bailleul, B., Cardol, P., Breyton, C., & Finazzi, G. (2010). Electrochromism: a useful probe to study algal photosynthesis. *Photosynthesis research*, 106(1-2), 179.

Ball, S., Colleoni, C., Cenci, U., Raj, J. N., & Tirtiaux, C. (2011). The evolution of glycogen and starch metabolism in eukaryotes gives molecular clues to understand the establishment of plastid endosymbiosis. *Journal of experimental botany*, 62(6), 1775-1801.

Barber, J., & Andersson, B. (1992). Too much of a good thing: light can be bad for photosynthesis. *Trends in biochemical sciences*, 17(2), 61-66.

Battchikova, N., & Aro, E. M. (2007). Cyanobacterial NDH-1 complexes: multiplicity in function and subunit composition. *Physiologia plantarum*, *131*(1), 22-32.

Battchikova, N., Eisenhut, M., & Aro, E. M. (2011). Cyanobacterial NDH-1 complexes: novel insights and remaining puzzles. *Biochimica et Biophysica Acta (BBA)-Bioenergetics*, 1807(8), 935-944.

Battchikova, N., Zhang, P., Rudd, S., Ogawa, T., & Aro, E. M. (2005). Identification of NdhL and Ssl1690 (NdhO) in NDH-1L and NDH-1M complexes of Synechocystis sp. PCC 6803. *Journal of Biological Chemistry*, 280(4), 2587-2595.

Benz, J. P., Lintala, M., Soll, J., Mulo, P., & Bölter, B. (2010). A new concept for ferredoxin–NADP (H) oxidoreductase binding to plant thylakoids. *Trends in plant science*, 15(11), 608-613.

Berardini, T. Z., Reiser, L., Li, D., Mezheritsky, Y., Muller, R., Strait, E., & Huala, E. (2015). The Arabidopsis information resource: making and mining the "gold standard" annotated reference plant genome. *genesis*, *53*(8), 474-485.

Berger, S., Ellersiek, U., Kinzelt, D., & Steinmüller, K. (1993). Immunopurification of a subcomplex of the NAD (P) H-plastoquinone-oxidoreductase from the cyanobacterium Synechocystis sp. PCC6803. *FEBS letters*, 326(1-3), 246-250.

Bergsten, J. (2005). A review of long-branch attraction. *Cladistics*, 21(2), 163-193.

Blankenship, R. E. (2010). Early evolution of photosynthesis. *Plant physiology*, 154(2), 434-438.

Blankenship, R. E., Sadekar, S., & Raymond, J. (2007). The evolutionary transition from anoxygenic to oxygenic photosynthesis. In *Evolution of primary producers in the sea* (pp. 21-35). Academic Press.

Blount, Z. D., Borland, C. Z., & Lenski, R. E. (2008). Historical contingency and the evolution of a key innovation in an experimental population of Escherichia coli. *Proceedings of the National Academy of Sciences*, 105(23), 7899-7906.

Boardman, N. K., & Anderson, J. M. (1967). Fractionation of the photochemical systems of photosynthesis. II. Cytochrome and carotenoid contents of particles isolated from spinach chloroplasts. *Biochimica et Biophysica Acta (BBA)-Bioenergetics*, 143(1), 187-203.

Boardman, N. T. (1977). Comparative photosynthesis of sun and shade plants. *Annual review of plant physiology*, 28(1), 355-377.

Bothe, H. (1969). Ferredoxin als Kofaktor der cyclischen Photophosphorylierung in einem zellfreien System aus der Blaualge Anacystis nidulans. *Zeitschrift für Naturforschung* B, 24(12), 1574-1582.

Bryant, D. A., Glazer, A. N., & Eiserling, F. A. (1976). Characterization and structural properties of the major biliproteins of Anabaena sp. *Archives of microbiology*, 110(1), 61-75.

Buchanan, B. B. (1980). Role of light in the regulation of chloroplast enzymes. *Annual Review of Plant Physiology*, 31(1), 341-374.

Buchert, F., Hamon, M., Gäbelein, P., Scholz, M., Hippler, M., & Wollman, F. A. (2018). The labile interactions of cyclic electron flow effector proteins. *Journal of Biological Chemistry*, 293(45), 17559-17573.

Burrows, P. A., Sazanov, L. A., Svab, Z., Maliga, P., & Nixon, P. J. (1998). Identification of a functional respiratory complex in chloroplasts through analysis of tobacco mutants containing disrupted plastid ndh genes. *The EMBO Journal*, 17(4), 868-876.

Campanella, J. J., Bitincka, L., & Smalley, J. (2003). MatGAT: an application that generates similarity/identity matrices using protein or DNA sequences. *BMC bioinformatics*, 4(1), 29.

Cardona, T. (2017). Photosystem II is a chimera of reaction centers. *Journal of molecular evolution*, 84(2-3), 149-151.

Castro-Chavez, F. (2010). The rules of variation: amino acid exchange according to the rotating circular genetic code. *Journal of theoretical biology*, 264(3), 711-721.

Cavalier-Smith, T. (2002). The phagotrophic origin of eukaryotes and phylogenetic classification of Protozoa. *International journal of systematic and evolutionary microbiology*, 52(2), 297-354.

Ceciliani, F., Caramori, T., Ronchi, S., Tedeschi, G., Mortarino, M., & Galizzi, A. (2000). Cloning, overexpression, and purification of Escherichia coli quinolinate synthetase. *Protein expression and purification*, 18(1), 64-70.

Chandler, C. J., Wilts, B. D., Brodie, J., & Vignolini, S. (2017). Structural color in marine algae. *Advanced Optical Materials*, 5(5), 1600646.

Charlebois, D., & Mauzerall, D. (1999). Energy storage and optical cross-section of PSI in the cyanobacterium Synechococcus PCC 7002 and a psaE-mutant. *Photosynthesis research*, 59(1), 27-38.

Cicchillo, R. M., Tu, L., Stromberg, J. A., Hoffart, L. M., Krebs, C., & Booker, S. J. (2005). Escherichia coli quinolinate synthetase does indeed harbor a [4Fe-4S] cluster. *Journal of the American Chemical Society*, 127(20), 7310-7311.

Clark, R. D., Hawkesford, M. J., Coughlan, S. J., Bennett, J., & Hind, G. (1984). Association of ferredoxin-NADP+ oxidoreductase with the chloroplast cytochrome bf complex. *FEBS letters*, 174(1), 137-142.

Clarke, A. K., & Eriksson, M. J. (1996). The cyanobacterium Synechococcus sp. PCC 7942 possesses a close homologue to the chloroplast ClpC protein of higher plants. *Plant molecular biology*, 31(4), 721-730.

DalCorso, G., Pesaresi, P., Masiero, S., Aseeva, E., Schünemann, D., Finazzi, G., ... & Leister, D. (2008). A complex containing PGRL1 and PGR5 is involved in the switch between linear and cyclic electron flow in Arabidopsis. *Cell*, 132(2), 273-285.

Dann, M., & Leister, D. (2019). Evidence that cyanobacterial Sll1217 functions analogously to PGRL1 in enhancing PGR5-dependent cyclic electron flow. Nature communications, 10(1), 1-7.

Dautant, A., Meyer, J. B., Yariv, J., Sweet, R. M., & Frolow, F. (1998). Structure of a monoclinic crystal form of cytochrome b1 (bacterioferritin) from E. coli. *Acta Crystallographica Section D: Biological Crystallography*, 54(1), 16-24.

Davies, E. C., & Bendall, D. S. (1987). The antimycin-binding site of thylakoid membranes from chloroplasts. In *Progress in Photosynthesis Research* (pp. 485-488). Springer, Dordrecht.

Demmig-Adams, B., & Adams, W. W. (1996). Xanthophyll cycle and light stress in nature: uniform response to excess direct sunlight among higher plant species. *Planta*, 198(3), 460-470.

Deng, Y., Ye, J., & Mi, H. (2003). Effects of low CO2 on NAD (P) H dehydrogenase, a mediator of cyclic electron transport around photosystem I in the cyanobacterium Synechocystis PCC6803. *Plant and Cell Physiology*, 44(5), 534-540.

Desplats, C., Mus, F., Cuiné, S., Billon, E., Cournac, L., & Peltier, G. (2009). Characterization of Nda2, a plastoquinone-reducing type II NAD (P) H dehydrogenase in Chlamydomonas chloroplasts. *Journal of Biological Chemistry*, 284(7), 4148-4157.

Edgar, R. C. (2004). MUSCLE: multiple sequence alignment with high accuracy and high throughput. *Nucleic acids research*, 32(5), 1792-1797.

Ejima, K., Kawaharada, T., Inoue, S., Kojima, K., & Nishiyama, Y. (2012). A change in the sensitivity of elongation factor G to oxidation protects photosystem II from photoinhibition in Synechocystis sp. PCC 6803. *FEBS letters*, 586(6), 778-783.

Emanuelsson, O., Nielsen, H., & Von Heijne, G. (1999). ChloroP, a neural network-based method for predicting chloroplast transit peptides and their cleavage sites. *Protein Science*, 8(5), 978-984.

Endo, T., Shikanai, T., Sato, F., & Asada, K. (1998). NAD (P) H dehydrogenase-dependent, antimycin A-sensitive electron donation to plastoquinone in tobacco chloroplasts. *Plant and cell physiology*, 39(11), 1226-1231.

Engler, C., Kandzia, R., & Marillonnet, S. (2008). A one pot, one step, precision cloning method with high throughput capability. *PloS one*, 3(11), e3647.

Englund, E., Liang, F., & Lindberg, P. (2016). Evaluation of promoters and ribosome binding sites for biotechnological applications in the unicellular cyanobacterium Synechocystis sp. PCC 6803. *Scientific reports*, 6, 36640.

Fallowfield, H. J., & Osborne, B. A. (1985). Growth and light absorptance of Cyanobacteria and Chlorophyceae with particular reference to Anabaena variabilis and Scenedesmus obliquus. *British Phycological Journal*, 20(1), 27-41.

Fan, D. Y., Fitzpatrick, D., Oguchi, R., Ma, W., Kou, J., & Chow, W. S. (2016). Obstacles in the quantification of the cyclic electron flux around Photosystem I in leaves of C3 plants. *Photosynthesis research*, 129(3), 239-251.

Felsenstein, J. (1978). Cases in which parsimony or compatibility methods will be positively misleading. *Systematic zoology*, 27(4), 401-410.

Felsenstein, J. (1985). Confidence limits on phylogenies: an approach using the bootstrap. *Evolution*, 39(4), 783-791.

Finazzi, Giovanni, and Giles N. Johnson. (2016). Cyclic electron flow: facts and hypotheses. *Photosynthesis Research*, 129(3), 227-230.

Finazzi, G., Johnson, G. N., Dallosto, L., Joliot, P., Wollman, F. A., & Bassi, R. (2004). A zeaxanthin-independent nonphotochemical quenching mechanism localized in the photosystem II core complex. *Proceedings of the National Academy of Sciences*, 101(33), 12375-12380.

Fothergill-Gilmore, L. A., & Michels, P. A. (1993). Evolution of glycolysis. *Progress in biophysics and molecular biology*, 59(2), 105-235.

Foy, R. H., & Gibson, C. E. (1982). Photosynthetic characteristics of planktonic blue-green algae: changes in photosynthetic capacity and pigmentation of Oscillatoria redekei Van Goor under high and low light. *British phycological journal*, 17(2), 183-193.

Fujisawa, T., Narikawa, R., Maeda, S. I., Watanabe, S., Kanesaki, Y., Kobayashi, K., ... & Suzuki, E. (2016). CyanoBase: a large-scale update on its 20th anniversary. *Nucleic acids research*, 45(D1), D551-D554.

Gandini, C., Schmidt, S. B., Husted, S., Schneider, A., & Leister, D. (2017). The transporter Syn PAM 71 is located in the plasma membrane and thylakoids, and mediates manganese tolerance in Synechocystis PCC 6803. *New Phytologist*, 215(1), 256-268.

Gantt, E., Grabowski, B., & Cunningham, F. X. (2003). Antenna systems of red algae: phycobilisomes with photosystem ll and chlorophyll complexes with photosystem I. In *Light-harvesting antennas in photosynthesis* (pp. 307-322). Springer, Dordrecht.

Gao, F., Zhao, J., Chen, L., Battchikova, N., Ran, Z., Aro, E. M., ... & Ma, W. (2016). The NDH-1L-PSI supercomplex is important for efficient cyclic electron transport in cyanobacteria. *Plant physiology*, 172(3), 1451-1464.

Gibson, D. G., Young, L., Chuang, R. Y., Venter, J. C., Hutchison III, C. A., & Smith, H. O. (2009). Enzymatic assembly of DNA molecules up to several hundred kilobases. *Nature methods*, 6(5), 343.

Glazer, A. N. (1977). Structure and molecular organization of the photosynthetic accessory pigments of cyanobacteria and red algae. *Molecular and cellular biochemistry*, 18(2-3), 125-140.

Głowacka, K., Kromdijk, J., Kucera, K., Xie, J., Cavanagh, A. P., Leonelli, L., ... & Long, S. P. (2018). Photosystem II subunit S overexpression increases the efficiency of water use in a field-grown crop. *Nature communications*, 9(1), 868.

Golding, A. J., & Johnson, G. N. (2003). Down-regulation of linear and activation of cyclic electron transport during drought. *Planta*, 218(1), 107-114.

Gorbunov, M. Y., Kuzminov, F. I., Fadeev, V. V., Kim, J. D., & Falkowski, P. G. (2011). A kinetic model of non-photochemical quenching in cyanobacteria. Biochimica et Biophysica Acta (BBA)-*Bioenergetics*, 1807(12), 1591-1599.

Gotoh, E., Matsumoto, M., Ogawa, K. I., Kobayashi, Y., & Tsuyama, M. (2010). A qualitative analysis of the regulation of cyclic electron flow around photosystem I from the post-illumination chlorophyll fluorescence transient in Arabidopsis: a new platform for the in vivo investigation of the chloroplast redox state. *Photosynthesis research*, 103(2), 111-123.

Grimm, B., Porra, R. J., Rüdiger, W., & Scheer, H. (Eds.). (2007). *Chlorophylls and bacteriochlorophylls: biochemistry, biophysics, functions and applications* (Vol. 25). Springer Science & Business Media.

Haig, D., & Hurst, L. D. (1991). A quantitative measure of error minimization in the genetic code. *Journal of molecular evolution*, 33(5), 412-417.

Havaux, M., Guedeney, G., Hagemann, M., Yeremenko, N., Matthijs, H. C., & Jeanjean, R. (2005). The chlorophyll-binding protein IsiA is inducible by high light and protects the cyanobacterium Synechocystis PCC6803 from photooxidative stress. *FEBS letters*, 579(11), 2289-2293.

He, Q., Dolganov, N., Björkman, O., & Grossman, A. R. (2001). The High Light-inducible Polypeptides inSynechocystis PCC6803 EXPRESSION AND FUNCTION IN HIGH LIGHT. *Journal of Biological Chemistry*, 276(1), 306-314.

Lüning, K. (1970). Tauchuntersuchungen zur Vertikalverteilung der sublitoralen Helgoländer Algenvegetation. *Helgoländer Wissenschaftliche Meeresuntersuchungen*, *21*(3), 271.

Hernandez-Prieto, M. A., Tibiletti, T., Abasova, L., Kirilovsky, D., Vass, I., & Funk, C. (2011). The small CAB-like proteins of the cyanobacterium Synechocystis sp. PCC 6803: their involvement in chlorophyll biogenesis for Photosystem II. *Biochimica et Biophysica Acta (BBA)-Bioenergetics*, 1807(9), 1143-1151.

Hertle, A. P., Blunder, T., Wunder, T., Pesaresi, P., Pribil, M., Armbruster, U., & Leister, D. (2013). PGRL1 is the elusive ferredoxin-plastoquinone reductase in photosynthetic cyclic electron flow. *Molecular cell*, 49(3), 511-523.

Hicks, Kali, "Characterization of Slr1098, a Protein with Similarity to the Bilin Lyase Subunit CpcE from the Cyanobacterium Synechocystis sp. PCC 6803" (2009). *University of New Orleans Theses and Dissertations*. 979. https://scholarworks.uno.edu/td/979

Hihara, Y., Kamei, A., Kanehisa, M., Kaplan, A., & Ikeuchi, M. (2001). DNA microarray analysis of cyanobacterial gene expression during acclimation to high light. *The Plant Cell*, 13(4), 793-806.

Hirano, M., & Katoh, S. (1981). ELECTROCHROMIC BAND SHIFTS OF CAROTENOID IN A BLUE-GREEN ALGA. *Photochemistry and Photobiology*, *34*(5), 637-643.

Hofmann, K., & Baron, M. D. (1996). Boxshade 3.21. Pretty printing and shading of multiple-alignment files. *Kay Hofmann ISREC Bioinformatics Group*, Lausanne, Switzerland.

Holtman, C. K., Chen, Y., Sandoval, P., Gonzales, A., Nalty, M. S., Thomas, T. L., ... & Golden, S. S. (2005). High-throughput functional analysis of the Synechococcus elongatus PCC 7942 genome. *DNA research*, 12(2), 103-115.

Hoseki, J., Okamoto, A., Masui, R., Shibata, T., Inoue, Y., Yokoyama, S., & Kuramitsu, S. (2003). Crystal structure of a family 4 uracil-DNA glycosylase from Thermus thermophilus HB8. *Journal of molecular biology*, 333(3), 515-526.

Houot, L., Floutier, M., Marteyn, B., Michaut, M., Picciocchi, A., Legrain, P., ... & Chauvat, F. (2007). Cadmium triggers an integrated reprogramming of the metabolism of Synechocystis

PCC6803, under the control of the Slr1738 regulator. *BMC genomics*, 8(1), 350.

Huang, L., McCluskey, M. P., Ni, H., & LaRossa, R. A. (2002). Global gene expression profiles of the cyanobacterium Synechocystis sp. strain PCC 6803 in response to irradiation with UV-B and white light. *Journal of bacteriology*, 184(24), 6845-6858.

Iwai, M., Takizawa, K., Tokutsu, R., Okamuro, A., Takahashi, Y., & Minagawa, J. (2010). Isolation of the elusive supercomplex that drives cyclic electron flow in photosynthesis. *Nature*, 464(7292), 1210.

Jahns, P., Graf, M., Munekage, Y., & Shikanai, T. (2002). Single point mutation in the Rieske iron–sulfur subunit of cytochrome b 6/f leads to an altered pH dependence of plastoquinol oxidation in Arabidopsis. *FEBS letters*, *519*(1-3), 99-102.

Jahns, P., & Holzwarth, A. R. (2012). The role of the xanthophyll cycle and of lutein in photoprotection of photosystem II. *Biochimica et Biophysica Acta (BBA)-Bioenergetics*, 1817(1), 182-193.

Jazmin, L. J., Xu, Y., Cheah, Y. E., Adebiyi, A. O., Johnson, C. H., & Young, J. D. (2017). Isotopically nonstationary 13C flux analysis of cyanobacterial isobutyraldehyde production. *Metabolic engineering*, 42, 9-18.

Jishage, M., Iwata, A., Ueda, S., & Ishihama, A. (1996). Regulation of RNA polymerase sigma subunit synthesis in Escherichia coli: intracellular levels of four species of sigma subunit under various growth conditions. *Journal of Bacteriology*, 178(18), 5447-5451.

Joët, T., Cournac, L., Horvath, E. M., Medgyesy, P., & Peltier, G. (2001). Increased sensitivity of photosynthesis to antimycin A induced by inactivation of the chloroplast ndhB gene. Evidence for a participation of the NADH-dehydrogenase complex to cyclic electron flow around photosystem I. *Plant Physiology*, 125(4), 1919-1929.

Johnson, G. N. (2005). Cyclic electron transport in C3 plants: fact or artefact?. *Journal of Experimental Botany*, *56*(411), 407-416.

Johnson, M. P. (2016). Photosynthesis. *Essays in biochemistry*, 60(3), 265-273.

Johnson, X., Steinbeck, J., Dent, R. M., Takahashi, H., Richaud, P., Ozawa, S. I., ... & Niyogi, K. K. (2014). Proton gradient regulation 5-mediated cyclic electron flow under ATP-or redox-limited conditions: a study of ΔATpase pgr5 and ΔrbcL pgr5 mutants in the green alga Chlamydomonas reinhardtii. *Plant physiology*, 165(1), 438-452.

Joliot, P., & Joliot, A. (2002). Cyclic electron transfer in plant leaf. *Proceedings of the National Academy of Sciences*, *99*(15), 10209-10214.

Joliot, P., & Joliot, A. (2006). Cyclic electron flow in C3 plants. *Biochimica et Biophysica Acta (BBA)-Bioenergetics*, *1757*(5-6), 362-368.

Källqvist, T. (1981). Hydroecological field experiment. Incubation of natural phytoplankton in Lake Gjersjøen. *Norwegian Institute for Water Research*, F-80402, Oslo, 21.

Kaneko, T., & Tabata, S. (1997). Complete genome structure of the unicellular cyanobacterium Synechocystis sp. PCC6803. *Plant and Cell Physiology*, 38(11), 1171-1176.

Karimova, G., Pidoux, J., Ullmann, A., & Ladant, D. (1998). A bacterial two-hybrid system based on a reconstituted signal transduction pathway. *Proceedings of the National Academy of Sciences*, 95(10), 5752-5756.

Kawashima, R., Sato, R., Harada, K., & Masuda, S. (2017). Relative contributions of PGR5-and NDH-dependent photosystem I cyclic electron flow in the generation of a proton gradient in Arabidopsis chloroplasts. *Planta*, 246(5), 1045-1050.

Keeling, P. J. (2010). The endosymbiotic origin, diversification and fate of plastids. Philosophical *Transactions of the Royal Society B: Biological Sciences*, 365(1541), 729-748.

Keren, N., Aurora, R., & Pakrasi, H. B. (2004). Critical roles of bacterioferritins in iron storage and proliferation of cyanobacteria. *Plant physiology*, 135(3), 1666-1673.

Kim, H., Esser, L., Hossain, M. B., Xia, D., Yu, C. A., Rizo, J., ... & Deisenhofer, J. (1999). Structure of antimycin A1, a specific electron transfer inhibitor of ubiquinol− cytochrome c oxidoreductase. *Journal of the American Chemical Society*, 121(20), 4902-4903.

Klich, M. G. (2000). Leaf variations in Elaeagnus angustifolia related to environmental heterogeneity. *Environmental and experimental botany*, 44(3), 171-183.

Kobayashi, Y., Takusagawa, M., Harada, N., Fukao, Y., Yamaoka, S., Kohchi, T., … & Nishimura, Y. (2015). Eukaryotic components remodeled chloroplast nucleoid organization during the green plant evolution. *Genome biology and evolution*, 8(1), 1-16.

Kojima, K., Oshita, M., Hayashi, H., & Nishiyama, Y. (2008). Role of Elongation Factor G in the Inhibition of the Synthesis of the D1 Protein of Photosystem II Under Oxidative Stress. In *Photosynthesis. Energy from the Sun* (pp. 1313-1316). Springer, Dordrecht.

Kojima, K., Motohashi, K., Morota, T., Oshita, M., Hisabori, T., Hayashi, H., & Nishiyama, Y. (2009). Regulation of translation by the redox state of elongation factor G in the cyanobacterium Synechocystis sp. PCC 6803. *Journal of Biological Chemistry*, 284(28), 18685-18691.

Kojima, K., Oshita, M., Nanjo, Y., Kasai, K., Tozawa, Y., Hayashi, H., & Nishiyama, Y. (2007). Oxidation of elongation factor G inhibits the synthesis of the D1 protein of photosystem II. *Molecular microbiology*, 65(4), 936-947.

Komenda, J., & Sobotka, R. (2016). Cyanobacterial high-light-inducible proteins—protectors of chlorophyll–protein synthesis and assembly. *Biochimica et Biophysica Acta (BBA)-Bioenergetics*, 1857(3), 288-295.

Kopečná, J., Komenda, J., Bučinská, L., & Sobotka, R. (2012). Long-term acclimation of the cyanobacterium Synechocystis sp. PCC 6803 to high light is accompanied by an enhanced production of chlorophyll that is preferentially channeled to trimeric photosystem I. *Plant physiology*, 160(4), 2239-2250.

Krogh, A., Larsson, B., Von Heijne, G., & Sonnhammer, E. L. (2001). Predicting transmembrane protein topology with a hidden Markov model: application to complete genomes. *Journal of molecular biology*, 305(3), 567-580.

Kromdijk, J., Głowacka, K., Leonelli, L., Gabilly, S. T., Iwai, M., Niyogi, K. K., & Long, S. P. (2016). Improving photosynthesis and crop productivity by accelerating recovery from photoprotection. *Science*, *354*(6314), 857-861.

Kukuczka, B., Magneschi, L., Petroutsos, D., Steinbeck, J., Bald, T., Powikrowska, M., ... & Hippler, M. (2014). Proton gradient regulation5-like1-mediated cyclic electron flow is crucial for

acclimation to anoxia and complementary to nonphotochemical quenching in stress adaptation. *Plant physiology*, 165(4), 1604-1617.

Kumar, S., Stecher, G., Li, M., Knyaz, C., & Tamura, K. (2018). MEGA X: molecular evolutionary genetics analysis across computing platforms. *Molecular biology and evolution*, 35(6), 1547-1549.

Laisk, A., Talts, E., Oja, V., Eichelmann, H., & Peterson, R. B. (2010). Fast cyclic electron transport around photosystem I in leaves under far-red light: a proton-uncoupled pathway?. *Photosynthesis Research*, 103(2), 79-95.

Lande, R. (1976). Natural selection and random genetic drift in phenotypic evolution. *Evolution*, 30(2), 314-334.

Laughlin, T. G., Bayne, A. N., Trempe, J. F., Savage, D. F., & Davies, K. M. (2019). Structure of the complex I-like molecule NDH of oxygenic photosynthesis. *Nature*, 566(7744), 411.

Laulhère, J. P., Labouré, A. M., Van Wuytswinkel, O., Gagnon, J., & Briat, J. F. (1992). Purification, characterization and function of bacterioferritin from the cyanobacterium Synechocystis PCC 6803. *Biochemical journal*, 281(3), 785-793.

Le Rouzic, A., & Carlborg, Ö. (2008). Evolutionary potential of hidden genetic variation. *Trends in ecology & evolution*, 23(1), 33-37.

Lee-Kaden, J., & Simonis, W. (1979). Photosystem I and photophosphorylation-dependent leucine incorporation in the blue-green alga Anacystis nidulans. *Plant and Cell Physiology*, 20(7), 1179-1190.

Leister, D. (2019). Genetic engineering, synthetic biology and the light reactions of photosynthesis. *Plant physiology*, 179(3), 778-793.

Leukart, P., & Lüning, K. (1994). Minimum spectral light requirements and maximum light levels for long-term germling growth of several red algae from different water depths and a green alga. *European Journal of Phycology*, 29(2), 103-112.

Li, L., Aro, E. M., & Millar, A. H. (2018). Mechanisms of photodamage and protein turnover in photoinhibition. *Trends in plant science*, 23(8), 667-676.

Li, W., Trabuco, L. G., Schulten, K., & Frank, J. (2011). Molecular dynamics of EF-G during translocation. *Proteins: Structure, Function, and Bioinformatics*, 79(5), 1478-1486.

Lindahl, M., Spetea, C., Hundal, T., Oppenheim, A. B., Adam, Z., & Andersson, B. (2000). The thylakoid FtsH protease plays a role in the light-induced turnover of the photosystem II D1 protein. *The Plant Cell*, 12(3), 419-431.

Lintala, M., Lehtimäki, N., Benz, J. P., Jungfer, A., Soll, J., Aro, E. M., ... & Mulo, P. (2012). Depletion of leaf-type ferredoxin-NADP+ oxidoreductase results in the permanent induction of photoprotective mechanisms in Arabidopsis chloroplasts. *The Plant Journal*, 70(5), 809-817.

Litchman, E. (2003). Competition and coexistence of phytoplankton under fluctuating light: experiments with two cyanobacteria. *Aquatic Microbial Ecology*, 31(3), 241-248.

Loogman, J. G. (1982). Influence of photoperiodicity on algal growth kinetics. *Ph.D. thesis, Univ. of Amsterdam.*

Lugo-Martinez, J., Pejaver, V., Pagel, K. A., Jain, S., Mort, M., Cooper, D. N., ... & Radivojac, P. (2016). The loss and gain of functional amino acid residues is a common mechanism causing human inherited disease. *PLoS computational biology*, 12(8), e1005091.

Luimstra, V. M., Schuurmans, J. M., Verschoor, A. M., Hellingwerf, K. J., Huisman, J., & Matthijs, H. C. (2018). Blue light reduces photosynthetic efficiency of cyanobacteria through an imbalance between photosystems I and II. *Photosynthesis research*, 138(2), 177-189.

Majewski, J., & Cohan, F. M. (1999). Adapt globally, act locally: the effect of selective sweeps on bacterial sequence diversity. *Genetics*, 152(4), 1459-1474.

Manasse, R. S., & Bendall, D. S. (1993). Characteristics of cyclic electron transport in the cyanobacterium Phormidium laminosum. *Biochimica et Biophysica Acta (BBA)-Bioenergetics*, 1183(2), 361-368.

Marchler-Bauer, A., Bo, Y., Han, L., He, J., Lanczycki, C. J., Lu, S., ... & Gwadz, M. (2016). CDD/SPARCLE: functional classification of proteins via subfamily domain architectures. *Nucleic acids research*, *45*(D1), D200-D203.

Martin, W. F., Bryant, D. A., & Beatty, J. T. (2017). A physiological perspective on the origin and evolution of photosynthesis. FEMS microbiology reviews, 42(2), 205-231.

Melis, A. (1999). Photosystem-II damage and repair cycle in chloroplasts: what modulates the rate of photodamage in vivo?. *Trends in plant science*, 4(4), 130-135.

Mi, H., Endo, T., Ogawa, T., & Asada, K. (1995). Thylakoid membrane-bound, NADPH-specific pyridine nucleotide dehydrogenase complex mediates cyclic electron transport in the cyanobacterium Synechocystis sp. PCC 6803. *Plant and Cell Physiology*, 36(4), 661-668.

Mi, H., Endo, T., Schreiber, U., Ogawa, T., & Asada, K. (1994). NAD (P) H dehydrogenase-dependent cyclic electron flow around photosystem I in the cyanobacterium Synechocystis PCC 6803: a study of dark-starved cells and spheroplasts. *Plant and cell physiology*, 35(2), 163-173.

Mi, H., Klughammer, C., & Schreiber, U. (2000). Light-induced dynamic changes of NADPH fluorescence in Synechocystis PCC 6803 and its ndhB-defective mutant M55. *Plant and Cell Physiology*, 41(10), 1129-1135.

Mills, J. D., Slovacek, R. E., & Hind, G. (1978). Cyclic electron transport in isolated intact chloroplasts. Further studies with antimycin. *Biochimica et Biophysica Acta (BBA)-Bioenergetics*, 504(2), 298-309.

Minagawa, J. (2011). State transitions—the molecular remodeling of photosynthetic supercomplexes that controls energy flow in the chloroplast. *Biochimica et Biophysica Acta (BBA)-Bioenergetics*, 1807(8), 897-905.

Miyake, C., Miyata, M., Shinzaki, Y., & Tomizawa, K. I. (2005). CO2 response of cyclic electron flow around PSI (CEF-PSI) in tobacco leaves—relative electron fluxes through PSI and PSII determine the magnitude of non-photochemical quenching (NPQ) of Chl fluorescence. *Plant and Cell Physiology*, 46(4), 629-637.

Moss, D. A., & Bendall, D. S. (1984). Cyclic electron transport in chloroplasts. The Q-cycle and the site of action of antimycin. *Biochimica et Biophysica Acta (BBA)-Bioenergetics*, 767(3), 389-395.

Mulkidjanian, A. Y., Galperin, M. Y., & Koonin, E. V. (2009). Co-evolution of primordial membranes and membrane proteins. *Trends in biochemical sciences*, 34(4), 206-215.

Mullineaux, C. W. (2014). Co-existence of photosynthetic and respiratory activities in cyanobacterial thylakoid membranes. *Biochimica et Biophysica Acta (BBA)-Bioenergetics*, *1837*(4), 503-511.

Mulo, P. (2011). Chloroplast-targeted ferredoxin-NADP+ oxidoreductase (FNR): structure, function and location. *Biochimica et Biophysica Acta (BBA)-Bioenergetics*, 1807(8), 927-934.

Munekage, Y., Hashimoto, M., Miyake, C., Tomizawa, K. I., Endo, T., Tasaka, M., & Shikanai, T. (2004). Cyclic electron flow around photosystem I is essential for photosynthesis. *Nature*, 429(6991), 579.

Munekage, Y., Hojo, M., Meurer, J., Endo, T., Tasaka, M., & Shikanai, T. (2002). PGR5 is involved in cyclic electron flow around photosystem I and is essential for photoprotection in Arabidopsis. *Cell*, 110(3), 361-371.

Munekage, Y., Takeda, S., Endo, T., Jahns, P., Hashimoto, T., & Shikanai, T. (2001). Cytochrome b6f mutation specifically affects thermal dissipation of absorbed light energy in Arabidopsis. *The Plant Journal*, *28*(3), 351-359.

Muramatsu, M., & Hihara, Y. (2012). Acclimation to high-light conditions in cyanobacteria: from gene expression to physiological responses. *Journal of plant research*, *125*(1), 11-39.

Murata, N., & Nishiyama, Y. (2018). ATP is a driving force in the repair of photosystem II during photoinhibition. *Plant, cell & environment*, 41(2), 285-299.

Nakano, H., Yamamoto, H., & Shikanai, T. (2019). Contribution of NDH-dependent cyclic electron transport around photosystem I to the generation of proton motive force in the weak mutant allele of pgr5. *Biochimica et Biophysica Acta (BBA)-Bioenergetics*, 1860(5), 369-374.

Nandha, B., Finazzi, G., Joliot, P., Hald, S., & Johnson, G. N. (2007). The role of PGR5 in the redox poising of photosynthetic electron transport. *Biochimica et Biophysica Acta (BBA)-Bioenergetics*, 1767(10), 1252-1259.

National Center for Biotechnology Information (NCBI)[Internet]. Bethesda (MD): National Library of Medicine (US), National Center for Biotechnology Information; [1988] – [cited 2019 Oct 07]. Available from: https://www.ncbi.nlm.nih.gov/

Nawrocki, W. J., Bailleul, B., Cardol, P., Rappaport, F., Wollman, F. A., & Joliot, P. (2019). Maximal cyclic electron flow rate is independent of PGRL1 in Chlamydomonas. *Biochimica et Biophysica Acta (BBA)-Bioenergetics*, 1860(5), 425-432.

Nei, M., & Kumar, S. (2000). *Molecular evolution and phylogenetics*. Oxford university press.

Nelson, N., & Ben-Shem, A. (2004). The complex architecture of oxygenic photosynthesis. *Nature Reviews Molecular Cell Biology*, 5(12), 971.

Nishikawa, Y., Yamamoto, H., Okegawa, Y., Wada, S., Sato, N., Taira, Y., ... & Shikanai, T. (2012). PGR5-dependent cyclic electron transport around PSI contributes to the redox homeostasis in chloroplasts rather than CO2 fixation and biomass production in rice. *Plant and Cell Physiology*, 53(12), 2117-2126.

Nishiyama, Y., Allakhverdiev, S. I., & Murata, N. (2006). A new paradigm for the action of reactive oxygen species in the photoinhibition of photosystem II. *Biochimica et Biophysica Acta (BBA)-Bioenergetics*, 1757(7), 742-749.

Nogales, J., Gudmundsson, S., Knight, E. M., Palsson, B. O., & Thiele, I. (2012). Detailing the optimality of photosynthesis in cyanobacteria through systems biology analysis. *Proceedings of the National Academy of Sciences*, 109(7), 2678-2683.

Nürnberg, D. J., Morton, J., Santabarbara, S., Telfer, A., Joliot, P., Antonaru, L. A., ... & Fantuzzi, A. (2018). Photochemistry beyond the red limit in chlorophyll f–containing photosystems. *Science*, 360(6394), 1210-1213.

Ogawa, T. (1991). A gene homologous to the subunit-2 gene of NADH dehydrogenase is essential to inorganic carbon transport of Synechocystis PCC6803. *Proceedings of the National Academy of Sciences*, 88(10), 4275-4279.

Ogawa, T., Harada, T., Ozaki, H., & Sonoike, K. (2013). Disruption of the ndhF1 gene affects Chl fluorescence through state transition in the cyanobacterium Synechocystis sp. PCC 6803, resulting in apparent high efficiency of photosynthesis. *Plant and cell physiology*, 54(7), 1164-1171.

Ogawa, T., Misumi, M., & Sonoike, K. (2017). Estimation of photosynthesis in cyanobacteria by pulse-amplitude modulation chlorophyll fluorescence: problems and solutions. *Photosynthesis research*, 133(1-3), 63-73.

Okegawa, Y., Long, T. A., Iwano, M., Takayama, S., Kobayashi, Y., Covert, S. F., & Shikanai, T. (2007). A balanced PGR5 level is required for chloroplast development and optimum operation of cyclic electron transport around photosystem I. *Plant and cell physiology*, 48(10), 1462-1471.

Okegawa, Y., Tsuyama, M., Kobayashi, Y., & Shikanai, T. (2005). The pgr1 mutation in the Rieske subunit of the cytochrome b6f complex does not affect PGR5-dependent cyclic electron transport around photosystem I. *Journal of Biological Chemistry*, 280(31), 28332-28336.

Olinares, P. D. B., Kim, J., & van Wijk, K. J. (2011). The Clp protease system; a central component of the chloroplast protease network. *Biochimica Et Biophysica Acta (BBA)-Bioenergetics*, *1807*(8), 999-1011.

Ollagnier-de Choudens, S., Loiseau, L., Sanakis, Y., Barras, F., & Fontecave, M. (2005). Quinolinate synthetase, an iron–sulfur enzyme in NAD biosynthesis. *FEBS letters*, 579(17), 3737-3743.

Ort, D. R., & Baker, N. R. (2002). A photoprotective role for O_2 as an alternative electron sink in photosynthesis?. *Current opinion in plant biology*, *5*(3), 193-198.

Parfrey, L. W., Lahr, D. J., Knoll, A. H., & Katz, L. A. (2011). Estimating the timing of early eukaryotic diversification with multigene molecular clocks. *Proceedings of the National Academy of Sciences*, 108(33), 13624-13629.

Patwa, Z., & Wahl, L. M. (2008). The fixation probability of beneficial mutations. *Journal of The Royal Society Interface*, 5(28), 1279-1289.

Peltier, G., & Cournac, L. (2002). Chlororespiration. *Annual review of plant biology*, 53(1), 523-550.

Petroutsos, D., Terauchi, A. M., Busch, A., Hirschmann, I., Merchant, S. S., Finazzi, G., & Hippler, M. (2009). PGRL1 participates in iron-induced remodeling of the photosynthetic apparatus and in energy metabolism in Chlamydomonas

reinhardtii. *Journal of Biological Chemistry*, 284(47), 32770-32781.

Pohorille, A., Wilson, M. A., & Chipot, C. (2003). Membrane peptides and their role in protobiological evolution. *Origins of life and evolution of the biosphere*, 33(2), 173-197.

Poorter, H., Niinemets, Ü., Ntagkas, N., Siebenkäs, A., Mäenpää, M., Matsubara, S., & Pons, T. (2019). A meta-analysis of plant responses to light intensity for 70 traits ranging from molecules to whole plant performance. *New Phytologist*, 223, 1073–1105.

Posada, D., & Crandall, K. A. (1998). Modeltest: testing the model of DNA substitution. *Bioinformatics (Oxford, England)*, *14*(9), 817-818.

Prommeenate, P., Lennon, A. M., Markert, C., Hippler, M., & Nixon, P. J. (2004). Subunit Composition of NDH-1 Complexes of Synechocystis sp. PCC 6803 identification of two new ndh gene products with nuclear-encoded homologues in the chloroplast Ndh complex. *Journal of Biological Chemistry*, 279(27), 28165-28173.

Rappsilber, J., Ishihama, Y., & Mann, M. (2003). Stop and go extraction tips for matrix-assisted laser desorption/ionization, nanoelectrospray, and LC/MS sample pretreatment in proteomics. *Analytical chemistry*, 75(3), 663-670.

Renger, T., & Schlodder, E. (2008). The primary electron donor of photosystem II of the cyanobacterium Acaryochloris marina is a chlorophyll d and the water oxidation is driven by a chlorophyll a/chlorophyll d heterodimer. *The Journal of Physical Chemistry B*, 112(25), 7351-7354.

Requejo, R., Hurd, T. R., Costa, N. J., & Murphy, M. P. (2010). Cysteine residues exposed on protein surfaces are the dominant intramitochondrial thiol and may protect against oxidative damage. *The FEBS journal*, 277(6), 1465-1480.

Richardson, K., Beardall, J., & Raven, J. A. (1983). Adaptation of unicellular algae to irradiance: an analysis of strategies. *New Phytologist*, 93(2), 157-191.

Rintamäki, E., Salo, R., & Aro, E. M. (1994). Rapid turnover of the D1 reaction-center protein of photosystem II as a protection mechanism against photoinhibition in a moss, Ceratodon purpureus (Hedw.) Brid. *Planta*, 193(4), 520.

Rippka, R., Deruelles, J., Waterbury, J. B., Herdman, M., & Stanier, R. Y. (1979). Generic assignments, strain histories and properties of pure cultures of cyanobacteria. *Microbiology*, 111(1), 1-61.

Ritchie, R. J. (2006). Consistent sets of spectrophotometric chlorophyll equations for acetone, methanol and ethanol solvents. *Photosynthesis research*, 89(1), 27-41.

Rochaix, J. D. (2011). Regulation of photosynthetic electron transport. *Biochimica et Biophysica Acta (BBA)-Bioenergetics*, 1807(3), 375-383.

Rodnina, M. V., & Wintermeyer, W. (2011). The ribosome as a molecular machine: the mechanism of tRNA–mRNA movement in translocation. *Biochemical Society Transactions*, *39*(2), 658-662.

Rodnina, M. V., Savelsbergh, A., Katunin, V. I., & Wintermeyer, W. (1997). Hydrolysis of GTP by elongation factor G drives tRNA movement on the ribosome. *Nature*, 385(6611), 37.

Rost, B. (1997). Protein structures sustain evolutionary drift. *Folding and Design*, 2, S19-S24.

Ruban, A. V., & Belgio, E. (2014). The relationship between maximum tolerated light intensity and photoprotective energy dissipation in the photosynthetic antenna: chloroplast gains and losses. *Philosophical Transactions of the Royal Society B: Biological Sciences*, 369(1640), 20130222.

Sacksteder, C. A., Kanazawa, A., Jacoby, M. E., & Kramer, D. M. (2000). The proton to electron stoichiometry of steady-state photosynthesis in living plants: a proton-pumping Q cycle is continuously engaged. *Proceedings of the National Academy of Sciences*, *97*(26), 14283-14288.

Sambrook, J., & Russell, D. W. (2001). Molecular cloning: A laboratory manual, the third edition.

Sandigursky, M., & Franklin, W. A. (1999). Thermostable uracil-DNA glycosylase from Thermotoga maritima a member of a novel class of DNA repair enzymes. *Current Biology*, 9(10), 531-534.

Sandigursky, M., Faje, A., & Franklin, W. A. (2001). Characterization of the full length uracil-DNA glycosylase in the extreme thermophile Thermotoga maritima. *Mutation Research/DNA Repair*, 485(3), 187-195.

Sato, S., Shimoda, Y., Muraki, A., Kohara, M., Nakamura, Y., & Tabata, S. (2007). A large-scale protein–protein interaction analysis in Synechocystis sp. PCC6803. *DNA research*, 14(5), 207-216.

Saunders, A. H., & Booker, S. J. (2008). Regulation of the activity of Escherichia coli quinolinate synthase by reversible disulfide-bond formation. *Biochemistry*, 47(33), 8467-8469.

Saura, P., & Kaila, V. R. (2019). Molecular dynamics and structural models of the cyanobacterial NDH-1 complex. Biochimica et Biophysica Acta (BBA)-Bioenergetics, 1860(3), 201-208.

Schägger, H., & Von Jagow, G. (1987). Tricine-sodium dodecyl sulfate-polyacrylamide gel electrophoresis for the separation of proteins in the range from 1 to 100 kDa. *Analytical biochemistry*, 166(2), 368-379.

Scheller, H. V., & Haldrup, A. (2005). Photoinhibition of photosystem I. *Planta*, 221(1), 5-8.

Schluchter, W. M., Zhao, J. I. N. D. O. N. G., & Bryant, D. A. (1993). Isolation and characterization of the ndhF gene of Synechococcus sp. strain PCC 7002 and initial characterization of an interposon mutant. *Journal of bacteriology*, 175(11), 3343-3352.

Schreiber, U., & Klughammer, C. (2008). New accessory for the Dual-PAM-100: the P515/535 module and examples of its application. *PAM Application Notes*, 1, 1-10.

Schuller, J. M., Birrell, J. A., Tanaka, H., Konuma, T., Wulfhorst, H., Cox, N., ... & Ikegami, T. (2019). Structural adaptations of photosynthetic complex I enable ferredoxin-dependent electron transfer. *Science*, 363(6424), 257-260.

Sergeyenko, T. V., & Los, D. A. (2000). Identification of secreted proteins of the cyanobacterium Synechocystis sp. strain PCC 6803. *FEMS microbiology letters*, *193*(2), 213-216.

Shikanai, T. (2007). Cyclic electron transport around photosystem I: genetic approaches. *Annu. Rev. Plant Biol.*, *58*, 199-217.

Shikanai, T. (2016). Regulatory network of proton motive force: contribution of cyclic electron transport around photosystem I. *Photosynthesis research*, 129(3), 253-260.

Shikanai, T., Endo, T., Hashimoto, T., Yamada, Y., Asada, K., & Yokota, A. (1998). Directed disruption of the tobacco ndhB gene impairs cyclic electron flow around photosystem I. Proceedings of the *National Academy of Sciences*, 95(16), 9705-9709.

Silva, P., Thompson, E., Bailey, S., Kruse, O., Mullineaux, C. W., Robinson, C., ... & Nixon, P. J. (2003). FtsH is involved in the early stages of repair of photosystem II in Synechocystis sp PCC 6803. *The Plant Cell*, 15(9), 2152-2164.

Simis, S. G., Huot, Y., Babin, M., Seppälä, J., & Metsamaa, L. (2012). Optimization of variable fluorescence measurements of phytoplankton communities with cyanobacteria. *Photosynthesis research*, 112(1), 13-30.

Singh, A. K., Elvitigala, T., Bhattacharyya-Pakrasi, M., Aurora, R., Ghosh, B., & Pakrasi, H. B. (2008). Integration of carbon and nitrogen metabolism with energy production is crucial to light acclimation in the cyanobacterium Synechocystis. *Plant physiology*, 148(1), 467-478.

Sjögren, L. L., MacDonald, T. M., Sutinen, S., & Clarke, A. K. (2004). Inactivation of the clpC1 gene encoding a chloroplast Hsp100 molecular chaperone causes growth retardation, leaf chlorosis, lower photosynthetic activity, and a specific reduction in photosystem content. *Plant physiology*, 136(4), 4114-4126.

Sjögren, L. L., Tanabe, N., Lymperopoulos, P., Khan, N. Z., Rodermel, S. R., Aronsson, H., & Clarke, A. K. (2014). Quantitative analysis of the chloroplast molecular chaperone ClpC/Hsp93 in Arabidopsis reveals new insights into its localization, interaction with the Clp proteolytic core, and functional importance. *Journal of Biological Chemistry*, 289(16), 11318-11330.

Slovacek, R. E., Mills, J. D., & Hind, G. (1978). The function of cyclic electron transport in photosynthesis. *FEBS Letters*, 87(1), 73-76.

Sonoike, K. (2011). Photoinhibition of photosystem I. *Physiologia Plantarum*, 142(1), 56-64.

Stal, L. J. (1995). Physiological ecology of cyanobacteria in microbial mats and other communities. *New Phytologist*, 131(1), 1-32.

Steinbeck, J., Ross, I. L., Rothnagel, R., Gäbelein, P., Schulze, S., Giles, N., ... & Stahlberg, H. (2018). Structure of a PSI–LHCI–cyt b6f supercomplex in Chlamydomonas reinhardtii promoting cyclic electron flow under anaerobic conditions. *Proceedings of the National Academy of Sciences*, 115(41), 10517-10522.

Stowell, M. H. B., McPhillips, T. M., Rees, D. C., Soltis, S. M., Abresch, E., & Feher, G. (1997). Light-induced structural changes in photosynthetic reaction center: implications for mechanism of electron-proton transfer. *Science*, 276(5313), 812-816.

Stroebel, D., Choquet, Y., Popot, J. L., & Picot, D. (2003). An atypical haem in the cytochrome b 6 f complex. *Nature*, 426(6965), 413.

Sugimoto, K., Okegawa, Y., Tohri, A., Long, T. A., Covert, S. F., Hisabori, T., & Shikanai, T. (2013). A single amino acid alteration in PGR5 confers resistance to antimycin A in cyclic electron transport around PSI. *Plant and cell physiology*, 54(9), 1525-1534.

Suorsa M Järvi S Grieco M Nurmi M Pietrzykowska M Rantala M Kangasjärvi S Paakkarinen V Tikkanen M Jansson S Aro EM . 2012. PROTON GRADIENT REGULATION5 is essential for proper acclimation of Arabidopsis photosystem I to naturally and artificially fluctuating light conditions. *The Plant Cell* 24, 2934–2948.

Suorsa, M. (2015). Cyclic electron flow provides acclimatory plasticity for the photosynthetic machinery under various environmental conditions and developmental stages. *Frontiers in plant science*, 6, 800.

Suorsa, M., Grieco, M., Järvi, S., Gollan, P. J., Kangasjärvi, S., Tikkanen, M., & Aro, E. M. (2013). PGR5 ensures photosynthetic control to safeguard photosystem I under fluctuating light conditions. *Plant signaling & behavior*, 8(1), e22741.

Suorsa, M., Järvi, S., Grieco, M., Nurmi, M., Pietrzykowska, M., Rantala, M., ... & Aro, E. M. (2012). PROTON GRADIENT REGULATION5 is essential for proper acclimation of Arabidopsis photosystem I to naturally and artificially fluctuating light conditions. *The Plant Cell*, 24(7), 2934-2948.

Tagawa, K., Tsujimoto, H. Y., & Arnon, D. I. (1963). Role of chloroplast ferredoxin in the energy conversion process of photosynthesis. *Proceedings of the National Academy of Sciences, 49*(4), 567.

Taira, Y., Okegawa, Y., Sugimoto, K., Abe, M., Miyoshi, H., & Shikanai, T. (2013). Antimycin A-like molecules inhibit cyclic electron transport around photosystem I in ruptured chloroplasts. *FEBS Open Bio*, 3(1), 406-410.

Takabayashi, A., Kadoya, R., Kuwano, M., Kurihara, K., Ito, H., Tanaka, R., & Tanaka, A. (2013). Protein co-migration database (PCoM-DB) for Arabidopsis thylakoids and Synechocystis cells. *SpringerPlus*, *2*(1), 148.

Takabayashi, A., Kishine, M., Asada, K., Endo, T., & Sato, F. (2005). Differential use of two cyclic electron flows around photosystem I for driving CO2-concentration mechanism in C4 photosynthesis. *Proceedings of the National Academy of Sciences*, 102(46), 16898-16903.

Takahashi, S., Milward, S. E., Fan, D. Y., Chow, W. S., & Badger, M. R. (2009). How does cyclic electron flow alleviate photoinhibition in Arabidopsis?. *Plant Physiology*, 149(3), 1560-1567.

Takahashi, H., Schmollinger, S., Lee, J. H., Schroda, M., Rappaport, F., Wollman, F. A., & Vallon, O. (2016). PETO interacts with other effectors of cyclic electron flow in Chlamydomonas. *Molecular plant*, *9*(4), 558-568.

Tibiletti, T., Rehman, A. U., Vass, I., & Funk, C. (2018). The stress-induced SCP/HLIP family of small light-harvesting-like proteins (ScpABCDE) protects Photosystem II from photoinhibitory damages in the cyanobacterium Synechocystis sp. PCC 6803. *Photosynthesis research*, 135(1-3), 103-114.

Tillich, U. M., Lehmann, S., Schulze, K., Dühring, U., & Frohme, M. (2012). The optimal mutagen dosage to induce point-mutations in Synechocystis sp. PCC6803 and its application to promote temperature tolerance. *PLoS One*, 7(11), e49467.

Tillich, U. M., Wolter, N., Franke, P., Dühring, U., & Frohme, M. (2014). Screening and genetic characterization of thermo-tolerant Synechocystis sp. PCC6803 strains created by adaptive evolution. *BMC biotechnology*, 14(1), 66.

Timmis, J. N., Ayliffe, M. A., Huang, C. Y., & Martin, W. (2004). Endosymbiotic gene transfer: organelle genomes forge eukaryotic chromosomes. *Nature Reviews Genetics*, 5(2), 123.

Tolleter, D., Ghysels, B., Alric, J., Petroutsos, D., Tolstygina, I., Krawietz, D., ... & Cuiné, S. (2011). Control of hydrogen photoproduction by the proton gradient generated by cyclic electron flow in Chlamydomonas reinhardtii. *The Plant Cell*, 23(7), 2619-2630.

Torzillo, G., & Masojidek, J. (2008). Mass Cultivation of Freshwater Microalgae. vol. Encyclopedia of Ecology, 2226-2235. Sven Erik Jorgensen and Brian Fath.

Tu, C. J., Shrager, J., Burnap, R. L., Postier, B. L., & Grossman, A. R. (2004). Consequences of a deletion in dspA on transcript accumulation in Synechocystis sp. strain PCC6803. *Journal of bacteriology*, 186(12), 3889-3902.

Uebe, R., Ahrens, F., Stang, J., Jäger, K., Böttger, L. H., Schmidt, C., ... & Schüler, D. (2019). Bacterioferritin of Magnetospirillum gryphiswaldense Is a Heterotetraeicosameric Complex Composed of Functionally Distinct Subunits but Is Not Involved in Magnetite Biomineralization. *mBio*, 10(3), e02795-18.

Valentini, G., Chiarelli, L., Fortin, R., Speranza, M. L., Galizzi, A., & Mattevi, A. (2000). The allosteric regulation of pyruvate kinase A site-directed mutagenesis study. *Journal of Biological Chemistry*, 275(24), 18145-18152.

Vamvaka, E. (2016). *Metabolic engineering of Synechocystis sp. PCC6803 for plant type pigment productions, and identification of new splicing factors in Arabidopsis thaliana* (Doctoral dissertation, LMU).

van Liere, L., & Mur, L. R. (1980). Occurrence of Oscillatoria agardhii and some related species, a survey. In *Hypertrophic ecosystems* (pp. 67-77). Springer, Dordrecht.

van Liere, L., & Mur, L. R. (1979). Growth kinetics of Oscillatoria agardhii Gomont in continuous culture, limited in its growth by the light energy supply. *Microbiology*, 115(1), 153-160.

van Thor, J. J., Geerlings, T. H., Matthijs, H. C., & Hellingwerf, K. J. (1999). Kinetic evidence for the PsaE-dependent transient ternary complex photosystem I/ferredoxin/ferredoxin: NADP+ reductase in a cyanobacterium. *Biochemistry*, 38(39), 12735-12746.

Viola, S. (2014). *Expression of higher plant photosynthetic proteins in the cyanobacterium Synechocystis sp. PCC 6803* (Doctoral dissertation, LMU).

Viola, S., Bailleul, B., Yu, J., Nixon, P., Sellés, J., Joliot, P., & Wollman, F. A. (2019). Probing the electric field across thylakoid membranes in cyanobacteria. *Proceedings of the National Academy of Sciences*, *116*(43), 21900-21906.

Wahl, L. M., & DeHaan, C. S. (2004). Fixation probability favors increased fecundity over reduced generation time. *Genetics*, 168(2), 1009-1018.

Wakasugi, T., Tsudzuki, J., Ito, S., Nakashima, K., Tsudzuki, T., & Sugiura, M. (1994). Loss of all ndh genes as determined by sequencing the entire chloroplast genome of the black pine Pinus thunbergii. *Proceedings of the National Academy of Sciences*, 91(21), 9794-9798.

Wang, C., Yamamoto, H., & Shikanai, T. (2015). Role of cyclic electron transport around photosystem I in regulating proton motive force. *Biochimica et Biophysica Acta (BBA)-Bioenergetics*, 1847(9), 931-938.

Wang, Y., Yao, H., Cheng, Y., Lovell, S., Battaile, K. P., Midaugh, C. R., & Rivera, M. (2015). Characterization of the bacterioferritin/bacterioferritin associated ferredoxin protein–protein interaction in solution and determination of binding energy hot spots. *Biochemistry*, 54(40), 6162-6175.

Weeden, N. F. (1981). Genetic and biochemical implications of the endosymbiotic origin of the chloroplast. *Journal of Molecular Evolution*, 17(3), 133-139.

Wellburn, A. R. (1994). The spectral determination of chlorophylls a and b, as well as total carotenoids, using various solvents with spectrophotometers of different resolution. *Journal of plant physiology*, 144(3), 307-313.

Whatley, F. W., and Daniel I. Arnon. (1963). [37] Photosynthesis phosphorylation in plants, *Methods in Enzymology,* Volume 6, 308-313.

Whelan, S., & Goldman, N. (2001). A general empirical model of protein evolution derived from multiple protein families using a maximum-likelihood approach. *Molecular biology and evolution*, 18(5), 691-699.

Wilson, A., Ajlani, G., Verbavatz, J. M., Vass, I., Kerfeld, C. A., & Kirilovsky, D. (2006). A soluble carotenoid protein involved in phycobilisome-related energy dissipation in cyanobacteria. *The Plant Cell*, 18(4), 992-1007.

Witt, H. T. (1979). Energy conversion in the functional membrane of photosynthesis. Analysis by light pulse and electric pulse methods: The central role of the electric field. *Biochimica et Biophysica Acta (BBA)-Reviews on Bioenergetics*, 505(3-4), 355-427.

Wong, S. G., Tom-Yew, S. A., Lewin, A., Le Brun, N. E., Moore, G. R., Murphy, M. E., & Mauk, A. G. (2009). Structural and mechanistic studies of a stabilized subunit dimer variant of Escherichia coli bacterioferritin identify residues required for core formation. *Journal of Biological Chemistry*, 284(28), 18873-18881.

Xu, H., Vavilin, D., Funk, C., & Vermaas, W. (2004). Multiple Deletions of Small Cab-like Proteins in the Cyanobacterium Synechocystis sp. PCC 6803 CONSEQUENCES FOR PIGMENT BIOSYNTHESIS AND ACCUMULATION. *Journal of Biological Chemistry*, 279(27), 27971-27979.

Yadav, K. S., Semchonok, D. A., Nosek, L., Kouřil, R., Fucile, G., Boekema, E. J., & Eichacker, L. A. (2017). Supercomplexes of plant photosystem I with cytochrome b6f, light-harvesting complex II and NDH. *Biochimica et Biophysica Acta (BBA)-Bioenergetics*, 1858(1), 12-20.

Yamamoto, H., & Shikanai, T. (2019). PGR5-dependent cyclic electron flow protects photosystem I under fluctuating light at donor and acceptor sides. *Plant physiology*, 179(2), 588-600.

Yamamoto, H., Takahashi, S., Badger, M. R., & Shikanai, T. (2016). Artificial remodelling of alternative electron flow by flavodiiron proteins in Arabidopsis. *Nature plants*, 2(3), 16012.

Yamori, W., & Shikanai, T. (2016). Physiological functions of cyclic electron transport around photosystem I in sustaining photosynthesis and plant growth. *Annual review of plant biology*, 67, 81-106.

Yang, J., Yan, R., Roy, A., Xu, D., Poisson, J., & Zhang, Y. (2015). The I-TASSER Suite: protein structure and function prediction. *Nature methods*, 12(1), 7.

Yeremenko, N., Jeanjean, R., Prommeenate, P., Krasikov, V., Nixon, P. J., Vermaas, W. F., ... & Matthijs, H. C. (2005). Open reading frame ssr 2016 is required for antimycin A-sensitive photosystem I-driven cyclic electron flow in the cyanobacterium

Synechocystis sp. PCC 6803. *Plant and Cell Physiology*, 46(8), 1433-1436.

Zavřel, T., Sinetova, M. A., & Červený, J. (2015). Measurement of chlorophyll a and carotenoids concentration in cyanobacteria. *Bio-protocol*, 5, e1467.

Zerulla, K., Ludt, K., & Soppa, J. (2016). The ploidy level of Synechocystis sp. PCC 6803 is highly variable and is influenced by growth phase and by chemical and physical external parameters. *Microbiology*, 162(5), 730-739.

Zevenboom, W., & Mur, L. R. (1984). Growth and photosynthetic response of the cyanobacterium Microcystis aeruginosa in relation to photoperiodicity and irradiance. *Archives of microbiology*, 139(2-3), 232-239.

Zhang, H., Whitelegge, J. P., & Cramer, W. A. (2001). Ferredoxin: NADP+ Oxidoreductase Is a Subunit of the Chloroplast Cytochrome b6fComplex. *Journal of Biological Chemistry*, 276(41), 38159-38165.

Zhang, P., Battchikova, N., Jansen, T., Appel, J., Ogawa, T., & Aro, E. M. (2004). Expression and functional roles of the two distinct NDH-1 complexes and the carbon acquisition complex NdhD3/NdhF3/CupA/Sll1735 in Synechocystis sp PCC 6803. *The Plant Cell*, 16(12), 3326-3340.